Convention on Long-range Transboundary Air Pollution

emep

Co-operative programme for monitoring and evaluation of the long-range transmission of air pollutants in Europe

STATUS REPORT
2/2021 July 2022

Assessment of heavy metal and POP pollution on global, regional and national scales

Status Report 2/2022

msc-e & ccc & ceip & imr & ciemat & ineris & enea & fmi

EMEP Status Report 2/2022

July 2022

Assessment of heavy metal and POP pollution on global, regional and national scales

METEOROLOGICAL SYNTHESIZING CENTRE - EAST

Ilia Ilyin, Nadezhda Batrakova, Aleksey Gusev, Mikhail Kleimenov, Olga Rozovskaya, Victor Shatalov, Irina Strizhkina, Oleg Travnikov, Nadezhda Vulykh

CHEMICAL CO-ORDINATING CENTRE

Knut Breivik, Pernilla Bohlin Nizzetto, Katrine Aspmo Pfaffhuber, Wenche Aas

umweltbundesamt

CEIP/Umweltbundesamt Austria

Stephan Poupa, Robert Wankmueller, Bernhard Ullrich

Institute of Marine Research, Norway

Michael Bank, Quang Tri Ho

Atmospheric Pollution Unit, Centro de Investigaciones Energéticas, Medioambientales y Tecnológicas (CIEMAT), Spain

Marta G. Vivanco, Mark R. Theobald, Juan Luis Garrido, Victoria Gil

National Institute for Industrial Environment and Risks (INERIS), France

Florian Couvidat, Augustin Collette

Italian National Agency for New Technologies, Energy and Sustainable Economic Development (ENEA), Italy

Mihaela Mircea, Mario Adani, Ilaria Delia

Finnish Meteorological Institute (FMI), Finland

Rostislav D. Kouznetsov, Evgeny V. Kadancev

Meteorological Synthesizing Centre - East (MSC-E)

2nd Roshchinsky proezd, 8/4, 115419 Moscow, Russia
Phone: +7 926 292 00 18, E-mail: msce@msceast.org, Internet: www.msceast.org

EXECUTIVE SUMMARY

Heavy metals and persistent organic pollutants (POPs) are toxic substances targeted by national and international environmental organizations and regulated by international agreements including the UNECE Convention on Long-range Transboundary Air Pollution (hereafter, CLRTAP or the Convention). Protocol on Heavy metals and Protocol on POPs to the Convention, aimed at reduction of emissions of these pollutants to the atmosphere, were adopted in 1998 and amended in 2012 and 2009, respectively. According to the Protocols, the priority heavy metals and POPs are lead (Pb), cadmium (Cd) and mercury (Hg), polychlorinated biphenyls (PCBs), polychlorinated dibenzo(p)dioxins and dibenzofurans (PCDD/Fs), hexachlorobenzene (HCB) and polyaromatic hydrocarbons (PAHs). The considered PAHs comprise benzo(a)pyrene (B(a)P), benzo(b)fluoranthene (B(b)F), benzo(k)fluoranthene (B(k)F), and indeno(1,2,3-cd)pyrene (I(cd)P). According to the amendments made in 2009 a number of Contaminants of Emerging Concern (CECs) were also included to the POP Protocol.

Scientific support of the implementation of the Protocols is carried out by the co-operative Programme for Monitoring and Evaluation of Long-range Transmission of Air Pollutants in Europe (EMEP, www.emep.int). EMEP activities on emission data, results of monitoring activity, model assessment of heavy metal and POP pollution, research and model development as well as cooperation with subsidiary bodies to the Convention, national and international organizations is described in the report. More detailed information is available in the Technical reports [*Ilyin et al*., 2022; *Aas et al*., 2022; *Pinterits et al.,* 2021; *Schindlbacher et al*., 2021] and the Supplementary Data Reports on heavy metals [*Strizhkina et al.,* 2022a] and POPs [*Strizhkina et al*., 2022b] as well as on the websites (www.msceast.org; https://projects.nilu.no/ccc/reports.html; https://www.ceip.at/).

Emissions

Completeness and consistency of submitted data have improved significantly since EMEP has been collecting information on emissions. In 2022 the emission data on heavy metals and POPs were submitted by 47 (92%) Parties. The quality of submitted data across countries differs quite significantly. Uncertainty of reported data (national totals, sectoral data) is considered to be relatively high. The completeness of reported data is not satisfactory for all pollutants and sectors either.

Analysis of the long-term heavy metal and POP emission trends from 2000 to 2020 demonstrated that temporal variability of the emissions differs significantly in the western and eastern parts of the EMEP domain. In the western part the reduction of PCDD/Fs, HCB , PCB and PAHs made up 61, 96, 59 and 16%, respectively. The reduction of heavy metal emissions was 47% (Cd), 59% (Hg) and 76% (Pb). The trends of heavy metal and POP emissions in the eastern part of the EMEP domain are inconsistent, mainly due to incomplete reporting.

“Industry” sector is the main contributor of Cd, Hg, Pb and PCB in the EMEP region, making up 39 – 83% to total emission. For PAHs (76%) and PCDD/Fs (47%) most of emissions are presented by the sector “Other stationary combustion”. For HCB the sectors “Public electricity and heat production”,

“Industry”, “Other stationary combustion” and “Other emissions from agriculture” have comparable proportions (22 – 28%) to the total emissions. For most of the considered pollutants emissions in the eastern part of the EMEP domain are characterized by higher contribution of sector “Public electricity and heat production” compared to the emissions in the western part.

Emission data for modelling were gridded over latitude-longitude grid based on the gridding system developed by CEIP. If no reported gridded data is available, data of Global Unintentional POPs Emissions data from the Emission Database for Global Atmospheric Research or particulate matter data from the Copernicus Atmospheric Monitoring Service were used as proxies. Final emission data sets for modelling were generated by MSC-E based on the inventories provided by CEIP and additional information on temporal variability, vertical distribution and chemical speciation of emissions. Global emission data were also prepared by MSC-E using the results of the related research projects and expert estimates.

Emission data for modelling were gridded over latitude-longitude grid based on the gridding system developed by CEIP. If no reported gridded data is available, relevant data from various research projects were used as proxies. Final emission data sets for modelling were generated by MSC-E based on the inventories provided by CEIP and additional information on temporal variability, vertical distribution and chemical speciation of emissions. Global emission data were also prepared by MSC-E using the results of the related research projects and expert estimates.

Monitoring

In 2020, there were 40 sites measuring heavy metals of the first and the second priority in both aerosols and precipitation, and altogether there were 67 measurement sites. Mercury in air or precipitation was measured at 27 sites. POP monitoring data were reported by 39 stations, and measurements in both air and precipitation were available at 25 stations. The data on heavy metals were reported by 21 Parties to the Convention, and the data on POPs by 17 Parties. The highest concentrations of heavy metals in air are mainly seen along the coast and especially around the English Channel. Relatively high levels of the concentrations in precipitation generally occur in Eastern Europe. For POPs higher levels are noted for the central and eastern parts of Europe while lower levels take place in the northern part.

Analysis of measured long-term trends of HCB revealed that air concentrations of HCB demonstrate very slow decline or even increase. The reasons for this remain poorly understood. Various factors possibly affecting the levels and long-term tendencies such as re-volatilization from previously contaminated surfaces, seasonal variability, peculiarities of atmospheric transport patterns and differences in sampling and analytical methodologies were discussed.

Status of heavy metal and POP pollution in 2020

Heavy metal (Pb, Cd, Hg) and POP (PAHs, PCDD/Fs, HCB, PCB-153) atmospheric pollution, in 2020 was analyzed for the whole the EMEP region, sub-regions and individual countries. The largest pollution levels of most contaminants are found in Central Europe. This region is characterized by the highest mean deposition fluxes of Pb, Cd, Hg and PAHs and significant pollution levels for PCDD/Fs, PCB-153 and HCB. Northern Europe and Caucasus and Central Asia are the regions with the lowest average pollution levels. According to the estimates, pollution changes between 2019 and 2020 caused by meteorological variability did not exceed ±15% on average for all considered contaminants in all the sub-regions.

Evaluation of the modelling results against observations was carried out for air concentrations and wet deposition fluxes available from the EMEP monitoring network. At most of the stations the modelled air concentrations of Pb and Cd and wet deposition fluxes of Pb, Cd and Hg agree with the observed levels within a factor of two. The model tends to overestimate air concentrations of Pb and Cd and underestimate their wet deposition fluxes. Modelled air concentrations of Hg match the observed levels within ±15%, and somewhat overestimate wet deposition fluxes. Evaluation of PAH, HCB and PCB-153 estimates demonstrate that the absolute value of mean bias between modelled and observed concentrations is below 14%. At the majority of stations the modelled and observed concentrations of PAHs agree within a factor of two. The model matches observed air concentrations of HCB, PCB-153 and PCDD/Fs within a factor of two at about half of the stations.

Deposition fluxes of heavy metals and POPs within the EMEP region are formed by the EMEP anthropogenic emissions, secondary emissions (wind re-suspension of dust particles containing Pb and Cd, natural/legacy emissions of Hg, re-emission of POPs), and emissions from sources located outside the EMEP region (non- EMEP sources). Contributions of anthropogenic and secondary sources to Pb deposition in the EMEP region are comparable, while in case of Cd the anthropogenic component prevails. The contribution of non-EMEP sources to Pb and Cd deposition is generally relatively low, except for Southern Europe and Caucasus and Central Asia. For Hg the contribution of non-EMEP sources exceeds that of the EMEP anthropogenic sources, while the contribution of secondary emissions from the EMEP domain is minor. Secondary sources are the main contributors to deposition of PCDD/Fs and PCB-153, and are the predominant source of HCB pollution in the EMEP region. The contribution of non-EMEP sources of these POP pollutants is relatively low.

In order to support the activities of the Working Group on Effects (WGE) on evaluation of adverse effects of heavy metal pollution on human health and biota, ecosystem-specific deposition fluxes of Pb, Cd and Hg were calculated. It was shown that deposition flux to high vegetation land-cover types (e.g., forests) is several-fold higher than that to low-vegetation types. Besides, the contribution of dry deposition to total deposition in forest is higher than that in other ecosystems. It is worth to note that an update of the critical loads estimates is needed to evaluate the present-day effect of the pollutants on the environment.

Results of the model simulations and measurements of PAH pollution levels in the EMEP domain were used to evaluate exposure of population to high levels of concentrations exceeding air quality

guidelines. Model estimates show that about 8% of the EMEP countries population in 2020 resided in areas with annual mean B(a)P air concentrations exceeded the EU target level. The upper assessment thresholds (UAT) and lower assessment thresholds (LAT) values were exceeded in the areas with about 15% and 25% of the population, respectively. The WHO Reference level was exceeded for about 66% of population of the EMEP countries. However, if the mixture of the four priority PAHs is considered, the percentage of population resided in areas, where the threshold levels are exceeded, is higher (e.g., 11% for the EU target value and 75% for the WHO reference level).

Atmospheric loads to the Arctic and to the marginal seas (the North, Baltic, Black, Mediterranean and Caspian) were also assessed. The assessment includes information on deposition levels and source attribution of heavy metals and POPs in 2020. Besides, results of the model simulations of the pollution on a global scale are shown. These simulations are used to estimate contribution of non-EMEP sources to heavy metal and POP pollution levels in the EMEP countries. However, inventories of heavy metals and POPs global scale emissions are subject of considerable uncertainties. Thus, improvement of the global-scale assessment requires additional efforts on development of global emissions inventories for heavy metals and POPs in co-operation with other international bodies (UN Environment, Stockholm Convention, Minamata Convention, etc.).

Research and development

Multi-model analysis of B(a)P pollution levels in Europe is being performed as a part of the joint TFMM/EuroDelta-Carb intercomparison exercise of national experts and MSC-E. Main objectives of the study on B(a)P are to explore the model performance, analyze sources of uncertainties of modelling results, and to contribute to the refinement of B(a)P emissions from the combustion of fossil fuel and biomass burning. Preliminary analysis of modelling results demonstrates generally reasonable level of agreement of model predictions with observed B(a)P concentrations. At the same time, for some of the stations modelled concentrations significantly deviated from the observed values indicating possible effect of uncertainties in emission estimates, modelling approaches, and measurements. It is planned to perform more detailed analysis to explore the reasons of the differences between the output of participating models, the deviations of the model predictions from observed B(a)P concentrations, and to compare other characteristics and parameters (e.g. B(a)P concentrations in precipitation and deposition fluxes, concentrations of species affecting B(a)P chemical transformations in the atmosphere).

Contaminants of emerging concern (CECs) comprise a wide range of substances having potential to adversely affect wildlife and human health. Some of the CECs are receiving increasing attention in many international and national environmental organizations. Selected CECs were added to the CLRTAP POP Protocol for regulation of their production and use, namely, hexachlorobutadiene (HCBD), octabromodiphenyl ether (octa-BDE), pentachlorobenzene (PeCB), pentabromodiphenyl ethers (PBDEs), perfluorooctane sulfonates (PFOS), polychlorinated naphthalenes (PCN) and short-chain chlorinated paraffins (SCCPs). Ambient concentrations of CECs (e.g. of PBDEs, SCCPs, and PFAS (per- and polyfluoroalkyl substances)) are measured at the EMEP monitoring stations and at a

number of sites of national monitoring networks. Furthermore, preparatory work for evaluation of CEC pollution levels, transport and fate in the environment is carried out.

Global character of Hg dispersion leads to contamination of terrestrial and aquatic ecosystems of the high latitude regions and the northern countries. A detailed study of Hg pollution on a country scale was performed for Norway as a part of the Norwegian Mercury Assessment 2022 (NMA 2022). The study was carried out in close collaboration with national experts and involving detailed national data on observations and emissions. Elevated Hg deposition levels were found in the southern part of the country and along the coast including the most northern areas, whereas low levels occur in the inland territories of the country. Mercury deposition to the country underwent relatively small reduction over past 30 years because of significant contribution of global emissions, which have been slowly changing. The study could useful for the effectiveness evaluation of national and international pollution reduction measures. Besides, further analysis of deviations between the modelling results and observations can help further improving the modelling approaches.

PAH pollution assessment on a national scale was continued in the framework of a country-scale study for Poland. The second phase of the study was focused on the model assessment of B(b)F, B(k)F, and I(cd)P. In particular, analysis and update of model parameterizations for these compounds was carried out. The GLEMOS model was used to evaluate previous and updated national emission inventories of these PAHs. Results of model simulations showed that updated national PAH emission inventory (reported to EMEP) allowed to achieve improvement of pollution assessment accuracy for B(b)F and B(k)F. At the same time, no improvements were seen in case of I(cd)P. On the whole, the study showed that the modelling results still tend to underpredict observed air concentrations of PAHs in the country. Thus, further activities to refine emission estimates and to reduce uncertainties of the model parameterizations for PAHs are of importance.

In order to evaluate the effect of wildfires on heavy metal and POP pollution levels, development of a model parameterization for wildfire emissions was initiated. Available databases on wildfire parameters were analyzed and pilot estimates Pb and B(a)P emissions from wildfires in the EMEP region were carried out. Analysis of the preliminary results showed that the annual mean contribution of wildfires to overall emissions and pollution levels of Pb and B(a)P is relatively low. Nevertheless, in particular countries and in certain months the wildfires can be significant contributors to the Pb and B(a)P pollution levels in the EMEP region. Further research will include sensitivity studies, involvement of wider range of measurement data for verification purposes and testing of the proposed approach to other heavy metals and POPs.

Cooperation

Main results of MSC-E in the field of research and model development were discussed at the virtual meeting of the Task Force on Measurements and Modelling (TFMM). In particular, participation of MSC-E in the assessment of Hg pollution of the Arctic and the results of the Hg case study for Norway were discussed. Besides, the parameterization of heavy metal and POP emissions from wildfires and preliminary results of the model simulations using the wildfire emissions were demonstrated. State-

of-the-art information about emissions, monitoring and modelling of CEC was overviewed. Finally, current results of the EuroDelta-Carb project and the country-scale study of PAH levels in Poland were presented.

MSC-E continues co-operation with the Task Force on Hemispheric Transport of Air Pollution (TF HTAP) on assessment of Hg and POP pollution. In particular, the Centre took part in the TF HTAP virtual meetings focused on global emissions and modelling of Hg (May 18, 2022) and POPs/CEC (May 25, 2022). The meetings were aimed at discussion of practical programs for fulfilment of the near-term plans of Hg and POP activities formulated at the TF HTAP Workshops (April 2021). It was agreed that near-term TF HTAP activities on Hg would benefit, if formulated in line with the on-going effectiveness evaluation procedure performed under the Minamata Convention on Mercury (MCM). It was concurred to consider opportunities of multi-pollutant studies of combustion-related POPs (e.g. PAHs, PCDD/Fs) and PM, and to continue reviewing the progress in the studies of CECs and microplastics on global and regional scales.

Long-term changes of heavy metal and POP deposition in comparison with observed concentrations of these pollutants in mosses and measured levels at the EMEP monitoring stations was analyzed in cooperation with ICP-Vegetation of WGE. The presented analysis showed that combined usage of the results of biomonitoring, the EMEP atmospheric monitoring and the modelling improves investigating long-term heavy metal and POP pollution changes in particular countries as well as at local scale. Results of the modelling and biomonitoring demonstrate similar rates of Pb, Cd, Hg and Cu reduction in most of EMEP countries. The moss measurements, observations at the EMEP monitoring stations and the modelling results demonstrate declining trends of BDE-99 levels and minor changes of PCB-153. Results of the moss surveys are important for evaluation of long-term trends of heavy metals and POPs in the EMEP region. Further cooperation between EMEP and ICP-Vegetation is highly appreciated.

MSC-E completed assessment of atmospheric loads of Pb, Cd and Hg to the marine regions of the North-East Atlantic under support of the OSPAR Commission. Long-term deposition trends for the period from 1990 to 2019 were calculated for each OSPAR maritime region and source-receptor relationships were estimated for 1995, 2005 and 2015. The modelling results were evaluated against observed data from the OSPAR Comprehensive Atmospheric Monitoring Programme (CAMP). It was shown that current estimates of long-term trends were comparable with the results of the previous studies. The results of this work were summarized in the Technical Report [*Ilyin et al*., 2022].

Furthermore, MSC-E continued cooperation with Task Force on Technical and Economic Issues (TFTEI), HELCOM and Stockholm Convention. MSC-E took part in the 7th TFTEI annual meeting. Updated results on long-term changes in measured and modelled B(a)P air concentrations had been demonstrated with emphasis on key emission source categories and exceedances of B(a)P air quality guidelines and population exposure. MSC-E took part in the preparation of the 3rd Global Monitoring Report of the Stockholm Convention, which compiled the most recent outcomes of research activities on monitoring and modelling of pollution levels and trends for legacy POPs as well as for CECs. In the framework of cooperation with HELCOM, the data on atmospheric emissions and modelled deposition of copper, HCB, and BDE-99 for the period 1990-2019 were prepared. In

addition to this, a review of information on regulation, emissions, monitoring, and model assessment of SCCPs and PFOS was performed. Results of this work are available in the joint report of the EMEP Centres for HELCOM [*Gauss et al.*, 2021].

Future activities

Future activities of the EMEP Centres are aimed at further improvement of the assessment of heavy metal and POP pollution levels in the EMEP countries. Detailed evaluation of PAH pollution in the EMEP region will be continued as a part of the TFMM/EuroDelta-Carb multi-model intercomparison study. Collection and evaluation of global emission inventories of Hg and POPs, multi-model studies of Hg air-surface exchange as well as source apportionment of combustion-related POPs will be continued in cooperation with TF HTAP, Minamata and Stockholm Conventions and AMAP. Preparatory work for assessment of CECs long-range transport and fate will be further conducted. Case studies of heavy metal and POP pollution on a country scale aimed at detailed analysis in co-operation with national experts will be initiated in accordance with demands from EMEP countries. MSC-E will proceed with long-term co-operation with WGE focusing on joint analysis of heavy metal measurements in moss in co-operation with ICP Vegetation, data support of ICP Integrated Monitoring and ICP Forests as well as data exchange with TF Health on PAH pollution levels and exceedances of air quality guidelines. It is planned to perform assessment of atmospheric pollution of the Baltic Sea and North-East Atlantic with heavy metals and POPs in co-operation with HELCOM and OSPAR Commissions.

ACKNOWLEDGEMENTS

The operational and research activities described in this report have been funded by the EMEP Trust Fund. Besides, the modelling activity on evaluation of marine pollution was funded by HELCOM and OSPAR. MSC-E is grateful to the colleagues from ICP-Vegetation and national experts for providing measurement data on concentrations of heavy metals and POPs in mosses.

CONTENTS

INTRODUCTION

Heavy metals and persistent organic pollutants (POPs) are toxic substances targeted by national and international environmental organizations and regulated by international agreements including the UNECE Convention on Long-range Transboundary Air Pollution (hereafter, CLRTAP or the Convention). Protocol on Heavy metals and Protocol on POPs to the Convention, aimed at reduction of emissions of these pollutants to the atmosphere, were adopted in 1998 and amended in 2012 and 2009, respectively. According to the Protocols, the priority heavy metals and POPs are lead (Pb), cadmium (Cd) and mercury (Hg), polychlorinated biphenyls (PCBs), polychlorinated dibenzo(p)dioxins and dibenzofurans (PCDD/Fs), hexachlorobenzene (HCB) and polyaromatic hydrocarbons (PAHs). The considered PAHs comprise benzo(a)pyrene (B(a)P), benzo(b)fluoranthene (B(b)F), benzo(k)fluoranthene (B(k)F), and indeno(1,2,3-cd)pyrene (I(cd)P). According to the amendments made in 2009 a number of Contaminants of Emerging Concern (CECs) were also included to the POP Protocol.

Scientific support of the implementation of the Protocols is carried out by the Co-operative Programme for Monitoring and Evaluation of Long-range Transmission of Air Pollutants in Europe (EMEP, www.emep.int). Information about emissions of heavy metals and POPs in the EMEP region is compiled by Centre on Emission Inventories and Projections (CEIP). Monitoring activity within EMEP is supported by Chemical Coordinating Centre (CCC). Model assessment of pollution levels and transboundary transport of heavy metals and POPs is performed by Meteorological Synthesizing Centre – East (MSC-E). The Working Group on Effects (WGE) is focused on evaluation of adverse impacts of the pollutants on the environment and human health.

The Status report summarizes the activity of the EMEP Centres in the field of assessment of heavy metal and POP pollution levels in 2020, following biennial work plan for the implementation of the Convention for 2022–2023 [ECE/EB.AIR/2021/2]. Chapter 1 summarizes information on heavy metal and POP emissions used in the model assessment of pollution levels in the EMEP region. Results of the monitoring activity are presented in Chapter 2. Model assessment of heavy metal and POP atmospheric pollution and information on transboundary transport in 2020 is described in Chapter 3. The results of the Chapter are based on emissions data of the previous reporting year (2019) and characterize pollution changes due to inter-annual meteorological variability. The updated results based on the new emissions reporting for 2020 are presented in Annex B. Recent model developments and research activities are overviewed in Chapter 4. Cooperation with national and international organizations as well as cooperation with the Subsidiary Bodies to the Convention are presented in Chapter 5. Finally, the main challenges and proposals for future work are formulated in Chapter 6.

More detailed information about results of the model assessment, research and cooperation activities, conducted by MSC-E, is presented in the supplementary and technical reports. In particular, detailed information on pollution levels and evaluation of the modelling results is available in the Supplementary Data Reports on heavy metals [*Strizhkina et al*., 2022a] and POPs [*Strizhkina et al*., 2022b]. Assessment of pollution of the North-East Atlantic by Pb, Cd and Hg prepared under support of OSPAR Commission, is given in [*Ilyin et al*., 2022]. Besides, evaluation of

long-term changes of atmospheric input of copper, HCB, and BDE-99 to the Baltic Sea is presented in the Joint report of EMEP Centres for HELCOM [*Gauss et al*., 2021]. Finally, the description of the current stable version of the Global EMEP Multi-media Modelling System (GLEMOS) and information on heavy metal and POP pollution of the EMEP region and individual countries can be found on the MSC-E website (www.msceast.org).

Chapter 1. EMISSIONS OF HEAVY METALS AND POPs

1.1. Official emission data for 2020

The EMEP Reporting guidelines [*UNECE*, 2014] request all Parties to the *LRTAP Convention* to report annually emissions and activity data of air pollutants (SO_x, NO_x, NMVOCs, NH_3, CO, heavy metals, POPs, particulate matter (PM) and voluntary black carbon (BC). Information on large point sources (LPS), projection data and gridded data should be reported every four years.

1.1.1. Reporting of emission inventories in 2022

Completeness and consistency of submitted data have improved significantly since EMEP has been collecting information on emissions (Fig. 1.1). 47 (92%) Parties submitted data to CEIP in 2022[1], 45 Parties reported data on priority heavy metals (Cd, Hg, Pb), from which 41 Parties provided the full time series, three Parties reported only 2020 data, 39 Parties reported data on five additional heavy metals (Arsenic (As), chromium (Cr), copper (Cu), nickel (Ni), selenium (Se), zinc (Zn) and their compounds) (Fig. 1.2). 44 Parties reported data on POPs (total PAHs, PCDD/Fs, HCB, PCBs), out of which all also reported data on additional PAHs (B(a)P, B(b)F, B(k)F, I(cd)P).

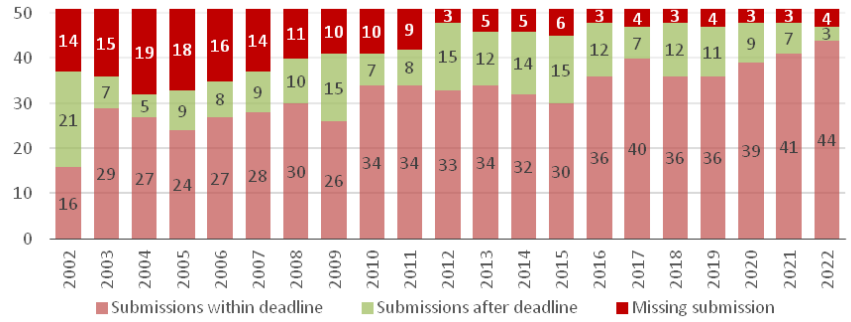

Fig. 1.1. *Number of parties reporting emission data to EMEP since 2002, as of 1 June 2022.*

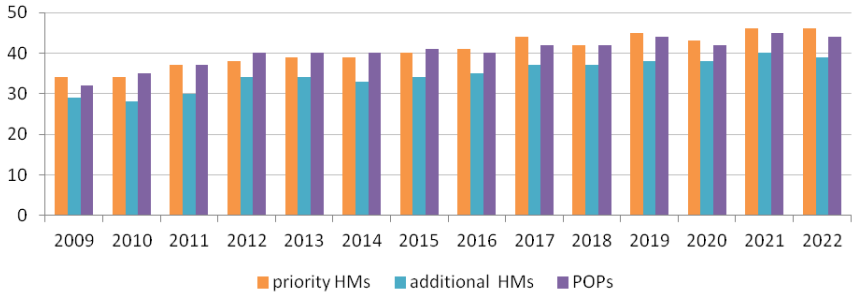

Fig. 1.2. *Number of parties reporting of heavy metals and POPs to EMEP since 2009, as of 1 June 2022.*

[1] *The original submissions from the Parties can be accessed via the CEIP homepage on* https://www.ceip.at/status-of-reporting-and-review-results/2022-submission

The quality of submitted data across countries differs quite significantly. When compiling the inventories, countries have to use the newest available version of the EMEP/EEA *air pollutant emission inventory guidebook*, which is the version of 2019 [*EMEP/EEA Guidebook*, 2019]. However, several countries still use the Guidebook 2016 [*EMEP/EEA Guidebook*, 2016] or older versions. Uncertainty of reported data (national totals, sectoral data) is considered to be relatively high [*CEIP/ Uncertainties*, 2021]. The completeness of reported data is not satisfactory for all pollutants and sectors either. Detailed information on recalculations, completeness and key categories, plus additional review findings, can be found in the annual CEIP technical inventory review reports and its Annexes[2,3].

1.1.2. Emission trends in the EMEP area – reported data

For priority heavy metals and POPs the emission trends and completeness of reported data show different pictures for the EMEP-East and EMEP-West regions. The EMEP-West region includes the EU27 countries, Monaco, Albania, Bosnia & Herzegovina, North Macedonia, Montenegro, Serbia, Iceland, Liechtenstein, Norway, Switzerland and the United Kingdom. The EECCA countries and Turkey are summarized in the EMEP-East region.

EMEP West area – POPs

The strong fluctuations in emission trends of POPs for the EMEP-West region (Fig. 1.3) are mostly due to the reporting of single countries. The high reductions of HCB from 2001 to 2002 are due to the strong decrease in emissions reported by Germany. Liechtenstein does not report PCB. Bosnia & Herzegovina does not report any data.

Main revisions in reporting

- Serbia strongly revised PCDD/F and PAHs which shows more reasonable (lower) emission values.

Emission trends of POPs 2000 to 2020

Table 1.1. shows reported data, and Figure 1.3 demonstrates the indexed trend (year 2000 = 100%) for POPs 2000 to 2020 in the EMEP WEST area.

[2] https://www.ceip.at/review-of-emission-inventories/technical-review-reports
[3] https://www.ceip.at/review-of-emission-inventories/review-process

Table 1.1. *POPs 2000-2020 in the EMEP West area (reported data)*

	B(a)P (t)	B(b)F (t)	B(k)F (t)	IcdP (t)	PAHs (t)	PCDD/F (g I-TEQ)	HCB (kg)	PCBs (kg)
2000	278	293	142	146	932	5 275	4 162	8 080
2001	282	296	144	147	940	4 738	4 269	7 520
2002	279	293	142	143	928	4 531	994	6 987
2003	286	300	145	147	953	4 116	579	6 538
2004	287	300	144	147	956	4 148	442	6 057
2005	297	309	148	150	982	3 858	452	5 818
2006	309	317	151	154	1 013	3 441	341	5 624
2007	300	309	147	154	992	2 828	330	5 334
2008	313	324	153	160	1 024	2 870	305	5 146
2009	307	312	146	158	975	3 175	261	4 679
2010	329	334	156	169	1 049	2 647	244	4 672
2011	303	308	144	155	973	2 518	262	4 479
2012	317	324	151	165	1 011	2 471	255	4 281
2013	309	317	148	162	987	2 435	316	4 057
2014	279	285	134	146	896	2 289	351	3 904
2015	280	287	135	147	902	2 330	227	3 810
2016	285	292	138	149	918	2 259	287	3 706
2017	278	286	134	146	900	2 254	313	3 653
2018	263	272	129	140	860	2 215	225	3 568
2019	242	251	119	132	796	2 112	220	3 459
2020	242	249	118	130	783	2 034	182	3 315
Trend 2000 to 2020	-13%	-15%	-17%	-11%	-16%	-61%	-96%	-59%
Change 2000 to 2020	-36	-44	-24	-15	-149	-3 241	-3 979	-4 765

From 2000 to 2020, **PCDD/F** emissions have been reduced by 61% (-3241 g I-TEQ) with major reductions between 2000 and 2010 (-49.8%). Major reductions are reported by France (-458 g I-TEQ), Slovakia (- 839 g I-TEQ), Romania (- 575 g I-TEQ) and Portugal (-281 g I-TEQ). All countries except Serbia (+39%) reported decreasing emissions since the year 2000.

The strongest PCDD/F emissions reductions occurred in GNFR-sectors *A_PublicPower* (-1172 g I-TEQ), *J_Waste* (-1310 g I-TEQ) and *B_Industry* (-474 g I-TEQ). PCDD/F emissions from *C_OtherStationaryComb* have the highest share (41%) in 2020 but have been reduced by only -161 g I-TEQ since 2000.

From 2000 to 2020, **HCB** emissions have been reduced by 96% (-3979 kg) with major reductions between 2000 and 2002 (-76%, -3168 kg) which is mainly due to the reporting of Germany for G-NFR sector *B_Industry* (-2860 kg). All countries except Latvia, Montenegro and Malta reported decreasing emissions since the year 2000. From 2002 to 2020, HCB emissions decreased by 82% (- 811 kg) with the largest decreases reported by Czechia (-221 kg), Spain (-169 kg), Hungary (-119 kg) and Portugal (-101 kg). In 2020, HCB emissions from *A_PublicPower* have the highest share (27%, 50 kg), followed by *L_AgriOther* (26%, 48 kg).

From 2000 to 2020, **PCB** emissions have been reduced by 59% (-4765 kg) with major reductions in sector *B_industry* (-3364 kg) and *J_Was*te (-954 kg). All countries except Albania, Greece, Lithuania and Norway reported decreasing emissions since the year 2000.

From 2000 to 2020, **PAH** emissions have been reduced by 16% (-149 t) with major reductions in sector *B_Industry* (-73 t) and *C_OtherStationaryComb* (-44 t). The decreasing trend 2017 to 2019 (-104 t) is dominated by Poland (-67 t) in sector *C_OtherStationaryComb*.

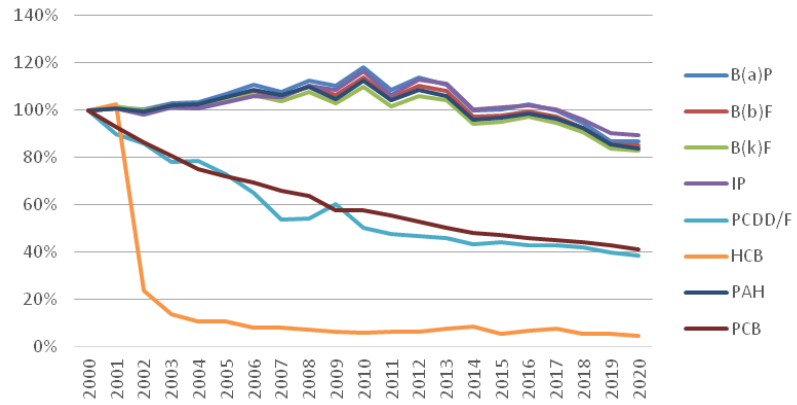

Fig. 1.3. *Emission trends of POPs 2000-2020 in the EMEP West area (reported data).*

EMEP East area – POPs

Reporting of POPs in the EMEP East region is quite incomplete and shows high peaks and inconsistent time series. The Russian Federation reported some POPs for the year 2000 only, and Turkey did not report any POPs at all. Belarus did not report PAH for the years 2000 and 2001. Ukraine reported very high levels of POPs for 2010 to 2013 (constant values) and data from 2017 to 2020. Azerbaijan reported data for the years 2000-2017 and comparatively high values of PCDD/F for 2007 to 2014. Georgia reported complete time series but comparatively high values of HCB for 2014-2017 and 2020 and unreasonable high levels of PCBs for 2000-2020 in G-NFR sector *B_Industry*. Kazakhstan reported complete time series but comparatively high values of PAH, especially for 2019 and 2020. Kyrgyzstan reported incomplete data for 2010-2012 and complete data for 2016 and 2017. Armenia reported incomplete data for 2007 and 2014 and complete data for 2018 to 2020.

Figure 1.4. shows POPs emissions trends from 2002 to 2018 for EMEP East without Russian Federation, Ukraine and without HCB from Kazakhstan and Georgia.

The trend and absolut values of PCDD/F emissions are dominated by reporting of Kazakhstan and for 2009 to 2014 also by Azerbaijan. The trend and absolut values of B(a)P emissions are dominated by Kazakhstan and Belarus. The strong increase in 2019 is also due to reporting of Kazakhstan. The increase of HCB emissions in 2009 is due to the reporting of Azerbaijan and Kazakhstan, and the trend from 2016 to 2020 is dominated by repoting of Belarus.

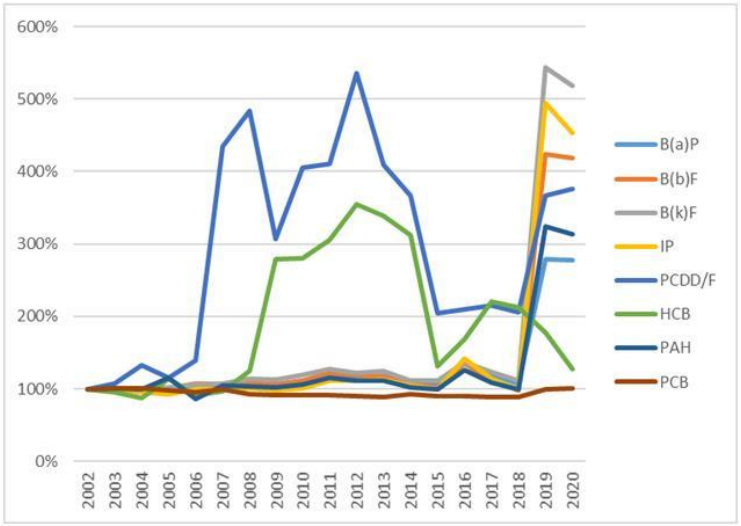

Fig. 1.4. *Emission trends of POPs 2002-2020 in the EMEP East area (reported data) without without Russian Federation, Ukraine and without HCB from Kazakhstan and Georgia.*

EMEP West area – priority heavy metals

Priority heavy metals of the EMEP West area show a rather smooth downtrend and a dip in the year 2009, which reflects the economic recession leading to lower industrial production in that year (Fig. 1.5). The strong decrease of Pb emissions from 2000 to 2002 is mainly due to lower emissions in the transport sector in Italy and Spain. The decreasing Hg emissions trend 2018 to 2020 (-17%) is mainly due to lower emissions reported by Germany (-24%), Spain (-36%), Poland (-13%) and Italy (-16%). The continuous decrease of Hg emissions since the year 2010 is mainly due to decreases reported by France, Germany, Italy and the United Kingdom.

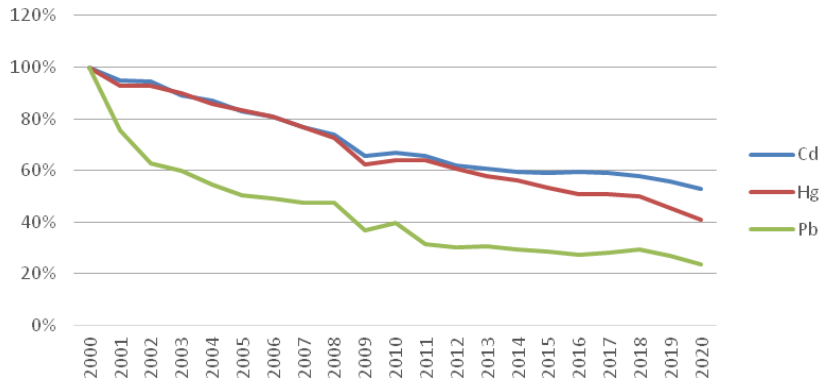

Fig. 1.5. *Emission trends of priority heavy metals 2000-2020 in the EMEP West area (reported data).*

The decreasing Pb emissions trend 2018 to 2020 (-19%) is mainly due to lower emissions reported by Bulgaria (-88%), Poland (-14%), Italy (-15%) and Serbia (-38%). The decrease in 2019 The decreasing Cd emissions trend 2018 to 2020 (-8%) is mainly due to lower emissions reported by Germany (-9%), Spain (-16%), Poland(-6%) and the Netherlands (-21%).

Table 1.2 and Figure 1.5 show reported data and trends for priority heavy metals 2000 to 2020 in the EMEP West area.

Table 1.2. *Priority heavy metals 2000-2020 in the EMEP West area.*

	Cd, t	Hg, t	Pb, t
2000	116	106	4 360
2001	110	99	3 291
2002	109	99	2 743
2003	103	96	2 606
2004	101	91	2 377
2005	96	89	2 201
2006	94	86	2 147
2007	89	82	2 081
2008	85	77	2 072
2009	76	66	1 602
2010	77	68	1 732
2011	76	68	1 378
2012	72	65	1 322
2013	70	61	1 345
2014	69	60	1 280
2015	69	57	1 250
2016	69	54	1 190
2017	68	54	1 231
2018	67	53	1 292
2019	65	48	1 181
2020	61	44	1 041
Trend 2000 to 2019	-47%	-59%	-76%
Change 2000 to 2019	-54	-63	-3 319

EMEP East area – priority heavy metals

Unlike EMEP West, *priority heavy metals of the EMEP East area show an unstable trend from 2000 to 2007*, which is mainly due to incomplete reporting (Fig 1.6). The dip in 2001 Pb and Cd emissions is mainly due to a gap in reporting of the Russian Federation, which reported for 2000, 2002-2006 and 2009 (jump in Cd emissions) only. Ukraine and Belarus did not report heavy metals for 2000.

Azerbaijan and Kyrgyzstan did not report data for 2018 to 2020 and Moldova did not report for 2020. Georgia, Kazakhstan and Turkey are the only countries, which reported complete time series for all three heavy metals since the year 2000.

The strong increase in Hg emissions from 2017 to 2020 is due unreasonable high emissions reported by Armenia for 2018 (GNFR sector “E_Solvents”, the value is about 400 times higher than for 2017 and 2019) and due to higher emissions reported by Kazakhstan and Ukraine for 2019 an 2020 (both a factor 5 to 7 higher than for previous years). The increase in Pb emissions 2019 is due to unreasonable high emissions reported by Ukraine (factor of 3 higher than for previous years) and Kazakhstan (factor of 2 higher than for previous years).

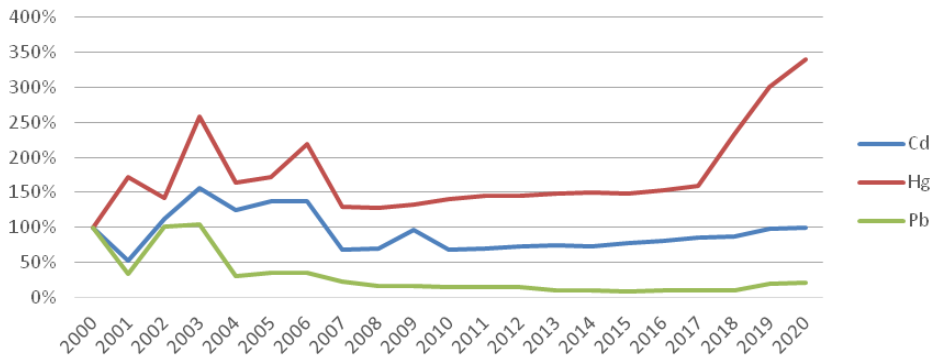

Fig. 1.6. *Emission trends of priority heavy metals 2000-2020 in the EMEP East area (reported data).*

1.1.3. Comparison of 2019 data reported in 2021 and in 2022

Emission data for 2019 reported in 2022 were compared with 2019 emissions reported in 2021. For 24 countries, data changed by more than ±15 % for one or several pollutants (see Fig. 1.7 and Annex A2). Four countries (Armenia, Belarus, Moldova, Ukraine) did not revise 2019 POPs and HMs data and are not displayed in Fig 1.7.

Several countries reported **significant recalculations** for some of the pollutants (see right part of Fig. 1.7, which is displayed in logarithmic scale).

Analysis shows that some of the 2019 values reported in the 2021 submissions were comparably low (e.g. Montenegro PAHs) or high (e.g. Serbia PAHs) which makes revisions reasonable.

Turkey revised heavy metal emissions remarkably upwards (by factors between +13 to +89), mainly from waste incineration.

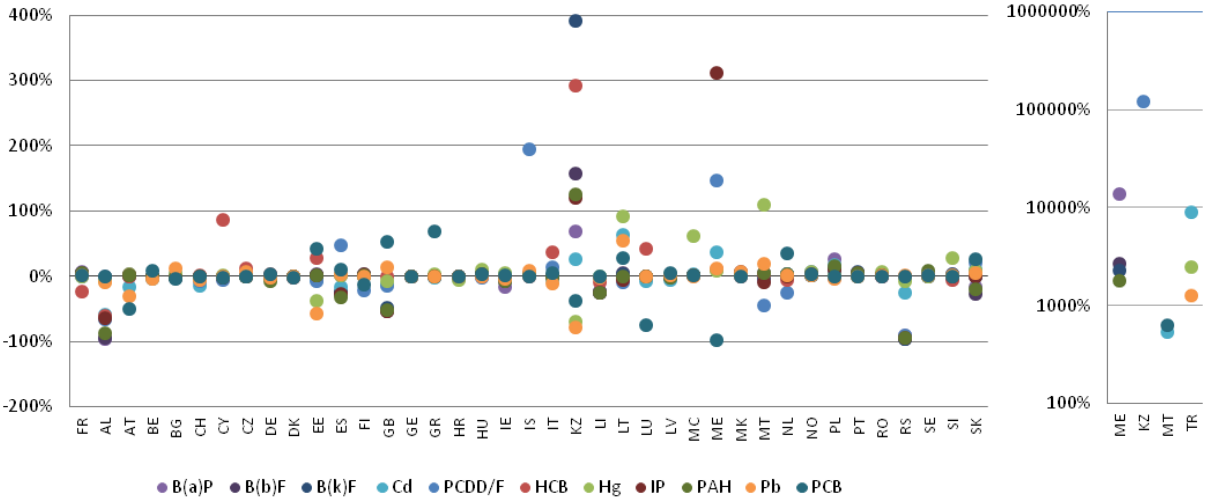

Fig. 1.7. *Recalculations between the 2022 and 2021 submission for 2019 values (reported data). The separate chart on the right shows countries and pollutants with recalculations > 400%, expressed as factors in logarithmic scale.*

1.1.4. Data sets for modellers in 2022

Data used by CEIP were reported by the Parties to the LRTAP Convention as sectoral emissions (NFR19) and National Total emissions according to the UNECE guidelines for reporting emissions and projections data under the LRTAP Convention, Annex I [*UNECE*, 2014].

Reported (NFR[4]) sector data were aggregated to 13 GNFR sectors. In several cases, no data were submitted by the countries, or the reporting is not complete or contains errors. Before modellers can use such emission data, missing or erroneous information has to be filled in or replaced by expert estimates. To gap-fill missing/erroneous data, CEIP typically applies different methods. The gap-filling procedure is fully documented every year in the technical reports which can be downloaded from the CEIP website[5]. After the gap-filling, sector emissions are used for spatial distribution (mapping) to the EMEP grids.

The Parties for which reported data were (partly) replaced are listed in Annex A3.

Contribution of individual sectors to total EMEP heavy metals and POPs emissions

Figure 1.8 shows the *contribution of each GNFR sector to the total emissions of individual air pollutants* (Cd, Hg, Pb, B(a)P, B(b)F, B(k)F, I(cd)P, PAHs, PCDD/F, HCB, PCB). To provide as complete a picture as possible of the share of the individual sectors in total EMEP emissions, data as used for EMEP models (i.e. gap-filled data) were used for the calculations. The analysis does not include sea regions.

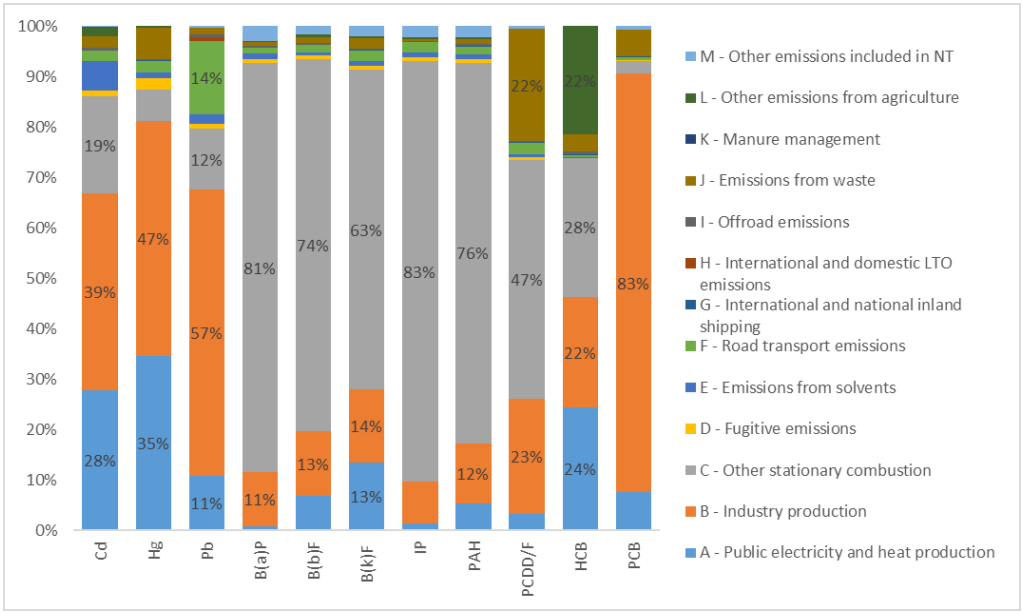

Fig. 1.8. *GNFR sector contribution to national total emissions in 2020, EMEP area without sea regions (only percentages above 10% are labelled).*

[4] NFR – Nomenclature for Reporting

[5] https://www.ceip.at/ceip-reports

It is evident that the combustion of fossil fuels and processing of raw materials is responsible for a significant part of heavy metals and POPs emissions.

Industry production emits about 39 % of **Cd** emissions, followed by 28% from public power and heat plants.

The industry production sector emit about 47% of total **Hg** emissions, followed by energy industries, which released 35% of total emissions, mainly from coal power plants.

About 57% of **Pb** emissions are released by the industry production sector, while each of the other sectors contributes to a maximum of about 14%. Road transport (leaded gasoline) only contributes 14%.

The largest source of **PAHs** and its compounds (B(a)P, B(b)F, B(k)F, I(cd)P) is the 'other stationary combustion' sector, which contributes 76% of total PAH emissions. The main source of PAH emissions are coal and wood stoves/boilers in households. About 12% of PAH emissions are related to the industry production sector.

With 47% of total emissions, the 'other stationary combustion' sector contributes most to **PCDD/F** emissions. The main source of PCDD/F emissions are coal and wood stoves/boilers in households. Industry production plants (metal industries) contribute 23% of total PCDD/F emissions and the waste sector (mainly waste incineration) contributes about 22%.

With 28% of total emissions, 'Other stationary combustion' contributes most to **HCB** emissions, followed by followed by public electricity and heat production with a share of 24% and industry production with a share of 22%. Another large source of HCB emissions is the agriculture sector with a share of 22%. The largest contributors of HCB to the agriculture sector in the EMEP West area are France (31%) the UK (27 %) and Spain (23%). However, the Ukraine (29 %) and Kazakhstan (20%) are the largest contributors to the agriculture sector in the total EMEP area.

The dominating sector for **PCB** emissions is the industrial sector, which contributes 83% to total emissions.

Figure 1.9 illustrates the sector contribution for the EMEP West region and the EMEP East region. North Africa is included in the EMEP East region. The comparison of both graphs highlights some significant differences between West and East.

The continuous revision of inventory data for many countries shows that POPs emissions have the highest uncertainties of all pollutant groups. In addition, data for MSC-E is subject to incomplete reporting or delays in reporting. Especially for POPs, one should therefore draw conclusions carefully when comparing the shares between MSC-E and MSC-W.

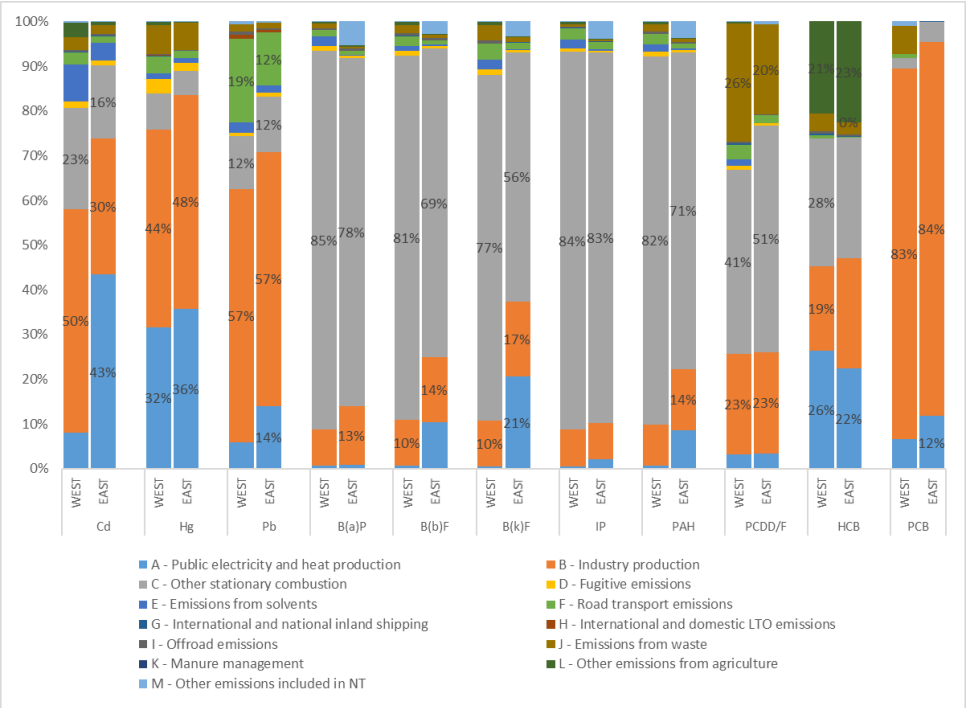

Fig. 1.9. *GNFR sector contribution to national total emissions in 2020 for the EMEP West and EMEP East areas (Only percentages above 10% are labelled. 'Remaining Asian Areas' are included in the EMEP East region and North Africa is included in the EMEP West region).*

Reporting of gridded data

After the first round of submissions in 2017, 2021 was the second year for which EMEP countries were obliged to report gridded emissions in the grid resolution of 0.1°x0.1° (long/lat). 34 of the 48 countries which are considered as a part of the EMEP area reported sectoral gridded heavy metal and POP emissions in the new resolution until June 2022. In 2022 four countries provided new information about their gridded emissions.

The majority of gridded sectoral emissions in 0.1°x0.1° (long/lat) resolution have been reported for the year 2015 (32 countries). For 2019 gridded sectoral emissions have been reported by 28 countries, for 2016 and 2017 by five countries and for 2018 and 2020 by four countries. Compared to the 2017 reporting, gridded data are available for 11 additional countries in 2022.

Reported gridded sectoral data in 0.1°x0.1° (long/lat) resolution, which can be used for the preparation of gridded emissions for modellers, covers less than 50% of the grid cells of all reporting parties. For the remaining areas missing emissions are gap-filled and spatially distributed using expert estimates. Reported grid data can be downloaded from the CEIP website[6]. An overview of gridded data in 0.1°x0.1° (long/lat) resolution reported in 2017, 2020, 2021 and 2022 is provided in Table 1.3.

[6] https://www.ceip.at/status-of-reporting-and-review-results/2022-submission

Table 1.3. *Gridded emissions reported until 2017, 2020, 2021 and 2022.*

Country	2017	2020	2021	2022	Comments
	Gridded data available for the years…	Gridded data available for the years…	Gridded data available for the years…	Gridded data available for the years…	
Austria	2015	2015	2000, 2005, 2010, 2015, 2019	2000, 2005, 2010, 2015, 2019	
Belgium	2015	2015	2015, 2019	2015, 2019	
Bulgaria	2015	2015	2015, 2019	2015, 2019	
Croatia	1990, 1995, 2000, 2005, 2010, 2015	1990, 1995, 2000, 2005, 2010, 2015	1990, 1995, 2000, 2005, 2010, 2015, 2019	1990, 1995, 2000, 2005, 2010, 2015, 2019	
Cyprus			1990, 1995, 2000, 2005, 2010, 2015, 2019	1990, 1995, 2000, 2005, 2010, 2015, 2019	
Czechia	2015	2015	2015, 2019	2015, 2019	
Denmark	2015	2015	2015, 2019	2015, 2019	
Estonia		1990, 1995, 2000, 2005, 2010, 2015	1990, 1995, 2000, 2005, 2010, 2015, 2019	1990, 1995, 2000, 2005, 2010, 2015, 2019	
Finland	2014, 2015	2014[(a)], 2015[(a)], 2016, 2017, 2018[(a)]	1990, 1995, 2000, 2005, 2010, 2015, 2016, 2017, 2019	1990, 1995, 2000, 2005, 2010, 2015, 2016, 2017, 2019, 2020	[(a)] Gridded data for 2014, 2015 and 2018 could not be used for the preparation of spatial distributed emission data in 2020
France		2015	2015, 2019	2015, 2019	
North Macedonia		2015	2015, 2019[(b)]	2015, 2019	[(b)] The submission of gridded emissions was too late to be considered for the preparation of gridded data for modelers in 2021
Georgia		2015	2015	2015	
Germany			1990, 1995, 2000, 2005, 2010, 2015, 2019	1990, 1995, 2000, 2005, 2010, 2015, 2019	
Greece		2015	2015, 2019	2015, 2019	
Hungary	2015[(c)]	2015	2015	2015	[(c)] The submission of gridded emissions was too late to be considered for the preparation of gridded data for modelers in 2017
Ireland	2015	2015	2015, 2019[(d)]	2015, 2019	[(d)] The submission of gridded emissions was too late to be considered for the preparation of gridded data for modelers in 2021

Italy		2015[e]	2015[e]	2015	[e] Reported gridded data was replaced by Copernicus Atmospheric Monitoring Service (CAMS) and EDGAR proxies
Latvia	2015	2015	2015, 2019	2015, 2019	
Lithuania	2015[f]	2015	2015, 2019[g]	2015, 2019	[f] Reported gridded emissions only on national total level, which could not be used for the gridding, which is done on sectoral level [g] The submission of gridded emissions was too late to be considered for the preparation of gridded data for modelers in 2021
Luxembourg	2015	2015	2015, 2019	2015, 2019	
Malta		2016	2016	2016	Grid reporting not in the defined 0.1°x0.1° coordinates
Monaco	2014, 2015	2014-2016	2014-2019	2014 - 2020	
Netherlands		1990, 1995, 2000, 2005, 2010, 2015	1990, 1995, 2000, 2005, 2010, 2015, 2019	1990, 1995, 2000, 2005, 2010, 2015, 2019	
Norway	1990, 1995, 2000, 2005, 2010, 2015	1990, 1995, 2000, 2005, 2010, 2015	1990, 1995, 2000, 2005, 2010, 2015, 2019	1990, 1995, 2000, 2005, 2010, 2015, 2019	
Poland	2014, 2015	2014, 2015, 2018	2014, 2015, 2018, 2019	2014, 2015, 2018, 2019	
Portugal	2015	2015	2015, 2019	2015, 2019	The spatial disaggregation of sector 'F – Road Transport' was replaced by CAMS proxies
Romania	2005	2005, 2015	2005, 2015	2005, 2015	
Serbia				2020	
Slovakia	2015	2015	2015, 2019	2015, 2019	
Slovenia	2015	2015	2015, 2019	2015, 2019	
Spain	1990-2015	1990-2018	1990-2019	1990-2019	The spatial disaggregation of sector 'F – Road Transport' was replaced by CAMS proxies
Sweden		1990, 2000, 2005, 2010, 2015	1990, 2000, 2005, 2010, 2015, 2019	1990, 2000, 2005, 2010, 2015, 2019	
Switzerland	1980-2015	1980-2018	1980-2019	1980-2020	
United Kingdom	2010, 2015	2010, 2015	2010, 2015, 2019	2010, 2015, 2019	

Gridded data of 2020 in resolution 0.1° x 0.1° (long/lat)

For this year, it was agreed with the modellers to perform gap-filling and gridding for the year 2020 in 0.1° x 0.1° longitude/latitude resolution on GNFR sector level.

The 0.1° x 0.1° GNFR grids of heavy metals (Cd, Hg, Pb) and POPs (B(a)P, B(b)F, B(k)F, I(cd)P, PCDD/Fs, HCB) were spatially distributed based on the gridding system developed by CEIP. A map of total Pb emissions in 2020 is shown in Figure 1.10 as an example. The system is module based and uses as a first step reported gridded emission data for each country and sector where it is available and usable. If no reported gridded data in the 0.1° x 0.1° (long/lat) resolution is available, Global Unintentional POPs Emissions data from the Emission Database for Global Atmospheric Research (EDGAR v6.0) is used as a proxy for spatial disaggregation of POP emissions. In case of HM emissions reported gridded PM data is used as a proxy for spatial disaggregation if no reported gridded data in the 0.1° x 0.1° (long/lat) resolution is available. If reported PM data or POP data from EDGAR v6.0 is not available either, PM data from the Copernicus Atmospheric Monitoring Service (CAMS-81, CAMS-REG-AP) and EDGAR 5.0 is used as a proxy.

Reported gridded data in 0.1° x 0.1° (long/lat) resolution was used from Austria, Belgium, Bulgaria, Croatia, Cyprus, Czechia, Denmark, Estonia, Finland, France, Georgia, Germany, Greece, Hungary, Ireland, Latvia, Luxembourg, Malta, Monaco, Netherlands, North Macedonia, Norway, Poland, Portugal, Romania, Slovakia, Slovenia, Spain, Sweden, Switzerland and the United Kingdom.

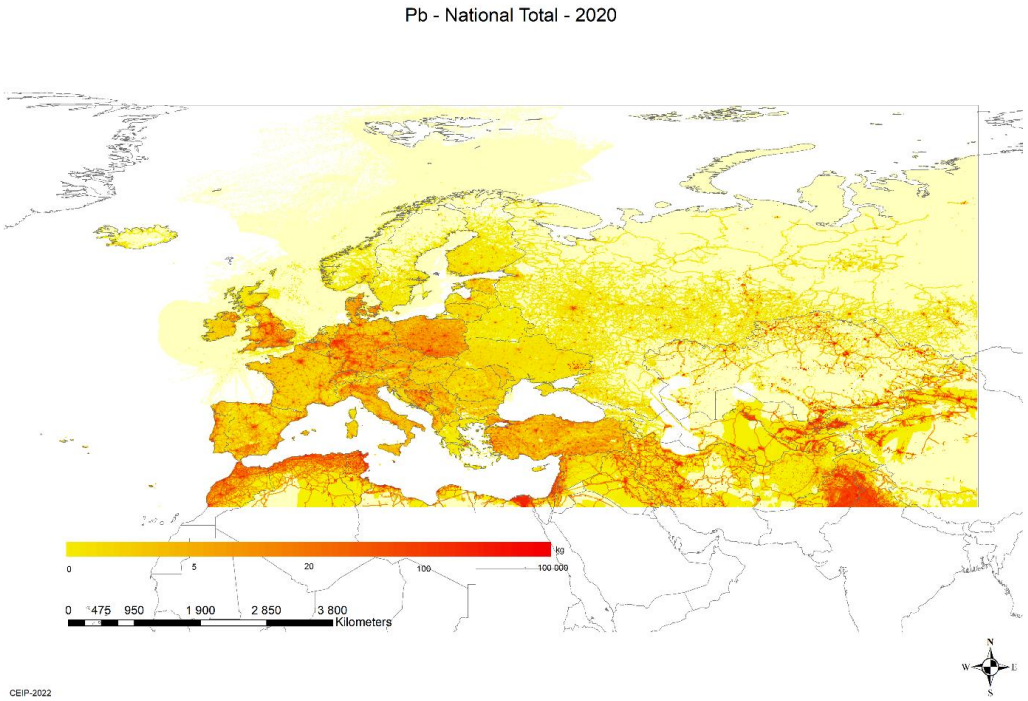

Fig. 1.10. *Visualized gap-filled and gridded Pb emissions in 0.1°x0.1° long-lat resolution.*

Significant changes in data set for modellers between 2022 and 2021

Compared are national totals of gap-filled data used in models in the year 2022 with national totals of gap filled-data used in 2021 (for more details see Annex A.2).

Table 1.4. shows countries and substances for which gap-filled data changed by more than ± 15%. Cases, where PAH has been calculated by adding up the four individual (reported) compounds are not listed.

Table 1.4. *Changes in gap-filled data larger than ± 15%.*

Country	Pollutant	Change	Comment[7]
Albania	PAH	679%	Mainly reported data with exceptions: Gap-filling of missing compounds. Replacement of C_OtherStationaryComb data (unreasonable low quantities) with (higher) 2018 reported data. (2021: sum of reported sector data)
Bosnia and Herzegovina	I(cd)P	283%	TNO data 2010 has been used for gapfilling (2021: Extrapolation of TNO data)
	PAH	140%	
	PCDD/F	54%	
Kazakhstan	PAH	166%	Reported sector data with sum correction of reported PAH/compounds (same methodology for both years).
	PCDD/F	43%	Reported data (2021: Extrapolation of TNO data)
Spain	PAH	-16%	Reported sector data. 2022: estimation of PAH compunds in iron and steel industries.
Turkey	Cd	24%	Reported sector data. 2022: Corrections for waste incineration.
	Hg	55%	Both years: Reported sector data and additional gap filling of non-reported sector "A_PublicPower" with Poland data, which has quite comparable coal consumption. 2022: corrections for waste incineration (IIR inventory report information looks more confident than reported data).
Turkmenistan	I(cd)P	-87%	Error correction of TNO data extrapolation for I(cd)P.
	PAH	-30%	
Ukraine	PCDD/F	-71%	Expert guess: 30% of 'National Implementation Plan of UA for the Stockholm Convention on POPs 2002' (2021: National Implementation Plan of UA for the Stockholm Convention on POPs 2002, extrapolated using population data)
Serbia	PAH	60%	Reported sector data from late resubmission 2022 (2021: omittance of agriculture data which is not reported in 2022).
Iceland	PAH	-30%	Reported sector data with correction of PAH (sum of compounds).
Poland	PAH	22%	Reported sector data with additional gapfilling of PAH compounds for iron and steel and product use (2021: sum of reported but inconsistent sector data)
Portugal	PAH	59%	Reported sector data with additional gapfilling of PAH compounds for industry production and shipping (2021: sum of reported but inconsistent sector data)
Slovakia	PAH	32%	Reported data with additional gapfilling of PAH compounds for industry production and product use (2021: sum of reported but inconsistent sector data)

[7] 'New reported' means, that 2019 data has been gap-filled and 2020 data has been reported.

Chapter 2. MEASUREMENTS OF HEAVY METALS AND POPs

2.1. Monitoring of POPs and heavy metals in 2020

Heavy metals and persistent organic pollutants (POPs) were included in the EMEP's monitoring program in 1999. However, earlier data have been reported and are available. The EMEP database, especially for heavy metals, thus also includes older data, even back to 1976 for a few sites. A number of countries have been reporting heavy metals and POPs within the EMEP area in connection with different national and international programmes such as HELCOM, AMAP and OSPAR.

The EMEP monitoring strategy [*UNECE,* 2019] defines the monitoring obligations for the Parties. For POPs, polycyclic aromatic hydrocarbons (PAHs), polychlorinated biphenyls (PCBs), hexachlorobenzene (HCB), chlordanes (CHLs), lindane/γ-hexachlorohexane (γ-HCH), α-HCH, and DDT/DDE are part of the compulsory monitoring programme, while for heavy metals, Hg, Cd and Pb are 1st priority elements while Cu, Zn, As, Cr, Ni are 2nd priority. In addition to these compounds several Parties report other POPs and trace elements. In addition to the regulated POPs, it is recommended to increase the attention on organic contaminants of emerging concern (CECs). A specific chapter is devoted to this topic.

All the data are available from the EBAS database (http://ebas.nilu.no/), and more detailed information about the sites and the measurement methods, these are found in the EMEP/CCC's data report on heavy metals and POPs [*Aas et al*., 2022].

Monitoring of heavy metals in 2020

In 2020, there were 40 sites measuring heavy metals in both aerosols and precipitation, and altogether there were 67 measurement sites (Fig. 2.1). 27 sites were measuring mercury in either air and precipitation, 17 of these with co-current measurements in air and precipitation. In total, 21 Parties to the Convention reports heavy metal data to EMEP.

Annual averages As, Cd, Cr, Cu, Ni, Pb and Zn concentrations in aerosols/air and precipitation in 2020 are presented in Figure 2.2., 2.3. There are more sites with precipitation in Northern Europe compared to aerosols, while the opposite for southern Europe. The sites in the United Kingdom have miss several months of precipitation measurements and are not included in the maps.

The highest concentrations vary depending on component and matrix, though elevated concentrations are especially for the aerosol components seen along the coast and especially around the English Channel. Cr has in addition to anthropogenic sources high concentrations in crustal material and that can be the reason for higher concentration of Cr in southern Europe. The concentration fields in precipitation are more scattered, but with higher levels generally seen towards Eastern Europe. For mercury, the highest concentration is seen in Poland while Spain showing extremely low concentrations of mercury in air (0.4 ng/m^3) indicating problems with the measurements.

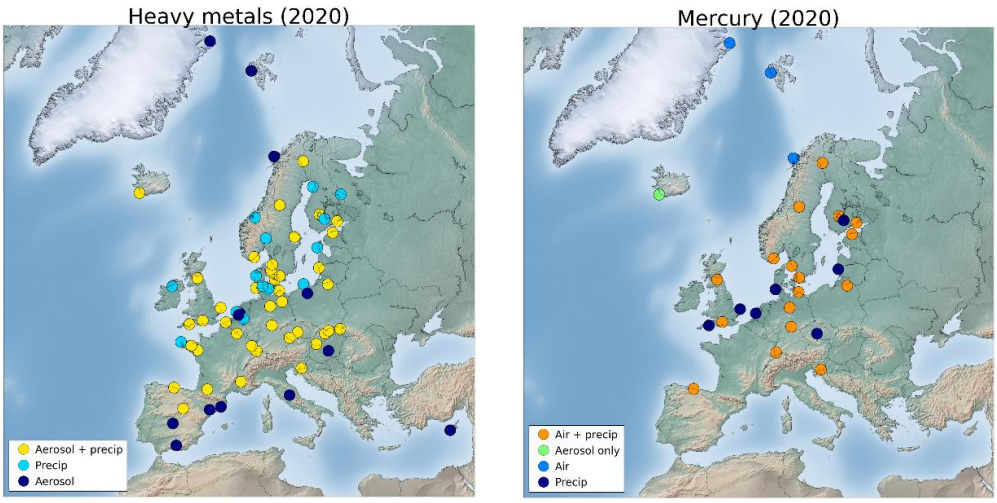

Fig. 2.1. *Sites reporting heavy metal and mercury data to EMEP.*

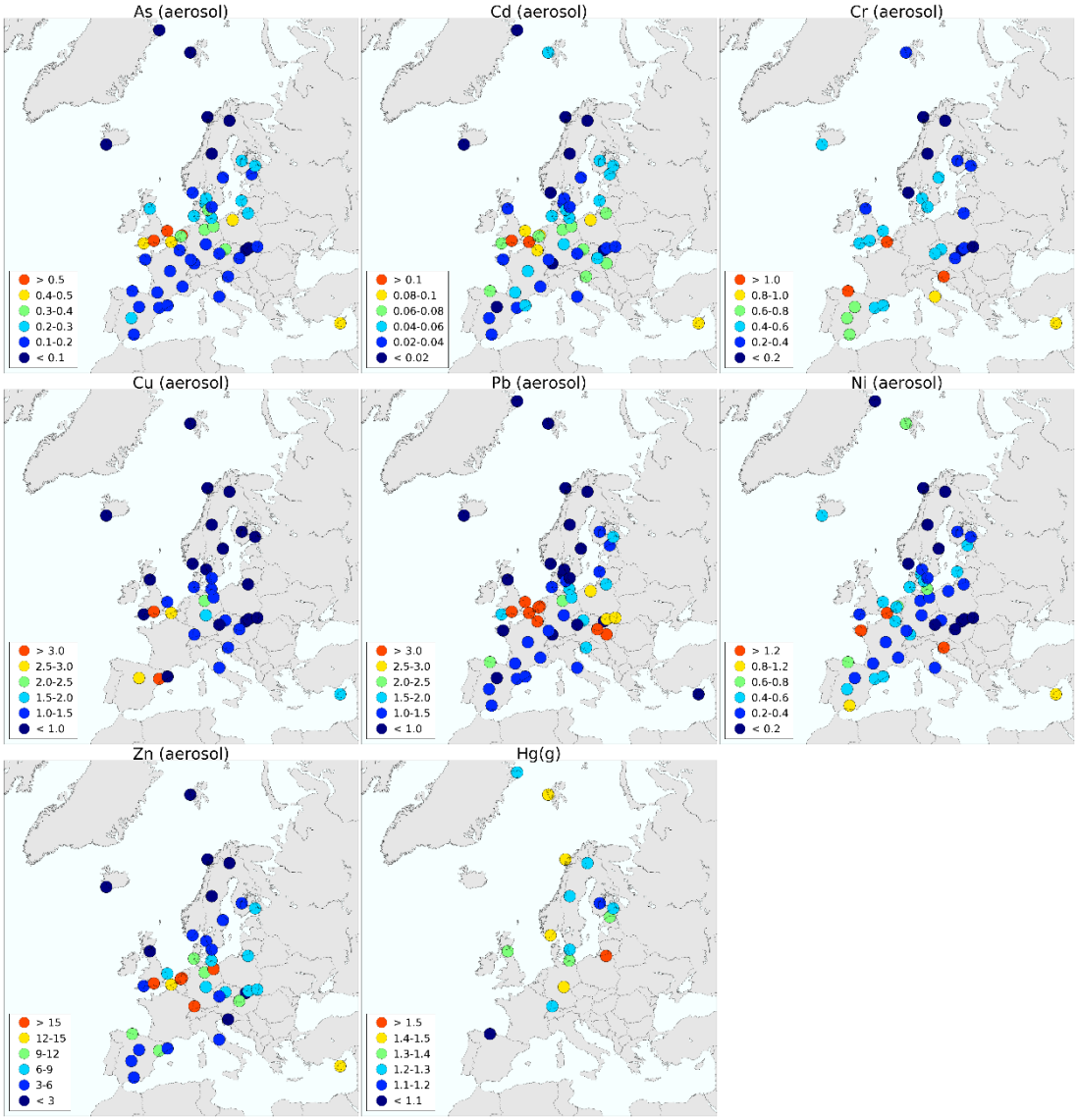

Fig. 2.2. *Annual mean concentrations of As, Cd, Cr, Cu, Ni, Pb and Zn in aerosols and Hg in air in 2020, unit ng/m³.*

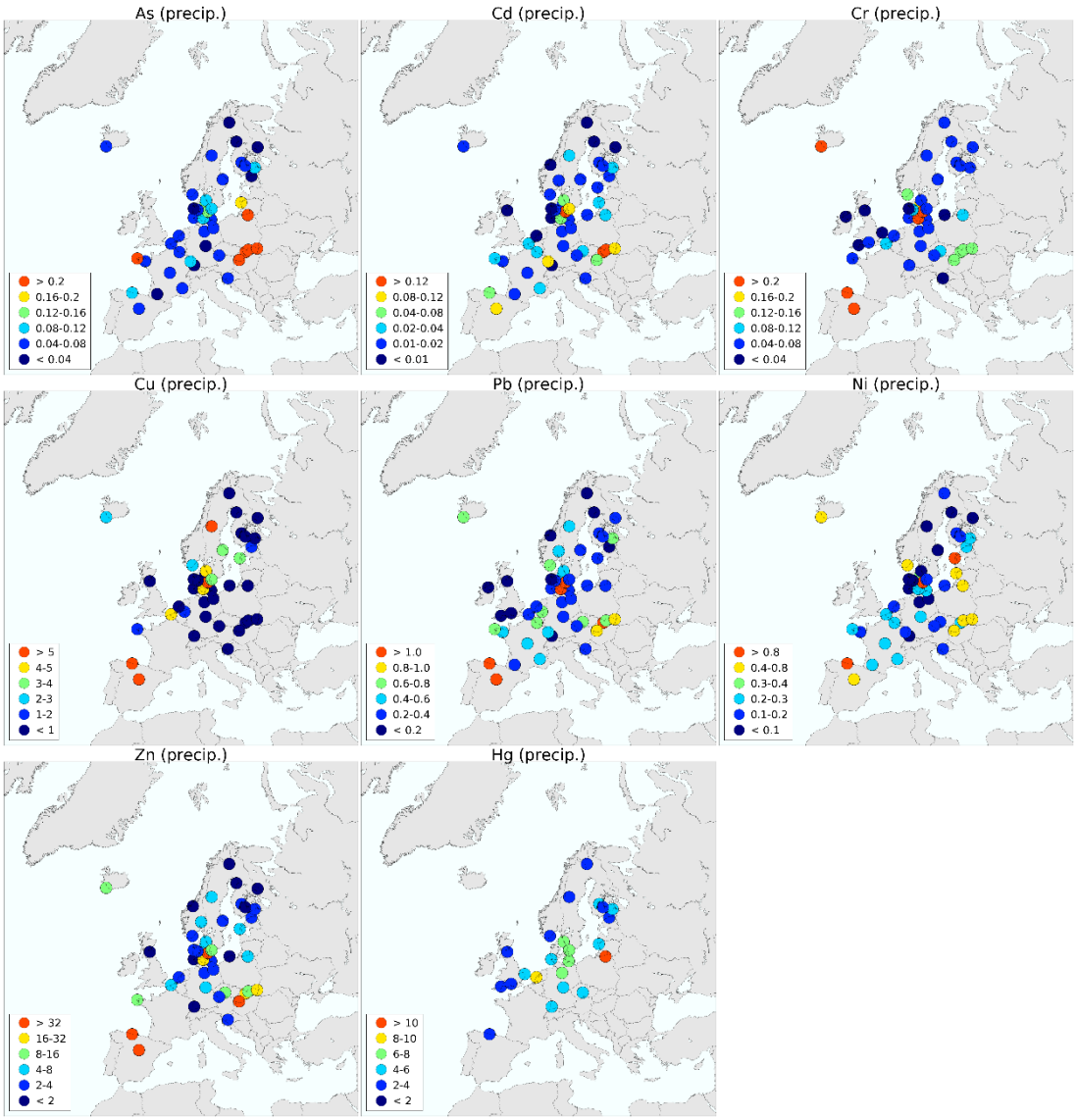

Fig. 2.3. *Annual mean concentrations of As, Cd, Cr, Cu, Ni, Pb, Zn (□g/L) and Hg (ng/L) in precipitation in 2020*.

Monitoring of POPs in 2020

The spatial coverage of POP monitoring in Europe is depending on which components in question. Concentration maps of selected POPs are shown in Figure 2.4. In total there are 39 sites reporting 2020 data on POPs whereof 25 sites with measurements in both air and precipitation. Data are available from 17 Parties. One should further notice that several of the Parties only measure PAHs (i.e. 9 Parties and 26 sites). For precipitation measurements, it is a challenge to compare the observations since the measurements are done using several different methods. There are four different matrixes defined for precipitation, i.e. total deposition (precip+dry_dep: 7 sites + 5 Spanish sites with campaign data), concentration in precipitation (precip: 12 sites); concentration in precipitation + POPs deposited in the funnel (precip_tot: 5 sites) and wet deposition (wet dep: 2 sites).

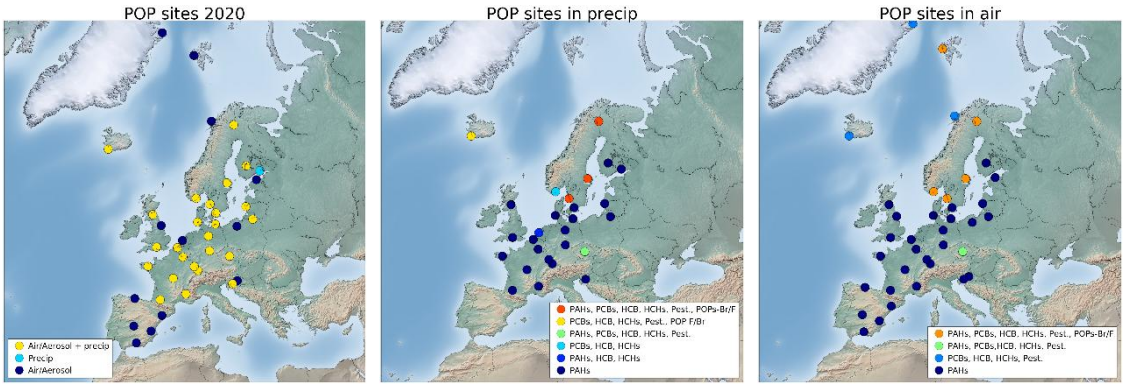

***Fig. 2.4. Sites** reporting POPs and the different data for 2020 reported to EMEP.*

HCB trends

Hexachlorobenzene (HCB) has been monitored in air under the EMEP program since 1993. Despite being among the first POPs that were initially regulated, HCB has recently received attention because of tendencies towards very slow or even increasing concentrations in air at several EMEP sites [*Hung et al*., 2010; *Hung et al.*, 2016; *Tørseth et al.*, 2012; *Wong et al.*, 2021]. The reason(s) for this remain poorly understood. In this year's report, we therefore present an update on the long-term and seasonal temporal and spatial trends of HCB and discuss the potential factors which may have dictated the observations.

Sources, fate properties and known sampling artefacts

HCB has miscellaneous primary emissions sources to the environment. It has been produced and used as a pesticide and for chemical manufacturing, and it is also emitted from various combustion sources and from biomass burning [*Bailey*, 2001; *Barber et al*., 2005]. Emissions from agriculture is likely to have been a major source historically, but the use as fungicide declined significantly in Europe since the 1970s and up to the mid-1990s [*Pacyna et al.,* 2001]. It has furthermore been suggested that HCB may be emitted in significant amounts into air by volatilization from secondary sources as contaminated in the past, such as soils [*Bailey,* 2001; *Barber et al.*, 2005]. The process of re-volatilization from contaminated surface reservoirs will be affected by temperature. It has been suggested that the significance of secondary emissions, relative to primary emissions in controlling atmospheric burdens, might have increased as result of climate change and reduced ice coverage in the Arctic [*Hung et al*., 2010].

Compared to many other POPs, HCB also has a considerable atmospheric lifetime in the atmosphere. Brubaker and Hites measured the rate constant in air for reaction with OH radicals and estimated the atmospheric lifetime to be ~930 days (about 2 and a half years) using a global average OH concentration [*Brubaker and Hites*, 1998]. This, in combination with a high volatility compared to many other POPs, leads to a significant potential for long-range atmospheric transport. The fate properties of HCB combined are anticipated to result in a limited spatial variability in background air. One would therefore expect relatively homogenous concentrations to be observed when comparing the spatial variability across EMEP background sites, for example in comparison to PAHs (Fig. 2.5).

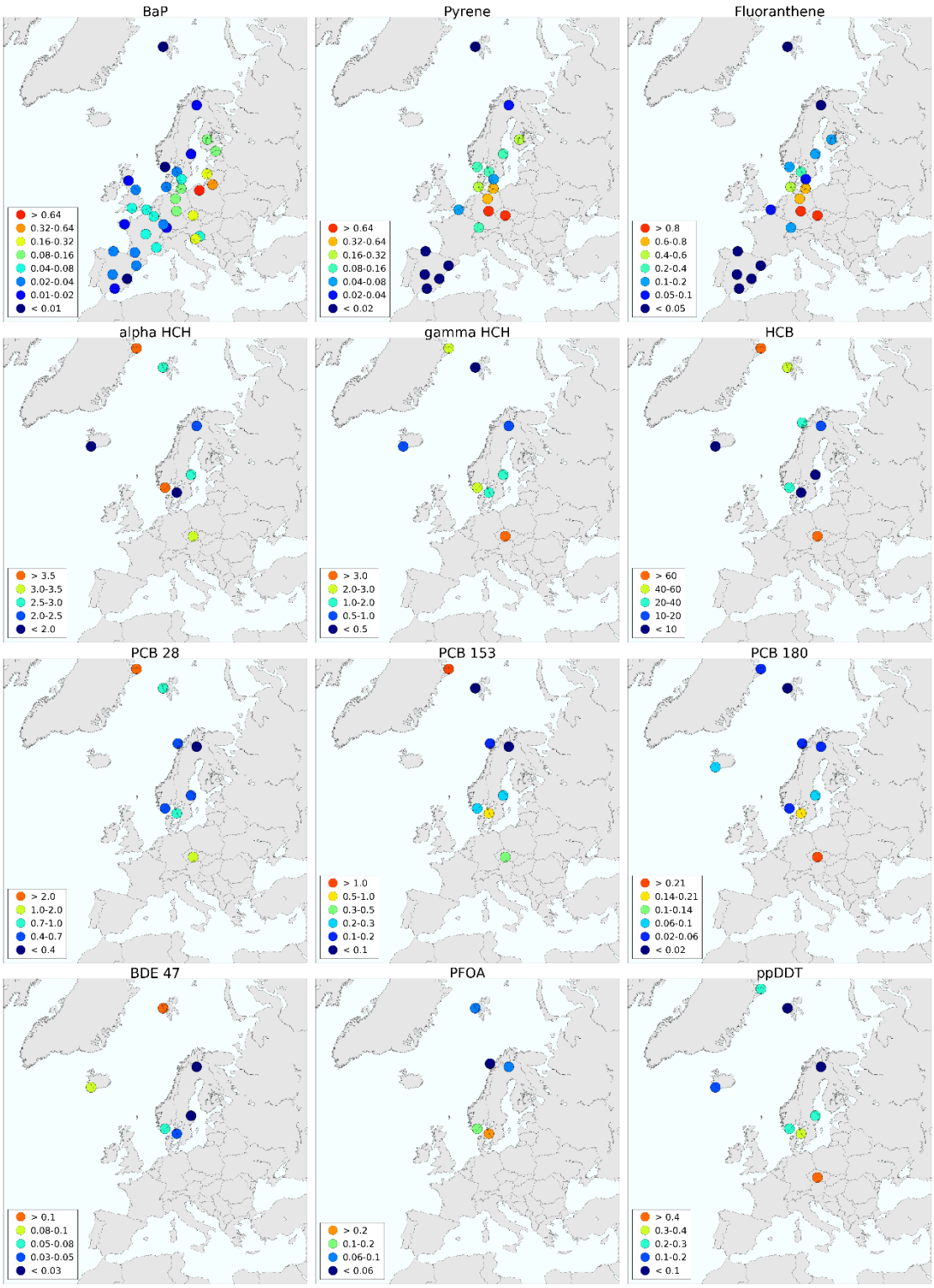

Fig. 2.5. *Annual mean concentrations of various PAHs (benzo[a]pyrene, Pyrene, Fluoranthene), (ng/m³), HCHs HCB, PCBs (28,153,180), BDE-47, PFOA and pp-DDT in air and aerosols (pg/m³), in 2020.*

However, a direct comparison between measurements obtained from various EMEP sites is difficult because of differences in sampling strategies. For example, it is well established that HCB may be subject to breakthrough using polyurethane (PUF) as sorbent [e.g. *Melymuk et al.*, 2014]. Breakthrough is of particular concern when temperatures and/or sampling volumes are high,

inevitably resulting concentrations being lower than they really are. The causes and implications for interpretation of HCB measurements from the EMEP program was earlier discussed in EMEP Status Report 3/2017 [*Gusev et al.*, 2017]. We note that a recent comprehensive review of long-term trends of concentrations of POPs (including HCB) and other organic contaminants in Arctic air, suggests that measurements based on PUF alone may be considered as semi-quantitative and biased low [*Wong et al.*, 2021].

It is thus conceivable that spatial and temporally variability in emissions, along with differences in sampling and analytical methodologies may lead to spatial and temporally variability in measured concentrations, whereas the long atmospheric lifetime of HCB may lead to limited spatial variability in observed concentrations. Additionally, seasonal and long-term variabilities in atmospheric transport patterns may have a profound influence on the observed trends.

Spatial and seasonal variability

While the spatial variability in average concentrations of HCB in air is shown in Figure 2.5, 2.6, shows the seasonal variability of HCB concentrations at EMEP sites in 2020. Three sites stand out as having consistently higher concentrations than the other sites throughout the year (Fig. 2.6). These are Kosetice (CZ03 in blue), the Villum research station at Station Nord on Greenland (DK10 in orange) and Zeppelin (NO42 in green). These stations thereby also have the highest annual mean concentrations in air with 66, 66 and 55 pg/m^3, respectively (Fig. 2.5).

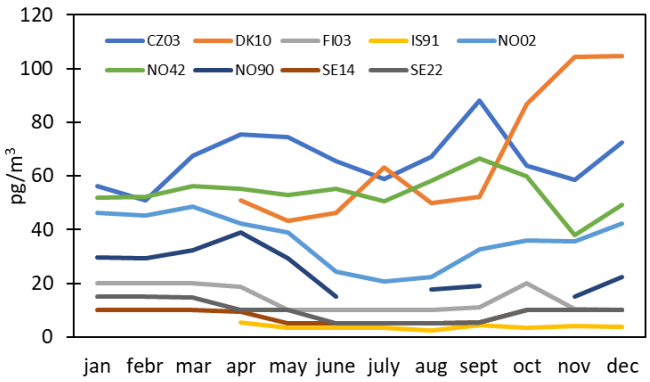

Fig. 2.6. *Monthly mean concentrations of HCB at EMEP sites in 2020.*

High concentrations in air at Kosetice is expected, given its location in central parts of Europe and proximity to potential source regions. On the other hand, Station Nord and Zeppelin are stations located in the high Arctic (north Greenland and Spitzbergen, respectively), and thereby distant to possible source regions in Europe. In the case of Station Nord, the potential for underestimated concentration in air is of lesser concern because samples are collected on a PUF-XAD-PUF sandwich kept at constant temperature [*Bossi et al.*, 2016; *Wong et al.*, 2021], rather than using PUF alone. Against this background, it is likely that the concentrations measured at Station Nord offer the more realistic representation of background concentrations of HCB in Arctic air, compared to the data from Zeppelin, Spitzbergen. The data from Zeppelin are discussed further below. Concentrations of HCB in air at Birkenes (NO0002R) are consistently lower than the three sites earlier mentioned and

throughout the year, albeit higher than the remaining sites. Concentrations of HCB in air also show a clear seasonal variability with concentrations being about twice as high during winter as during summer. In this case, breakthrough may represent one explanation for the seasonal variability. However, seasonal variability in transport and/or primary/secondary emissions may also have impacted seasonal time trends. A similar reasoning applies for the monitoring data from Andøya (NO09). Yet, little is known about the seasonal variability of primary emissions. However, the impact of secondary emissions is prone to vary seasonally with higher emissions during summer. It is thus notable that the monthly data from Station Nord indicate that concentrations are the highest in early winter, rather than the summer. The Arctic haze period is typically late winter and early spring. Regrettably, data from this period are lacking in the data from Station Nord 2022.

Long-term time trends of HCB concentrations in air

A main motivation to look closer into HCB in this report is the divergent long-term time trends in air. Figure 2.7 shows the long-term temporal trends at EMEP sites for which long-term monitoring data are available. These are evaluated using the Digital Filtration Technique (DF), which is a statistical approach which highlights seasonal cycles and inter-annual trends in observations (Hung et al., 2005). The concentrations are presented in natural log of concentrations (ln C) on the y-axis, and the results are indicated with arrows in Fig.2.7. Apparent first order half-lives ($t_{1/2}$, years) for HCB at the six EMEP sites with long-term monitoring in air are given in for six EMEP sites with long-term trends and for the entire monitoring periods, whereas apparent first order half-lives at Birkenes and Zeppelin are further broken down into three different time periods in Table 2.1.

When it comes to the estimated first order half-lives across the entire monitoring time periods in Table 2.1, there is a downwards trend for most sites except for Kosetice with an extremely low increase (CZ03), and a very slow decline for Zeppelin (NO42). However, none of these trends are statistically significant and thus difficult to determine. Lack of statistical significance is not an issue for the other four sites with half-lives ranging from ~10 years for the German stations (Zingst and Westerland), 21 years for Station Nord, and 39 years for Birkenes.

Table 2.1. *Apparent first order half-lives (t1/2, years) for HCB at the six EMEP sites with long-term monitoring in air.*

Station code	Station name	$t_{1/2}$	r^2
CZ03	Kosetice	-342	0.001*
DE09	Zingst	9.5	0.55
DE01	Westerland	9.8	0.75
NO02	Birkenes	39	0.45
DK10	Station Nord	21	0.24
NO42	Zeppelin	157	0.04*

*No significant trend can be determined.

As can be readily observed in Fig 2.7, there are sites for which the long-term trends for certain periods have both increased and decreased during the entire monitoring periods. This is further shown based on data from Birkenes (NO02) and Zeppelin (NO42) in Table 2.2.

Table 2.2. *Apparent first order half-lives (t1/2, years) for HCB at Birkenes and Zeppelin covering four time periods.*

Station code	Station name	Start-2020		Start-04		04-20		2016-2020	
		$t_{1/2}$	r^2	$t_{1/2}$	r^2	$t_{1/2}$	r^2	$t_{1/2}$	r^2
NO02	Birkenes	39	0.45	13	0.36	25	0.63	7.4	0.99
NO42	Zeppelin	157	0.04*	10	0.87	516	0.003*	6.3	0.98

As a general observation we see from Fig. 2.7 that there are sites which often show a seasonal variability with summer maximum and a winter minimum. This applies to Station Nord (DK10) and Zeppelin (NO42). There are also stations which alternate between a summer minimum and winter maximum and the other way around. A prime example is Kosetice (CZ03). And then there are sites which tend to show a minimum concentration during summer and a maximum during winter (Zingst, DE09; Westerland, DE01 and Birkenes, NO02). As there are several reasons why differences in seasonal patterns are observed across sites as noted in the introduction to this chapter, it is premature to offer any unequivocal mechanistic explanations for the various seasonal trends depicted in Fig. 2.7. However, a transport-based analysis was recently carried out for the time-period with the highest concentrations in recent years [*Platt et al.*, 2022].

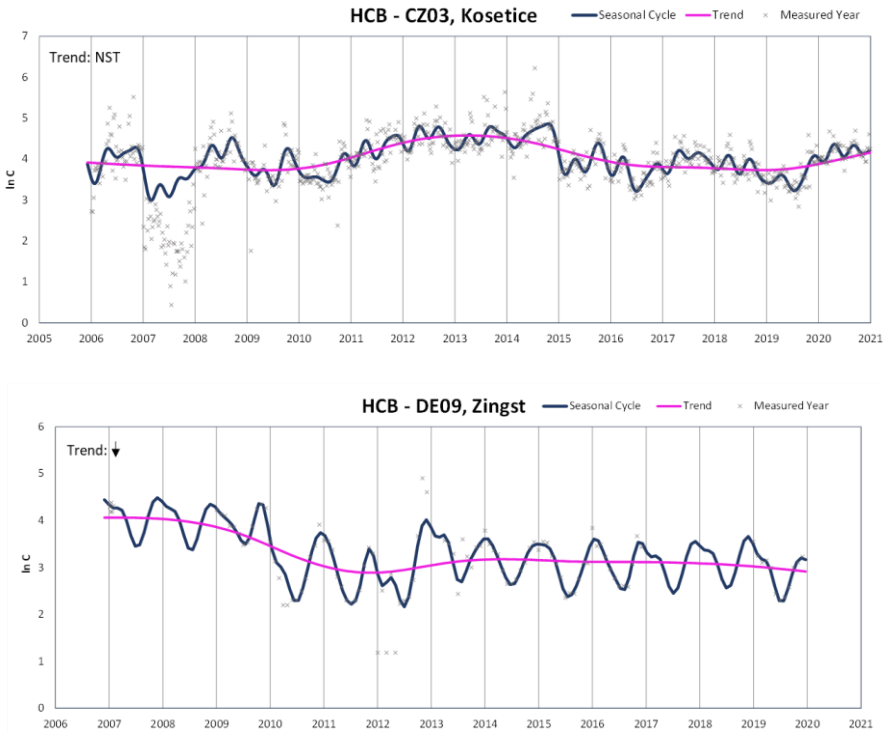

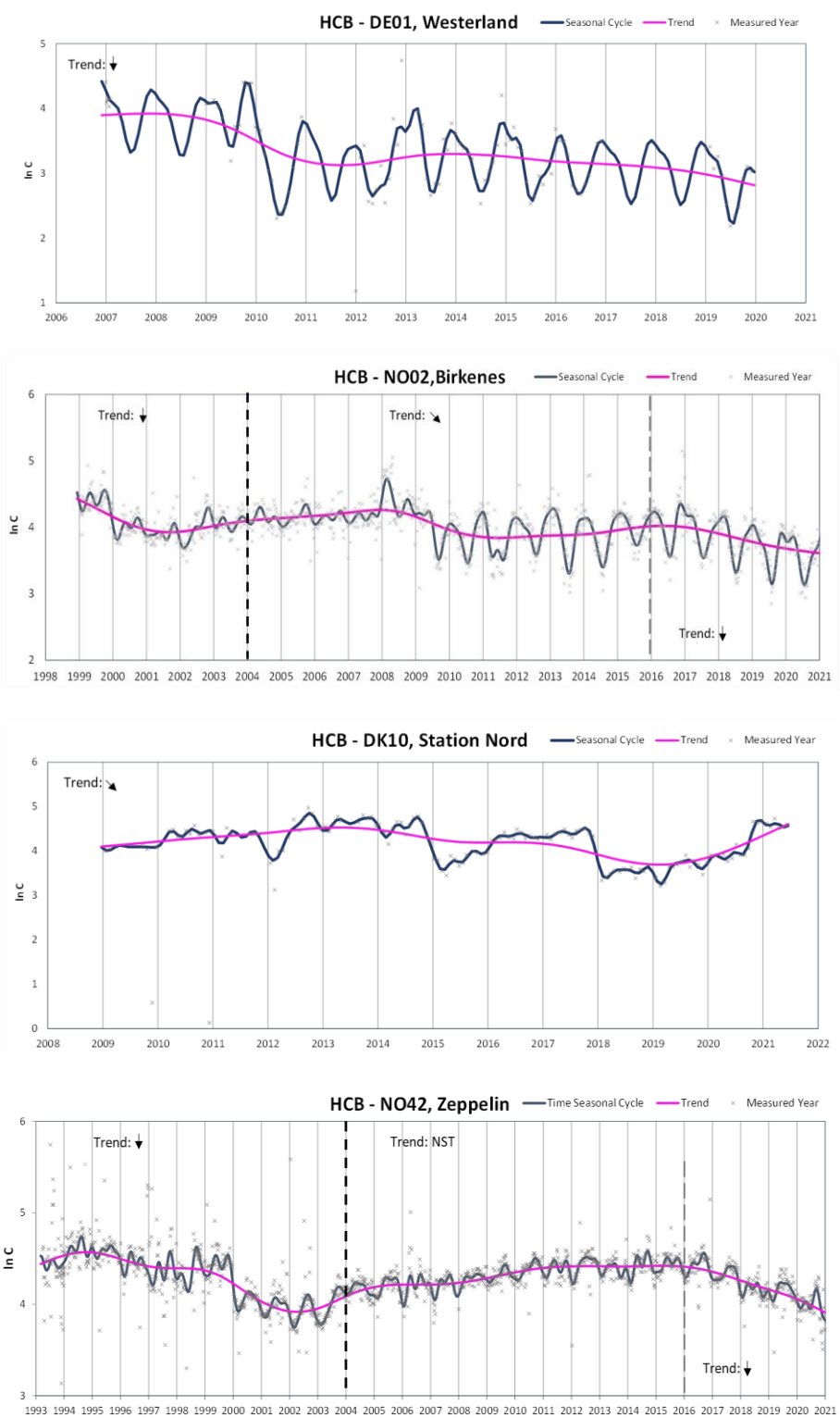

Fig. 2.7. *Temporal trends of HCB in air at six EMEP sites. The concentrations are presented in natural log of concentrations (ln C) on the y-axis. The results of trend analyses are indicated with arrows.*

Zeppelin is the site for which HCB has been monitored for the longest time-period [*Tørseth et al.* 2012]. The temporal trend from this site shows a particularly interesting trend whereby the lowest concentrations were measured around 2002, and in recent years. At Zeppelin, the concentrations

increased from 2002 and declined from 2016 onwards. This pattern would not be anticipated if primary emissions of HCB were steadily declining over the time-period considered and reflected in the measurements. Nor would one expect such a pattern in inter-annual trends under a scenario for which secondary emissions are steadily increasing as result of warmer temperatures and/or reduced ice coverage and dominating the overall time trend for almost 30 years. Additional hypotheses put forward earlier to explain the lack of decreasing trends are that HCB is a combustion by-product and used in the manufacturing of chlorinated solvents and other chemicals. None of these factors alone are likely to explain the observed pattern at Zeppelin over the last two decades, nor where the main source regions are located. Against this background, Platt et al. used the FLEXPART model to investigate seasonal variability in transport patterns to estimate so-called footprint emission sensitivities during periods with high and low concentrations of HCB in air at Zeppelin during the Arctic haze period from 2014 to 2017 [*Platt et al.*, 2022]. This transport analysis also investigated when HCB was significantly elevated compared to other years. The modelling results highlighted that Arctic haze periods are typically associated with transport of air masses from Asia, whereas atmospheric transport from large ice-free ocean areas is associated with low concentrations. The latter contradicts the hypothesis of enhanced secondary emissions of HCB from seawater having a significant impact on atmospheric burdens at Zeppelin for the years investigated. Further research will be required to better understand why concentrations at Zeppelin have been declining over the last few years.

2.2. Supplementary measurements

EMEP monitoring data are involved in the assessment of heavy metal and POP pollution levels as well as evaluation of the modelling results. These data characterize pollution levels typical for rural or remote locations that are not affected by major emission sources. However, these measurements are mainly carried out in the northern, central, southern and western parts of Europe, whereas the eastern and south-eastern parts of the EMEP region remain uncovered with the EMEP measurement network. In order to extend the abilities of the pollution level assessment, EMEP monitoring data were complemented with measurements of air concentrations from European Environmental Agency (EEA) data base AQ e-reporting (https://www.eea.europa.eu/data-and-maps/data/aqereporting-9). This database contains measurement information on large spectrum of atmospheric pollutants, including heavy metals and POPs, observed at the national monitoring stations of the EU countries.

The EU national monitoring networks are represented by stations of different types. From viewpoint of the predominant sources industrial, traffic and background stations are distinguished. Background type of station indicates that it is not possible to identify a predominant type of emission source. In order to characterize location of the station, rural, urban and sub-urban types are considered. Therefore, the EEA measurements are also useful for evaluation of heavy metal and POP levels in more polluted and densely populated regions compared to the EMEP monitoring data.

Monitoring data on PAHs from this EEA data base were used for the analysis of pollution in the EMEP region. In particular, amount of population exposed by PAH concentrations exceeding various

threshold limits was estimated (See section 3.5.2). Fig. 2.8 demonstrates example of B(a)P annual mean concentrations in air in 2020. The data on B(a)P concentrations is available from more than 800 stations. The highest levels are noted for Poland, where B(a)P annual mean concentrations exceed 0.6 ng/m^3 at most of the stations. Other regions of relatively high B(a)P levels are the northern part of Italy, Hungary, Bulgaria, Croatia and Slovenia. Relatively low levels are noted for Denmark, the Netherlands, Belgium, Switzerland, and a number of regions of Spain, France, Italy, Finland and Norway.

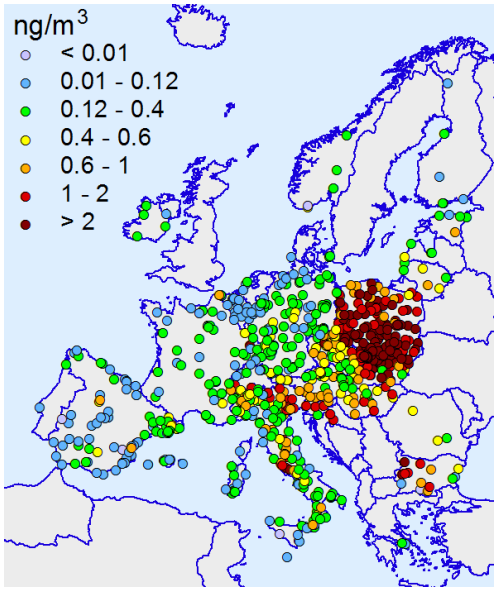

Fig. 2.8. *Concentrations of B(a)P in air observed in 2020 in the EMEP region from EEA AQ e-reporting database.*

Chapter 3. STATUS OF HEAVY METAL AND POP POLLUTION IN 2020

3.1. Meteorological conditions of 2020

Meteorological conditions is one of the key factors governing atmospheric transport and deposition of heavy metals and POPs in the EMEP region. Dispersion of the pollutants is affected by wind patterns and atmospheric stability. Deposition fluxes depend on atmospheric precipitation and processes in the surface boundary layer. Chemical reactions in the atmosphere are influenced by air temperature and humidity. Re-suspension of dust particles is determined by soil moisture and near-surface wind velocity.

Meteorological conditions of a particular year differ from those of the other years due to inter-annual variability and long-term climatic changes. Meteorological conditions of the considered year (2020) are compared with those of the previous year (2019) and with climatic norms. Comparison of meteorological conditions is important for interpretation of changes between pollution levels simulated for these years.

Anomalies of air temperature and annual precipitation sums were considered for the comparison of meteorological conditions of the current year with climatic norms. An anomaly is a difference between the value in the current year and the climatic norm. Positive value of the anomaly means that temperature or precipitation sum in this year is higher than the climatic norm, and vice versa. Climatic norm is considered as the average for the period from 1981 to 2010 [*Blunden and Boyer*, 2021].

The year 2020 was one of the warmest since the beginning of meteorological records [*Blunden and Boyer*, 2021]. The global mean surface air temperature was 0.6°C higher than the climatic mean calculated for 1981-2010 period. In Europe this year was the warmest for the period since 1900 with anomaly +1.9°C [*Blunden and Boyer*, 2021]. In 2020 anomalies of annual mean air temperature exceeding 1°C occurred almost over whole Europe except for Iceland, Ireland and the northern part of the United Kingdom (Fig. 3.1a). The highest positive anomaly exceeding 5°C took place over the northern part of Russian Siberia. Small negative anomaly (0 - -1°C) was observed over Ireland and the north-eastern part of the Atlantic. In the eastern part of the EMEP domain positive anomalies were observed over Russia and the northern part of Kazakhstan, while over other countries of Central Asia negative anomalies reaching -2.5°C predominated. The temperature anomalies demonstrate distinct seasonal variability [*Blunden and Boyer*, 2021]. Winter (December 2019 – February 2020) was characterized by high positive anomalies (1 – 5° C) taken place over entire Europe and Central Asia. In spring relatively low (0 - 2°C) anomalies were observed in Europe, while in the eastern part of the EMEP domain high positive anomalies (2 - 6°C) remained. In summer positive anomalies did not exceed 2°C over most part of the EMEP region. In autumn most of countries of Europe experienced positive anomalies ranging from 1°C to 5°C, while negative anomalies reaching -3°C took place in Central Asia.

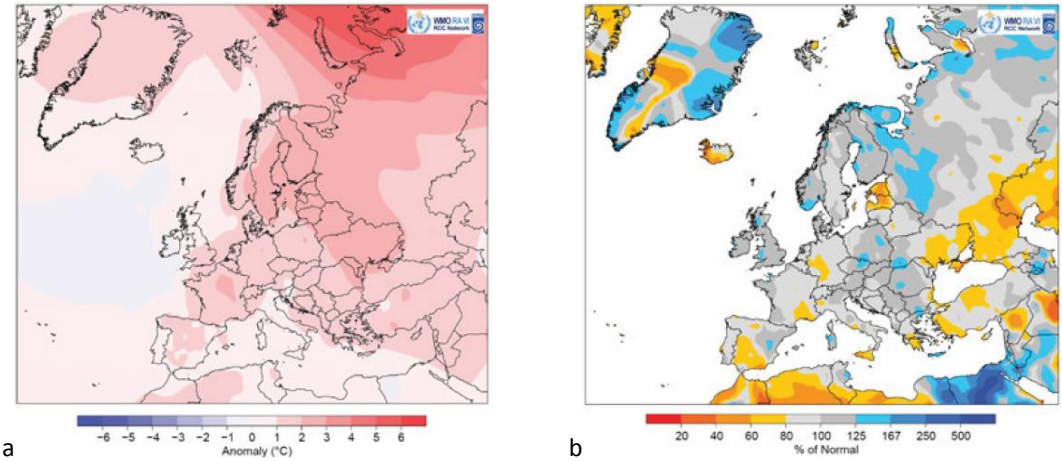

Fig. 3.1. *Anomaly of mean annual air temperature (a) and annual precipitation sum (b) in 2020 [Blunden and Boyer, 2021].*

Over the most part of Europe annual sums of precipitation in 2020 lied in the limits from 80% to 125% of the climatic norm (Fig. 3.1b). The deficit of precipitation is noted for the Black Sea region, southern Spain, Estonia, Latvia, some areas in the Mediterranean countries, and Iceland. Besides, precipitation sums below the norm by 20 – 40% were observed in Central Asia. Excess of the precipitation took place in a number of areas of the eastern part of Europe, in the United Kingdom and Scandinavia.

Winter of 2020 was substantially drier compared to climatic mean in most part of Southern Europe, North Africa, the Caspian Sea region, Estonia, and Latvia. In Scandinavia, Poland, north of Germany and France, over the British Isles, and north of Russia it was 25 – 150% wetter than normal. In spring Central Europe, the British Isles, most part of Scandinavia, and the Black Sea region experienced 20%-60% deficit of precipitation, while excess of the precipitation occurred over the Iberian Peninsula, most part of Russia, the Balkan Peninsula and the northern part of Scandinavia. In summer strong deficit of precipitation, reaching 20% of the climatic norm, was observed in the south of the Iberian Peninsula and the southern part of Turkey. Precipitation sum in autumn was characterized by the deficit in the central, western and southern parts of Europe, in southern Russia, Turkey and the Baltic Sea region.

Precipitation sums higher than the norm were observed in Scandinavia and Poland. Precipitation in Central Asia was substantially higher than the norm in winter and spring. In summer precipitation in this region was moderately lower than the norm, and in autumn the significant excess took place.

Zonal circulation in the EMEP region in winter and beginning of spring of 2020 was significantly higher than the climatic norm [*HMCR*, 2021]. In the rest of the year the zonal component was close to the norm. Meridional component of the circulation did not differ much from the norm.

Annual precipitation sums in 2020 (Fig. 3.2a) were compared with those of 2019. Relative difference between these two fields is shown in Fig. 3.2b. Compared to 2019, the increase (15% – 50%) of precipitation took place in the western and south-western parts of Europe (western France, north-west of the United Kingdom and Ireland, western coast of Scandinavia, most of Iberian Peninsula),

the northern part of the Baltic Sea, large areas in the eastern and south-eastern parts of Europe, the eastern part of Russia (within the EMEP region) and the northern part of Kazakhstan. Decrease (15% – 50%) of the precipitation occurred in the southern parts of Scandinavia and the Baltic Sea, the central part of Europe (Germany), most of southern Europe and the Mediterranean Sea, some parts of eastern Europe, most part of European Russia, and in Central Asia.

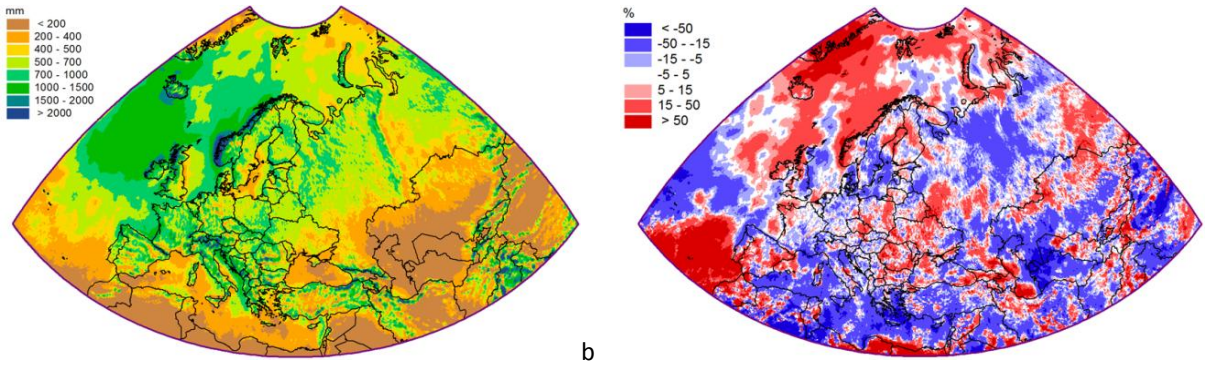

a b

Fig. 3.2. *Annual precipitation sums in 2020 (a) and relative difference between precipitation in 2020 and 2019 (b). Positive values mean increase and negative – decrease of precipitation in 2020 relative to 2019.*

Concentrations in air of a number of pollutants, e.g., PAHs, have distinct seasonal variability with the difference between winter maximum and summer minimum reaching an order or magnitude. Smaller, but still substantial seasonal changes in air concentrations of heavy metals also take place. Therefore, for the analysis of changes of pollution levels between 2019 and 2020 the changes of air temperature in warm (April-September) and cold (January-March and October-December) seasons are considered separately. Compared to 2019, warm season air temperature in 2020 demonstrated relatively low change from -1°C to 1°C over major part of the EMEP domain (Fig. 3.3a). Strong increase (> 1.5°C) of air temperature is noted for the north-eastern part of Russia (within the EMEP domain). In Turkmenistan, Uzbekistan and the southern part of Kazakhstan the decrease of the temperatures about 1°C - 1.5°C took place. The pattern of difference of mean air temperatures in 2020 and 2019 in cold period is similar to that for temperatures in warm period. However, the contrast between areas of the increase and decrease of temperatures was higher (Fig. 3.3b).

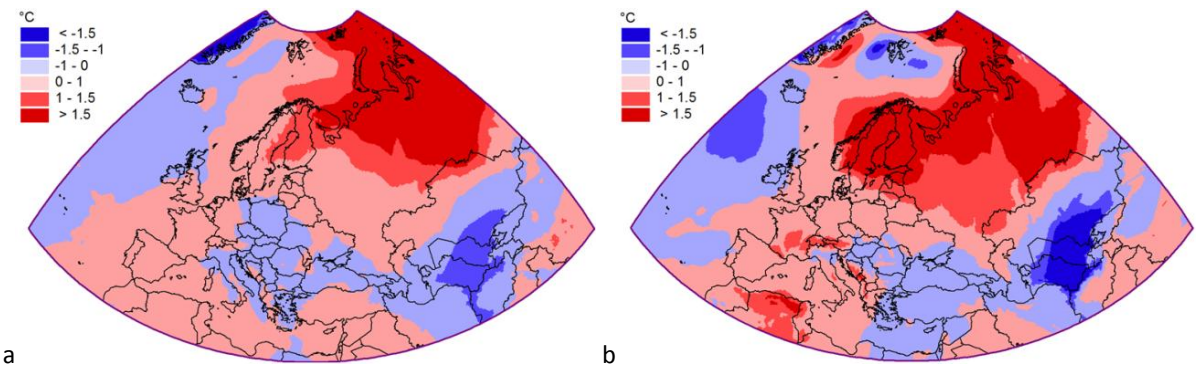

a b

Fig. 3.3. *Difference of warm (a) and cold (b) season mean air temperatures in the atmospheric boundary layer (~1 km) between 2019 and 2020.*

For the analysis of changes in atmospheric transport patterns between 2019 and 2020 source-receptor matrices for air concentrations of a passive tracer were calculated (i.e., without taking into account wet and dry removal and chemical reactions). Since scavenging and chemical transformations are not taken into account, the contributions of source countries to a receptor is governed entirely by atmospheric transport. Therefore, relative changes in contributions of the source countries to concentrations in the receptor countries characterize the changes in the atmospheric transport between the current and previous years.

The concentration matrices calculated for particular EMEP countries, were generalized to the matrices for the sub-regions of the EMEP domain (Fig. 3.8). Definition of the sub-regions is given in section 3.4.1. Analysis of contributions of sub-regions to passive tracer concentrations in 2019 and 2020 allows deriving general features of changes in the atmospheric transport patterns in the EMEP domain as a whole (Fig. 3.4). Positive value of the change means the increase of atmospheric transport from a source to receptor sub-regions, and vice versa. As follows from the Figure, the relative changes of atmospheric transport to more remote sub-regions are typically higher than the changes in the transport to neighbouring areas. For example, the highest change (about 40-50%) is noted for atmospheric transport from Caucasus and Central Asia sub-region to Western, Central and Northern Europe. It should be noted that in absolute terms atmospheric transport from Caucasus and Central Asia to these sub-regions is small. Hence, even low absolute changes lead to high relative changes. The changes in atmospheric transport between neighbouring sub-regions mostly do not exceed 20%. Atmospheric transport from Eastern and Northern Europe decreased to all other sub-regions.

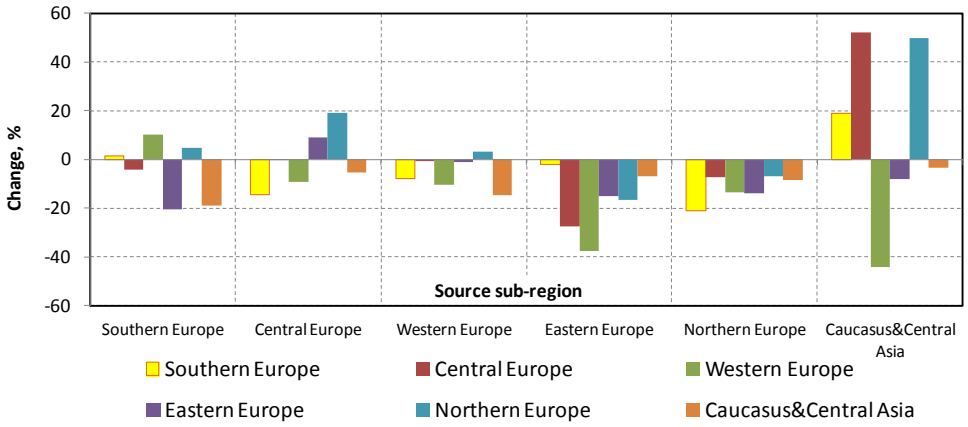

Fig. 3.4. *Relative change of atmospheric transport from the source to receptor sub-regions between 2019 and 2020. Positive value indicates the increase of atmospheric transport from source to receptor sub-regions, and vice versa.*

This approach can be applied to the analysis of changes in atmospheric transport patterns in particular countries of the EMEP domain. For instance, transport to Germany from France, Switzerland, and Spain increased, while the transport from Poland, Czechia and the countries of the Scandinavian Peninsula decreased (Fig. 3.5a). The exchange between the United Kingdom and other EMEP countries in 2020 slowed down compared to 2019. Atmospheric transport to Sweden, from Germany, France and Poland increased, while the transport from Russia, Finland and the United

Kingdom declined (Fig. 3.5b). Similar analysis can be applied to any country of the EMEP region and could be helpful for the interpretation of the pollution level changes between 2019 and 2020.

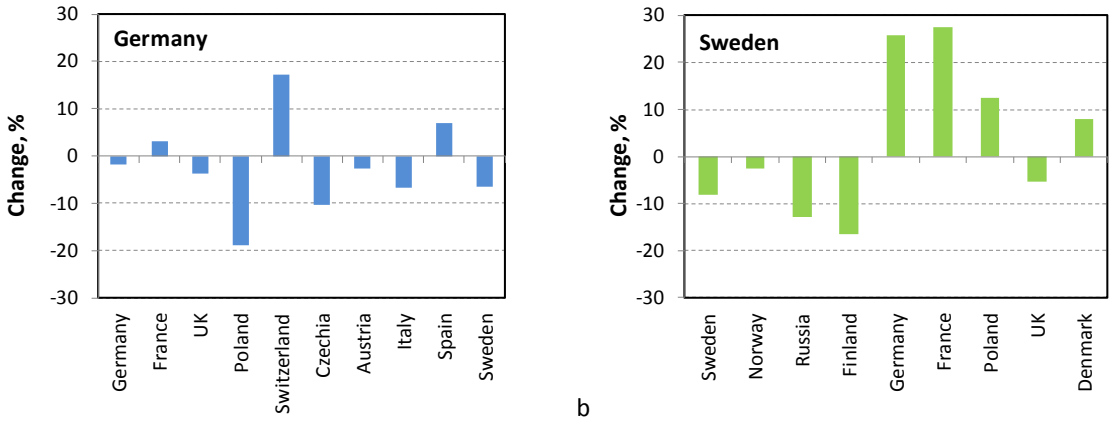

Fig. 3.5. *Relative change (%) of atmospheric transport to Germany (a) and Sweden (b) from main countries-contributors in 2020.*

3.2. Model setup

The operational model assessment of heavy metal and POP pollution in 2020 has been performed using the GLEMOS model, version v2.2.2. Description of the current stable version of the model is available at the MSC-E website (http://en.msceast.org/index.php/j-stuff/glemos). New research directions aimed at improvement of the model parameterizations, which will be included to the next versions of the model, are discussed in Chapter 4 of the report.

Modelling of pollution levels in the EMEP countries as well as estimates of the transboundary transport between them (source-receptor relationships) have been carried out on a regional scale within the EMEP domain (https://www.ceip.at/the-emep-grid). Anthropogenic emission data for modelling of all pollutants have been prepared based on the gridded emissions fields provided by CEIP (Section 1) and complemented with additional emission parameters required for model runs (Section 3.3). Natural and secondary Hg emissions from soil and seawater have been estimated depending on Hg concentration in soil and the environmental parameters [*Travnikov and Ilyin*, 2009]. Data on wind re-suspension of particle-bound heavy metals (Pb and Cd) from land and sea surface has been generated using the dust pre-processor [*Gusev et al*., 2006; 2007].

Meteorological information for the model simulations has been generated from the operational analysis data of the European Centre for Medium Range Weather Forecasts [*ECMWF*, 2022] using the meteorological pre-processor based on the Weather Research and Forecast modelling system (WRF) [*Skamarock et al.,* 2008]. Atmospheric concentrations of chemical reactants and particulate matter, which are required for description of Hg and POP chemistry, were derived from the GEOS-Chem model simulations (see below).

Boundary conditions for the regional scale simulations of all considered pollutants have been obtained from the GLEMOS model runs on a global scale (Section 3.8). Initial conditions for the evaluation of pollution levels of the long-living POPs (e.g. PCBs, HCB, and PCDD/Fs) in the EMEP region have been extracted from the long-term global model spin-up based on expert estimates of historical emissions.

Model updates

The new version (v2.2.2) of GLEMOS contains a number of updates including the new input data on land cover and concentration of chemical reactants (O_3, OH, Br, SO_2, $PM_{2.5}$, etc.) in the atmosphere as well as numerous technical updates. More recent and comprehensive land cover dataset was incorporated into the model based on the Moderate Resolution Imaging Spectroradiometer (MODIS) satellite product - The Terra and Aqua combined MODIS Land Cover Type (MCD12Q1, version 6) [*Friedl et al*., 2019]. This product provides global distribution of land cover types at yearly intervals with 500-m spatial resolution. Comparison of the previous and the new land cover datasets is given in [*Ilyin et al*., 2021]. The dataset of chemical reactants in the atmosphere from the MOZART (Model for Ozone and Related chemical Tracers, version 4) model in the previous version of GLEMOS was replaced by the 3D concentration data generated with GEOS-Chem (version 12.5.0). Detailed description and evaluation of the new dataset is available in [*Travnikov et al.*, 2020].

The effect of the model updates on the modelling results was evaluated in a number of sensitivity tests. The tests show that update of the land cover information leads to some increase (5-20%) of air concentrations of Pb, Cd, and B(a)P in Western and Northern Europe. In other parts of the domain no significant changes or slight concentration decrease are obtained. Deposition of these pollutants decreased by 5-20% in some areas of Central and Western Europe as well as in the eastern and southern parts of the domain, besides, B(a)P deposition increased in Northern Europe. The variation of land cover in the region does not affect significantly Hg^0 concentration in air but causes mosaic changes (±20%) of Hg deposition in various parts of the domain. The changes do not affect noticeably correlation and the relative bias between the modelling results with observations.

Update of the data on air concentration of chemical reactants and particular matter results in slight general increase (5%) of Hg^0 concentration over the region and similar decrease (5-10%) in Hg deposition. An exception is increased Hg deposition in some locations of the Arctic and over the southernmost part of the domain. The updates also caused increase (about 20%) of both air concentration and deposition of B(a)P over the most part of Europe with some deposition decrease in Central Asia and Turkey. The changes of air concentrations and deposition fluxes of PCDD/Fs, PCB-153 and HCB vary in different parts of the region but mostly do not exceed ±20%. The updated model results better agree with observations in terms of relative bias in comparison with previous ones keeping similar spatial correlation.

3.3. Emission for modelling

Regional emissions

Model assessment of heavy metal and POP pollution in the EMEP domain was made on the basis of gridded emission data with spatial resolution 0.1°x0.1° provided by CEIP (http://www.ceip.at). Pollution levels of heavy metals and POPs in 2020 were evaluated using emission data, reported for the previous year 2019. Detailed description of estimated heavy metal and POP emissions in the EMEP countries, gap-filling methods, and expert estimates used for preparation of the emission inventory, can be found in the CEIP Technical report 6/2021 [*Poupa*, 2021].

Model simulations for Pb, Cd, Hg and PAHs were based on the officially reported emission data. For PCBs, PCDD/Fs and HCB a combination of official emission data and expert estimates was applied for modelling. In particular, for the assessment of PCB pollution officially reported inventories were combined with available expert estimates of emissions. Currently reported PCB emissions provide only total amount of PCBs without specifying particular congener emissions. However, modelling of PCBs requires definition of emissions of particular PCB congeners. Therefore, to evaluate transport and fate of individual PCB congeners, the congener specific emission inventory by *K.Breivik et al*. [2007] was used for modelling. The indicator congener PCB-153 was selected to characterize transboundary transport and pollution by PCBs. Spatial distribution of PCB-153 emissions was constructed on the base of gridded PCB emissions officially provided by 32 EMEP countries (namely, Austria, Belgium, Bulgaria, Croatia, Cyprus, Czechia, Denmark, Estonia, Finland, France, Georgia, Germany, Greece, Hungary, Ireland, Italy, Latvia, Lithuania, Luxembourg, North Macedonia, Monaco, Netherlands, Norway, Poland, Portugal, Romania, Slovakia, Slovenia, Spain, Sweden, Switzerland and the United Kingdom). For other EMEP countries, which did not report gridded emission data, gridded population density was used for spatial allocation of emissions.

Estimates of PCDD/F emissions, officially reported by the EMEP countries, may incorporate considerable uncertainties due to incomplete coverage of all potential sources [*Breivik et al.*, 2004; *Fiedler*, 2007; *Pulles et al.*, 2005; 2006] that might lead to underestimation of releases to the atmosphere. For this reason, a scenario, representing maximum level of PCDD/F emissions, was used in the model simulations. The maximum emission scenario was prepared on the basis of the uncertainty range reported by 15 EMEP countries in their inventory information reports (namely, Austria, Belarus, Belgium, Croatia, Cyprus, Denmark, Estonia, Finland, France, Latvia, Poland, Republic of Moldova, Sweden, Switzerland, and the United Kingdom). Difference between the maximum and average estimates of PCDD/F emissions in these countries varied from a factor of 1.33 for Latvia up to a factor of 4.4 for Denmark. For other EMEP countries, which did not report uncertainty range in their inventories, the maximum level of national PCDD/F emissions was assumed to be 3-fold higher compared to the officially reported emissions in accordance with the expert estimates [*Pulles et al.*, 2006; *Bogdal et al.*, 2014]. Thus, total PCDD/F emission in the EMEP countries according to the maximum emission scenario exceeded reported data in the inventories by a factor of 2.9 on average. This approach has already been applied in the model assessment [*Gusev et al*., 2018].

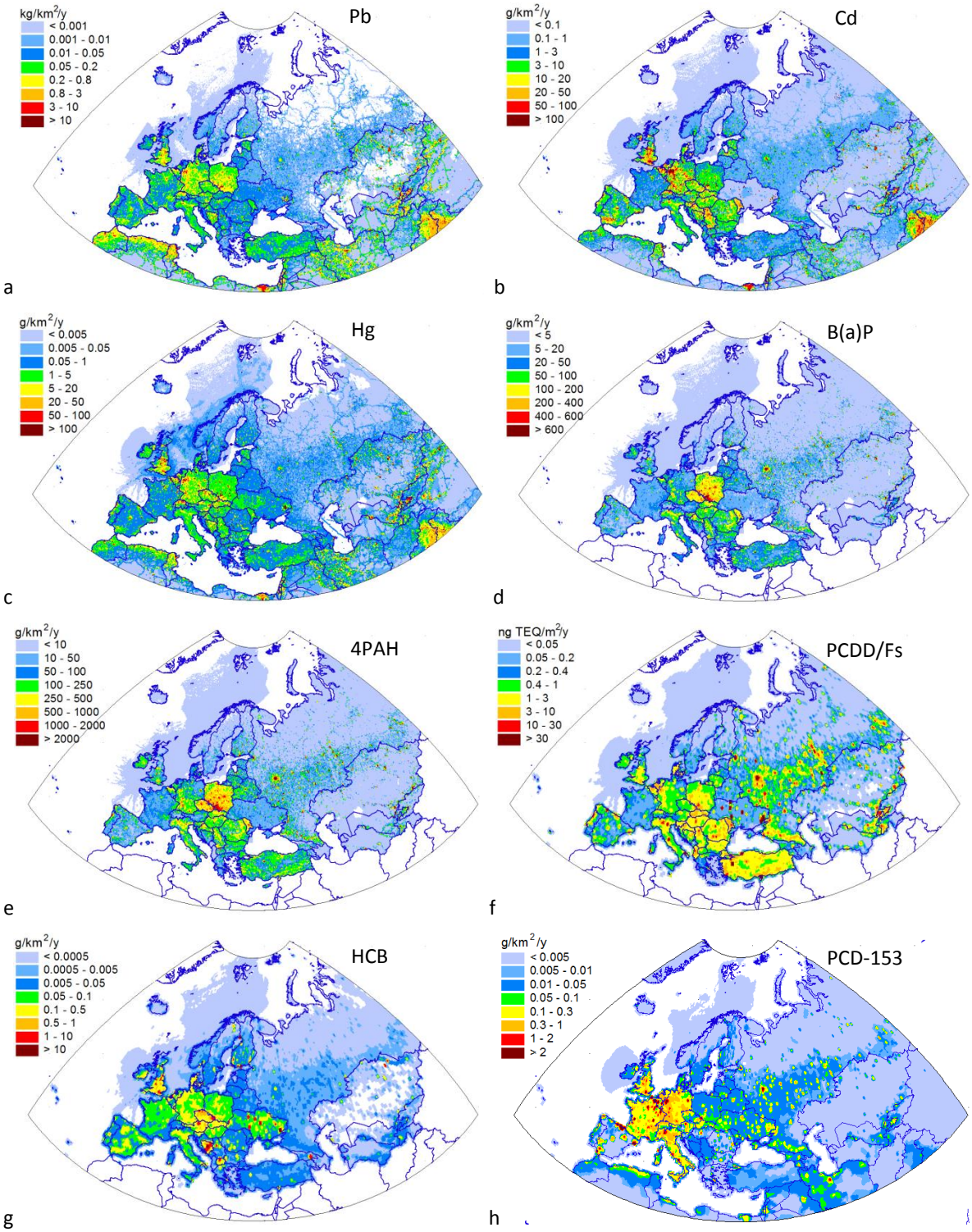

Fig. 3.6. *Spatial distribution of Pb (a), Cd (b), Hg (c), B(a)P (d), sum of 4 PAHs (e), PCDD/Fs (f), HCB (g) and PCB-153 (h) emissions in the EMEP region used in model simulations for 2020.*

Similarly, a scenario representing maximum level of emissions to the atmosphere was prepared and applied for HCB model simulations. The scenario was based on the data on the uncertainty range of HCB emissions reported by 14 EMEP countries in their inventory information reports (namely, Austria, Belarus, Belgium, Croatia, Cyprus, Denmark, Estonia, Finland, France, Latvia, Poland, Republic of Moldova, Switzerland, and the United Kingdom). Difference between the maximum and

average estimates of HCB emissions in these countries varied from a factor of 1.09 for Cyprus up to a factor of 5.7 for Denmark. For other EMEP countries, which did not report uncertainty range in their inventories, difference between the maximum and average emissions was set to a factor 2.3 (average difference based on the data for above-mentioned countries). The total HCB emissions in the EMEP countries according to the maximum emission scenario were higher than reported data in the inventories by a factor of 2.3 on average.

Maps illustrating spatial distributions of the pollutants, namely, Pb, Cd, Hg, B(a)P, sum of 4 PAHs, PCDD/Fs, HCB and PCB-153 emission fluxes from anthropogenic sources in the EMEP region, used in the model simulations for 2020, are presented in Fig. 3.6.

Along with gridded emission data, the GLEMOS modelling system requires additional information on heavy metal and POP emissions, namely, intra-annual variations, distribution of emissions with height and chemical speciation of Hg, PCB and PAH emissions. Necessary vertical and temporal disaggregation of the emissions was generated using the emission pre-processing tool, developed in MSC-E for the GLEMOS modelling system. More detailed information on the emission pre-processing procedure is presented in the heavy metal Status Report [*Ilyin et al*., 2018].

Global emissions

A number of pollutants, such as mercury and some POPs, are known for their ability to disperse in the atmosphere over the global scale. In order to take into account contribution of intercontinental transport to pollution levels in the EMEP countries and to evaluate boundary and initial conditions required for the regional EMEP modelling, global-scale model simulations are carried out.

Global-scale modelling of Hg is based on gridded emission data produced in the framework of the UNEP Global Mercury Assessment 2018 [*AMAP/UNEP*, 2019] and related to 2015. More detailed information can be found in the EMEP Status Report 2/2021 [*Ilyin et al*., 2021]. Intercontinental transport of PAHs is simulated based on the inventory, developed by the research group of Peking University [*Shen et al*., 2013]. Global PAH emission inventories with 0.1°x0.1° spatial resolution were elaborated using a bottom-up approach for the period from 1960 to 2014. For the evaluation of global-scale transport and fate of PCDD/Fs, HCB, and PCBs expert estimates of global emissions were utilized. In particular, global gridded emissions of PCDD/Fs to the atmosphere and soil were prepared using the national emission inventories reported by countries to the Stockholm Convention [*Gusev et al.*, 2014; *Shatalov et al.*, 2014]. Model simulations of HCB global-scale transport were carried out on the basis of experimental emission scenario of historical HCB releases during the period covering several recent decades [*Shatalov et al.*, 2010]. For the PCB-153 modelling, data on global emissions were derived from the inventory of *Breivik et al.* [2007]. Spatial distributions of Hg and B(a)P emissions, used in the global-scale model simulations for 2020, are shown in Fig. 3.7.

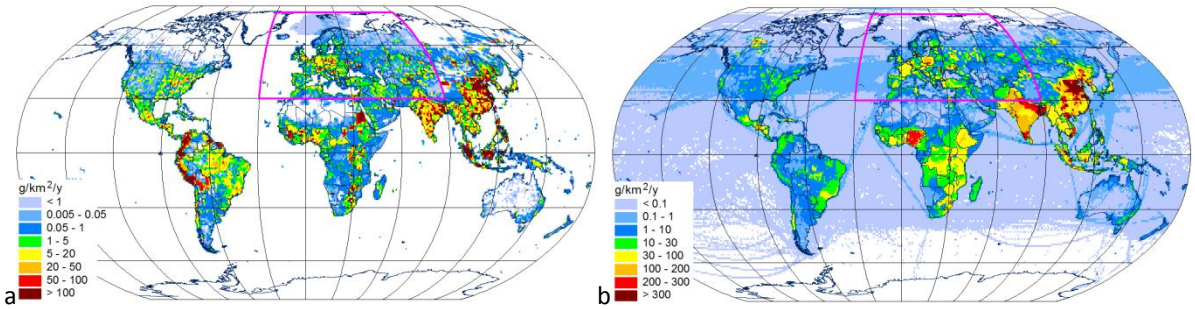

Fig. 3.7*. Spatial distribution of global annual emissions of Hg (a) and B(a)P (b) with spatial resolution 1°x1°, used in the model simulations for 2020. Pink line depicts boundary of the EMEP region.*

3.4. Levels of Heavy Metal and POP pollution

3.4.1. Pollution summary

Information on pollution levels of heavy metals and POPs was prepared on the base of monitoring data and atmospheric modelling of transboundary transport. Emission data for 2019 were used in the model calculations. Meteorological information and other time-dependent input data, such as land cover and chemical reactants related to 2020. Assessment of pollution levels includes spatial distributions of concentrations in air and deposition fluxes, source-receptor relationships for the EMEP countries, and changes in the levels between current (2020) and previous (2019) years. More detailed information on pollution levels of each of considered pollutant is available in Sections 3.4.2-3.4.6.

The purpose of this section is to summarize information on pollution levels of the considered pollutants (Pb, Cd, Hg, PAHs, PCDD/Fs, PCB-153, HCB) in 2020. Concentrations, deposition and their changes between 2019 and 2020 are presented for six sub-regions of the EMEP domain, namely Western Europe, Southern Europe, Northern Europe, Eastern Europe, Central Europe and Caucasus and Central Asia (Fig. 3.8). For comparability spatially-mean deposition fluxes of the pollutants in each sub-region were normalized and converted to dimensionless form. In general, the highest pollution levels are noted for Central Europe (Fig. 3.9a). Compared to other sub-regions, this sub-region is characterized by the highest mean deposition fluxes of Pb, Cd, Hg and PAHs and takes the second position for PCDD/Fs, PCB-153 and HCB. Northern Europe and Caucasus and Central Asia are the regions with the lowest spatially-averaged levels of pollution.

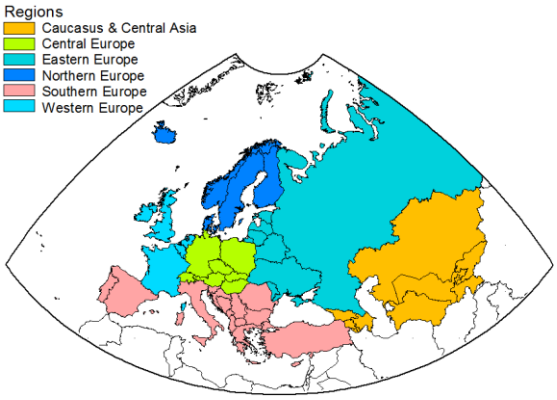

Fig. 3.8. *Definition of sub-regions of the EMEP region used in the report.*

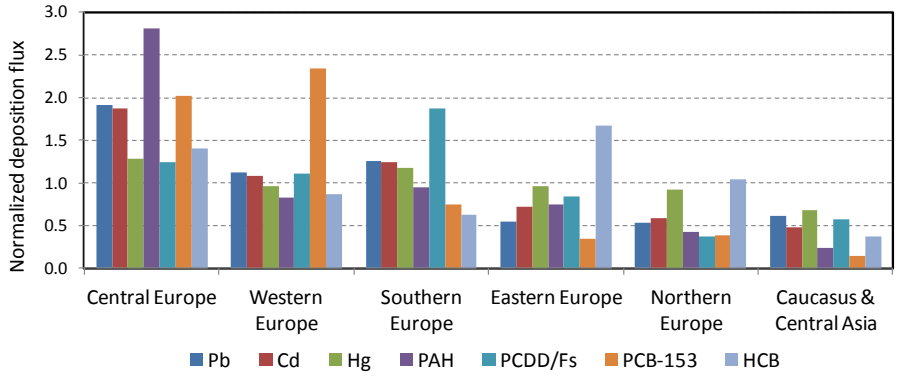

a

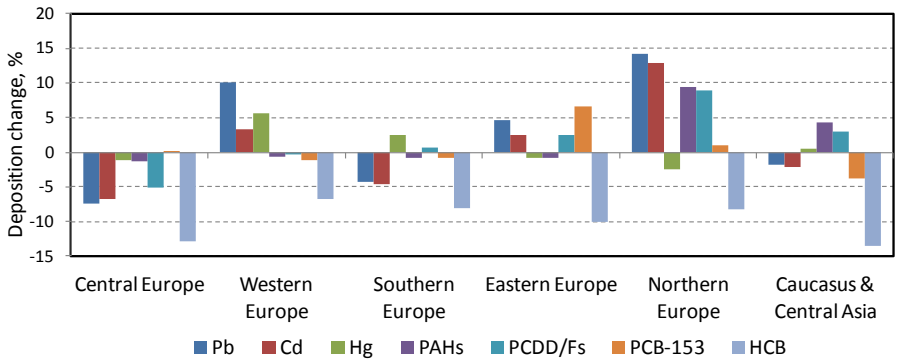

b

Fig. 3.9. *Normalized mean deposition flux in 2020 (a) and relative changes of heavy metals and POP deposition between 2020 and 2019 (b) in sub-regions of the EMEP region.*

The change between modelling results (X) of the current and previous year, caused by inter-annual meteorological variability, is calculated as a difference between the value of 2019 and 2020 related to 2019, according to the formula:

$$\Delta = \frac{(X_{2020} - X_{2019})}{X_{2019}} \cdot 100\%$$

Positive value of the change means that pollution levels increased in 2020 compared to 2019, and vice versa. The same approach is applied to evaluate the changes between current and previous year to particular pollutants (sections 3.4.2 – 3.4.6).

The considered pollutants are characterized by different spatial distribution of emissions, atmospheric properties and behavior in the environment. Pb and Cd are fully particulate species which atmospheric properties are determined by the properties of the aerosol particles-carriers. Hg presents in the atmosphere in various forms with wide range of atmospheric lifetime. Considered POP species are present in the atmosphere in gaseous and particulate phases and partitioning between these two phases depends on air temperature and properties of atmospheric aerosols. Besides, Hg and POPs take part in gaseous exchange between the atmosphere and other environmental compartments. Therefore, the changes in the meteorological conditions between 2019 and 2020 have different effect on the change of pollution levels of heavy metals and POPs.

In Central Europe general reduction of deposition of all pollutants except for PCB-153 is noted (Fig. 3.9b). Most significant increase of deposition is noted for Northern Europe. The increase of deposition of Pb, Cd, PAHs and PCDD/Fs was 9 – 14%. Western Europe is characterized by increase of heavy metal deposition. In contrast, in Southern Europe decline of Pb and Cd levels occurred. In Eastern Europe deposition of Pb, Cd, PCDD/Fs and PCB-153 demonstrate moderate (2% – 7%) increase. In all sub-regions the decline of HCB deposition takes place.

More detailed information on evaluation of modelling results against measurements, source - receptor relationships, ecosystem-dependent deposition and pollution of marginal seas is summarized in Supplementary Data Reports for heavy metals [*Strizhkina et al*., 2022a] and for POPs [*Strizhkina et al*., 2022b].

3.4.2. Lead

Lead is presented in the atmosphere as a component of aerosol particles. Industry sector is the main anthropogenic emission source of lead in the EMEP region followed by road transport and domestic heating. Lead harmfully affects brain and nervous system of humans, increases risks of high blood pressure and kidney damage, and has adverse impact on fetus (https://www.who.int/news-room/fact-sheets/).

Air concentrations

Annual mean concentrations of Pb in 2020 ranged from 0.3 ng/m^3 to more than 20 ng/m^3. The lowest levels took place in the northern part of the EMEP region (Scandinavian Peninsula, Iceland, north of Russia) (Fig. 3.10a). The highest levels are found in the northern part of Italy, southern part of Poland, north-western part of Germany and a number of regions in the south-eastern Europe and Central Asia. Central Europe is characterized by the highest spatially mean concentrations (about 4.5 ng/m^3) followed by Western Europe (Fig. 3.10b). The lowest spatially mean concentrations (about 0.5 ng/m^3) took place in Northern Europe. Relatively low concentrations in Eastern Europe are explained by large areas in Russia with the low levels varying from 0.3 to 1 ng/m^3. However, in other parts of Eastern Europe the concentrations are comparable with those in other regions.

Modelled annual mean concentrations of Pb in air were compared with the available EMEP measurement data. On average the model somewhat (+12%) overestimates the observed levels. At 80% of stations the difference between modelled and observed concentrations is within a factor of two. Spatial correlation coefficient is about 0.7 which means that the model reproduced in general main spatial gradients of concentrations in air. It is important to take into account that for particular countries the agreement between modelled and observed levels may differ from the average value. More detailed information on the evaluation of modelling results against measurements is presented in Supplementary Data Report [*Strizhkina et al*., 2022a].

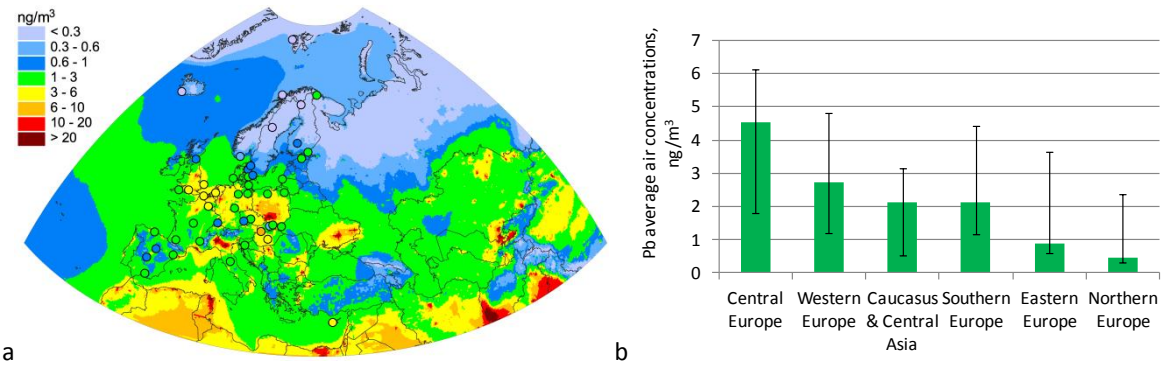

Fig. 3.10. *Annual mean air concentrations of Pb (circles on the map show observed values in the same colour scale) (a) and average air concentrations of Pb in EMEP sub-regions (b) in 2020. Whiskers show the range of concentrations in particular countries of the sub-region.*

Deposition fluxes

Spatial distribution of Pb deposition flux in the EMEP region in 2020 is demonstrated in Fig. 3.11a. Deposition flux depends on a number of factors, including location of main emission sources, precipitation amount, properties of underlying surface and contribution of re-suspension. Similar to air concentrations, the highest deposition flux (0.8–2.0 kg/km^2/y) occurred in the regions of significant emissions such as the southern part of Poland, north-west of Germany and north of Italy. Relatively high levels took place in regions with high precipitation sums, e.g., upwind coasts of the Scandinavian Mountains, north-eastern coast of Turkey, the western part of the Balkan region. Deposition consists of wet and dry component. Wet deposition contributes three quarters to the total one on the average. Like for air concentrations, the highest spatially mean deposition flux is noted for Central Europe (about 0.6 kg/km^2/y), and the lowest one for Northern Europe (almost 0.2 kg/km^2/y) (Fig. 3.11b).

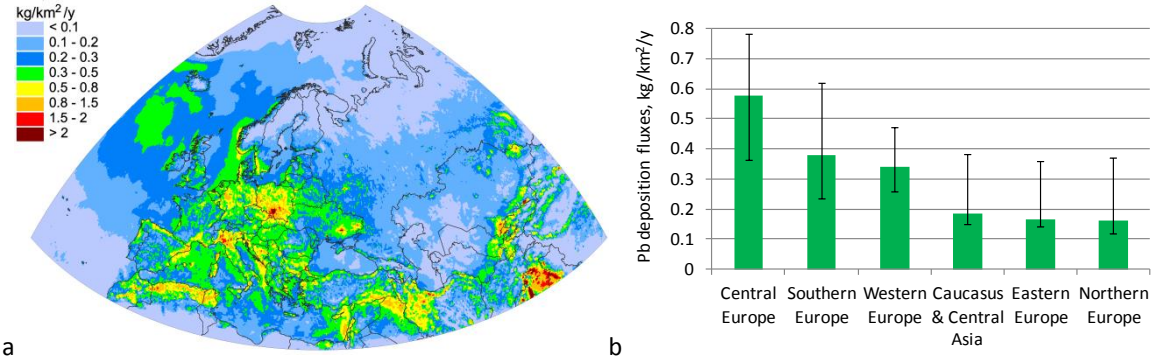

Fig. 3.11. *Annual total deposition flux of Pb (a) and mean total deposition fluxes of Pb to EMEP sub-regions (b) in 2020. Whiskers show the range of country-average concentrations across countries in each sub-region.*

Mean modelled wet deposition flux underestimates the mean flux observed at the EMEP stations by about 23%. At about 60% of stations modelled values agree with the observed fluxes within a factor of two. Spatial correlation coefficient is about 0.5. These statistical indicators reveal that the model

generally reproduces the observed levels. Nevertheless, there is a tendency of some underestimation of the observed levels, especially in Northern Europe. Results of the model evaluation are described in Supplementary Data Report [*Strizhkina et al*., 2022a] in more detail.

Three groups of emission sources of the Pb deposition are considered in the model simulations. They include EMEP anthropogenic sources, secondary sources (re-suspension) in the EMEP domain and contribution of sources located outside the EMEP countries (non-EMEP sources).

Spatial distribution of Pb deposition from the EMEP anthropogenic emissions is correlated with the locations of emission sources (Fig. 3.12a). However, due to the influence of meteorological factors deposition field is smoother than the field of emissions. The highest spatial mean deposition flux from anthropogenic sources in 2020 took place in Central Europe, and the lowest – in Northern Europe.

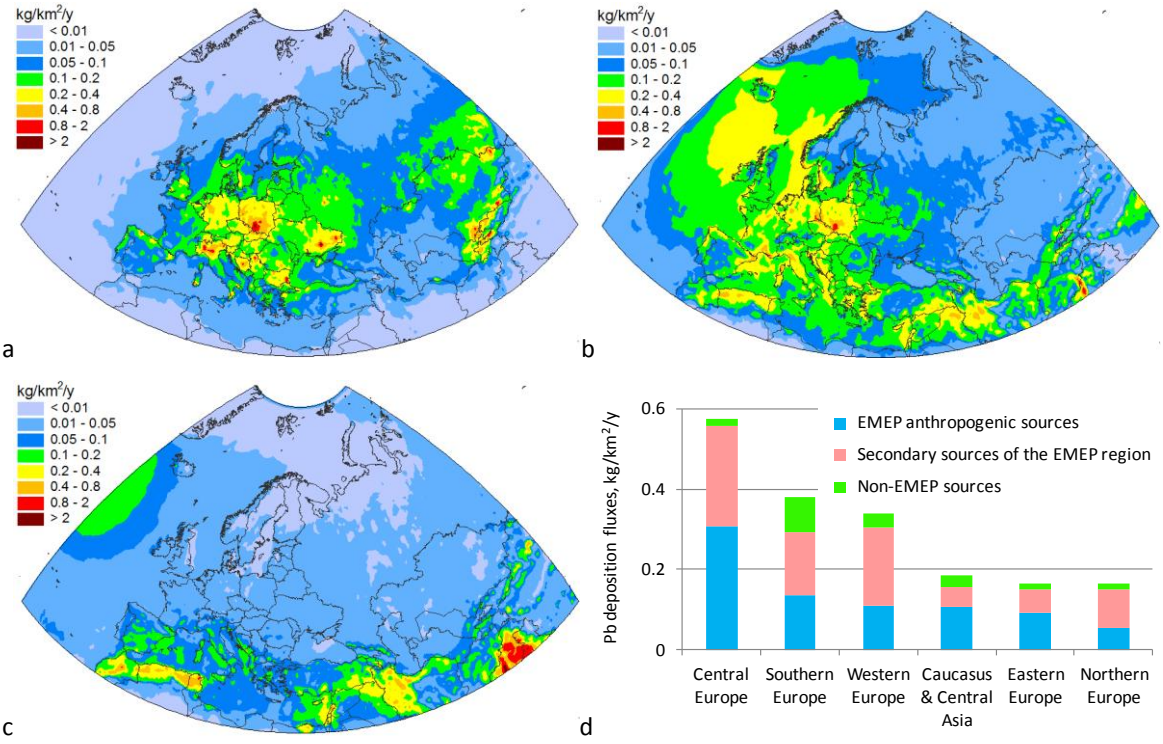

Fig. 3.12. *Annual Pb deposition in 2020 from EMEP anthropogenic sources (a), secondary sources (wind re-suspension) (b) and non-EMEP sources (c), and mean deposition fluxes from these sources to the EMEP sub-regions (d).*

Accumulation of deposition over long-term period led to increase of heavy metal concentrations in the top soil or urban dust. Therefore, regions with high deposition from anthropogenic sources become also sources of re-suspension (e.g., Poland, Northern Germany). Besides, significant re-suspension occurs in regions with relatively high background concentration of Pb in soils, e.g., in the southern part of France [*Salminen*, 2005]. Broad area of elevated deposition over the Atlantic is caused by wind suspension and consequent deposition of sea spray aerosol. The contribution of re-suspension in the EMEP countries varies from 25% in Caucasus and Central Asia sub-region to almost

60% in Northern and Western Europe. This high contribution of re-suspension is explained by low anthropogenic emissions of Pb in countries of the latter two sub-regions. Besides, it is important to keep in mind that modelling of re-suspension is subject to high uncertainties.

Contribution of non-EMEP sources to Pb deposition flux in the sub-regions of the EMEP domain is relatively low ranging from 3% in Central Europe to 23% in Southern Europe (Fig. 3.12d). Relatively high contribution of these sources to deposition in Southern Europe is caused by the influence of emission sources in non-EMEP countries located outside or within the EMEP domain (e.g., Algeria, Egypt, Iran). Besides, Pb is re-suspended from the deserts of Africa and Asia located outside the EMEP domain and is transported through the southern border of the EMEP domain.

More detailed information concerning contributions from the EMEP anthropogenic sources, wind re-suspension and non-EMEP anthropogenic sources to Pb deposition in 2020 in the EMEP countries is available in Supplementary Data Report [*Strizhkina et al.,* 2022a].

Changes of the pollution levels between 2019 and 2020

This section contains description of changes between pollution levels in 2019 and 2020 because of meteorological variability. Compared to 2019, the changes of annual mean Pb concentrations due to meteorological variability over most of the EMEP countries varied within ±50% (Fig. 3.13a). In particular, significant increase (20-50%) took place in Western Europe, over the north of Italy, the Baltic Sea, north-eastern part of Russia and over some regions of south-eastern part of Europe. At the same time, substantial decrease occurred over the northern part of the United Kingdom and Ireland, the southern part of Norway and the Mediterranean Sea. Meteorological variability resulted in the increase of spatially averaged concentrations in all six sub-regions of the EMEP domain (Fig. 3.13b). The highest increase took place in Western Europe (about 20%), and the lowest one in Central Europe (1%).

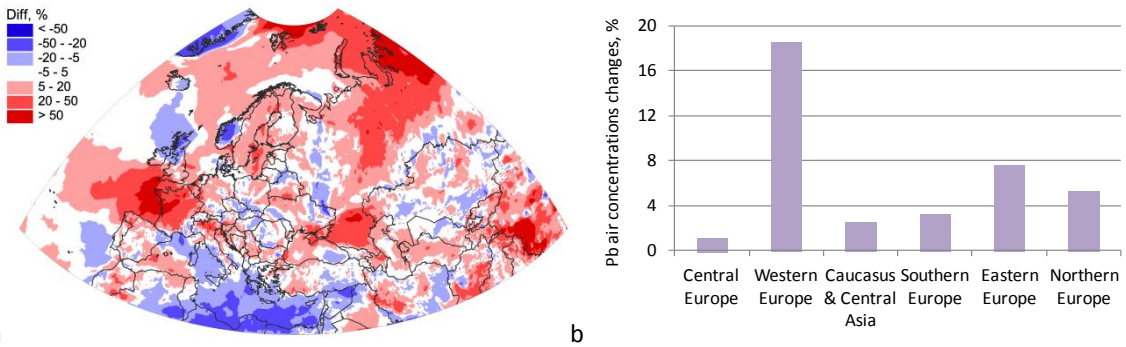

a b

Fig. 3.13. *Relative changes of Pb air concentrations due to the changes in meteorological conditions over the EMEP domain (a), and in the EMEP sub-regions (b) between 2019 and 2020.*

Changes in meteorological conditions between 2019 and 2020 resulted in the decline of Pb deposition in most of countries in Central and Southern Europe, the Mediterranean Sea and the

western part of Central Asia (Fig. 3.14a). The increase of Pb deposition occurred in the southern and south-western parts of Europe (e.g., west of Spain, France), in a number of regions of Eastern Europe, Scandinavia and Central Asia. The highest increase of spatially mean deposition flux took place in Northern Europe (almost 15%) followed by Western Europe (10%) (Fig. 3.14b) mostly because of the increase of contribution of re-suspension that depends on meteorological conditions. In Central Europe the deposition declined by about 5% due to reduction of contributions of all considered groups of sources. In the Caucasus and Central Asia sub-region deposition caused by the EMEP anthropogenic sources and non-EMEP sources declined, while the impact of re-suspension increased. The overall change of the deposition in this sub-region was low reaching around -2%. In most of the particular EMEP countries the changes due to meteorological variability lie within ±30%.

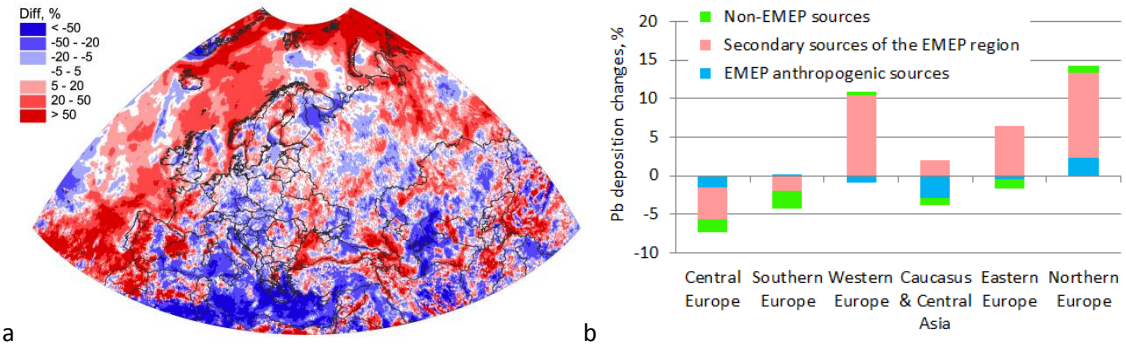

a b

Fig. 3.14. *Relative changes of Pb total deposition due to the changes in meteorological conditions over the EMEP domain (a), and in the EMEP sub-regions (b) between 2019 and 2020.*

Effects of changes of meteorological variability between 2019 and 2020 on changes of Pb pollution levels varied for different parts of the EMEP region. Significant increase of deposition and air concentrations in Western Europe is mostly caused by increased contribution of wind re-suspension.

The main changes with regard to the wind re-suspension in the Western Europe took place in winter and spring. Compared to 2019, January and February of 2020 were characterized by stronger wind which favoured the increase of re-suspension flux from land and sea surfaces. Besides, precipitation in a number of countries of the Western Europe in 2020 was significantly higher than that in 2019. For example, precipitation amount in the Netherlands, Belgium, the United Kingdom and main part of France in winter (February) of 2020 were 1.5 – 4 fold higher compared to that in 2019. It resulted in the corresponding increase of total deposition flux in February by 90 - 170% in these countries. For example, in France the increase made up 130% (Fig. 3.15). Hence, lead re-suspended to the air was scavenged and increased deposition flux in 2020 compared to 2019.

Increase of annual mean air concentrations in 2020 compared to 2019 in Western Europe is mainly determined by the increase of air concentrations in spring. The increase is caused by the growth of wind re-suspension. In its turn, the re-suspension increased due to combination of drier weather conditions and relatively strong near-surface winds. For example, in spring precipitation amount in the Netherlands and Belgium declined by 40 – 50% relative to the corresponding period of 2019.

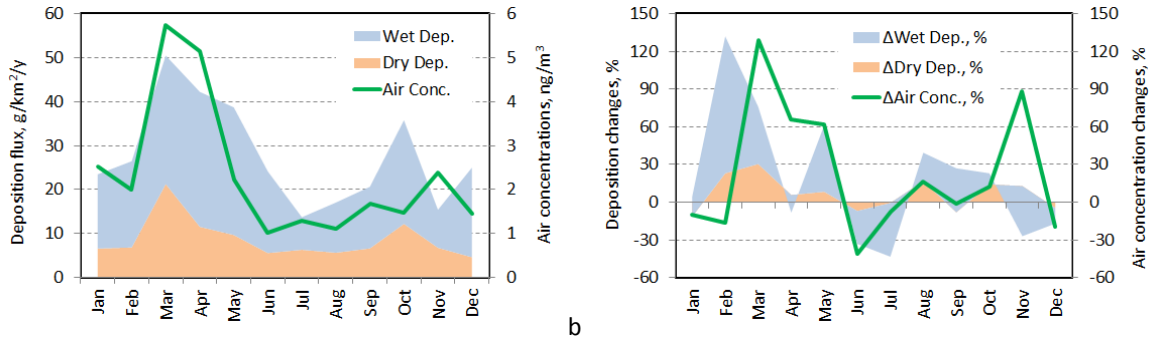

Fig. 3.15. *Spatial mean deposition flux and concentration in air of Pb in France in 2020 (a) and their changes relative to 2019 (b).*

Decrease of precipitation amount in Central Europe led to the decline of deposition and some increase of air concentrations. Increase of air concentrations and deposition fluxes in Northern Europe is explained by the effect of wind re-suspension. In particular, due to stronger winds in 2020, especially in winter and autumn, compared to 2019 over the Baltic and North Seas, re-suspension of sea-spay aerosol containing Pb increased and it led to the growth of Pb levels in Northern Europe. Another factor is an increase of atmospheric transport from Central Europe. The change in Southern Europe, Eastern Europe and Caucasus and Central Asia is relatively low lying within ±8%.

Transboundary transport

Anthropogenic component of deposition to the EMEP countries is divided into two parts: deposition caused by national sources and deposition caused by transboundary atmospheric transport from the foreign sources of the EMEP countries. The highest spatially averaged anthropogenic flux (0.4 kg/km^2/y) is noted for Poland followed by Slovakia and Bosnia and Herzegovina (Fig. 3.16a). The lowest takes place in Iceland and Malta. In 37 countries of total 51 more than a half of anthropogenic deposition is caused by transboundary transport, and in 27 countries the contribution of foreign sources makes up 75%. The highest contribution of foreign sources, reaching 97 – 99%, is noted for the countries with small territory (e.g., Liechtenstein, Monaco) or low national emissions, e.g. Montenegro. The lowest contribution of transboundary transport (20 – 25%) is simulated for the countries with substantial national emissions and relatively large territory, e.g., Poland, Kazakhstan, Italy. Predominant influence of national sources is noted for Portugal, the United Kingdom and Spain due to their location in the western part of the EMEP region. Due to predominant westerly atmospheric transport and relative remoteness from major foreign emission sources, the emission sources of their "eastern" neighbours have relatively small impact on Pb pollution in these countries.

Changes of deposition to each EMEP country from national and foreign sources between 2019 and 2020 are demonstrated in Fig. 3.16b. The change of anthropogenic deposition ranges within ±20% in the majority of the EMEP countries. The exception is Iceland where almost two-fold decline of anthropogenic deposition takes place, caused by the reduction of transboundary transport to this country from other EMEP countries. In some countries (e.g., Estonia) deposition from national sources declined while the impact of transboundary transport increased in 2020.

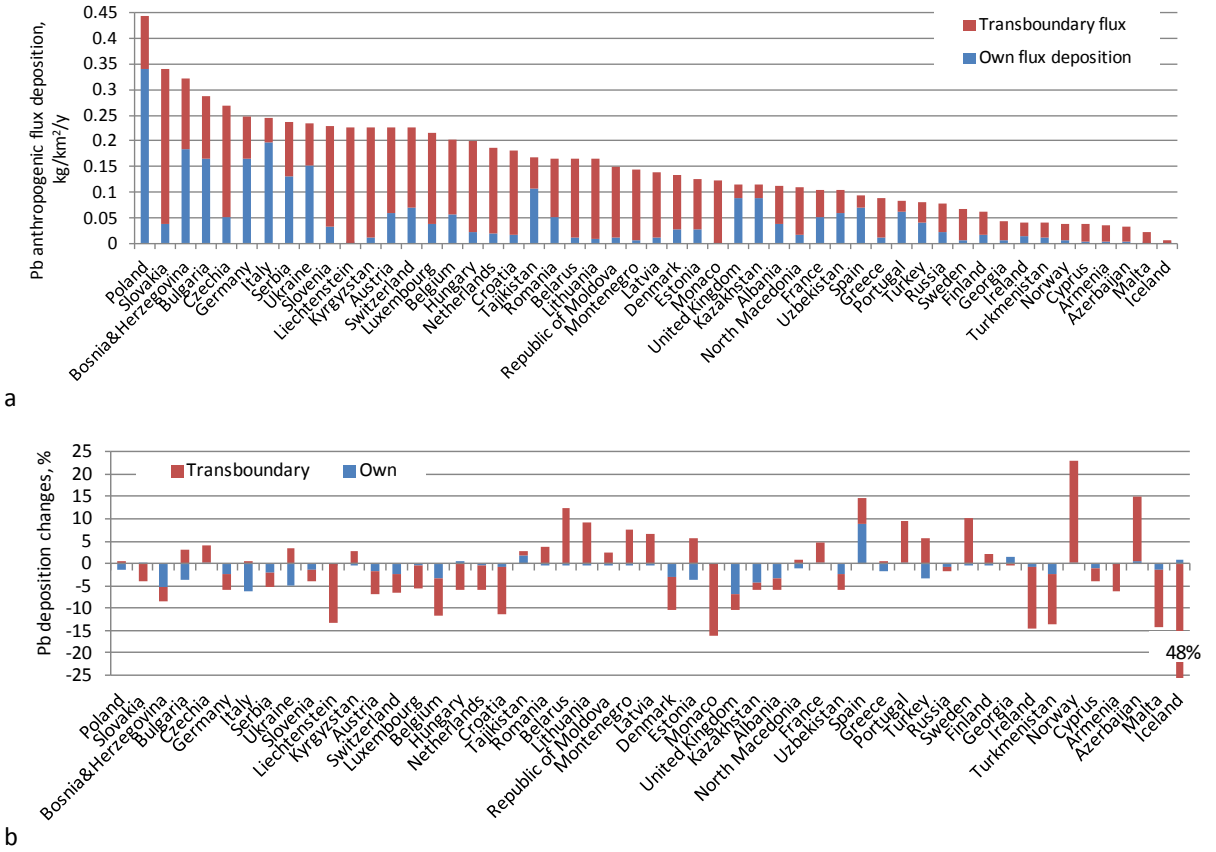

Fig. 3.16. *Spatially averaged deposition flux of Pb in the EMEP countries from national and foreign sources in 2020 (a) and relative change of the deposition fluxes between 2019 and 2020 (b).*

Changes of Pb pollution levels between 2019 and 2020 are caused by inter-annual meteorological variability. The changes in Pb total deposition are within ±30% limits in most of the EMEP countries. It is important to note that the changes of meteorological conditions have both direct (e.g., changes of precipitation, transport patterns) and indirect (changes of re-suspension fluxes) effects on the variability of the Pb levels between 2019 and 2020.

3.4.3. Cadmium

Cadmium in the atmosphere is bound to aerosol particles. The main anthropogenic emission sectors of Cd in the EMEP region are industry, production of electricity and residential combustion. However, in particular countries the contributions of other sectors can also be important. Cadmium is a toxic element known for harmful effects on the kidney, skeletal and respiratory system and is classified as a carcinogen.

Air concentrations

Annual modelled and observed atmospheric concentrations of Cd in 2020 ranged mainly from 0.01 to 0.2 ng/m^3 over the most part of the EMEP region (Fig. 3.17a). On average, the highest values were noted for Central Europe, followed by Western Europe (Fig. 3.17b). However, Western Europe is characterized by the widest range of concentrations. High levels of Cd up to 0.5 ng/m^3 occured in particular areas of the south-western part of Germany, the southern part of Poland, the northern part of Serbia and southeast of Sicily. These peak values are mostly explained by the high anthropogenic emissions in these regions. The lowest Cd concentrations are modelled over Norway, Sweden, Finland, Iceland and Russia as well as over most parts of Turkey and Central Asian countries. Modelled data agree with the measured concentrations within a factor of two at more than 50% measurement sites involved into the comparison. More information on agreement between modelled and observed Cd air concentrations is given in the Supplementary Data Report [*Strizhkina et al.,* 2022a].

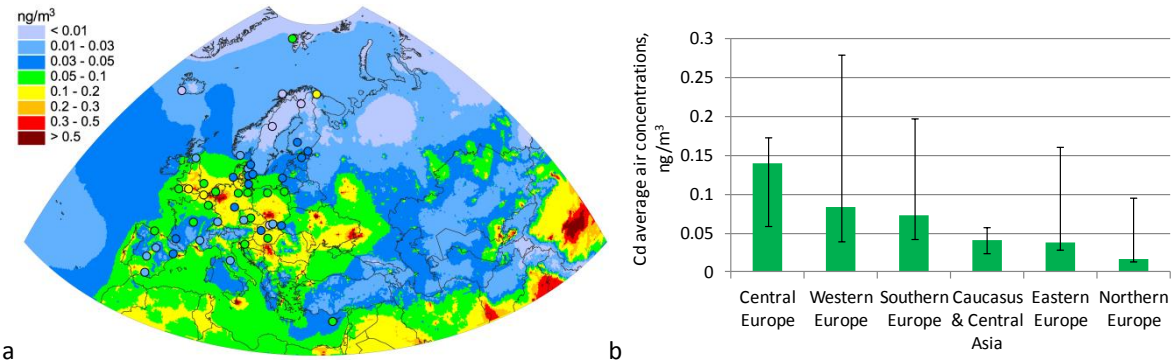

Fig. 3.17. *Annual mean air concentrations of Cd (circles on the map show observed values in the same colour scale) (a) and average air concentrations of Cd in EMEP sub-regions (b) in 2020. Whiskers show the range of country-average concentrations across countries in each sub-region.*

Deposition fluxes

Cadmium total deposition fluxes varied from 5 to 60 g/km^2/y over a major part of the EMEP region in 2020 (Fig. 3.18a). The highest deposition fluxes occurred over the countries located in Central Europe followed by Southern Europe (Fig. 3.18b) and also over the central part of European Russia as well as in the south-eastern part of Turkey. These data generally agree with the spatial distribution of anthropogenic emission in these regions. Cadmium deposition fluxes were relatively low in Western Europe except for the areas over the Netherlands and Belgium, where they were closer to the levels in Central Europe . Also the Middle East is characterized as the region with significant Cd deposition fluxes that are partly explained by wind re-suspension of the pollutant from the ground. The levels below 5 g/km^2/y occured in Northern Europe and in the Russian Arctic because of low emissions and low precipitation in these regions. Along with this, low deposition fluxes are noted for Central Asia also due to low precipitation amounts.

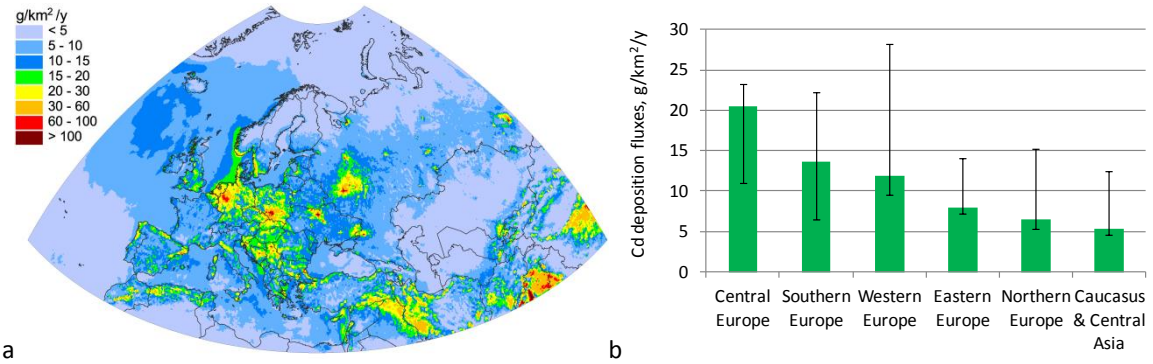

Fig. 3.18. *Annual total deposition flux of Cd (a) and mean total deposition fluxes of Cd to EMEP sub-regions (b) in 2020. Whiskers show the range of country-average concentrations across countries in each sub-region.*

The contribution of various types of Cd emission sources to deposition levels is shown in Figure 3.19. The assessment considers the influence of three groups of sources, in particular, Cd anthropogenic emissions of the EMEP countries (Fig. 3.19a), secondary sources of Cd in the EMEP region due to wind re-suspension (Fig. 3.19b) and Cd emission sources located outside of the EMEP region or non-EMEP sources (Fig. 3.19c). As it can be seen, anthropogenic emissions from the EMEP countries dominate in most of the EMEP sub-regions contributing about 50% of total Cd deposition in Southern, Western, and Northern Europe and even more in Central and Eastern Europe (Fig. 3.19d).

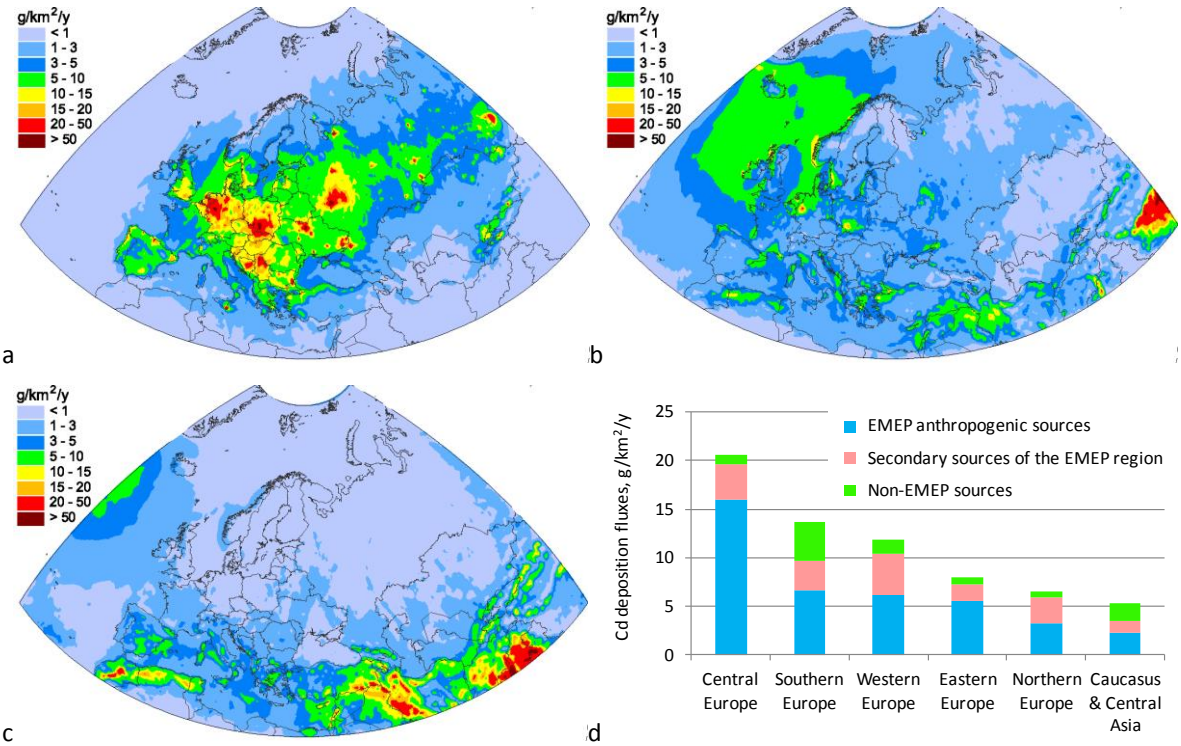

Fig. 3.19. *Annual Cd deposition in 2020 from EMEP anthropogenic sources (a), secondary sources (wind re-suspension) (b) and non-EMEP sources (c), and mean deposition fluxes from these sources to the EMEP sub-regions (d).*

In addition to this, it is assumed that in such regions topsoil is enriched with Cd due to elevated Cd pollution levels. According to the model parameterization, it causes comparatively high deposition of

re-suspended Cd, for instance in the south-eastern part of Poland and the western part of Germany. The highest mean deposition flux from re-suspension (around 4 g/km^2/y) is noted for Central and Western Europe. However, the relative contribution of re-suspension does not exceed 40% of total deposition level (Western Europe).

The contribution of non-EMEP Cd emission sources is noticeable over Turkey, Greece and Spain as well as in Caucasus and Central Asia due to proximity to non-EMEP sources in Northern Africa, the Middle East and Southern Asia. The deposition fluxes from this type of sources range from 0.5 g/km^2/y in Northern Europe to 4.6 g/km^2/y in Southern Europe (Fig. 3.19d). Besides, the highest relative contribution of these sources to total deposition is noted for the Caucasus and Central Asia (around 40%) followed by Southern Europe (about 25%). More detailed information on the contributions from the EMEP anthropogenic sources, wind re-suspension and non-EMEP anthropogenic sources to Cd deposition in 2020 in the particular EMEP countries can be found in Supplementary Data Report [*Strizhkina et al*., 2022a].

Changes of the pollution levels in 2020

Cd air pollution and deposition fluxes over the EMEP region have been changed since 2019. Changes caused by variability of meteorological conditions are considered in this section. The description of the overall changes due to both meteorological conditions and emissions can be found in Annex B. In 2020 due to changes in meteorological conditions Cd air concentrations increased on average from 1.5 to 6.5% depending on the particular sub-region (Fig. 3.20b). The highest regional-mean relative increase is estimated for Caucasus and Central Asia, while the lowest one for Southern Europe. At the same time, the changes in particular countries of the EMEP region are more substantial (Fig. 3.20a). In particular, air concentrations increased by 5-20% in Poland, Finland, Sweden, Hungary, Slovakia, Bosnia and Herzegovina, Croatia, over the northern part of Italy, and more than by 20% in France, Russia (especially in the Arctic and in the southern part). Cadmium concentrations also increased over the Black Sea, the Caspian Sea, over the Bay of Biscay and the Arctic Ocean. At some locations over the Arctic Ocean the relative increase exceeds 50% (Fig. 3.20a). Some of the areas are characterized by declining levels of concentrations. In particular, a 5-20% decrease is seen in the United Kingdom, Norway, Latvia, Lithuania, and Belarus as well as over the most part of the Mediterranean Sea. On the contrary, in most countries of Central Europe, Cd concentrations in the air are changed only slightly (from -5% to 5%) . The absolute differences range from -0.1 to 0.1 ng/m^3 in almost all sub-regions of the EMEP domain.

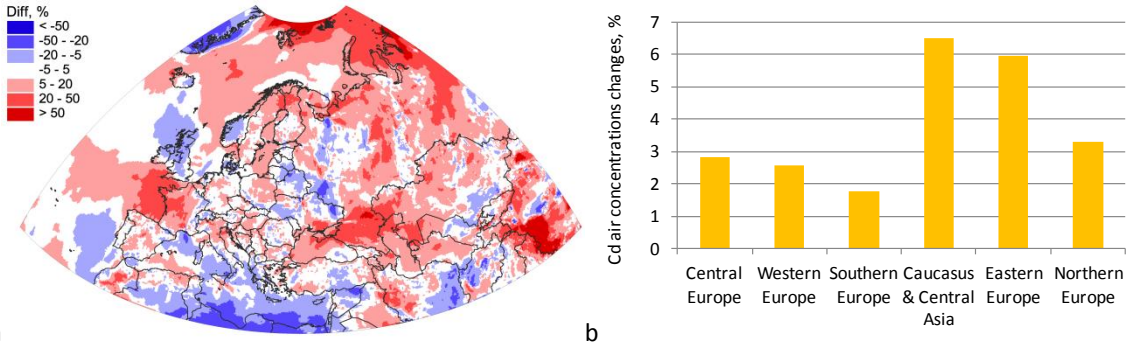

a b

Fig. 3.20. *Relative changes of Cd air concentrations due to the changes in meteorological conditions over the EMEP domain (a), and in the EMEP sub-regions (b) between 2019 and 2020.*

Following air concentrations, the total deposition fluxes of Cd also changed in 2020. Variability of meteorological conditions led to a noticeable decrease in Southern Europe (Italy and countries of the Adriatic coast) and Central Europe as well as over the Mediterranean Sea, White Sea, and in Central Asia due to the decrease of precipitation in these regions (Fig. 3.21a,b). Compared to the previous year, the highest relative increase of Cd deposition fluxes is seen in France, Spain, Azerbaijan, Armenia, Georgia as well as over the Bay of Biscay, the Caspian Sea, and the western part of Black sea. Along with this 5-20% increased deposition fluxes are seen in some parts of Sweden, Norway and Finland which is explained by increased atmospheric transport from Central Europe. Patterns of Cd pollution level changes are similar to those for Pb (Section 3.4.2). Taking into account this and similarity of atmospheric behavior of Pb and Cd, it is justified to state that the reasons for Cd level changes are similar to those of Pb discussed in section 3.4.2.

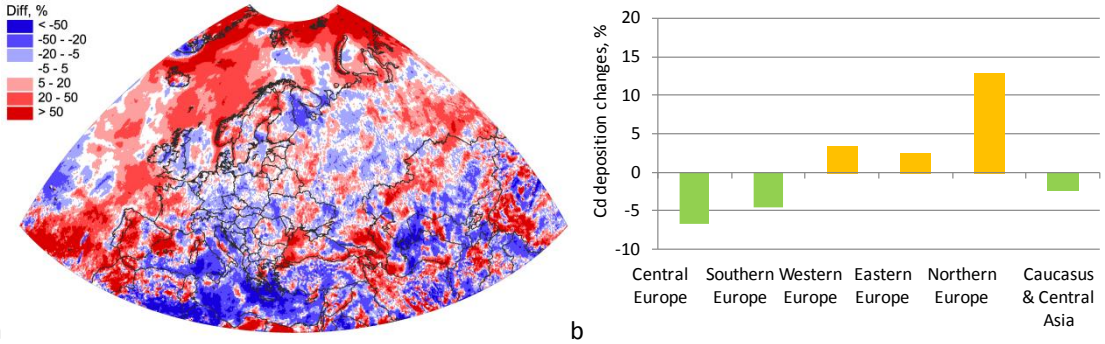

a b

Fig.3.21. *Relative changes of Cd total deposition due to the changes in meteorological conditions over the EMEP domain (a), and in the EMEP sub-regions (b) between 2019 and 2020.*

Transboundary transport

In 2020, there were 39 countries of total 51where the contribution of transboundary transport to Cd deposition exceeded 50%, and it should be noted that this number did not change compared to 2019. At the same time, the number of countries where the contribution of transboundary transport to deposition levels exceeds 75% increased by 1 and amounted to 19. Total anthropogenic Cd deposition flux in the EMEP parties split by types of sources is illustrated in Figure 3.22a. The largest

contribution of transboundary transport is seen in Monaco (more than 99%), Liechtenstein (98%), Iceland (96%), Malta (96%) and Lithuania (92%). The dominance of foreign sources in the pollution of these countries is explained by the low levels of their own anthropogenic emissions and their small areas. In some particular cases, for instance in Iceland, national emissions are so small that despite remoteness from major European sources, the contribution of long-range transport to Cd deposition in these countries exceeds 95%. High contribution of transboundary transport also takes place for Lithuania, Latvia, Estonia, Finland, Denmark, Sweden, Norway, Croatia, and Montenegro, where the impact of national sources is relatively small. There is 15-25% deposition increase in Norway and Azerbaijan and 10% in Sweden compared to 2019 due to the increase of contribution of foreign sources (Fig. 3.22b). At the same time atmospheric transport, mostly in charge of deposition, decreased in Iceland, Malta, Ireland, Austria, Belgium and Liechtenstein. The smallest contribution of foreign sources is noticeable in Spain (about 18%), the United Kingdom (20%), Portugal (25%), Russia (almost 30%) and Germany (around 30%).

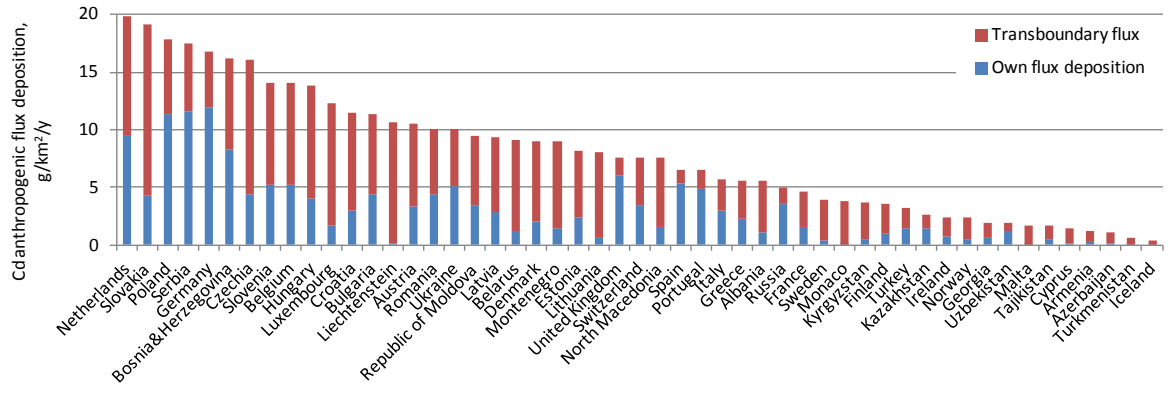

a

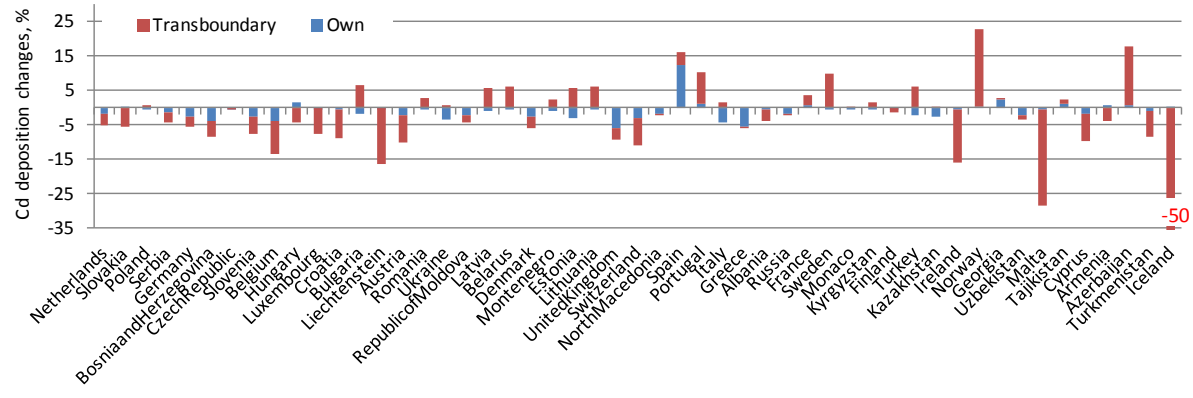

b

Fig. 3.22. *Spatially averaged deposition flux of Cd in the EMEP countries from national and foreign sources in 2020 (a) and relative change of the deposition fluxes between 2019 and 2020 (b).*

The impact of transboundary transport is the most noticeable in Central Europe as well as in western part of Eastern Europe and the northern part of Southern Europe. According to the officially reported data, Cd emissions are relatively high in Germany, Serbia and Poland (Fig. 3.22a). Therefore, compared to other countries, the largest national deposition fluxes in absolute terms (more than 12 g/km^2/year) are noted for these countries. But beside high levels of deposition to their own territory, contribution of Cd deposition from transboundary transport in these countries is also significant (up

to 67% in Serbia and about 50 % in Poland and Germany). For other countries of Central Europe, the foreign sources mostly contribute more than national ones. In the westernmost countries, such as Spain and the United Kingdom, the situation is the opposite. National sources contribute more than the foreign ones. In Central Asia, the farther south the country is, the lower its national emissions, and the greater the role of long-range transport in pollution levels. The modelling results for 2020 show the decreasing role of the Cd transboundary transport in a number of countries, namely Iceland, Malta, Croatia, Liechtenstein, Belgium, Switzerland and the United Kingdom compared to 2019 (Fig. 3.22b). Also there is an increase in Cd deposition caused by both foreign and national sources in Spain and Portugal.

3.4.4. Mercury

Mercury is a toxic pollutant capable of long-range transport, bioaccumulation in ecosystems and leading to adverse effects on human health and biota. Mercury mainly occurs in the free and lower troposphere in the gaseous elemental form (Hg^0) with a small contribution of oxidized forms (Hg^{II}). Besides, mercury deposition is determined by Hg^{II}, which is directly emitted from anthropogenic sources and formed chemically in the atmosphere from Hg^0, as well as by air-vegetation exchange of Hg^0. Thus, Hg deposition depends on a number of factors including spatial patterns of anthropogenic and natural emission, chemical composition of the atmosphere as well as meteorological conditions.

Air concentrations

Annual atmospheric concentrations of Hg^0 in the surface layer range from 1.2 to 2 ng/m^3 with an average of 1.4 ng/m^3 over the whole EMEP region in 2020 (Fig. 3.23a). The relatively small variation of atmospheric Hg^0 concentrations is explained by the fact that, in contrast to other heavy metals, Hg^0 is characterized by long resistance time in the atmosphere that leads to forming evenly distributed background levels. According to the modelling results, concentrations of elemental gaseous Hg exceeding 1.6 ng/m^3 are noted for Portugal, Greece, Hungary, Albania, Bulgaria, North Macedonia, Croatia, Poland, Uzbekistan, Turkmenistan, the Netherlands and the western part of Turkey. Also Hg^0 air pollution levels that exceed the average EMEP value are noticeable over the Baltic and North seas, the coastal zones of the Mediterranean sea and especially over the Black and Caspian seas. In some particular areas of Bosnia and Herzegovina, Serbia, Uzbekistan, Spain and Italy air pollution reaches 1.7 ng/m^3, in particular areas in the northern part of Italy levels are greater than 3 ng/m^3. However, mean air concentrations of Hg^0 in all EMEP sub-regions are within 1.3-1.4 ng/m^3 (Fig. 3.23b). Hg^0 concentrations lower than 1.4 ng/m^3 are seen in the central part of France as well as in remote regions (e.g. the Arctic). Modelling results agree with measured Hg^0 concentrations, obtained from the EMEP monitoring network, with relative bias ranging from -15% to 15%. Detailed information on agreement between modelled and observed concentrations is presented in Supplementary Data Report [*Strizhkina et al.,* 2022a].

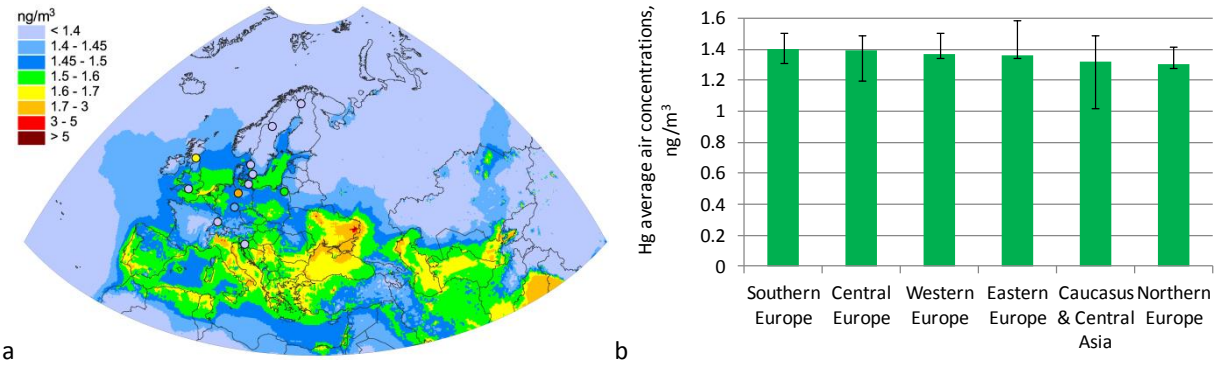

a b

Fig. 3.23. *Annual mean air concentrations of Hg (circles on the map show observed values in the same colour scale) (a) and mean air concentrations of Hg in EMEP sub-regions (b) in 2020. Whiskers show the range of country-average concentrations across countries in each sub-region.*

Deposition fluxes

On average, the greatest Hg deposition fluxes occured in Central Europe, whereas the largest range of Hg deposition is noted in Southern Europe (Fig. 3.24b). The most intensive mercury deposition (higher than 25 g/km^2/y) is modelled for some areas in Poland, Italy, Bosnia and Herzegovina, Romania, Serbia, Turkey and Azerbaijan (Fig. 3.24a). Besides, relatively high mercury deposition fluxes (exceeding 17 g/km^2/y) are noted in Germany, Greece, Slovakia, Bulgaria, over the northern part of the Kola Peninsula and the Black Sea coast. Also elevated fluxes are seen in the high Arctic. It is caused by intensive Hg^0 oxidation and deposition in springtime during the Atmospheric Mercury Depletion Events (AMDEs). However, it should be noted that a major part of the mercury deposited on the snow is later re-emitted to the atmosphere. The agreement between the modelled and measured wet deposition levels is within factor of 2. The more detailed information on comparison between the modelled and measured wet deposition is presented in the Supplementary Data Report [*Strizhkina et al.,* 2022a].

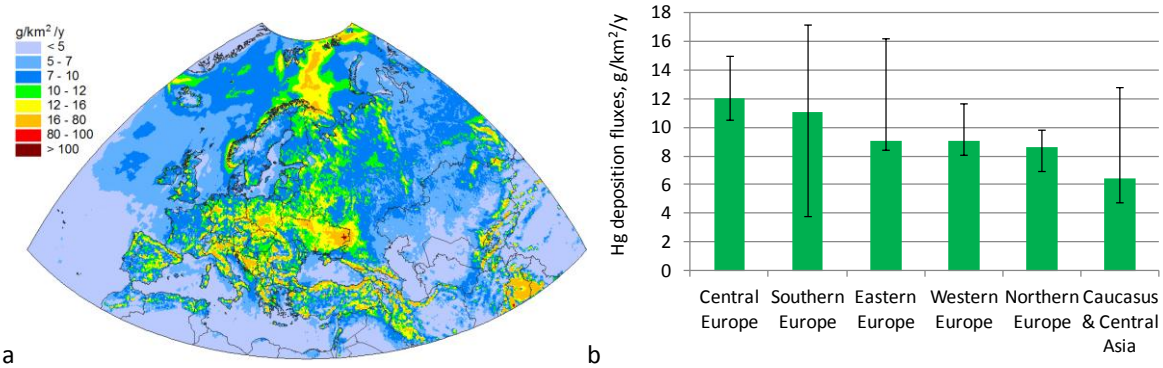

a b

Fig. 3.24. *Annual total deposition flux of Hg (a) and mean total deposition fluxes of Hg to EMEP sub-regions (b) in 2020. Whiskers show the range of country-average concentrations across countries in each sub-region.*

The spatial distribution of Hg total deposition originated from different groups of sources is shown in Fig. 3.25. The largest average relative contribution of EMEP anthropogenic sources is seen in Central

Europe and amounted to 45% to total deposition. In other sub-regions it does not exceed 30% (Fig. 3.25d). The minimum contribution of this type of sources is noted for Northern Europe (13%). The spatial distribution of Hg deposition originated from the EMEP sources is mainly consistent with spatial pattern of Hg emission (Fig. 3.25a, Fig. 3.6c). It can be seen that high deposition fluxes in some particular areas in Poland, Bosnia and Herzegovina and Germany are largely caused by the EMEP anthropogenic sources. Besides, significant fluxes in countries in Southern Europe (e.g. Spain, Italy, Turkey, Romania, Serbia) as well as over the Caucasus and the high Arctic are mostly originated from the non-EMEP sources.

Figure 3.25c shows that the non-EMEP sources contribute a large part to total mercury deposition and their relative contribution ranges from 52% in Central Europe to 85% in Northern Europe. In other sub-regions it amounts to 70-74%. It should be noted that due to the long-time residence of Hg in the atmosphere, non-EMEP sources might contain some fraction of the mercury input from the EMEP anthropogenic sources that was transported out through the boundaries of the region, mixed with inputs from other anthropogenic sources, and transported back into the region in composition of the non-EMEP sources. Mercury emitted from natural and secondary sources within the EMEP domain is mostly transported outside the region, therefore contribution of these sources does not exceed 3% over all EMEP sub-regions (Fig. 3.25b).

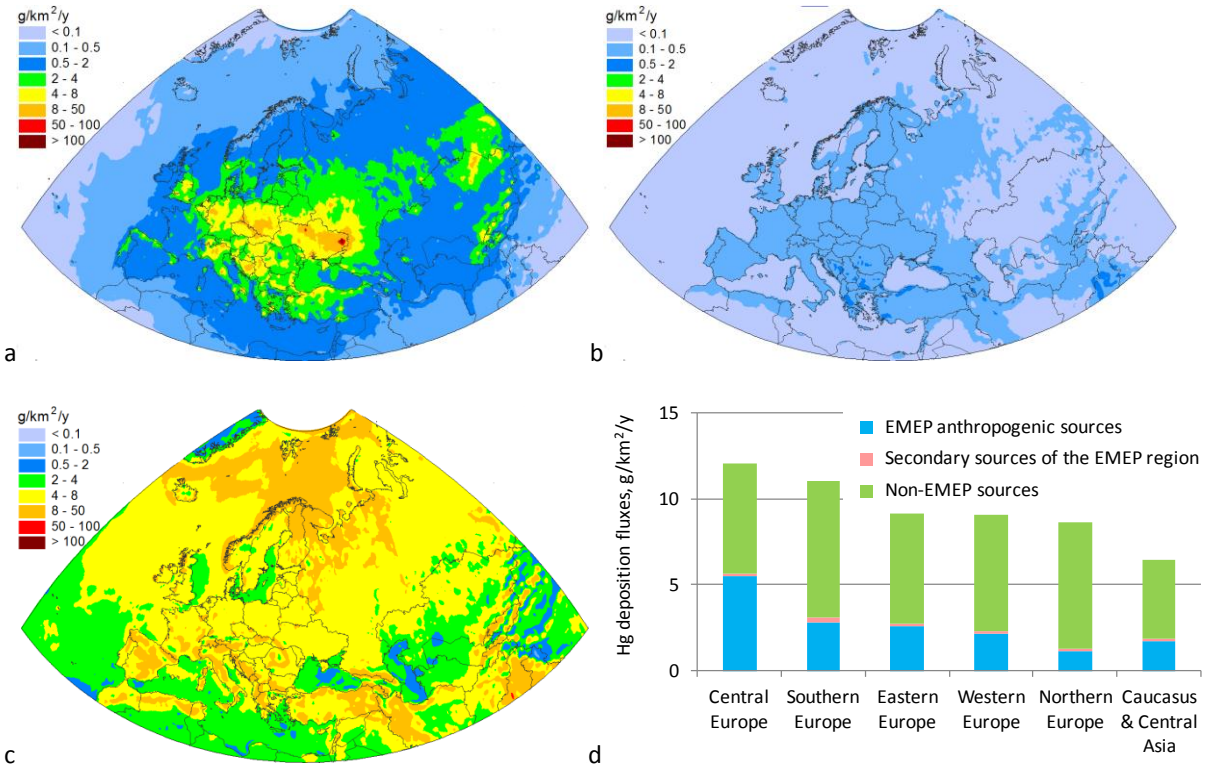

Fig. 3.25. *Annual Hg deposition in 2020 from EMEP anthropogenic sources (a), EMEP secondary sources (natural and re-emission) (b) and non-EMEP sources (c), and mean deposition fluxes from these sources to the EMEP sub-regions (d)*

Changes of the pollution levels between 2019 and 2020

Changes of the mercury pollution levels between 2019 and 2020 due to changes in meteorological conditions are considered in this section. Changes in meteorological conditions led to negligible 1.5 - 2.5% decrease in Hg air concentrations over all EMEP sub-regions (Fig. 3.26b). In particular, decrease is seen over the western part of Russia, the central and southern parts of Italy, Switzerland, Austria, the northern parts of Sweden and Finland, and the southern part of Turkey (Fig. 3.26a). At the same time, there is a slight increase in Portugal, in the north of Italy and over the high Arctic.

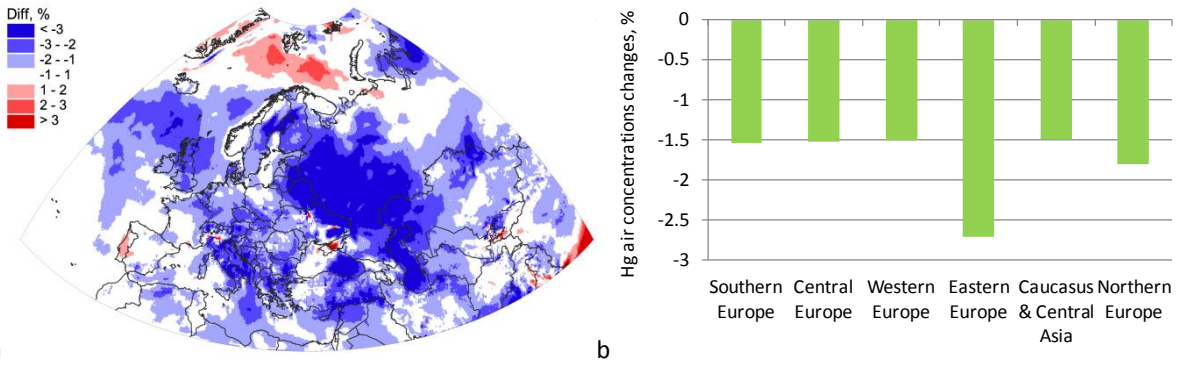

a b

Fig. 3.26. *Relative changes of Hg air concentrations due to the changes in meteorological conditions over the EMEP domain (a) and in the EMEP sub-regions (b) between 2019 and 2020.*

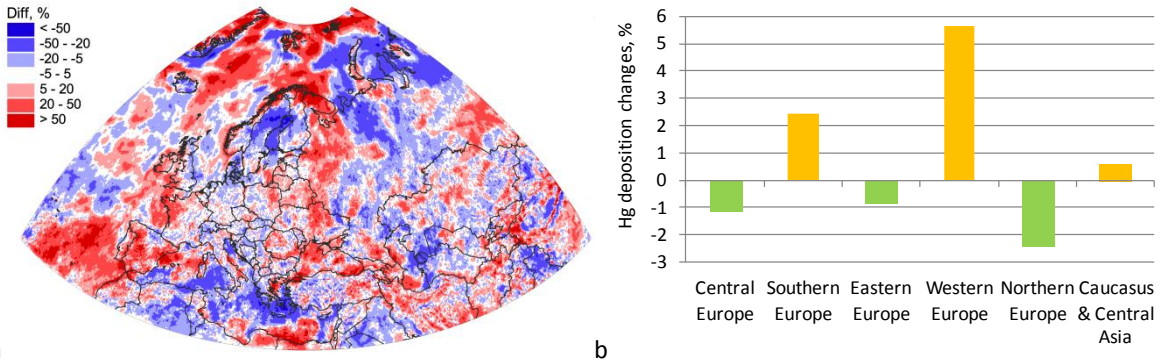

a b

Fig. 3.27. *Relative changes of Hg total deposition due to the changes in meteorological conditions over the EMEP domain (a) and in the EMEP sub-regions (b) between 2019 and 2020.*

Total mercury deposition levels also changed in 2020. Changes in meteorological conditions led to decrease in Central, Eastern and Northern Europe (Fig. 3.27b). In particular, it is seen in Hungary, Austria, Switzerland, Denmark, Slovakia, Albania, Greece, Bosnia and Herzegovina, Finland, the Netherlands and Iceland (Fig. 3.27a). The most significant (more than 20%) decrease is noted in Sweden, Gulf of Bothnia and the Russian Arctic. Also, it is found over the Tyrrhenian, Aegean, Ionian Seas, the northern part of the Adriatic Sea and the Gulf of Venice. At the same time, the meteorological variability caused an increase in deposition fluxes in Southern Europe and, especially, in Western Europe. The most drastic increase of deposition fluxes is noted in Spain, Portugal, Poland, Latvia, the western part of France, the eastern part of Belarus, Romania, Georgia, Armenia,

Azerbaijan and along the northern coastline of Norway as well as over the middle Atlantic, the Celtic Sea, the Bay of Biscay, the Black Sea and the Arctic.

Transboundary transport

In 2020 there were 14 EMEP countries, where contribution of transboundary transport to total mercury deposition from anthropogenic sources does not exceed 50%. They include countries in Central and Southern Europe with high Hg pollution levels caused by national emission sources, namely Bosnia and Herzegovina (37%), Germany (35%), Poland (40%), and Serbia (48%). Besides, these are countries relatively distant from major European emission sources and with low contribution of national anthropogenic sources, in particular, the United Kingdom, Spain, Portugal, Turkey and Kazakhstan (Fig. 3.28a). The predominant role of transboundary transport that explains more than 90% of mercury pollution from anthropogenic sources is seen in 11 countries, including Lithuania, Armenia, Latvia and Belarus. It should be noted that Hg deposition in some countries of that list is characterized by the negligible contribution of their national emissions (Monaco, Liechtenstein, Malta, Cyprus) and remoteness from major emission sources (Kyrgyzstan) in the EMEP region.

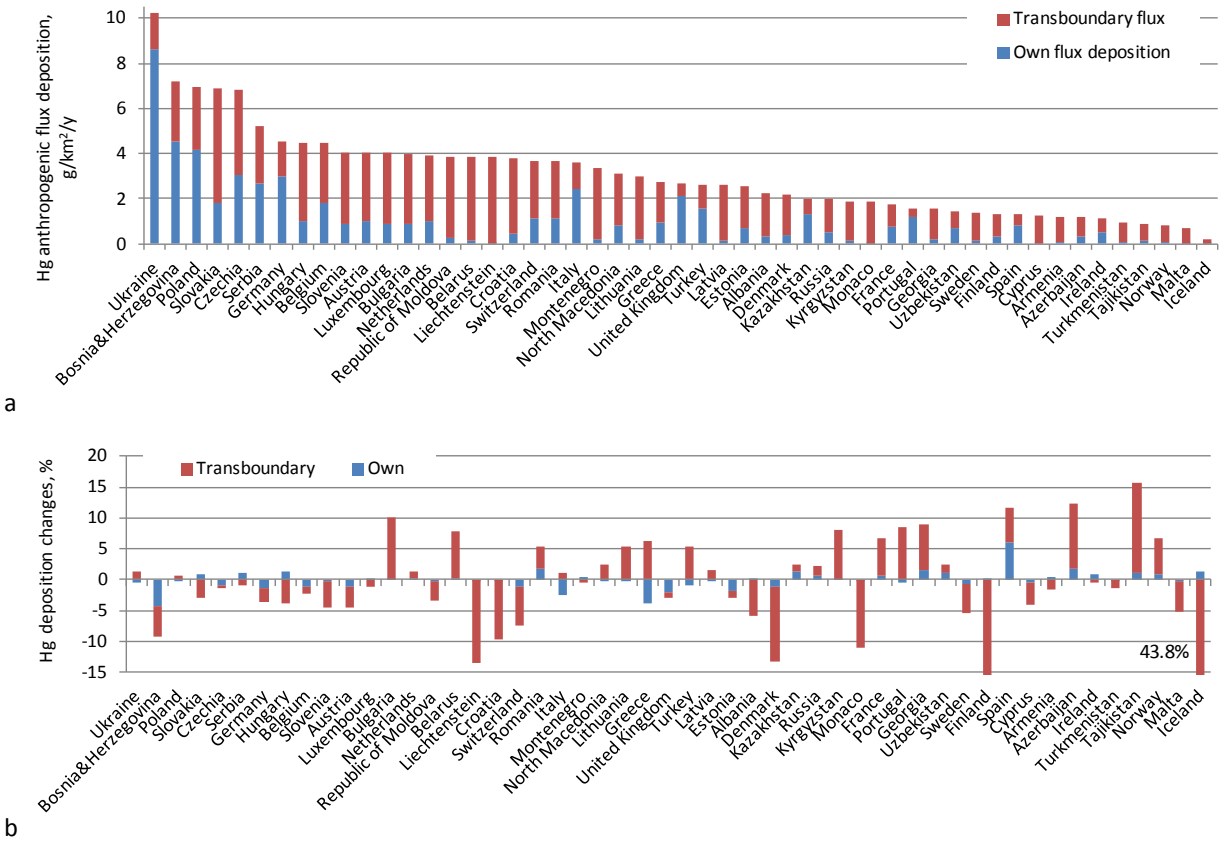

***Fig. 3.28.** . Spatially averaged deposition flux of Hg in the EMEP countries from national and foreign sources in 2020 (a) and relative change of the deposition fluxes between 2019 and 2020 (b).*

In most EMEP countries changes of Hg deposition in 2020 in comparison with the previous year are explained by changes of contribution of the foreign sources (transboundary transport). The most significant relative decrease of deposition (more than 5%), caused by reducing the role of foreign sources, is noted in Iceland, Finland, Monaco, Denmark, Switzerland, Croatia and Liechtenstein (Fig. 3.28b). Also, a 5% decrease is seen in Sweden, Albania and Cyprus. On the other hand, a significant increase (more than 5%) is noticeable in Bulgaria, Belarus, Kyrgyzstan, France, Portugal, Tajikistan, Norway and Azerbaijan. The visible impact of the changes in deposition from national sources is noted in Spain, where it is responsible for a 5% deposition increase, and in Bosnia and Herzegovina, where it led to a 5% decrease.

3.4.5. Polycyclic Aromatic Hydrocarbons (PAHs)

Polycyclic Aromatic Hydrocarbons comprise a large group of organic chemicals that are released to the environment both from natural and anthropogenic emission sources. The most significant part of anthropogenic PAH emissions originates from incomplete combustion of various types of fossil fuels and biomass burning. PAHs belong to semi-volatile compounds that present in the atmosphere in gaseous and particulate phase and undergo chemical reactions. Entering the atmosphere PAHs can be transported over long distances. It was recognized that some of the PAHs have carcinogenic, mutagenic, and teratogenic properties and can pose serious risk to human health [*Keyte et al.*, 2013; *Kim et al.*, 2013].

Assessment of PAH pollution levels and exceedances of air quality guidelines is made for the 4 selected PAH compounds, targeted by the LRTAP Protocol on POPs (namely benzo(a)pyrene, benzo(b)fluoranthene, benzo(k)fluoranthene, and indeno(1,2,3-cd)pyrene). In this section overview of PAH pollution levels and long-range transport in the EMEP region is presented based on the results of monitoring and model simulations for 2020. Information on exceedances of air quality guidelines for 4 PAHs is given in Section 3.5.2. More detailed results of modelling and monitoring of PAH pollution levels can be found in the Supplementary Data Report [*Strizhkina et al.*, 2022b].

Air concentrations

Observed and modelled annual mean air concentrations of the sum of 4 PAHs in 2020 are illustrated in Fig. 3.29a. PAH concentrations in air in the EMEP region vary from less than 0.1 ng/m^3 up to 3 ng/m^3 and higher. The highest average atmospheric concentrations are estimated for the countries of Central Europe followed by Southern and Eastern Europe (Fig. 3.29b). Model simulations indicate high levels of pollution (above 1.5 ng/m^3) in Poland, Czechia, Slovakia, and Hungary. High level of concentrations is also noted for selected areas of Italy, Croatia, Serbia, Romania, and a number of regions of the eastern part of Europe. In some of these countries pollution levels exceeded air quality guidelines established for B(a)P by the EU and WHO (Section 3.5.2). Other areas of the EMEP region are characterized by relatively low air concentrations of 4 PAHs (0.1 - 1.5 ng/m^3) with the lowest levels (below 0.1 ng/m^3) in Northern Europe (Fig. 3.29b).

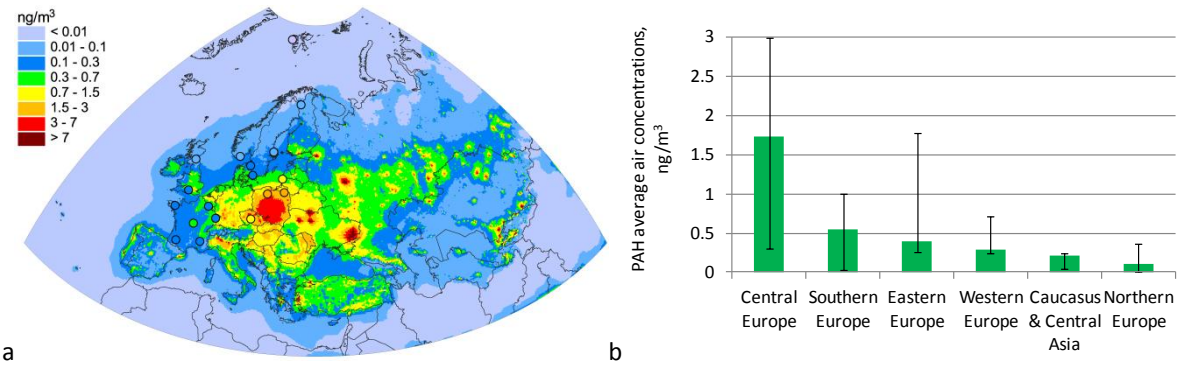

a b

Fig.3.29. *Annual mean air concentrations of the sum of 4PAHs (circles on the map show observed values in the same color scale) (a) and average air concentrations of the sum of 4 PAHs in the EMEP sub-regions (b) in 2020. Whiskers show the range of concentrations in particular countries of the sub-region.*

Monitoring of 4 PAHs in 2020 was carried out at 34 monitoring sites in 14 EMEP countries. Evaluation of the modelling results against EMEP measurements shows good agreement of modelled and observed concentrations of the sum of 4 PAHs with low bias (-3%) and high spatial correlation (0.91). For about 80% of the monitoring stations, the differences between the modelling results and measured concentrations are within a factor of 2. Evaluation of modelling results for individual 4 PAH compounds against the EMEP measurements indicates -9%, 14%, -6%, -3% bias for B(a)P, B(b)F, B(k)F and I(cd)P, respectively. The model satisfactory reproduced the spatial distribution of observed 4 PAH air concentrations with correlation coefficients about 0.80-0.95.

In addition to this, modelled B(a)P concentrations for 2020 were compared with observed concentrations collected in the EEA AQ e-Reporting database. Measurements of B(a)P in air at background rural and suburban stations in 22 countries were selected for the comparison. Model predictions showed generally higher bias between modelled and observed concentrations of EEA compared to EMEP measurements. In particular, the model tended to under-predict observed B(a)P concentrations by 54%. At the same time, modelling results showed good spatial correlation with measurements (correlation coefficient about 0.8). The differences between the modelled and measured concentrations were within a factor of 2 for about 50% of the monitoring stations.

Deposition fluxes

Spatial distribution of the sum of 4 PAHs deposition fluxes in the EMEP region in 2020 is shown in Fig. 3.30a. Deposition flux of PAHs depends on a number of factors that include distribution of emission sources, properties of underlying surface and precipitation amount. The highest deposition fluxes (200-400 g/km^2/y and higher) were estimated for some of the countries of Central and Eastern Europe. Moderate levels of deposition (70-200 g/km^2/y) took place in countries of Western and Southern Europe. Similar to air concentrations, the highest spatially averaged deposition fluxes of 4 PAHs are noted for Central Europe (about 170 g/km^2/y), and the lowest ones for Caucasus and Central Asia (about 15 g/km^2/y) (Fig. 3.30b).

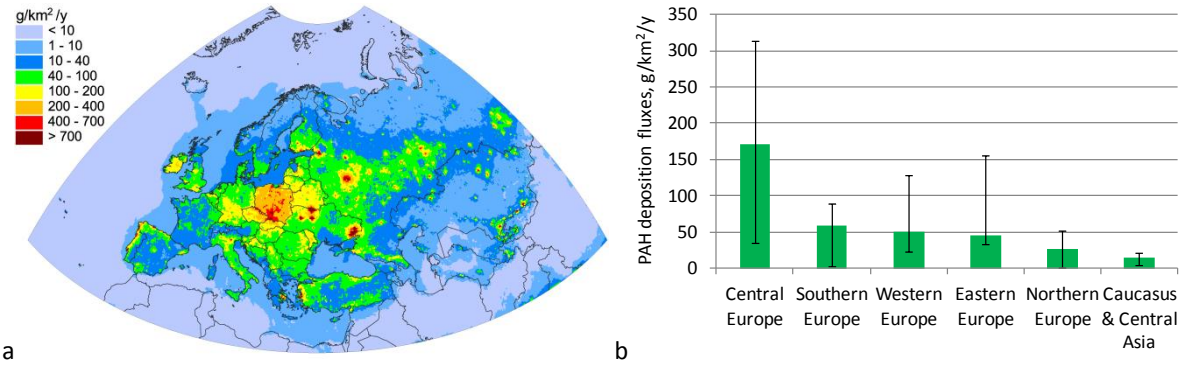

a b

Fig. 3.30. *Annual total deposition flux of the sum of 4 PAHs (a) and average total deposition fluxes of the sum of 4 PAHs to the EMEP sub-regions (b) in 2020. Whiskers show the range of deposition fluxes in particular countries of the sub-region.*

Three groups of emission sources of PAH deposition are considered in the model simulations, namely, EMEP anthropogenic sources, secondary sources (re-volatilization from surface compartments) in the EMEP domain and emission sources located outside the EMEP countries (non-EMEP sources). The largest contribution (more than 80%) is made by the EMEP anthropogenic sources, while other types of emission sources contributed less than 20%.

Changes of pollution levels between 2019 and 2020

Relative changes of PAH air concentrations between 2019 and 2020 due to meteorological variability are shown for the whole EMEP domain (Fig. 3.31a), and as spatially averaged air concentrations in six sub-regions (Fig. 3.31b). Over the most part of the EMEP countries differences of air concentrations between two years varied within ±50%. The largest decrease of spatially averaged air concentrations is estimated for Western Europe (about 16%), while the lowest one for Central Europe (about 1%). For other sub-regions model simulations show decline of PAH concentrations by 7-9%. For some of the areas of Northern, Western, and Central Europe increase of air concentrations is estimated (e.g. Iceland, northern parts of Norway and Sweden). More significant increase of air concentrations is noted for Mediterranean Sea, Atlantic Ocean, and Arctic region. At the same, time these areas are characterized by significantly lower pollution levels compared to EMEP countries.

Relative changes of total deposition fluxes of 4 PAHs from 2019 to 2020 are illustrated in Fig. 3.32a. Similar to air concentrations, deposition fluxes varied within the range of ±50% between 2019 and 2020 for most of EMEP countries. Contrary to air concentrations an increase of spatially averaged PAH deposition fluxes is estimated for Northern Europe as well as for Caucasus and Central Asia sub-regions by almost 10% and 4%, respectively (Fig. 3.32b). Other sub-regions are characterized by negligible decline. Similar to air concentrations, more significant relative increase of deposition fluxes is estimated for the Arctic region and some areas of Atlantic Ocean and the Mediterranean Sea. Estimated changes in PAH concentrations and deposition fluxes from 2019 to 2020 can be attributed to inter-annual variations of meteorological conditions, namely, temperature and atmospheric circulation patterns, described in Section 3.1.

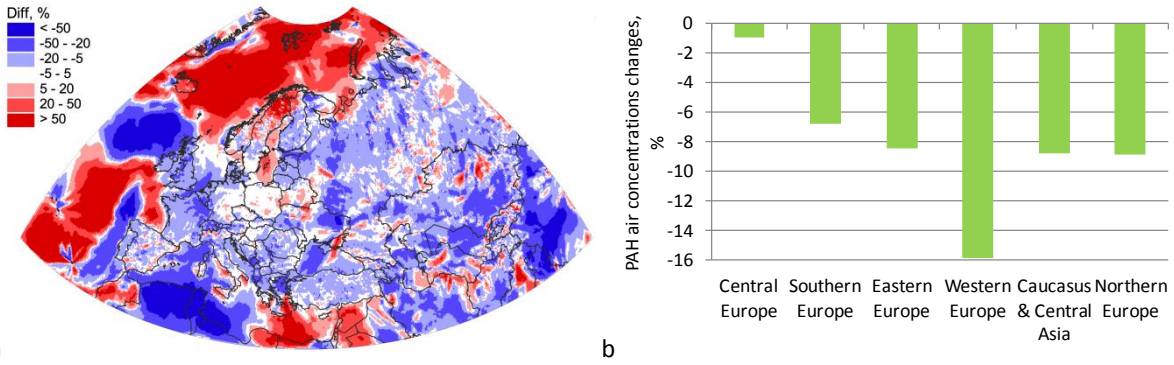

Fig. 3.31. *Relative changes of the sum of 4 PAHs air concentrations between 2019 and 2020 over the EMEP domain due to meteorological conditions (a). The bar chart (b) shows relative changes of concentrations of the sum of 4 PAHs in EMEP sub-regions.*

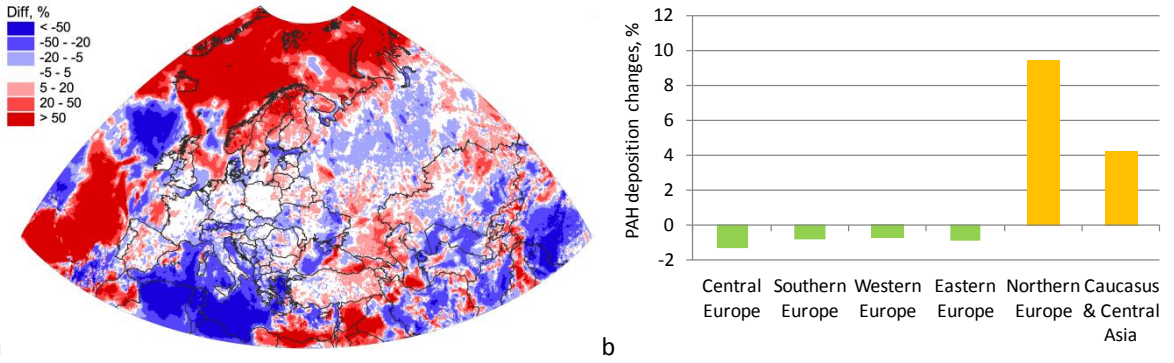

Fig. 3.32. *Relative changes of the sum of 4 PAHs deposition between 2019 and 2020 over the EMEP domain due to meteorological conditions (a). The bar chart (b) shows relative changes of deposition fluxes of the sum of 4 PAHs in the EMEP sub-regions.*

Transboundary transport

Modelling of PAH long-range transport and country-to-country deposition fluxes permit to characterize relative contributions of national and foreign emission sources to total PAH deposition in particular countries. Spatially averaged deposition fluxes of the sum of 4 PAHs to EMEP countries are shown in Fig. 3.33a. The highest deposition flux is estimated for Poland (about 250 g/km^2/y) followed by Czechia and Slovakia, while the lowest one is calculated for Iceland and Malta (about 1 g/km^2/y). PAH deposition from transboundary transport exceeds deposition from national sources in 16 EMEP countries (e.g. Slovakia, Sweden, and Estonia). The highest contribution of transboundary transport (about 97 – 99%) is noted for Liechtenstein, Monaco and Montenegro due to their relatively small territory or low national emissions. The lowest contribution of transboundary transport (below 10%) is estimated for Portugal, Italy, Spain, Turkey and Ireland due to their relative remoteness from major foreign emission sources. Detailed information on transboundary pollution for each EMEP country and for all selected PAHs is presented in Supplementary Data Report [*Strizhkina et al.*, 2022b].

Changes of PAH deposition to each EMEP country from national and foreign emission sources between 2019 and 2020 are shown in Fig. 3.33b.

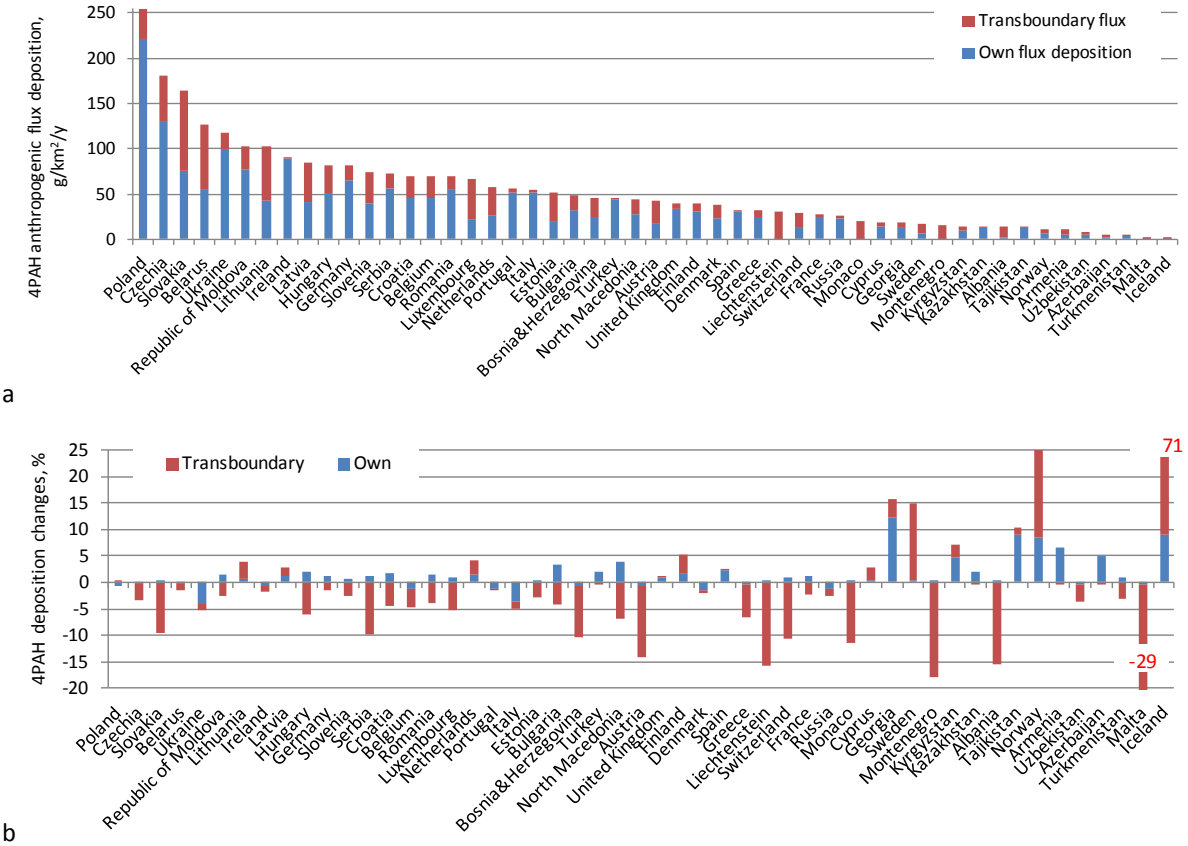

Fig. 3.33. *Spatially averaged deposition flux of the sum of 4 PAHs in the EMEP countries from national (national flux) and foreign (transboundary flux) anthropogenic emission sources in 2020 (a) and relative change of the deposition fluxes between 2019 and 2020 due to meteorological variability (b).*

For most of the countries difference between PAH deposition fluxes in 2019 and 2020 ranges within ±15%. A few exceptions include Iceland, Malta, Norway and Montenegro. Changes of transboundary fluxes were more significant compared to the changes of deposition fluxes from national sources. In some countries (e.g. Bulgaria, Hungry, Germany) deposition from national emission sources increased in 2020 while deposition from foreign emission sources declined. Difference of estimates of PAH pollution levels between 2019 and 2020 is explained by the effect of inter-annual variability of meteorological parameters.

3.4.6. PCDD/Fs, PCBs and HCB

This section provides a summary of modelled and observed pollution levels of PCDD/Fs, PCBs, and HCB in 2020 in the EMEP region. These pollutants are known to be semi-volatile, persistent and widely dispersed in the environment. Studies of their adverse effects indicate that they pose risk to human health and biota [*WHO*, 2000; 2003; *Starek-Świechowicz et al.,* 2017]. PCDD/Fs, PCBs, and

HCB are formed as unintentional by-products during various anthropogenic activities (e.g. combustion of fossil fuels, chemical manufacture processes, waste incineration) and can be released into the atmosphere and other environmental compartments. Long-term accumulation in the terrestrial and aquatic compartments can lead to their secondary emissions (re-volatilization) to the atmosphere making significant contribution to the pollution levels.

Air concentrations

Annual mean modelled PCDD/Fs, PCB-153 and HCB air concentrations in the EMEP domain simulated for 2020 are presented in Figs. 3.34a,c,e. Model predictions of PCDD/Fs and PCB-153 concentrations in the EMEP countries vary in a wider range for PCDD/Fs and PCB-153 compared to HCB concentrations. Relatively homogeneous distribution of HCB can be attributed to its more significant persistence in the atmosphere. Along with the modelling results annual mean concentrations, measured at the EMEP monitoring stations in 2020, are shown on the maps.

Averaged levels of concentrations for six sub-regions of the EMEP region are given in Figs. 3.34b,d,f. The highest concentrations of PCDD/Fs are estimated for some of the countries in Eastern and Southern Europe (about 16 fg I-TEQ/m^3), of PCB-153 for Western Europe (about 6 pg/m^3), and for HCB for Eastern and Central Europe (about 50 pg/m^3). The lowest pollution levels are noted for countries in Northern Europe as well as in Caucasus and Central Asia.

Comparison of the modelling results with observed PCB-153 and HCB concentrations in 2020 at the EMEP monitoring network shows reasonable agreement between measurements and modelled concentrations. Relative bias between modelled and observed concentrations is about 6% for PCB-153 and -11% for HCB. For half of the stations, the model predictions are within a factor of 2 compared to measured concentrations. Differences higher than a factor 2 were found for the stations CZ0003R, IS091R, NO0090R and NO0042R in case of PCB-153, and for IS091R, NO0042R, SE0014R and SE0022R in case of HCB.

Measurements of PCDD/F air concentrations in 2020 were carried out at two EMEP stations SE0014R and SE0022R. Comparison of modelled and observed air concentrations shows satisfactory agreement for SE0014R with some overestimation about 8%. In case of SE0022R the model tended to underestimate observed concentrations with the bias of about -65%. More detailed information on agreement between the modelled and observed concentrations of POPs is given in Supplementary Data Report [*Strizhkina et al.*, 2022b].

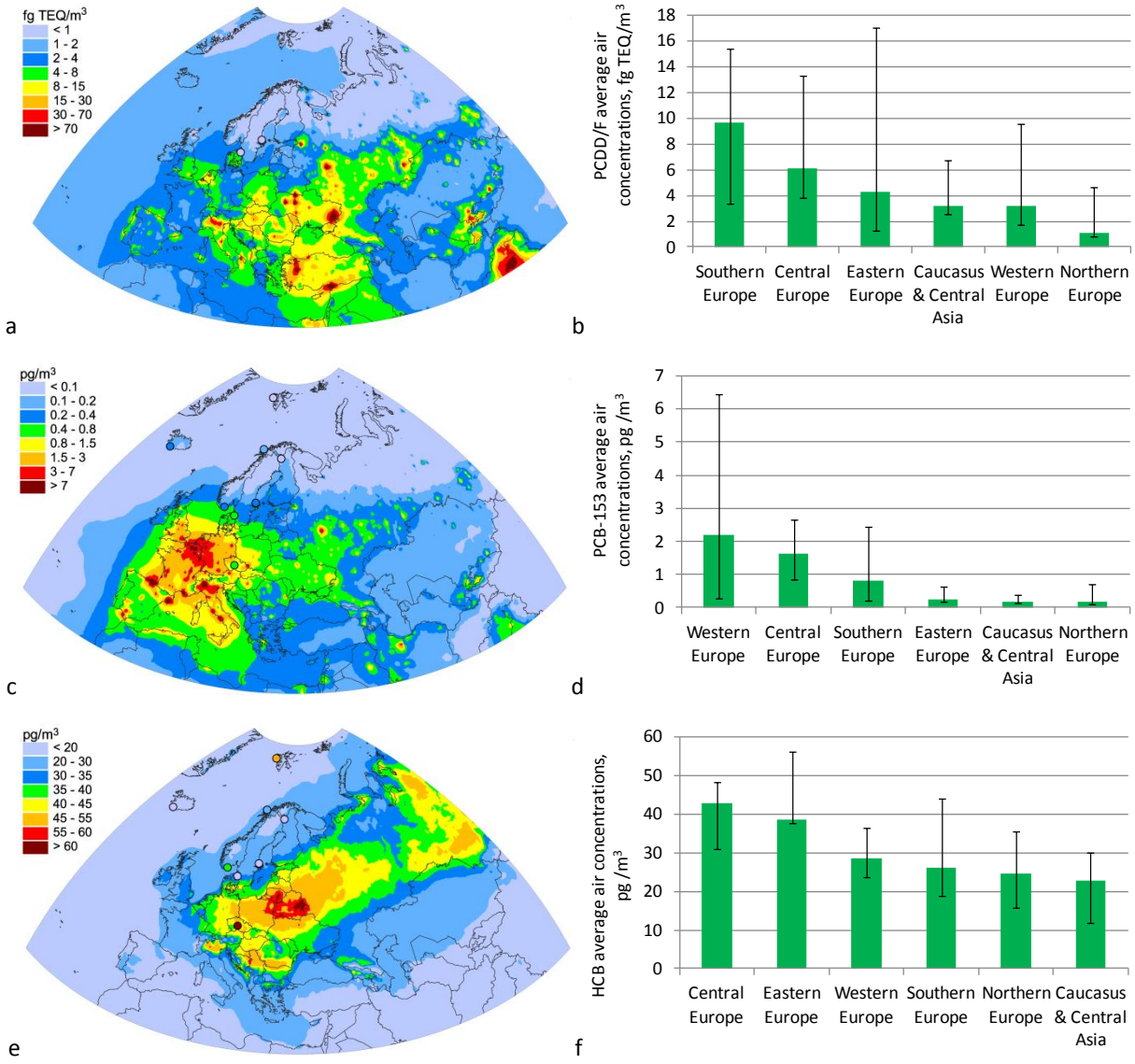

Fig. 3.34. *Annual mean modelled and observed air concentrations of PCDD/Fs (a), PCB-153 (c), and HCB (e) (circles on the map show observed values in the same color scale) and averaged air concentrations of PCDD/Fs (b), PCB-153 (d), and HCB (f) in the EMEP sub-regions in 2020. Whiskers show the range of concentrations in particular countries of the sub-regions.*

Deposition fluxes

Modelled PCDD/Fs, PCB-153 and HCB annual deposition fluxes in the EMEP domain, simulated for 2020, are demonstrated in Fig. 3.35a,c,e. Annual deposition fluxes depend on a number of factors, including location of main emission sources, precipitation amounts, properties of underlying surface and contribution of secondary emissions.

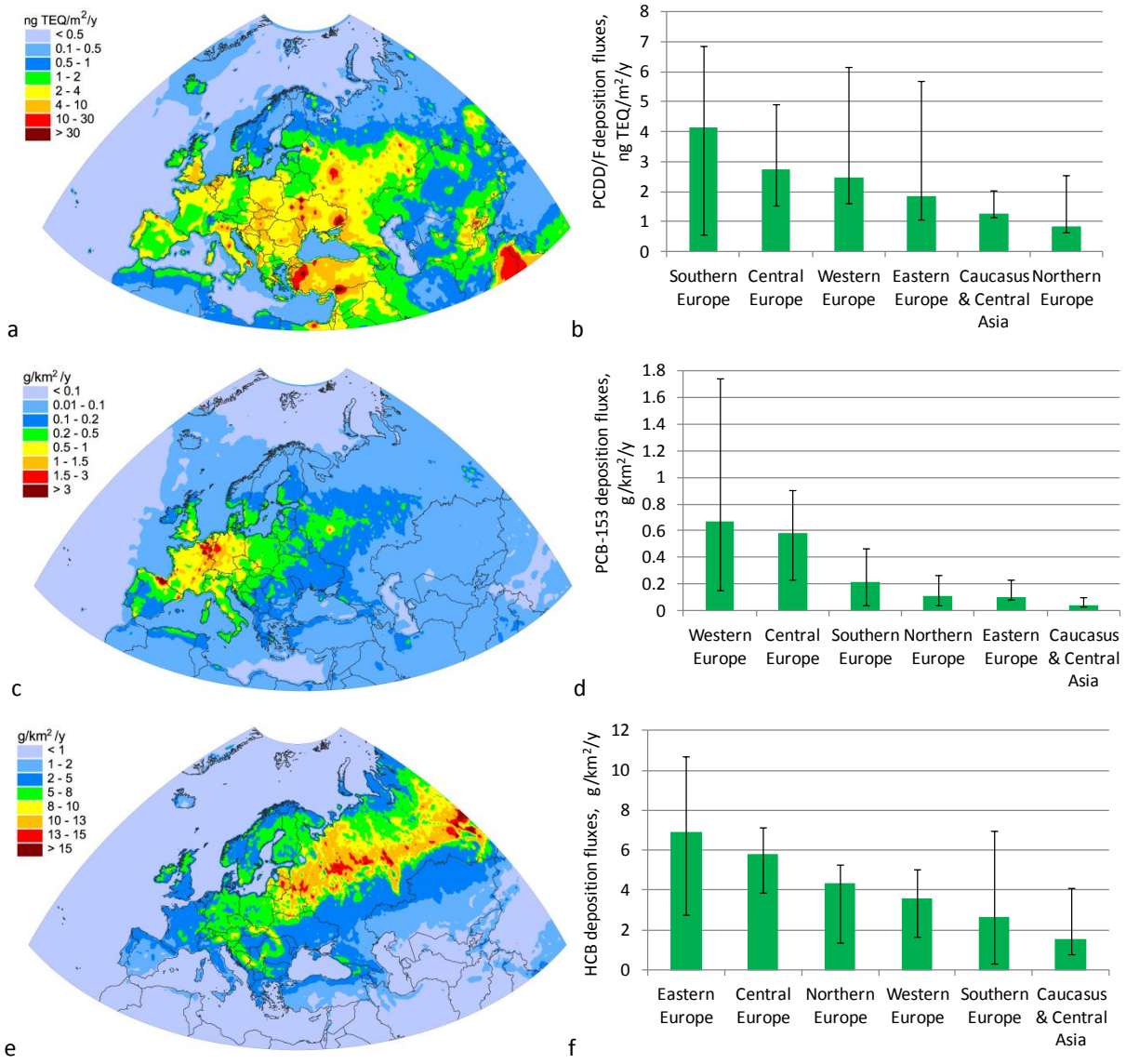

Fig. 3.35. *Annual modelled deposition fluxes of PCDD/Fs (a), PCB-153 (c), and HCB (e) and averaged deposition fluxes of PCDD/Fs (b), PCB-153 (d), and HCB (f) in the EMEP sub-regions in 2020. Whiskers show the range of deposition fluxes in particular countries of the sub-regions.*

Spatial distributions of PCDD/Fs, PCB-153 and HCB deposition fluxes generally follow the distribution of air concentrations of these pollutants. In particular, maximum values of deposition fluxes are estimated for countries in Western, Central and Southern Europe in case of PCDD/Fs and PCB-153. For HCB relatively high deposition fluxes are indicated for Eastern, Central and Northern Europe.

Average annual total deposition fluxes of PCDD/Fs, PCB-153 and HCB for different EMEP sub-regions are illustrated in Fig. 3.35b,d,f. The highest average annual deposition fluxes took place in Southern Europe for PCDD/Fs, in Western Europe for PCB-153 and in Eastern Europe for HCB. The lowest pollution levels are estimated for Northern Europe in case of PCDD/Fs, and for Caucasus and Central Asia in case of PCB-153 and HCB.

Three groups of emission sources were considered in the model simulations, namely, EMEP anthropogenic sources, secondary sources (re-volatilization) in the EMEP domain and emission sources located outside the consolidated area of all EMEP countries (non-EMEP sources). The contributions of these three groups of sources to average annual deposition fluxes in six sub-regions of EMEP domain are shown in Fig. 3.36.

Modelling results show that the highest contributions to deposition fluxes was made by secondary emission sources of the EMEP domain (55%, 69% and 78% on average for PCDD/Fs, PCB-153 and HCB, respectively). The second most important contributors for PCDD/Fs and PCB-153 were the EMEP anthropogenic emissions (about 34% and 27% respectively). For HCB the second most important contributor was the emission outside the EMEP domain boundaries while the EMEP anthropogenic emissions contributed less than 1%.

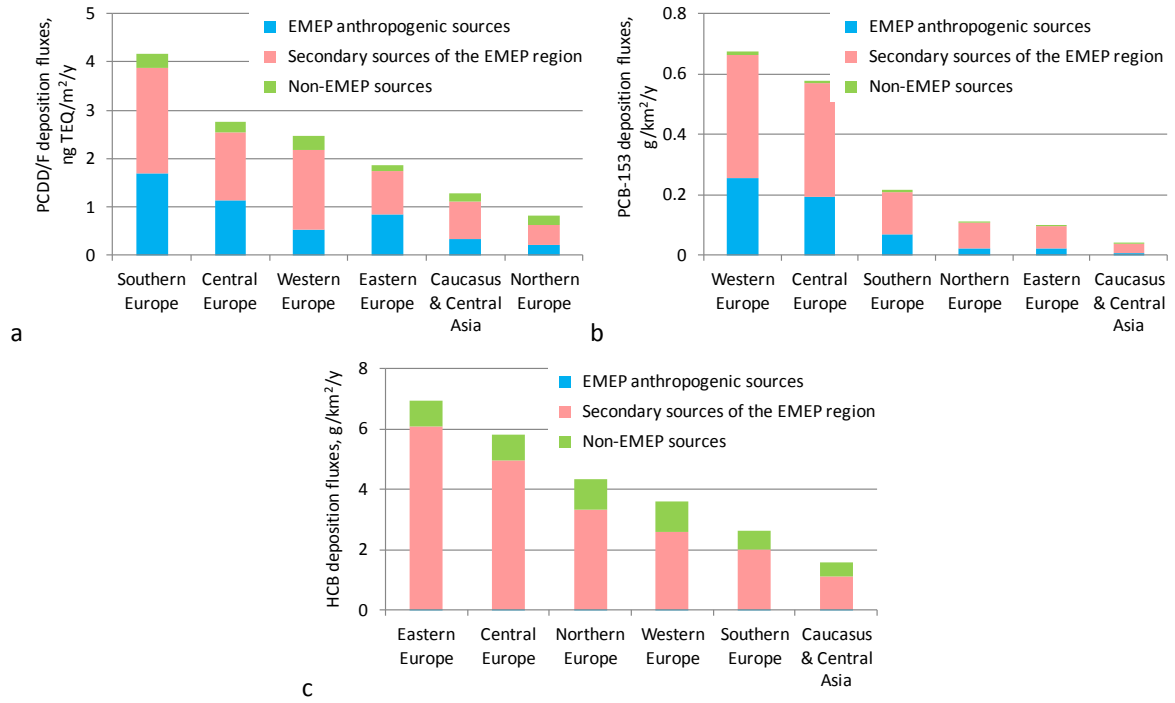

Fig. 3.36. *Annual average deposition fluxes of PCDD/Fs (a), PCB-153 (b) and HCB (c) to EMEP sub-regions in 2020 from the EMEP anthropogenic sources, secondary sources (re-volatilization) and non-EMEP sources.*

Changes of the pollution levels between 2019 and 2020

This section describes inter-annual changes of pollution levels between 2019 and 2020 due to variability of meteorological conditions. To evaluate the effect of changes of meteorological parameters, sensitivity model simulations were carried out using meteorological data for 2019 and 2020 and the same emission dataset for 2019.

Relative changes of PCDD/Fs, HCB, and PCB-153 annual mean air concentrations between 2019 and 2020 are shown in Fig. 3.37. For all sub-regions PCDD/F air concentrations declined with the exception of Central Europe. The largest decline was estimated for Western Europe (about 7%)

followed by Eastern Europe (about 6%). For Central Europe small increase of concentrations was calculated by the model. In case of PCB-153, the largest decline is noted for Western Europe (about 6%) as well as for Caucasus and Central Asia (about 5%). Southern and Eastern Europe are characterized by negligible increase of pollution levels. HCB air concentrations declined in all the sub-regions with the largest decrease in Central Europe (about 16%) followed by Southern Europe (about 14%).

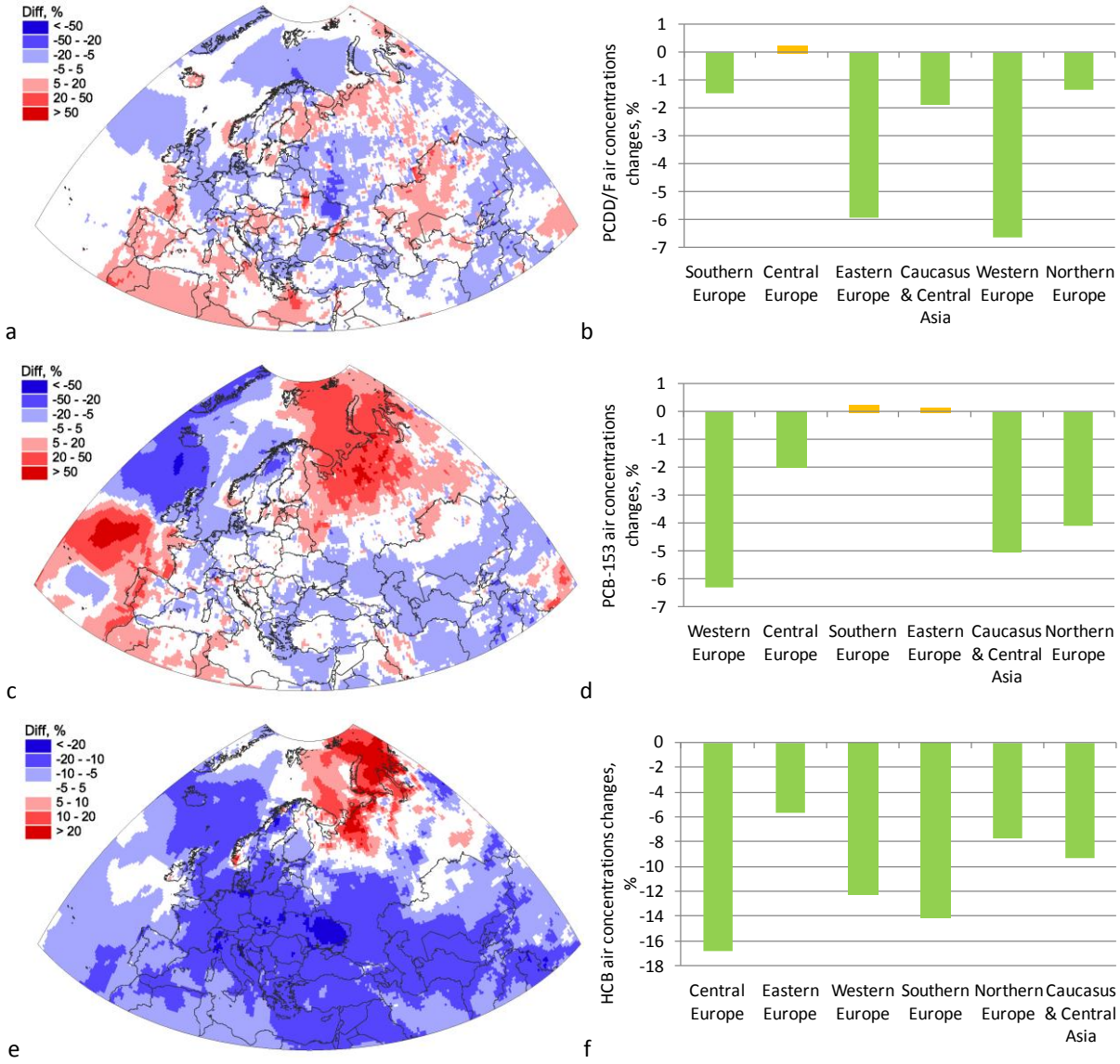

Fig. 3.37. *Relative changes of PCDD/Fs, PCB-153 and HCB air concentrations between 2019 and 2020 in the EMEP domain (a,c,e) and in its six sub-regions (b,d,f).*

Relative changes of PCDD/Fs, HCB, and PCB-153 annual deposition fluxes between 2019 and 2020 are demonstrated in Fig. 3.38. Deposition of PCDD/Fs increased in Northern Europe, Caucasus and Central Asia and Eastern Europe by 6%, 3% and 2%, respectively. In Central Europe decline of deposition fluxes by 5% is noted. Deposition fluxes of PCB-153 in Eastern Europe were higher by 6% in 2020 compared to 2019. At the same time, in Caucasus and Central Asia decrease of PCB-153 deposition by about 4% took place. Similar to air concentrations, deposition fluxes of HCB decreased

in all the sub-regions. The largest change was estimated for Central Europe (about -14%) followed by Southern Europe (about -13%). Inter-annual changes of air concentrations and deposition fluxes described above can be attributed to the changes of air temperature, precipitation amount and pathways of atmospheric circulation.

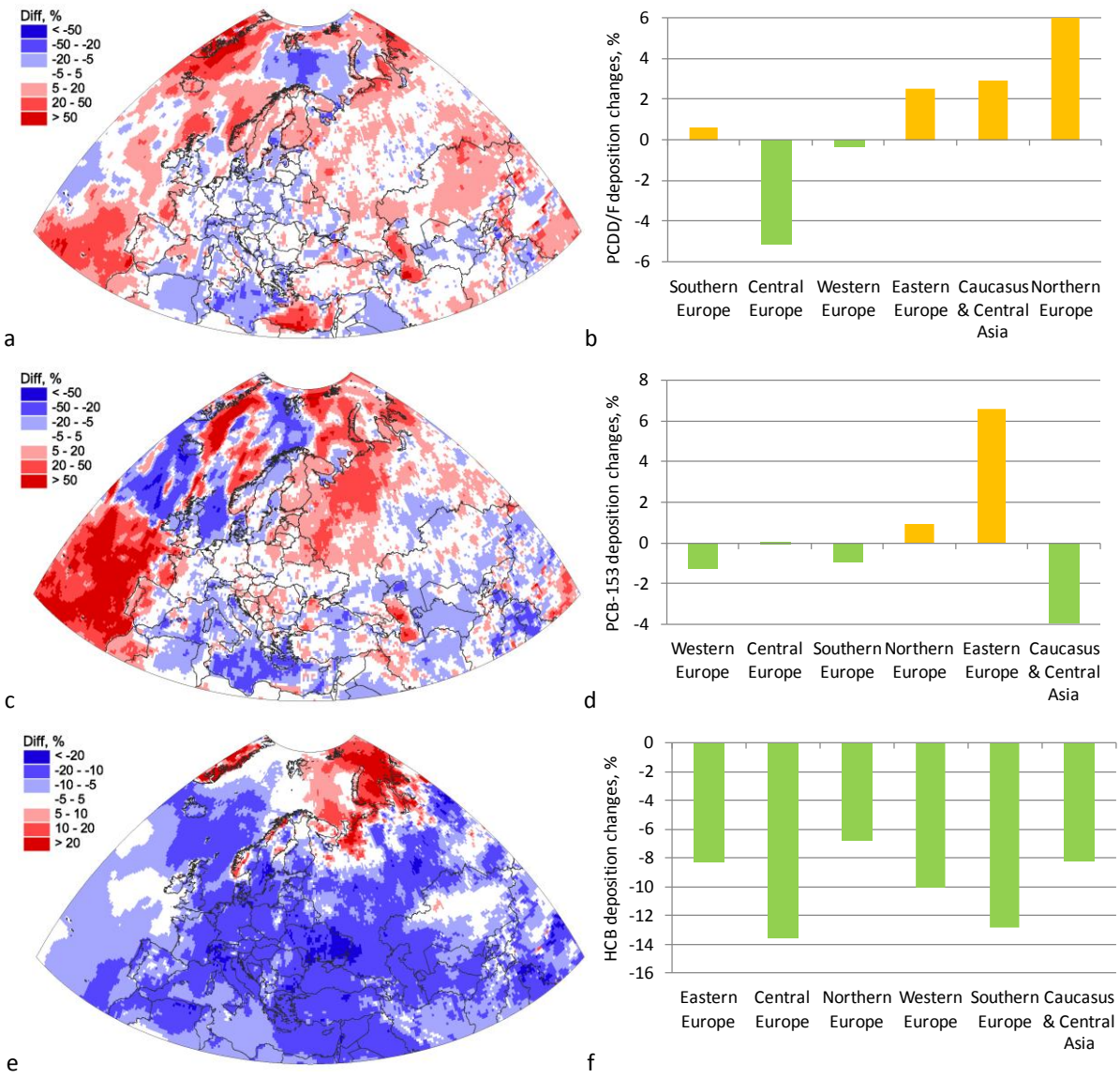

Fig. 3.38. *Relative changes of PCDD/Fs, PCB-153 and HCB deposition fluxes between 2019 and 2020 in the EMEP domain (a,c,e) and in its six sub-regions (b,d,f).*

Transboundary transport

Anthropogenic component of deposition to the EMEP countries can be split into two parts: deposition caused by national emission sources and deposition caused by transboundary atmospheric transport from the sources of other EMEP countries (foreign sources). The example of modelling results, evaluating contributions of national and foreign sources to PCB-153 deposition, is presented in Fig. 3.39. The largest deposition fluxes were estimated for the Benelux countries

(Belgium, Luxembourg and the Netherlands), while the lowest ones for the Central Asian countries and Iceland.

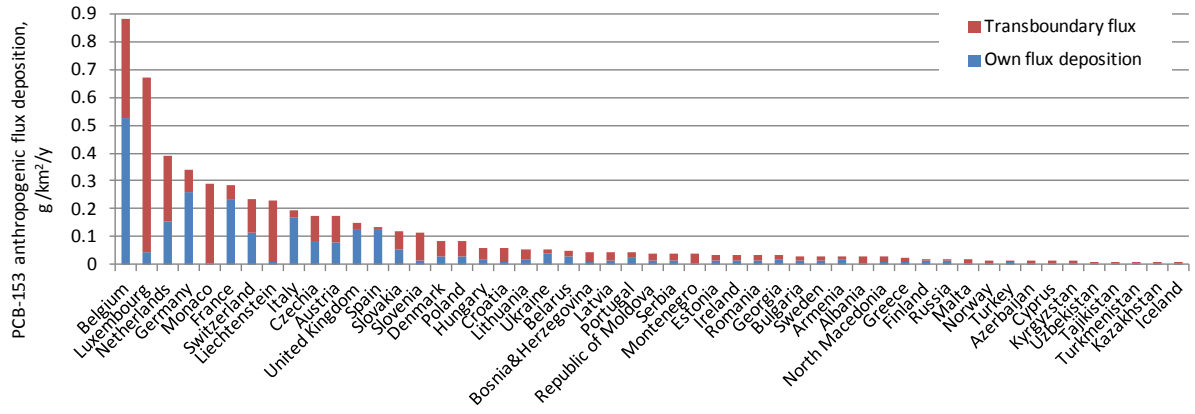

Fig. 3.39. *Spatially averaged deposition flux of PCB-153 over EMEP countries from national and foreign sources in 2020.*

Modelling results indicate that the fraction of transboundary transport exceeds 50% in 20 from 51 EMEP countries for PCDD/Fs, in 36 countries for PCB-153 and in 37 countries for HCB. Thus, model simulations indicate that transboundary transport of POP pollution plays important role in the contamination of the EMEP countries. The highest contribution of transboundary transport is noted for the countries with small territory and/or low national emissions (e.g. in Liechtenstein, Monaco, Montenegro). The lowest contribution of transboundary transport is estimated for the countries with substantial national emissions and relatively large territory (e.g. in Poland, Kazakhstan, Italy). Furthermore, significant influence of national sources is noted for the countries located in the western part of the EMEP region due to predominant westerly atmospheric transport and relative remoteness from major foreign emission sources.

According to the modelling results variability of meteorological conditions between 2019 and 2020 resulted in changes of PCDD/Fs, PCB-153 and HCB deposition fluxes from -10% to 10% in the majority of EMEP countries. As an example, in Fig. 3.40 the differences of PCB-153 deposition fluxes caused by inter-annual meteorological variability between 2019 and 2020 are illustrated. The largest increase of deposition (by 21%) is estimated for Norway, while the largest decrease of deposition (by 26%) for Iceland. In most of the countries estimated changes of PCB-153 deposition were due to the change of transboundary contribution. Some of the countries are characterized by the changes of national and transboundary components of deposition in opposite directions (e.g. Denmark, Estonia, Iceland). More detailed information on POP deposition levels and contributions of national and foreign sources as well as their changes from 2019 to 2020 can be found in Supplementary Data Report [*Strizhkina et al.*, 2022b].

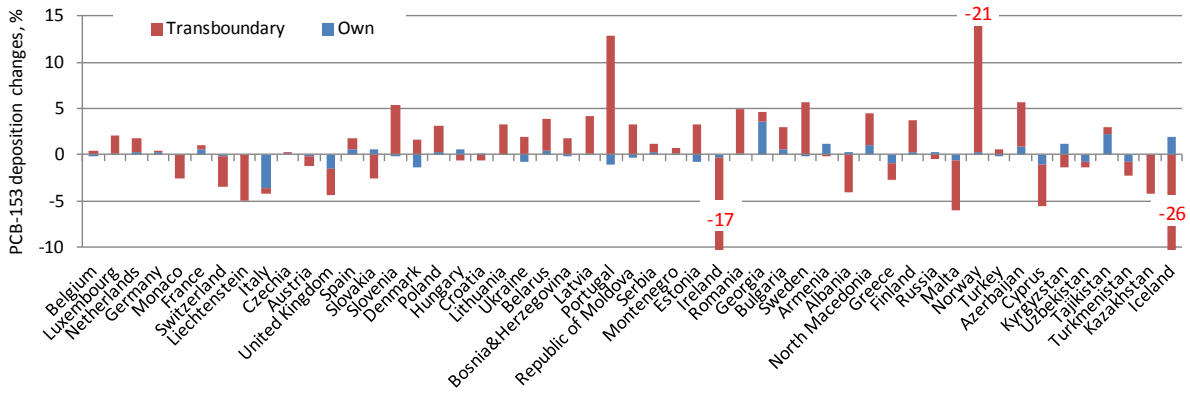

Fig. 3.40. *Relative changes of the deposition fluxes of PCB-153 contribution between 2019 and 2020.*

3.4.7. Country-specific information

Dissemination of the assessment results and other relevant information, aimed at supporting political decisions, is of high importance. Annual reports containing current status of heavy metals and POPs pollution within the EMEP region are supplemented by presentation of information on the web. It provides more flexible and targeted assistance to national experts and authorities with data required for the environment protection regulations.

Detailed information on heavy metals and POPs pollution is given for each individual EMEP country. This country-specific information includes variety of data on the model assessment for particular country collected in one place to make easier access to information and its analysis by national experts. Information is presented in the form of diagrams, maps and data files for all the EMEP countries at the MSC-E website (http://msceast.org/index.php/pollution-assessment/emep-countries-menu). In addition, the country-specific information for the EECCA countries is also available in Russian (http://www.ru.msceast.org/index.php/pollution-assessment/eecca-countries-menu).

Country-specific information includes the following elements:

- Spatial distribution of pollution levels;
- Transboundary pollution of a country;
- Contribution of national sources to transboundary transport;
- Ecosystem-specific deposition (17 land cover categories).

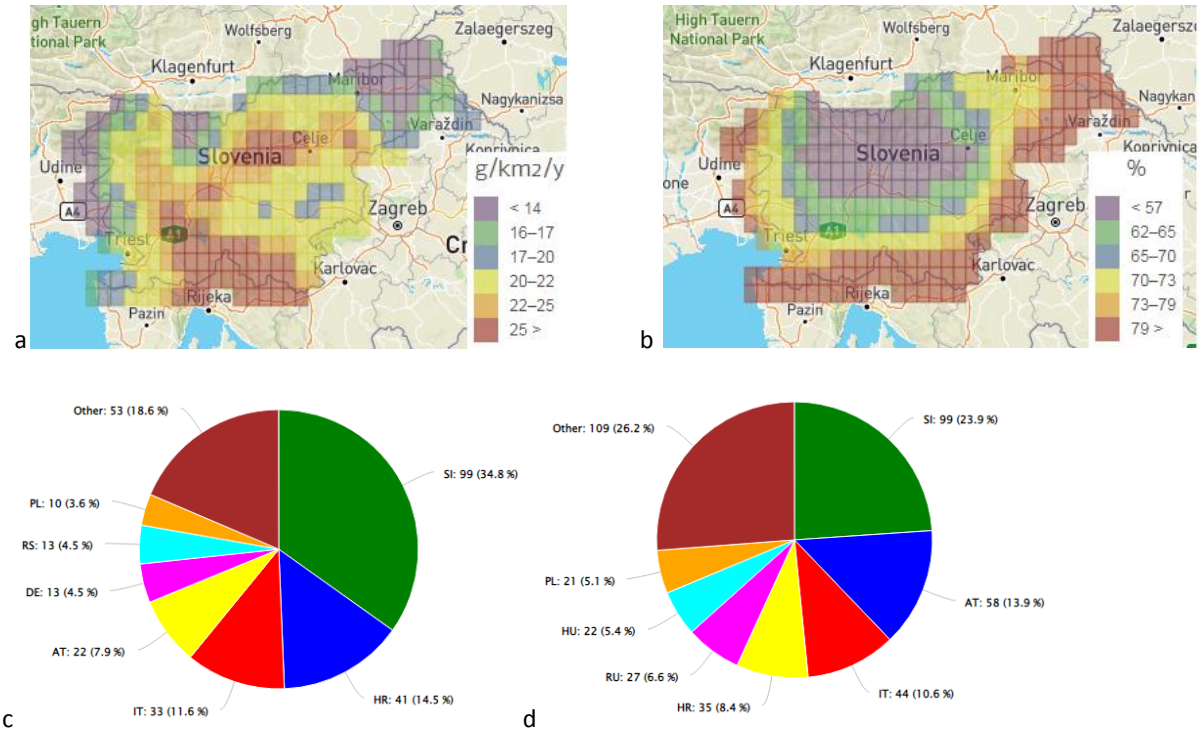

Fig. 3.41. *Characteristics of transboundary transport of Cd to Slovenia: (a) –deposition map, (b) – relative contributions of foreign sources; (c) – main contributors to anthropogenic deposition in the country; (d) main receptors of deposition from the country.*

Detailed information on transboundary pollution of individual countries includes maps of total deposition fluxes to a country's territory (Fig. 3.41a) and relative contributions of foreign sources to anthropogenic deposition (Fig. 3.41b). Besides, source apportionment of anthropogenic deposition to the country's territory is presented (Fig. 3.41c). Each country contributes to atmospheric pollution of other EMEP countries. Spatial distribution of deposition caused by country's sources is available for the entire EMEP region. Besides, country's total deposition to main receptor regions and its fraction of deposition within the EMEP region are indicated (Fig. 3.41d).

Detailed information on source-receptor relationships between all EMEP countries is also available in the database on the website along with other data on heavy metals and POP pollution of the EMEP domain (http://msceast.org/index.php/pollution-assessment/emep-domain-menu/data-hm-pop-menu).

3.5. Information for exposure assessment

3.5.1. Ecosystem-specific deposition of heavy metals

Heavy metals depositing to the underlying surface from the atmosphere negatively affect terrestrial and aquatic ecosystems [*Naeem et al*., 2020]. Adverse effects of heavy metals on human health are also well documented [*Mitra et al*., 2022; *ECHA*, 2013; *ECHA*, 2018; *Rice et al*., 2014; *Karcioglu and Arslan*, 2019]. Effect-based approach aimed at establishing link between atmospheric deposition and impact of heavy metals on human health and biota was developed by the Working Group of Effects. According to this approach, concentrations of heavy metals in soils above which effects are expected, were determined [*de Vries et al*., 2015a,b; *CLRTAP*, 2017]. These concentrations are called critical limits. The approach assumes steady-state conditions, i.e. sources of heavy metals in soils are balanced by sinks. One of the sources is atmospheric deposition. Deposition flux providing steady-state critical level is critical load. If actual deposition flux exceeds critical load, the difference is called exceedance [*Hettelingh et al*., 2015].

For the support of WGE with the development of critical load, ecosystem-dependent deposition fluxes are calculated. Critical loads differ for particular ecosystems. Besides, dry deposition velocities also depend on types of the underlying surface (http://msceast.org/index.php/j-stuff/glemos). The calculations were carried out for 17 types of land cover (forests, arable land, urban area, water surface etc.). Modelled ecosystem-specific deposition fluxes for each EMEP country in 2020 are available on the MSC-E website (https://www.msceast.org/pollution-assessment/emep-countries-menu) and in Supplementary Data Report [*Strizhkina et al*., 2022a].

Figure 3.42 demonstrates example of Pb deposition fluxes to croplands (a) and mixed forests (b). As seen, the fluxes to the underlying surface covered with low vegetation (i.e., croplands) are lower than the fluxes to the surfaces with high vegetation (mixed forests). Deposition flux of Pb to croplands in the western and central parts of Europe varies from 200 to 500 g/km^2/y, while the flux to mixed forests ranges from 300 to 1000 g/km^2/y. Similar to the field of total Pb deposition (Fig. 3.42), the highest fluxes are noted for the southern part of Poland, north-western part of Germany, north of Italy. The lowest fluxes take place over the Scandinavian Peninsula, Finland and north of Russia.

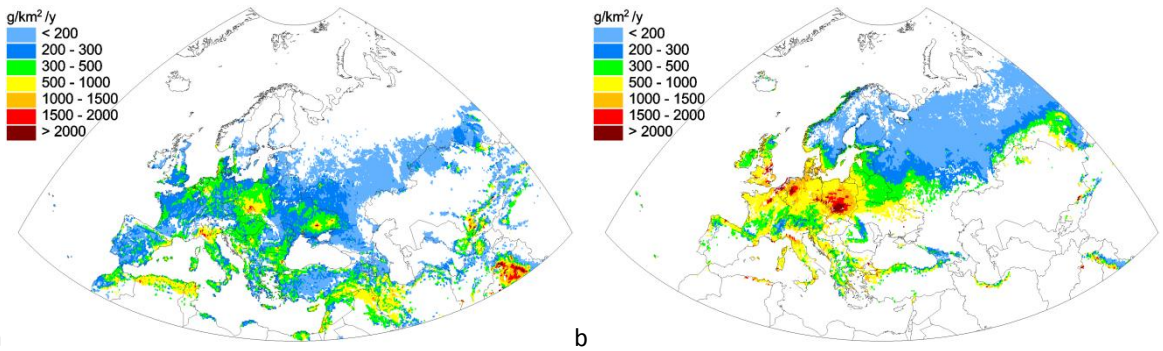

a b

Fig. 3.42. *Annual deposition flux of Pb to croplands (a) and mixed forests (b) in 2020.*

Mean deposition fluxes of Pb to all land-cover types considered by the model are demonstrated in Fig. 3.43. Mean deposition flux is split into wet and dry component, and range between minimum and maximum country-averaged deposition flux is indicated. The highest mean deposition flux (about 900 g/km^2/y) in 2020 was noted for evergreen broadleaf forests. In general, relatively high deposition levels occurred over forests (except deciduous needleleaf forests) and urban areas, while the lowest fluxes (about 100 g/km^2/y) took place over snow/ice, bare lands, open shrubs and wetlands. Besides, low deposition is noted for deciduous needleleaf forests. The reason for this was the location of these forests mostly in the western part of Siberia, where large emission sources are scarce. However, upper limit of deposition range is quite similar to that of other types of forests. It is interesting to note that contribution of dry deposition to total deposition in forests (30 – 65%) is much higher than that to other land cover types (5- 20%). Relatively high deposition to urban areas is explained by their close location to main emission sources.

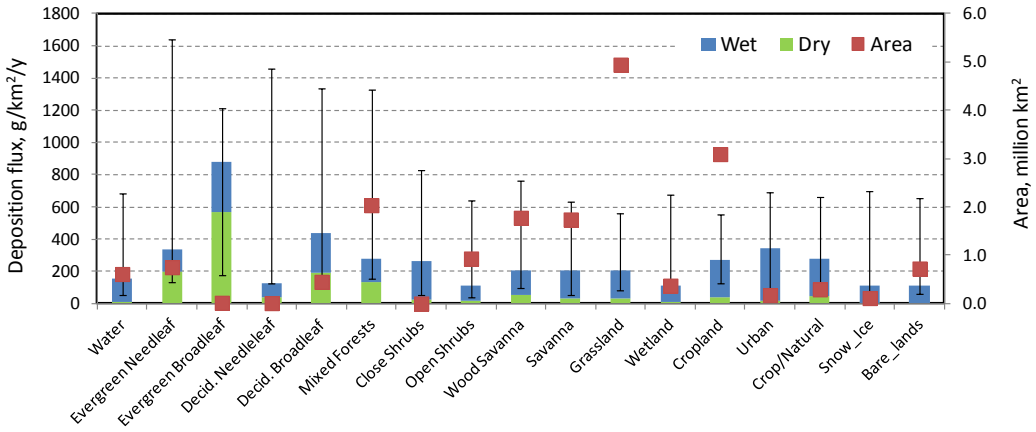

Fig. 3.43. *Deposition (wet and dry) flux of Pb to various ecosystem types within the EMEP domain in 2020. Bars show average value for all EMEP countries; whiskers show range of deposition flux variation (minimum and maximum values) among the EMEP countries.*

The most recent estimates of critical load exceedances of heavy metal deposition are related to 2010 [*de Wit et al.*, 2015]. In order to evaluate up-to-date effect of heavy metal deposition on human health and biota new estimates of the exceedances are needed.

3.5.2. Exceedances of air quality guidelines for PAHs

Results of model simulations and measurements of PAH pollution levels in the EMEP domain were used to evaluate population exposure to high levels of concentrations exceeding air quality guidelines. Several threshold values were established in European Union for B(a)P as an indicator compound (European Directive 2004/107/EC). The threshold values include target value of B(a)P air concentration equal to 1 ng/m^3 as well as the upper and lower assessment thresholds (UAT and LAT) equal to 0.6 and 0.4 ng/m^3 respectively. Along with this, the reference level of 0.12 ng/m^3 for B(a)P has been defined by World Health Organization (WHO) as a level of air concentrations corresponding to the excess lifetime cancer risk level of 10^{-5} [*WHO*, 2017].

Modelled annual mean B(a)P air concentrations for 2020 are shown in Fig. 3.44a. Based on these data amount of population in the areas, where levels of concentrations exceeded air quality guidelines, was estimated (Fig. 3.44b). Data on gridded distribution of urban and rural areas have been adapted from the outcome of the project GRUMP1 [*SEDAC*, 2011].

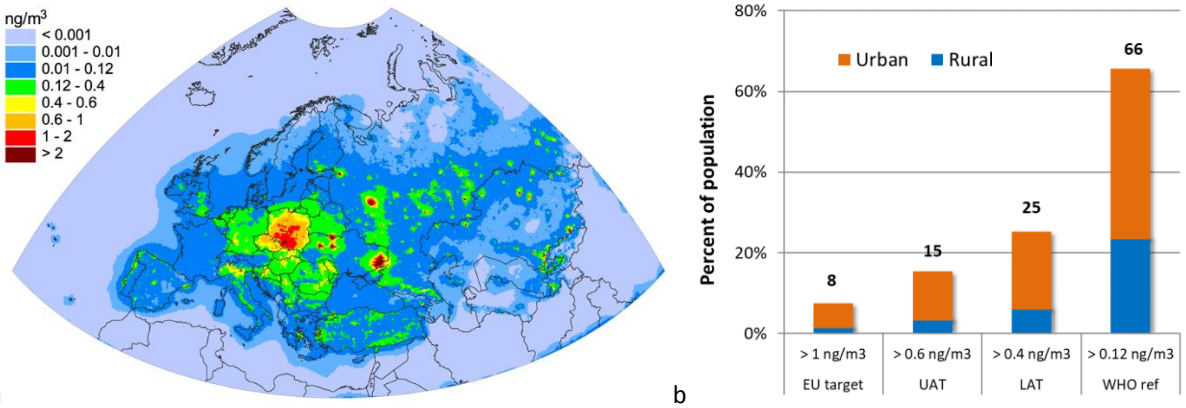

Fig. 3.44. *Spatial distribution of annual mean B(a)P air concentrations for 2020 (a) and percentage of urban and rural population of the EMEP countries in the areas with annual mean B(a)P air concentrations in 2020 exceeding the EU limit values and WHO reference level (b).*

Model estimates show that about 8% of the population of EMEP countries in 2020 were in areas with exceeded EU target level for annual mean B(a)P air concentrations. The upper assessment thresholds (UAT) and lower assessment thresholds (LAT) values were exceeded in the areas with about 15% and 25% of population, respectively. The WHO Reference level was exceeded for about 66% of population of EMEP countries.

To evaluate population exposure to mixture of 4 PAHs the approach based on toxic equivalency factors was used [*Liu et al*., 2019]. Information on toxic properties is available for some of the PAH compounds that allows to define specific toxic equivalence factors (TEF) for them to characterize their potent toxicity relative to that of B(a)P [*ALS*, 2013]. The TEFs can be applied to characterize the carcinogenic potency of each considered PAH and calculate B(a)P equivalent concentration of PAH mixture. Distribution of equivalent B(a)P concentration of the 4 PAHs (namely, B(a)P, B(b)F, B(k)F, I(cd)P) in the EMEP domain calculated for 2020 is shown in Fig. 3.45a. B(a)P equivalent concentrations are calculated as the sum of concentrations of individual PAHs multiplied by corresponding values of TEFs. It is seen that model estimates of B(a)P equivalent concentrations show higher percentage of population in the areas of exceeded EU target value and WHO reference level, namely, 11% and 75%, respectively.

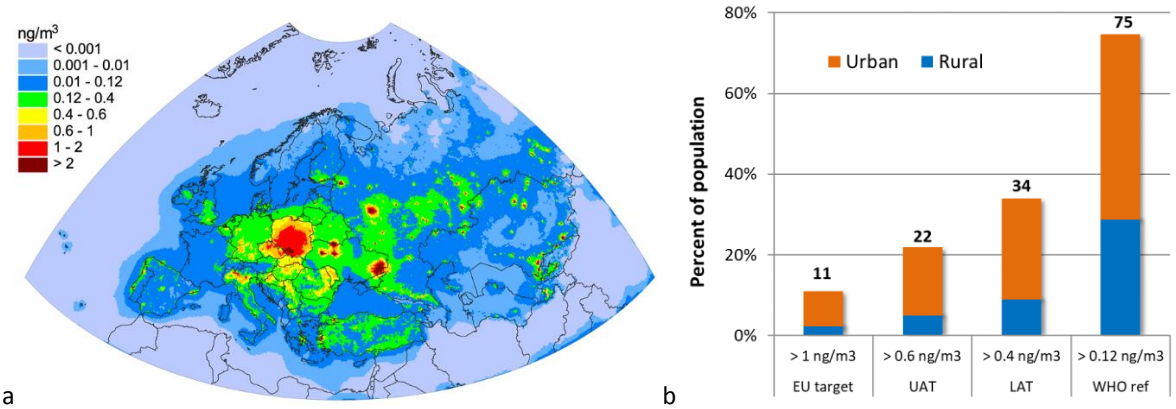

***Fig. 3.45**. Calculated B(a)P equivalent concentrations of the sum of 4 PAHs in the EMEP region for 2020 (a) and percentage of urban and rural population of the EMEP countries in the areas with equivalent B(a)P air concentrations exceeding the EU limit values and WHO reference level in 2020 (b).*

Measurements of PAH air concentrations, performed by national monitoring networks in 2020 (EEA air quality database AQ e-Reporting), show exceedances of air quality guidelines in the EU countries. Averaged annual mean B(a)P air concentrations measured at several hundreds of national monitoring stations in almost 30 countries are shown in Fig. 3.46.

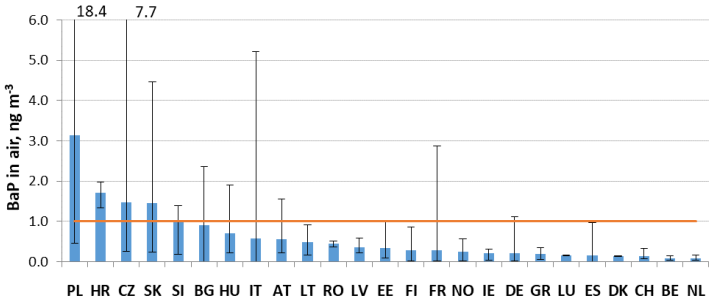

***Fig. 3.46.** Averaged annual mean B(a)P air concentrations observed in the EU countries in 2020. Whiskers denote the range from minimum to maximum values of measured B(a)P concentrations. Red line indicates EU target value of B(a)P air concentration equal to 1 ng/m³.*

High levels of B(a)P air concentrations above the EU target value were observed in 2020 in 4 EU countries, namely, Poland, Croatia, Czechia and Slovakia. It is seen also that exceedances of EU target values for at least one of monitoring site took place in 11 EU countries. The most significant air concentrations were observed at the urban background stations. In case of WHO reference level exceedances of averaged annual mean B(a)P concentrations in 2020 took place in 25 countries.

The information on exceedances of the EU and WHO air quality guidelines for B(a)P as well as data on B(a)P equivalent air concentrations of PAHs can be used to support activities of the Task Force on Health and Working Group on Effects with regard to the analysis of population exposure to toxic substances and their impacts on human health.

3.6. Atmospheric loads to the marginal seas

Anthropogenic pollution of marine ecosystems is one of main environmental problems. This problem is targeted both on national and international levels. In particular, protection of regional seas surrounding the EMEP countries (the Baltic, North, Mediterranean, Black and Caspian Seas) is coordinated by HELCOM, OSPAR, Barcelona Convention, Bucharest Convention, and Tehran Convention, respectively. Besides, protection of waters around Europe is the aim of Marine Strategy Framework Directive.

Information on atmospheric loads of heavy metals and POPs to the regional seas is summarized in this section. Examples of deposition fluxes and contributions of emission sources to deposition to the seas are given for Cd, Hg, HCB and PCB-153. More detailed data on the atmospheric loads to the seas are available in the Supplementary Data Reports [*Strizhkina et al*., 2022a; *Strizhkina et al*., 2022b]. In addition to this, special sections of this report are focused on pollution of the Baltic Sea (Section 5.2.2) and the North-East Atlantic area including the North Sea (Section 5.2.3).

Deposition of heavy metals and POPs to the marginal seas in 2020 differs markedly depending on location of emission sources and peculiarities of atmospheric conditions. The highest mean deposition flux of Cd is noted for the North Sea (Fig. 3.47a). The same situation takes place for Pb. Contribution of Cd anthropogenic sources varies from about 25% for the Mediterranean Sea to around 60% for the Baltic Sea. The contribution of secondary sources ranges from 20% to 50%. Significant contribution of secondary sources to total deposition is caused by wind suspension of sea spray aerosols, containing Pb and Cd. Further deposition of the metals, suspended with the sea spray makes large contribution to total deposition. In case of the Mediterranean and Caspian Seas large contribution to deposition from secondary sources is made by wind-blown dust form deserts of Africa and Asia, respectively.

The highest deposition flux of Hg (6.5 g/km^2/y) is noted for the North Sea, and the lowest one (3 g/km^2/y) for the Caspian Sea (Fig. 3.47b). The difference can be attributed to the distribution of atmospheric precipitation over the EMEP region. Precipitation sums over the North Sea are higher than those over the other seas. Unlike Pb and Cd, the main contribution to Hg deposition to the marginal seas is made by non-EMEP sources. However, it is worth mentioning that deposition of Hg from non-EMEP emission sources can include some share of the EMEP anthropogenic emissions, which left the EMEP domain and then returned back due to long residence time of Hg in the atmosphere. Therefore, the contribution of Hg from non-EMEP emissions sources can be somewhat overestimated.

The highest mean deposition flux of HCB takes place in the Baltic Sea (0.45 g/km^2/y), and the lowest one in the Mediterranean Sea (about 0.3 g/km^2/y) (Fig. 3.47c). Unlike most of heavy metals and POPs, deposition of HCB is almost fully presented by contributions of re-emission and non-EMEP sources, whereas the contribution of the EMEP anthropogenic sources is below 1%. Due to strong restrictions anthropogenic emissions in the EMEP region significantly declined, and the main source of HCB is re-emission from soils of HCB accumulated over the previous decades. Deposition flux of the re-emitted HCB contributes 55 – 80% to total deposition over the marginal seas. Other significant

contributor is atmospheric transport through the domain borders from the sources located outside the EMEP region.

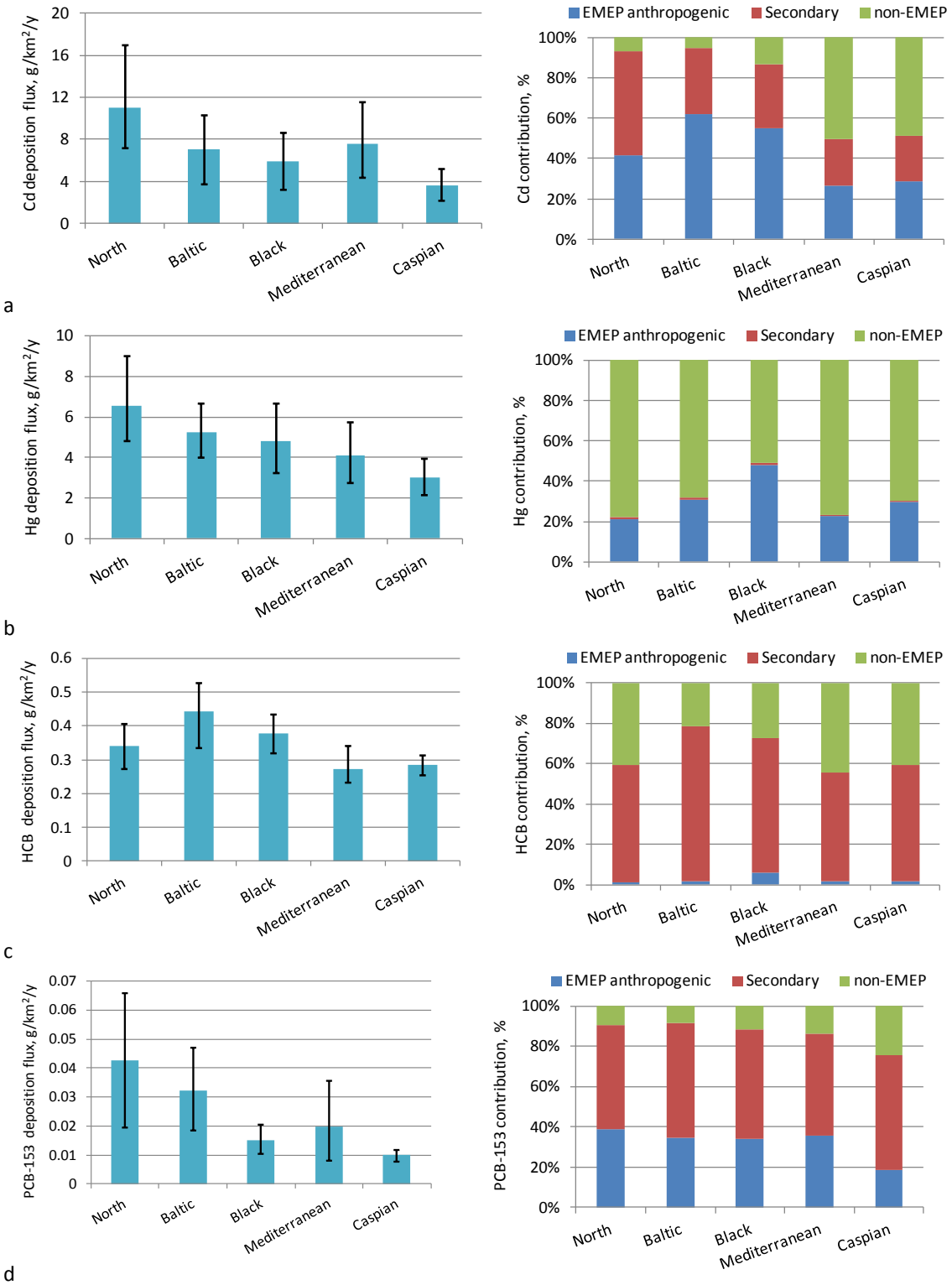

Fig. 3.47. *Mean deposition fluxes (left) and relative contribution of various source types to deposition (right) of Cd(a), Hg(b), HCB(c) and PCB-153(d) to the marginal seas of the EMEP region in 2020.*

The highest deposition flux of PCB-153 occurs over the North Sea, while the Caspian Sea is characterized by the lowest deposition flux (Fig. 3.47d). This difference of deposition fluxes is explained by distribution of emission sources. In particular, countries surrounding the North and the Baltic Seas are characterized by higher emissions compared to those located near the Caspian Sea. As a result, contributions of anthropogenic emission sources as well as secondary sources to deposition of PCB-153 to the North and the Baltic Seas are higher than the contributions to the Caspian Sea.

The main factors affecting spatial distribution of heavy metal and POP deposition to the marginal seas are location of main emission sources and regional meteorological peculiarities. Figure 3.48 demonstrates examples of spatial distribution of Hg and PCB-153 annual deposition flux to the Mediterranean Sea. There are two areas of elevated (> 10 g/km^2/y) Hg deposition to the Mediterranean Sea. The deposition over the area to the east of Greece (the Aegean Sea) is explained mainly by significant emissions in Greece, compared to other countries of the Mediterranean region. Another area is the eastern part of the Adriatic Sea. High Hg deposition fluxes in this region are mainly explained by high precipitation amount along the eastern Adriatic coast (Fig. 3.48a). In the southern part of the Mediterranean Sea Hg deposition is relatively low (around 3 g/km^2/y) mostly due to arid climatic conditions.

Among the Mediterranean countries the most significant EMEP anthropogenic emissions of PCB-153 take place in Italy, France and Spain (Fig. 3.48b). Besides, large non-EMEP emissions occur along Algerian and Libyan coasts. The same source areas are also characterized by the annual highest re-emission flux in 2020. Therefore, the highest PCB-153 deposition fluxes to the Mediterranean Sea are noted in the western part of the sea, especially along coasts of the southern France, Italy, Spain and North Africa. The lowest PCB-153 deposition is estimated in the southern and eastern parts of the sea. Similar results for other considered pollutants and the seas are presented in the Supplementary Data Reports [*Strizhkina et al.*, 2022a,b].

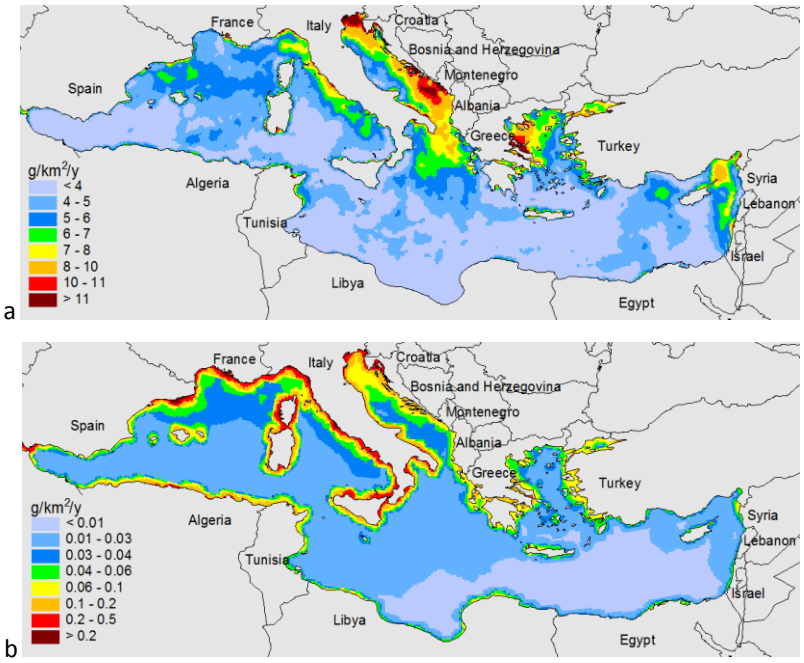

Fig. 3.48. *Deposition flux of Hg (a) and PCB-153(b) to the Mediterranean Sea in 2020.*

3.7. Pollution of the Arctic

This section provides information on pollution of the Arctic by heavy metals (Pb, Cd, Hg) and POPs (PAHs, PCDD/Fs, HCB, PCBs) in 2020. This information comprises the spatial distribution of total deposition fluxes of heavy metals and POPs as well as net Hg deposition fluxes, which were estimated using global-scale simulations. In case of Hg net deposition flux is used instead of total deposition in order to take into account quick re-emission of Hg from snow surface during Atmospheric Mercury Depletion Events (AMDEs) [*Dastoor et al.*, 2022]. Besides, apportionment of heavy metal and POP anthropogenic deposition to the Arctic area within the EMEP domain is given. The borders of the Arctic area are defined according to the AMAP formulation.

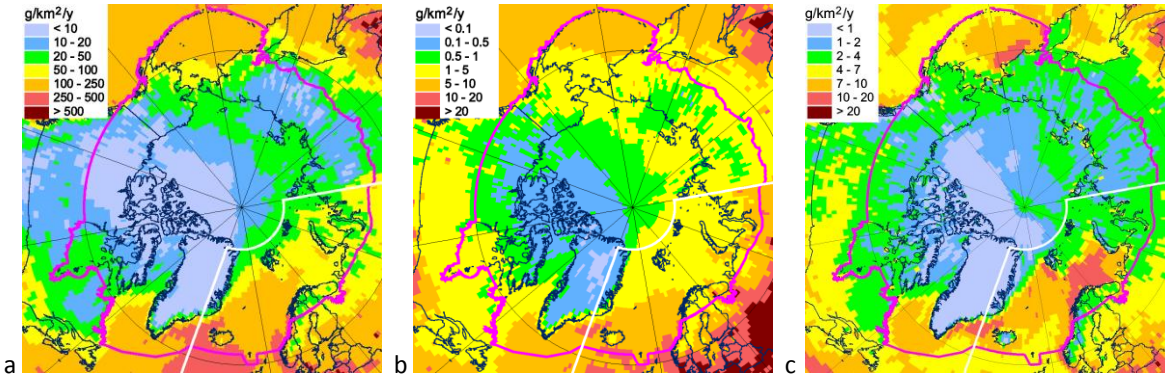

Fig. 3.49. *Total deposition fluxes of Pb (a) and Cd (b) and net deposition flux of Hg (c) to the Arctic in 2020. Purple line denotes the border of the Arctic region adopted by AMAP, and white line denotes a border of the EMEP domain.*

In general, heavy metal deposition fluxes in the Arctic are much lower than those in temperate latitudes. This can be explained by the remoteness of the Arctic from the main sources of emissions located in Europe, Asia and North America, as well as the relatively low precipitation amount (Fig. 3.49). For instance, Pb deposition fluxes in 2020 for the Arctic region are in the range 10-100 g/km^2/y while for the middle latitudes they are about 250 g/km^2/y. Similar contrast can be noted for Cd deposition fluxes in the Arctic ranging from 0.1 to 10 g/km^2/y, whereas the fluxes over most of the EMEP area varies from 5 to 60 g/km^2/y. Higher deposition levels of Pb and Cd take place over the sea surfaces of the Atlantic and Pacific Oceans due to higher precipitation amounts compared to central and continental parts of the Arctic. Besides, over the oceans significant contribution to atmospheric load is caused by re-suspension of trace metals with sea spray aerosols. Over the continental part of the Arctic the higher deposition fluxes occur in the European sector, and the lowest ones in the North American sector. It is explained mainly by distribution of anthropogenic emission sources. Mercury is a global pollutant. Therefore the differences between Hg net deposition fluxes in the Arctic and in other parts of the EMEP region are smaller. Net deposition fluxes of Hg range from 1 to 10 g/km^2/y (Fig. 3.49c) over most of Arctic. Similar to Pb and Cd, higher levels occur over the Atlantic and Pacific Oceans, and lower levels take place over land areas of the Arctic. The lowest net fluxes are noted for the Canadian Arctic Archipelago, Greenland and the American sector of the Arctic Ocean. The highest Hg net fluxes (> 10 g/km^2/y) take place in the Barents Sea and near the south-

eastern coast of Greenland. These high values are explained by combination of two factors, namely, significant load due to AMDEs and substantial atmospheric precipitation.

Deposition fluxes of POPs in the Arctic are also generally lower than those in temperate latitudes. For instance, B(a)P deposition fluxes in the Arctic are in the range 0.1-5 g/km^2/y, while the fluxes over most of the EMEP area vary from 2 to 150 g/km^2/y. Over most of water areas B(a)P deposition fluxes are below 0.1 g/km^2/y. Some hotspots of elevated B(a)P deposition fluxes take place in northern Canada, the eastern part of Russia and Kola Peninsula, which can be explained by the presence of significant emission sources in these regions (Fig. 3.50a). For PCDD/Fs deposition fluxes in the Arctic are much lower than in temperate latitudes, but some hotspots take place (Fig. 3.50b). Deposition fluxes of PCB-153 range from 0.002 to 0.05 g/km^2/y over land areas of the Arctic and North Atlantic. Over the Arctic Ocean, most of Greenland and the Arctic part of the Pacific Ocean deposition the fluxes are around 0.002 – 0.004 g/km^2/y (Fig. 3.50c). The highest fluxes are noted for the north of Europe (Scandinavian and Kola Peninsulas), Iceland and the central part of Alaska.

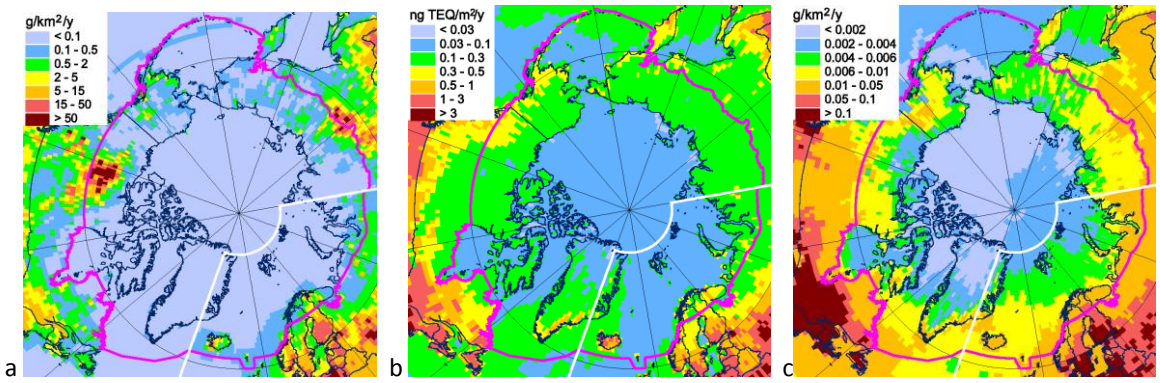

Fig. 3.50. *Total deposition fluxes of B(a)P (a), PCDD/Fs (b) and PCB-153 (c) to the Arctic in 2020. Purple line denotes the border of the Arctic region adopted by AMAP, and white line denotes a border of the EMEP domain.*

The sources responsible for the deposition of pollutants in the Arctic were divided into three groups, similar to the calculations for the EMEP region. They include anthropogenic emissions from the EMEP countries, secondary emissions and non-EMEP sources. For Pb, the largest contribution to deposition in the Arctic within the EMEP area is made by secondary sources (almost 60%) due to significant re-suspension from the sea surface and remoteness of the Arctic from the main sources of anthropogenic emissions (Fig. 3.51). The contribution of the EMEP anthropogenic sources to deposition of Pb is about 27%. The contribution of secondary sources is significant also for HCB (about 75%), PCB-153 (about 65%) and PCDD/Fs (about 45%), which can be explained by the re-emission of historically accumulated pollutants in environmental media (soils, waters, etc). EMEP anthropogenic sources are predominant in pollution of the Arctic by B(a)P and Cd (73% and 44%, respectively). The contribution of non-EMEP sources in the Arctic region is the most significant for Hg (over 90%), while for the other pollutants the contribution of this group of sources ranges from <1% to 35%.

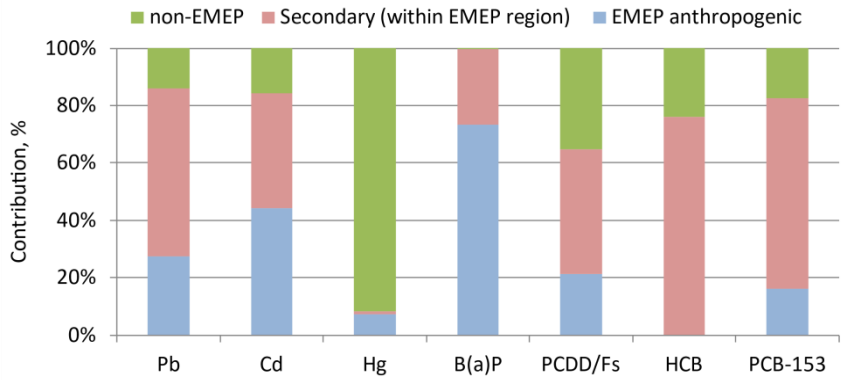

Fig. 3.51. *Relative contributions of the EMEP anthropogenic, secondary and non-EMEP sources to deposition in the Arctic (within the EMEP domain) in 2020.*

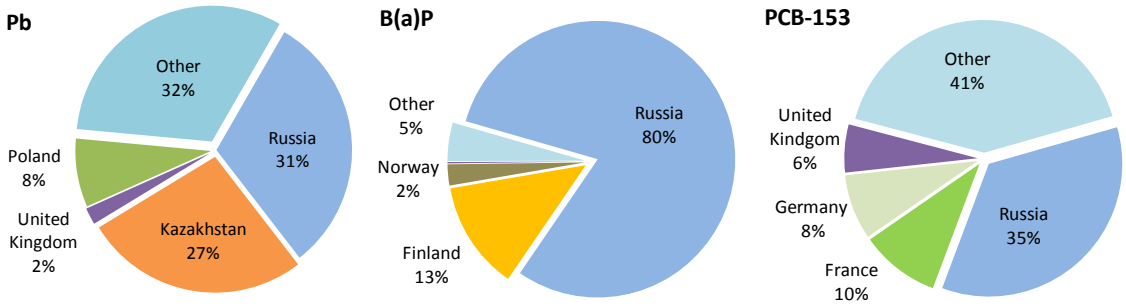

Fig. 3.52*. Source apportionment of heavy metal and POP anthropogenic deposition to the Arctic (within the EMEP domain) in 2020.*

The contribution of particular countries to heavy metal and POP deposition to the Arctic is illustrated in Fig. 3.52. This contribution depends on a number of factors, such as magnitude of national emissions of the country, the remoteness of sources from the Arctic, the physicochemical characteristics of pollutants, meteorological conditions, etc. Russia makes the main contribution to air pollution in the Arctic for all considered pollutants (about 30% for Pb, 35% for PCB-153 and 80% for B(a)P). This is explained by the location of the large part of the territory of Russia and a number of industrial sources within the Arctic region. For Pb, significant contribution is made by Kazakhstan (27% for Pb), which has one of the highest levels of heavy metal emissions among the EMEP countries. Therefore, in spite of its remoteness from the Arctic the contribution of its emission sources to deposition in the Arctic is considerable. The substantial contribution of French and German emission sources to deposition of PCB-153 in the Arctic can be explained by similar reasons. For B(a)P, notable contribution is made by sources of Finland and Norway, which are located partly within or close to the Arctic region.

3.8. Global scale pollution by heavy metals and POPs

Pollution levels of heavy metals and POPs in the EMEP countries are determined by emission sources located both inside and outside the EMEP domain. In case of contaminants, which are characterized by long residence time in the atmosphere (e.g. Hg and some POPs), intercontinental atmospheric transport can contribute substantially to the pollution of the EMEP region. Global-scale simulations were performed to take into account contribution of non-EMEP sources to pollution levels in the EMEP countries. The boundary conditions for the regional modelling were derived from the global-scale simulations. In addition, the global-scale modelling results were also used for assessment of heavy metal and POP pollution in other regions and over the globe in co-operation with other international bodies (e.g. UN Environment, Stockholm and Minamata Conventions, AMAP, etc.) (see Section 5.2 for details).

Figure 3.53 shows simulated global patterns of annual mean air concentrations of Pb, Cd and Hg^0 in 2020. The highest air concentrations of Pb and Cd are estimated for Southeast and South Asia (above 15 ng/m^3 for Pb and 0.5 ng/m^3 for Cd), mainly because of large emissions in China and India (Fig. 3.53a and b). Elevated concentrations are also simulated in arid areas of the south-western part of Asia, Middle East and Northern Africa due to significant wind re-suspension of heavy metals in these regions. The lowest concentrations of Pb and Cd occur over the Arctic and Antarctic regions. Concentrations of Pb and Cd near the western, northern and eastern borders of the EMEP domain are lower by an order of magnitude than those in the middle of the domain. However, the concentrations along the southern border are comparable with the levels in the EMEP countries.

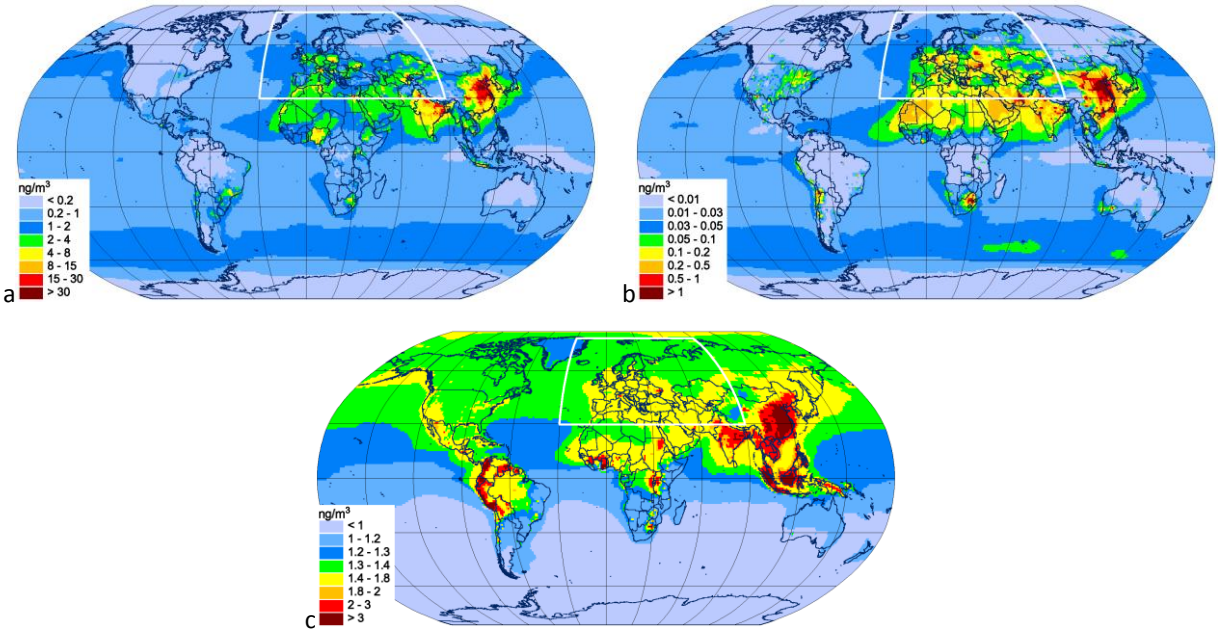

Fig. 3.53. *Global distributions of annual mean air concentration of Pb (a), Cd (b) and Hg^0 (c) in 2020. White line depicts boundary of the EMEP region.*

Air concentration of Hg^0 is more evenly distributed over the globe with lower concentrations (0.8-1.3 ng/m^3) in the Southern Hemisphere and higher concentrations (1.3-2.5 ng/m^3) in the Northern Hemisphere (Fig. 3.53c). East and Southeast Asia are characterized by the highest Hg concentrations (above 2 ng/m^3) due to large anthropogenic emissions. High concentration levels are also obtained for equatorial Africa, South America and Southeast Asia as a result of emissions from artisanal and small-scale gold mining in these regions. In addition to this, elevated Hg concentrations are found over Southern Europe and the western coast of North and South Americas because of natural emissions from Hg-enriched soils. The lowest concentrations are simulated over the Southern Ocean and Antarctica.

Simulated global distributions of B(a)P, PCDD/Fs, PCB-153 and HCB concentrations in air in 2020 are shown in Fig. 3.54. The highest concentrations of B(a)P are estimated in East and South Asia, where B(a)P levels can exceed 1 ng/m^3 (Fig. 3.54a). Relatively high concentrations are also predicted in some countries of Central, Eastern, and Southern Europe as well as in Central Africa. Other continents and regions, namely, North and South America, Northern Africa and Australia are characterized by lower concentrations (below 0.1 ng/m^3). The highest levels of PCDD/Fs are estimated in some areas of South and East Asia, and Central Africa (above 25 fg TEQ/m^3) (Fig. 3.54b). Concentrations of PCDD/Fs in Europe, North and South Americas, and Australia are generally lower (below 10 fg TEQ/m^3) except for a number of hot spots in areas with significant emissions.

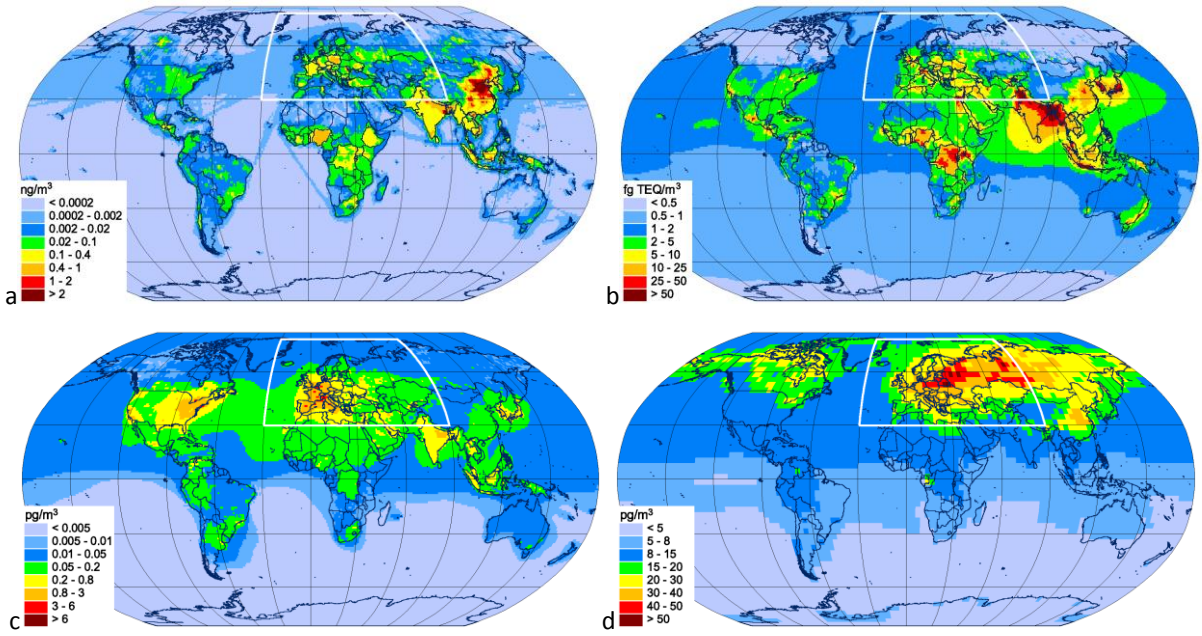

Fig. 3.54. *Global distribution of annual mean air concentration of B(a)P (a), PCDD/Fs (b), PCB-153(c), and HCB (d) in 2020. White line depicts boundary of the EMEP region.*

Elevated air concentrations of PCB-153 are characteristics of Europe, North America and South Asia (0.2-6 pg/m^3) (Fig. 3.54c). In other regions, the levels of PCB-153 are mostly within 0.01-0.2 pg/m^3 in the Northern Hemisphere and below 0.005 pg/m^3 in the Southern Hemisphere. Spatial distribution of HCB levels in air is more homogeneous due to its persistence and significant contribution of

secondary emission (Fig. 3.54d). HCB concentrations mostly vary within 8-50 pg/m^3 in the Northern Hemisphere and below 5 pg/m^3 in the Southern Hemisphere. The most significant levels (above 40 pg/m^3) are predicted for Europe and Western Siberia.

It should be noted that the global scale modelling of heavy metal and POP pollution requires reliable and up-to-date global emission inventories. However, no or limited data on contemporary emissions is available for some priority contaminants (e.g. Pb, Cd, HCB and PCDD/Fs). Thus, improvement of the global-scale pollution assessment requires additional efforts for the development of global emissions inventories for heavy metals and POPs in co-operation with other international bodies (UN Environment, Stockholm Convention, Minamata Convention, etc.).

Chapter 4. RESEARCH ACTIVITIES

4.1. Eurodelta-Carb activities

The Eurodelta-Carb intercomparison of B(a)P models was initiated by the TFMM in the beginning of 2021 in the framework of a broader scientific study, devoted to the modelling of secondary organic aerosol and black carbon. The main objectives of the Eurodelta-Carb study on B(a)P are to analyze performance of models and sources of uncertainties in the modelling results. The study is also aimed to contribute to the refinement of B(a)P emissions from the combustion of fossil fuel and biomass burning and to the further improvement of modelling approaches. Four regional chemistry transport models were applied to simulate the concentrations of B(a)P in Europe. The modelled concentrations were compared with the measurements of B(a)P carried out by the EMEP monitoring network. Evaluation of the modelling results was performed in close cooperation with national experts in B(a)P modelling. In this section, a summary of current progress in the analysis of the multi-model B(a)P simulations is presented.

Model simulations setup and input data

The Eurodelta-Carb B(a)P modelling exercise is focused on the time period from the beginning of December 2017 to the end of 2018. Simulations of B(a)P were performed using four chemical transport models (CTMs): CHIMERE, GLEMOS, MINNI and SILAM, being developed and applied by the modelling teams of INERIS (France), CIEMAT (Spain), MSC-E (EMEP), ENEA (Italy), and FMI (Finland) to study air pollution levels on regional and national scales. All the models used a prescribed modelling domain and gridded B(a)P annual emissions data for 2018, generated by CEIP (Fig. 4.1). Other input data and parameterizations, such as meteorological input, intra-annual variations of B(a)P emissions, emissions of other pollutants, boundary conditions, model parameterizations, and other parameters of the model setup were specific to each model. The participating models have different degrees of complexity with regard to B(a)P modelling. In particular, CHIMERE, GLEMOS, and MINNI consider B(a)P as a reactive semi-volatile substance that undergoes gas-particle partitioning and degradation in the atmosphere due to chemical reactions with OH in the gaseous form. Also, GLEMOS and MINNI include the chemical reaction of B(a)P with ozone in particulate form. All three models consider deposition of gaseous and particulate B(a)P. In the case of SILAM, the model simulations were carried out assuming that B(a)P is an inert substance emitted to the atmosphere in particulate phase and subject only to dry and wet deposition processes.

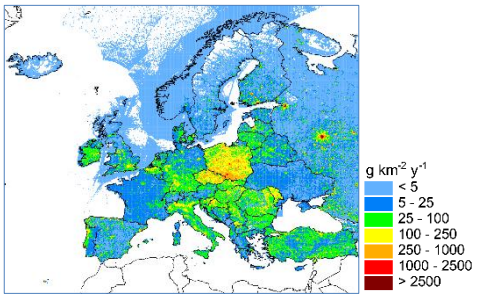

Fig. 4.1. *Eurodelta-Carb modelling domain and spatial distribution of annual B(a)P emission fluxes for 2018.*

The program of model simulations includes the base case run for the specified time period with the prescribed B(a)P emission data using independently defined model setups. In addition, a number of sensitivity runs are also being discussed that can be used to analyse factors affecting B(a)P long-

range transport and pollution levels (e.g. unified emission temporal profiles, B(a)P degradation in particulate phase, modelling of B(a)P as an inert substance). In particular, model simulations treating B(a)P as an inert substance have been performed by the GLEMOS and SILAM, and will be analysed later in the study.

Modelling results and analysis

Spatial distributions of annual mean total B(a)P air concentrations, simulated by CHIMERE, GLEMOS MINNI and SILAM for the base case run for 2018, are shown in Figure 4.2. The three models that treat B(a)P as a reactive semi-volatile substance predicted similar patterns of B(a)P pollution levels for most regions in Europe. SILAM, on the other hand, that treats B(a)P as an inert substance, estimated substantially higher concentrations. The largest concentrations were estimated by all three models for the countries in Central Europe as well as for Northern Italy and some areas in Eastern Europe. The lowest concentrations were predicted for the countries of Northern Europe and remote areas. In general, relatively higher concentrations were simulated by SILAM, followed by CHIMERE GLEMOS and MINNI. Other than the fact that SILAM treats B(a)P as an inert substance, the differences between the simulated B(a)P concentrations may be attributed to the effect of different model parameterizations applied (e.g. for gas-particle partitioning, degradation, and deposition processes) as well as the different meteorological inputs. Additional contributions could also have been made by different emission temporal profiles and concentrations of reactants used in the models to estimate B(a)P chemical transformations.

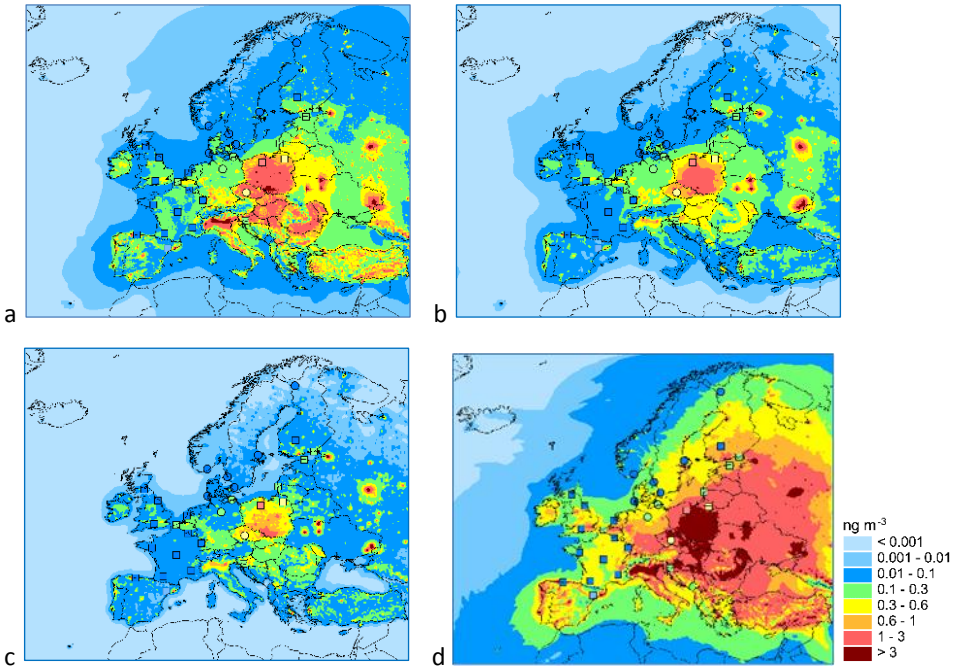

Fig. 4.2. *Maps of annual mean modelled total (gaseous + particulate phase) B(a)P atmospheric concentrations in 2018 simulated by CHIMERE (a), GLEMOS (b), and MINNI (c) and SILAM (d) for the base case model run. For the comparison, observed total and particulate phase B(a)P concentrations, reported by the EMEP monitoring stations, are shown as colored circles and squares, respectively, on the same scale as the modelled values.*

Evaluation of the model output against measurements for the base case model run was carried out using the data of 29 EMEP monitoring stations for the year 2018. Of these, 9 stations located in Central and Northern Europe measured total B(a)P concentrations, whilst B(a)P concentrations in particulate form were measured at 20 stations covering a wider geographical area (Fig. 4.2).

For the model-measurement comparison (excluding SILAM), the daily mean modelled total or particulate phase concentrations, depending on the type of measurement, were extracted from the model output files for the station locations. Modelled values were then averaged to the temporal resolution and periods of the observations (e.g. daily or weekly). A summary of the statistical analysis of the modelled and observed annual mean B(a)P concentrations is presented in Table 4.1. All the models reproduced the spatial pattern of observed total and particulate B(a)P concentrations well with correlation coefficients (R) of 0.84-0.96. CHIMERE and GLEMOS tended to slightly overestimate observed total B(a)P levels with a mean bias of about 4%, whereas MINNI underestimated the measured values with a mean bias of -53%. For the particulate B(a)P concentrations, CHIMERE overestimated concentrations with a mean bias about 9%, while GLEMOS and MINNI underestimate the observed concentrations with mean biases of -19% and -52%, respectively. Estimated total B(a)P concentrations were within a factor of 2 of the measured values for 89%, 78%, and 11% of monitoring stations for CHIMERE, GLEMOS, and MINNI, respectively, whereas for B(a)P in particulate phase they were within a factor of 2 for 80%, 70%, and 40% of monitoring stations. The fraction of model values that were within a factor of 3 from measurements is larger. In particular, modelled concentrations of CHIMERE and GLEMOS were within the agreement of a factor of 3 for all the stations that measured total B(a)P concentrations, and for 90% and 85%, respectively, for stations that measured particulate B(a)P concentrations.

Table 4.1. *Summary of statistical metrics, calculated on the basis of annual mean total and particulate phase B(a)P air concentrations for 2018, observed at EMEP monitoring stations and estimated by CHIMERE, GLEMOS and MINNI in the base case model run.*

Models	Mean ($ng\ m^{-3}$)	NMB[a] (%)	R[a]	RMSE[a] ($ng\ m^{-3}$)	F2[a] (%)	F3[a] (%)
Total B(a)P concentrations (9 stations), mean observed 0.116 ng m^{-3}						
CHIMERE	0.120	3.9	0.93	0.058	89	100
GLEMOS	0.121	4.3	0.91	0.087	78	100
MINNI	0.054	-53.3	0.86	0.090	11	22
Particulate B(a)P concentrations (20 stations), mean observed 0.156 ng m^{-3}						
CHIMERE	0.170	8.9	0.84	0.128	80	90
GLEMOS	0.126	-19.3	0.96	0.095	70	85
MINNI	0.075	-52.1	0.93	0.168	40	70

[a] *NMB is normalized mean bias; R is the spatial correlation between modelled and observed concentrations; RMSE is the root mean square error; F2 and F3 represent fractions of sites for which the modelled value is within a factor of 2 and 3, respectively, of the observed value.*

The evaluation of annual mean modelled B(a)P concentrations against the measurements of total and particulate B(a)P concentrations from individual EMEP monitoring stations is shown in the scatter plots in Figure 4.3. An overestimation of observed particulate B(a)P concentrations was found for two Spanish stations ES0008R and ES0014R for all three models. For other stations, different

kinds of discrepancies were obtained. In particular, for CHIMERE, an overestimation by more than a factor of 2 was found for the stations GB0048R, GB1055R, and NL0091R that measured particulate B(a)P. In the case of GLEMOS, the largest underestimation (more than a factor of 3) was found for total B(a)P observed at DE0009R and FI0036R, and for particulate B(a)P at FR0023R and FR0025R. In case of MINNI, the greatest deviations (underestimation by more than a factor of 5) were found for the stations DE0001R, DE0009R, and FI0036R that measured total B(a)P, and for LV0010R and FR0023R that measured particulate B(a)P.

The scatter plots indicate that CHIMERE modelling results have the highest regression slope value (0.81) followed by GLEMOS (0.77) and MINNI (0.44). The scattering of modelled-observed pairs is best for GLEMOS (coefficient of determination 0.88) compared with MINNI and CHIMERE (0.83 and 0.80, respectively).

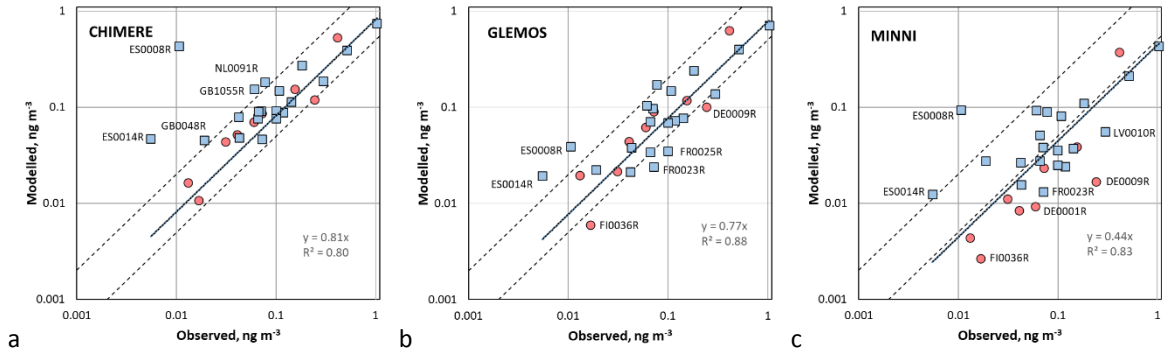

Fig. 4.3. *Scatter plots on a log-log scale of the comparison of modelled B(a)P air concentrations (total and particulate) simulated by CHIMERE (a), GLEMOS (b), and MINNI (c) for the base case model run with measurements of EMEP monitoring stations in 2018. The region between the dashed lines indicates the model estimates within a factor of two of the measured values and the solid line is the linear regression of all data points. Total B(a)P concentrations are shown as red circles and particulate B(a)P concentrations are shown as blue squares. The stations, for which the models have the largest deviations from the measurements, are indicated by their names.*

Figure 4.4 shows examples of modelled and observed B(a)P time series for two EMEP monitoring stations, namely, CZ0003R and PL0009R that measured total and particulate B(a)P concentrations, respectively. For these stations, the comparison of modelled and observed concentrations shows, in general, a good level of agreement. Model estimates capture the high levels of observed concentrations in the cold season, and low concentrations in the warm season, as well as peak concentrations. However, in some of the episodes, especially in winter months, the models underestimate measured concentrations. Differences between the modelled and measured intra-annual variations of B(a)P concentrations may be explained both by an underestimate of emissions and by the uncertainties in the temporal disaggregation of B(a)P emissions that were applied in the model simulations.

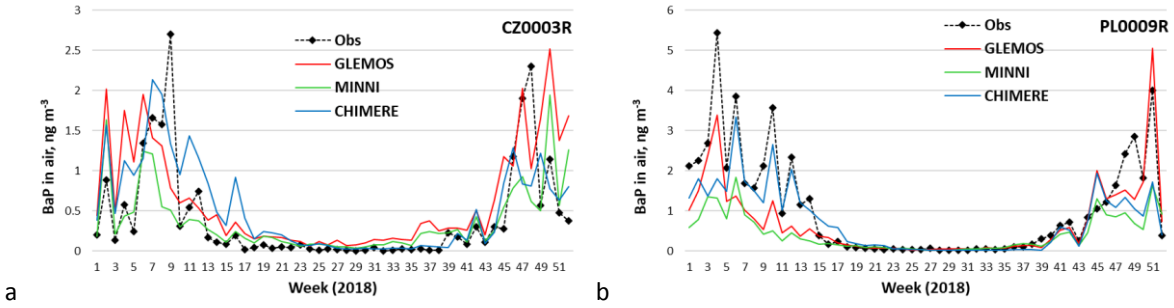

Fig. 4.4. *Intra-annual variations of total B(a)P air concentrations, observed at the EMEP station CZ0003R (a), and particulate B(a)P concentrations, observed at the station PL0009R (b), and the total and particulate B(a)P concentrations simulated by CHIMERE, GLEMOS, and MINNI in the base case model run for 2018.*

This preliminary analysis of model simulations with prescribed officially reported B(a)P emissions demonstrates a generally reasonable level of agreement between model estimates and both annual mean observed B(a)P concentrations and their intra-annual variations. On the other hand, for some of the stations, modelled concentrations significantly deviated from the observed values indicating possible uncertainties in emission estimates, modelling approaches and measurements. More detailed analyses are, therefore, required to explore the reasons for the differences between the outputs of participating models and substantial over- and underestimates of observed B(a)P concentrations for some of the stations. The next stage of the study will focus on the sensitivity analyses, an evaluation of the meteorological drivers and an analysis of other model outputs such as B(a)P concentrations in precipitation and deposition fluxes and concentrations of species affecting B(a)P chemical transformations in the atmosphere.

4.2. Contaminants of emerging concern

Contaminants of emerging concern (CECs) comprise a wide range of substances having potential to adversely affect wildlife and human health. Many of CECs are being used in consumer and personal care products and in building materials. CECs include new POPs recently started to be regulated and characterized by limited data on their pollution levels, fate and effects, and substances which are currently unregulated due to the properties falling partly outside existed criteria to be considered as POPs. In spite of limited knowledge, significant attention is paid to the CECs in recent and ongoing research activities including monitoring and assessment of their distribution in the environment and potential risks.

Some of the CECs are included in the annexes of the Stockholm Convention and are listed by AMAP, HELCOM, OSPAR for the analysis of their pollution levels, exposure assessment, and regulatory activities. Selected CECs were added to the CLRTAP POP Protocol for regulation of their production and use, namely, hexachlorobutadiene (HCBD), octabromodiphenyl ether (octa-BDE), pentachlorobenzene (PeCB), pentabromodiphenyl ethers (PBDEs), perfluorooctane sulfonates (PFOS), polychlorinated naphthalenes (PCN) and short-chain chlorinated paraffins (SCCPs). Ambient concentrations of CECs (e.g. of PBDEs, SCCPs, and per- and polyfluoroalkyl substances (PFAS)) are

being monitored at EMEP monitoring stations in Northern Europe in accordance with the new EMEP monitoring strategy [ECE/EB.AIR/144/Add.1]. Besides, national monitoring networks carry out measurements of selected CECs in mosses in framework of ICP-Vegetation Programme activities. Furthermore, preparatory work for evaluation of CEC pollution levels, transport and fate in the environment is performed in accordance with the EMEP work plan for 2022-2023. As a part of this activity, a workshop on CEC monitoring and model assessment is planned to be organized in 2023 in co-operation with TFMM, TF HTAP and CCC.

In framework of co-operation with HELCOM, MSC-E carried out compilation of information on some of the CECs (e.g. SCCPs, PFOS, (hexabromocyclododecanes (HBCDDs), PBDEs) with the focus on the Baltic Sea area. In this section an overview of information on these substances including regulatory activities, their production, usage and emissions, as well as results of monitoring and model assessment of their transport and fate in the environment are presented. More detailed information can be found in the Joint reports of the EMEP Centres for HELCOM [*Gauss et al.*, 2021].

Short-chain chlorinated paraffins (SCCPs)

Chlorinated paraffins (alkanes) are a group of saturated hydrocarbons with different chlorine content and different length of carbon chain. Short-chain chlorinated paraffines comprise a complex mixture, which are characterized by a carbon chain-length from 10 to 13 carbon atoms and the degree of chlorination of more than 48% by weight. Assuming that SCCPs do not contain dechlorinated carbon atoms and branched chains, there can be 7820 SCCP isomers and 46 congener groups [*Diefenbacher et al.*, 2015, *Krogseth et al.*, 2013].

SCCPs are considered as substances posing risk both for human health and the environment. International Agency for Research on Cancer (IARC) has classified SCCPs with average carbon chain length 12 (C12) and average chlorination 60% as possible carcinogens for humans (group 2B) [*IARC*, 1990]. In accordance with the EU REACH (1907/2006/EC) and CLP Regulation (1272/2008/EC), SCCPs are classified as carcinogens (Category 2), as very toxic to aquatic life with long lasting effects (Category 1), and as persistent, bioaccumulative, and toxic substances (PBT).

Regulation

Taking into account hazardous properties, SCCPs are included in the work programs of various national and international activities, aimed to collect the information on their environmental levels and trends as well as to develop measures for the restriction of their usage and reduction of emissions. SCCPs are recognized as contaminants of concern by the CLRTAP (since 2009) and Stockholm Convention (since 2017). Besides, SCCPs are considered as pollutants of priority action and specific concern in the regulatory activities of OSPAR and HELCOM. In the European Union, the manufacturing, placing on the market and use of SCCPs shall be restricted in accordance with the Article 3 of the EU Regulation (EU) 2019/1021 on POPs.

Production, use, and emissions

Technical mixtures of SCCPs have been widely used in Europe, America, Asia, Australia, and South Africa. The major areas of chlorinated paraffins usage include application in metal working fluids or lubricants, water repelling agents, flame retardants, and plasticizers. SCCPs were used in the production of polyvinyl chloride and consumer goods on its basis, for filling of expansion and movement joints in building and general engineering, filling of joints for protection from spillages, and in other areas where resistance to water, chemicals, alkalis, solvents and biological agents was required. Besides, SCCPs were used in sealants, rubbers, textiles, paints and coatings [*Fiedler et al.*, 2010; *Lassen et al.*, 2014].

Large-scale commercial production of chlorinated paraffins (CPs) was initiated in USA in 1930s. Since 1977 they started to be produced also in Europe and Japan. The highest volume of production was reached after 2006, when China increased sharply manufacturing of CPs. SCCP releases to the environment can occur at all stages of their life cycle including production, formulation, use, and disposal [*Breivik et al.*, 2012]. However, it is widely believed that production and application of SCCPs for manufacturing of other products take place in the closed systems, thus main releases of SCCPs to the environment can take place at the use and disposal stages.

Although SCCPs are included in the Protocol on POPs to LRTAP Convention, no officially reported information on their emissions to the atmosphere is currently available, since SCCPs are not considered to be subject to emission reporting obligations under the Convention in accordance with the Guidelines for Reporting Emissions and Projections Data under the Convention [*UNECE*, 2014]. As an exception, the inventory of SCCP emissions in Finland [*Finland*, 2021] can be noted. The European Pollutant Release and Transfer Register (E-PRTR) contains specifications for the reporting of SCCP releases to the environmental compartments. However, SCCP emissions to the atmosphere are not currently submitted by the EU countries. At the same time, it can be noted that under the Stockholm Convention, development of the guidance on preparing inventories of SCCP releases was initiated. Developed methodology for the inventory of SCCP emissions was made available at the end of 2020 [*UNEP*, 2021].

Monitoring

In accordance with the EMEP monitoring strategy for the period 2020-2029 [ECE/EB.AIR/144/Add.1], it is recommended to monitor SCCPs at the research-based stations (Level 3). Chlorinated paraffins were included in the monitoring campaigns of several countries in Northern Hemisphere [*Šebková et al.*, 2021; *Harner et al.*, 2021]. In Norway, measurements of SCCPs are carried out at the Zeppelin and Birkenes stations. In the period 2017-2019, measured concentrations varied from 60 to 900 pg m^{-3}. Over these three years, some decrease of pollution levels by 30% - 40% was indicated at these two stations. In Sweden, concentrations of SCCPs in air have been regularly monitored at the stations Råö and Aspvreten since 2009. In 2009-2017, SCCP pollution levels ranged from 7 to 220 pg m^{-3} at Råö, and from 6 to 2100 pg m^{-3} at Aspvreten. No clear temporal trend in airborne SCCP concentrations was observed at these stations. However, for the past two years a slight decrease of SCCPs in air can be noted [*Swedish EPA*, 2020].

Data on SCCP content in atmospheric deposition have been reported by Swedish stations since 2009 [*Swedish EPA*, 2020]. Sampling was carried out at two stations Råö and Aspvreten 4 times a year. Average annual deposition of SCCPs varied over a wide range from 4.3 to 840 ng m^{-2} day^{-1} at Råö and from 1.6 to 190 ng m^{-2} day^{-1} at Aspvreten [*Fredricsson et al.*, 2018]. The maximum SCCP deposition flux was observed at Råö in December 2015, while in subsequent years deposition fluxes at this station decreased significantly.

Modelling

Distribution, transport and fate of SCCPs in the environment was investigated using several multi-media models [*Vulykh et al.*, 2007; *Gluge et al.*, 2013; *Gawor and Wania*, 2013; *Krogseth et al.*, 2013; *Chen et al.*, 2019]. A number of aspects related to environmental pollution by SCCPs was studied including physical-chemical properties, emissions, and approaches to describe their fate. It should be noted that model assessment of chlorinated paraffins represents a challenging task due to the complexity of composition of their mixtures [*Chen et al.*, 2019] and wide range of variations of isomers properties that leads to remarkable variability of their behaviour in the environment [*Gawor and Wania*, 2013].

Estimates of long-range transport potential and persistence in the environment for selected SCCPs were obtained using numerical multi-media model MSCE-POP [*Vulykh et al.*, 2007]. The model predictions using conventional point emission source in Europe showed atmospheric half-lives of the selected three isomers in the range from 2 to 4 days, and transport distance in the atmosphere from 1700 up to 2600 km.

Systematic investigation of the SCCP physico-chemical properties was carried out in the study [*Glüge et al.*, 2013]. The study of [*Gawor and Wania*, 2013] describes an approach to analyze variability of physical-chemical properties of individual isomers within the complex mixtures (e.g. SCCPs), determined using quantitative structure–property relationships methods.

Investigation of environmental fate of SCCPs in the western part of the Baltic Sea region was carried out using the combination of environmental fate model CoZMoPOP and bioaccumulation model ACC-HUMAN [*Krogseth et al.*, 2013]. The study indicated the large variability of environmental fates of individual isomers within the group of SCCPs that needs to be taken into account in the assessment of SCCP pollution. The global environmental fate of SCCPs was studied using a mechanistic fugacity-based multimedia fate model BETR-Global [*Chen et al., 2019*]. The obtained results showed that the effect of usage of single and multiple sets of SCCP physical-chemical properties was less remarkable in areas with substantial emissions comparing to the areas with negligible emissions.

Perfluorooctane sulfonic acid and its derivatives (PFOS)

Perfluorooctane sulfonic acid and its derivatives (perfluorooctane sulfonates) comprise a group of fully fluorinated chemicals with eight carbons chain length, belonging to the larger group of chemicals, known as per- and poly-fluoroalkyl substances (PFAS).

PFOS are substances of anthropogenic origin. They are widely distributed in the environment both in the vicinity of emission sources and in the remote regions. PFOS can occur in the ionic form as a fully fluorinated anion or as a part of PFOS-related substances, which can degrade and form PFOS [*Brooke et al.*, 2004]. For example, the precursors of PFOS are volatile PFAS.

Although PFOS are related to POPs, their physical-chemical properties differ markedly from those of traditional POPs. PFOS do not undergo hydrolysis, photolysis or biodegradation in the environment, and, hence, they are extremely persistent [*OECD*, 2002]. Compared to other POPs, PFOS and their precursors are easier dissolved in water. Because of relatively low vapour pressure and small air-water partition coefficient, PFOS themselves are not expected to volatilize significantly [*UNEP*, 2006]. Therefore, most likely they present in the atmosphere in particulate phase that was confirmed experimentally by the study [*Ahrens et al.*, 2012] demonstrated that about 90% of PFOS in air of Toronto was bound to aerosol particles. However, a number of PFOS-related substances, e.g., precursors of PFOS, have much higher vapour pressure than PFOS itself. Therefore, the PFOS precursors can volatilize and disperse in the atmosphere over the globe and degrade to PFOS even in remote locations.

Regulation

PFOS are identified as highly persistent [*Frömel et al.*, 2010; *Young et al.*, 2010], potentially bioaccumulative [*Conder et al.*, 2008] and toxic substances [*OECD*, 2013]. Studies of PFOS in different regions of the world indicated their widespread occurrence in the environment including the presence in biota and humans [*Giesy et al.*, 2001; *Vestergren et al.*, 2009]. Since 2000, PFOS were included in the work programs of various national and international organizations, aimed to collect the information on their environmental levels and trends as well as to develop measures for the restriction of their use (in particular, by CLRTAP, Stockholm Convention, OECD, AMAP, OSPAR and HELCOM). PFOS are identified as priority hazardous substances by the EU Regulation (EU) 2019/1021 on POPs, Water Framework Directive (2000/60/EC), Directive on environmental quality standards in the field of water policy (2008/105/EC), Directive on the quality of water intended for human consumption (2020/2184), and Directive on Industrial Emissions (2010/75/EU).

Production, use, and emissions

PFOS and related substances are used in various industrial applications including metal plating, production of fire-fighting foams, photographic processes, photolithography and semiconductors, hydraulic fluids for aviation, treatment of metal, glass, leather and fabrics, etc. [*OSPAR*, 2006]. Manufacturing and disposal of PFOS causes their release to the environment. In order to evaluate levels and trends of PFOS content in the environment, biota, and humans several inventories of their production, application, disposal, and emissions were elaborated.

Although PFOS is included in the Protocol on POPs to CLRTAP, no official emission data are collected currently. Nevertheless, there is a number of research activities describing emission expert estimates of PFOS and their precursors. According to [*Paul et al.*, 2009] total global emissions of PFOS to air and water for the period from 1970 to 2002 ranged from 450 to 2700 tonnes. Similar magnitude of emissions (353 – 3252 tonnes) in the period 1957-2010 was estimated by *Armitage et al.*, [2009].

The most recent global PFOS emission inventory [*Wang et al.*, 2017] is based on new methodology, the information and knowledge published in the literature as well as data reported to the UNEP Stockholm Convention after 2009. PFOS emissions were estimated for the period 1958-2015 and projections of emissions up to 2030. According to this inventory total direct and indirect emissions of PFOS are estimated as 1228–4930 tonnes, and emissions of PFOS precursors as 1230–8738 tonnes. The largest part of these emissions took place between 1958 and 2002. The subsequent period of time is characterised by substantial decrease of emissions due to reduction of production of PFOS and POSF-based products. At the same time, they are still produced in different countries and thus can be released into the environment.

Monitoring

In accordance with the EMEP monitoring strategy for the period 2020-2029 [ECE/EB.AIR/144/Add.1], per- and polyfluoroorganic compounds (PFAS) are classified as organic pollutants of growing concern. It is recommended to monitor these compounds at the research-based stations (Level 3).

Information on concentrations of PFAS in air, observed at the EMEP stations, is available since 2013. Measurements have been carried out at three Norwegian stations Birkenes, Zeppelin and Andøya, at Finnish station Pallas/Matarova and at Swedish station Råö. Observed annual mean concentrations at Pallas were lower than the detection limit value [*Aas and Bohlin-Nizetto*, 2019, 2020]. In case of Råö, the measured values are substantially higher (0.36 – 1.46 pg m^{-3}) compared to those at other stations.

Observed annual mean concentrations of PFOS, including measured monthly mean concentrations, are available from the results of Norwegian national monitoring programme for the period from 2013 to 2019 [*Nizzetto and Aas*, 2014, 2016; *Nizzetto et al.*, 2015, 2017, 2018, 2019, 2020]. Measured concentrations range from 0.02 to 0.16 pg m^{-3}. Similar to the EMEP data, a large fraction of the observed values is below the detection limit.

Measurements of PFOS at national monitoring network of Sweden have been carried out since 2009. For the period from 2009 to 2015 PFOS air concentrations ranged from 0.35 to 1.4 pg m^{-3}, and concentrations in precipitation varied from 0.58 to 3.7 ng L^{-1} at station Råö [*Fredricsson et al.*, 2021]. The highest concentrations in air were observed in 2011 and 2013. Concentrations in precipitation exhibit declining trend for 2009 – 2019 period.

AMAP monitoring network carried out measurements of PFOS in air. Along with the Norwegian Arctic monitoring stations Zeppelin and Andøya, monitoring of PFOS was performed at the station Alert [*Wong et al.*, 2018]. It was shown that as much as 96% of measurements collected at Alert station from 2006 to 2014 were above the detection limit, and median concentrations were 0.07 pg m^{-3}.

Modelling

Several attempts have been made to model environmental levels of PFOS or its precursors. Most of the works are focused on evaluation of the pollution levels in water bodies, and some take into account atmospheric processes involving PFOS. Modified BETR model was applied to simulate fate and transport of PFOS in the Bohai costal region (Northeastern China) [*Lui at al.*, 2015]. It was shown that soil and coastal waters are the most important sinks of PFOS in the considered region, storing more than 90% of PFOS at steady-state conditions.

Zhang et al. [2017] investigated processes of transport, accumulation and temporal evolution of PFOS in waters of Northern Atlantic using simulations of ocean circulation model MITgcm. Time-dependent inventory of PFOS inputs from wastewaters was prepared for the period from 1958 to 2010. It was assumed that generation of PFOS from degradation of its precursors in the atmosphere is insignificant. Evaluation of modelling results against measurement data showed general underestimation (~75%) of the observed levels. Temporal long-term variability of PFOS levels demonstrated increase until 2000s and further decline.

An effort to predict the long-term fate and concentrations of PFOS in water, sediment and fish of San-Francisco Bay was made by *Sánchez-Soberón et al.* [2020], using the multi-box model originally developed by *Mackay* [1994], which was adopted for simulations of PFOS. It was predicted that PFOS concentrations exhibited exponential decline from 2009 to 2059, and about 500 years would be required to reach stable concentrations of PFOS in sediments and fish.

In order to simulate long-term fate of PFOS and transport of volatile precursors to remote locations (e.g Arctic) global CliMoChem model was applied by *Armitage et al.* [2009]. It was shown that air and water concentrations of the pollutants increased from 1970 to 2000. Although concentrations of the precursors in air and water dropped after 2000, concentrations of PFOS in the Arctic waters continued to increase. Model assessment revealed the ability of PFOS to disperse over the global scale reaching even remote regions of the Northern hemisphere.

Most of researches consider transport and dispersion of PFOS and related species taking into account anthropogenic emissions or releases to water or air. A Norwegian Earth System Model (NorESM) was used to simulate global-scale suspension of PFOS to the atmosphere via sea spray aerosols and consequent atmospheric transport to land [*Johansson et al.*, 2019]. Modelling of wind suspension of sea spray aerosols from water surface allowed estimating emissions of PFOS in the range from about 40 to 800 tonnes per year which represented significant source comparing to anthropogenic emissions.

General peculiarity of the available modelling studies for PFOS was the consideration of water bodies as the main environmental compartment for their dispersion, while other compartments including the atmosphere played less important role.

Hexabromocyclododecanes (HBCDDs)

HBCDDs are the most often used brominated flame retardants throughout the world. Technical HBCDD mixture consists of a number of stereoisomers. Main stereoisomers, namely α-HBCDD, β-HBCDD and γ-HBCDD have different physical-chemical properties which lead to the different character of their behavior in the environment. The most complete information on physical-chemical properties of HBCDD stereoisomers is available for γ-HBCDD. Technical HBCDD products contain about 10% of α-HBCDD, 5% of β-HBCDD and 80% - 85% of γ-HBCDD. However, in biological samples α-HBCDD is a predominant stereoisomer [*Covaci et al.*, 2006; *DEFRA*, 2010].

Regulation

Toxicological and ecotoxicological properties of HBCDDs were intensively investigated beginning from early 2000s. The EU CLP Regulation 1272/2008 marks them as reproductive toxicants. In other notified classifications, submitted by industry enterprises, HBCDDs are considered also as toxic compounds for aquatic wildlife. In 2013, HBCDDs were included into the Stockholm Convention for elimination without specific exemptions. In May 2019 HBCDDs were included into Annex III (List of Banned or Restricted Chemicals) of Rotterdam Convention. The latter document classifies HBCDDs as substances of very high hazard for aquatic toxicity (both acute and chronic), high persistence and very high bioaccumulation potential. HBCDDs is a candidate for the inclusion into the Protocol on POPs to the CLRTAP. HBCDDs are included as part of the brominated flame retardants group in the List of Substances for Priority Action of the OSPAR Convention. Additional information on HBCDD regulation can be found in [*WHO*, 2013].

Production, use, and emissions

HBCDD technical mixtures were mainly applied as additive-type brominated flame retardants (BFR) for extruded and expanded polystyrene foams. Other applications include their use in crystal and high-impact polystyrene, resins, textile, adhesives, and coatings. HBCDDs can enter the environment at all stages of their life-cycle. Main pathways of emissions include production of BFRs or the manufacture of flame-retarded products, leaching from consumer products, or following disposal as wastes [*Covaci et al.*, 2006; *ECHA*, 2009].

Monitoring

First data on the presence of HBCDD in the environment were obtained in the beginning of 1990s [*De Wit,* 2002; *Lee et al.*, 2016]. Most widely the presence of HBCDD in the atmosphere in Sweden and Finland in 2000 – 2001 was investigated by [*Remberger et al.*, 2004]. An urban site had concentrations between 76 pg m^{-3} and 610 pg m^{-3} whereas the remote sites showed the concentrations between less than 1 pg m^{-3} and 280 pg m^{-3}.

During the recent decade measurements of HBCDD in Sweden and Finland were performed at two EMEP sites Pallas and Råö in 2015–2018. Observed values of HBCDD concentrations ranged from less than 0.1 pg m^{-3} up to 10 pg m^{-3}.

Modelling

A number of studies were recently performed to evaluate levels of HBCDD concentrations in the environment using available modelling approaches. In particular, BETR-Global model [*MacLeod et al.*, 2011] with emissions estimates obtained using dynamic substance flow model CIP-CAFÉ [*Li and Wania*, 2016; *Li and Wania*, 2017; *Li et al.*, 2017] was used. As stated in *Li and Wania* [2017], BETR-Global models succeeded in reproducing concentrations of sum of three main HBCDD isomers observed at GAPS monitoring stations [*Lee et al.*, 2016]. Besides, long-range atmospheric transport potential and persistence of HBCDDs were evaluated using the MSCE-POP multicompartment hemispheric transport model [*Vulykh et al.*, 2009]. The model predicted that the residence time of HBCDD mixture in the atmosphere was about 3 days and the transport distance was about 1800 km.

Concluding remarks and further activities

CECs comprise a large group of pollutants that are characterized by a wide range of physical-chemical properties and different behavior in the environment. These substances are receiving increasing attention in many international and national environmental organizations due to potential risk for wildlife and human health. However, literature overview demonstrates, that information on physical-chemical properties of CECs, on concentrations in environmental compartments, and on levels of emission is not sufficient or lacking.

Model assessment of pollution by CECs requires more detailed monitoring data on their content in the environment and temporal trends as well as elaboration of emission inventories. Besides, further improvement of understanding of processes governing their fate is of importance for the assessment of pollution levels (e.g. of gas-particle partitioning in the atmosphere, air-surface exchange, degradation in media). Furthermore, improvements of existing modelling approaches are needed to apply them for some of the new POPs and CECs (e.g. polar, ionizable compounds), which have different behavior in the environment comparing to traditional POPs.

4.3. Mercury pollution: A case study for Norway

Mercury is known as a toxic pollutant capable of long-range transport and pollution of remote areas. Long residence time in the atmosphere and ability to cycle among the environmental media determine global character of Hg dispersion and significant pollution levels in regions located far from emission sources (polar regions, open ocean, etc.). Recent studies of the Arctic pollution with mercury [*AMAP*, 2021; *Dastoor et al*., 2022] showed that more than 98% of Hg pollution in the region is transported from outside through atmospheric and oceanic transport. It leads to contamination of terrestrial and aquatic ecosystems of the high latitude regions and northern countries.

A detailed study of Hg pollution on a country scale was performed for Norway as a part of the Norwegian Mercury Assessment 2022 [*NMA,* 2022]. The study continues a series of country-scale researches performed by MSC-E over the past decade and focused on analysis of heavy metal and

POP pollution in selected EMEP countries (Croatia, the Czech Republic, the Netherlands, Belarus, Poland, Germany, the UK, Spain and France). These studies are carried out in close collaboration with national experts and involving detailed national data on observations and emissions.

In the current project MSC-E supported NMA 2022 with modelling data and participated in the analysis of spatial patterns of Hg levels in Norway and adjacent seas, long-term trends of Hg emissions, concentration and deposition to the country as well as Hg levels and trends in biota. A summary of the research results is discussed below.

Data used

A variety of modelling data were involved to the analysis of Hg atmospheric pollution and trends in Norway. Spatial patterns of Hg levels in the country were analysed using national-scale fine-resolution simulations with the GLEMOS model (v2.2.2) for the years 2000, 2005, 2010, 2015 and 2019. The analysis of pollution trends over the period 1990-2019 was based on the long-term regional GLEMOS simulations performed as a part of the project focused on assessment of heavy metal pollution of the OSPAR maritime areas [*Ilyin et al*., 2022]. In addition to this, multi-model global-scale simulations performed within the AMAP Mercury Assessment 2021 [*AMAP*, 2021] were used for the analysis of Hg atmospheric loads to the North Atlantic and the Arctic aquatic regions.

The country-scale modelling results were evaluated against the EMEP monitoring data for stations located in Norway and other Scandinavian countries. Detailed evaluation of the long-term regional simulations is presented in [*Ilyin et al*., 2022]. Description and evaluation of the global-scale results of the multi-model ensemble are given in [*AMAP*, 2021; *AMAP/UNEP,* 2019]. Spatial distribution of Hg deposition in Norway was compared with observed Hg concentrations in moss from the data collected by ICP-Vegetation [*Harmens and Norris*, 2008; *Harmens et al*., 2013; *Frontasyeva et al*., 2020]. Simulated Hg deposition to the marine areas was also compared with Hg measurements in fish [*Bank et al*., 2021; *Ho et al*., 2021].

Spatial patterns

Modelled spatial patterns of Hg^0 air concentration and wet deposition in the Scandinavian region are shown in Figs. 4.5 and 4.6 for 2000, 2010 and 2019 in comparison with observed levels at available measurement sites. Air concentrations of Hg^0 slightly vary along the country with somewhat higher concentrations in the southern part of the country, which is closely located to major European emission sources, and lower levels in the northern part (Fig. 4.5). Besides, Hg^0 are somewhat higher over the aquatic regions in comparison with terrestrial areas due to stronger Hg^0 dry deposition over land through the vegetation uptake. There is evident concentration decrease between 2000 (1.3-1.6 ng/m^3) and 2019 (1.2-1.4 ng/m^3) that is confirmed by observations.

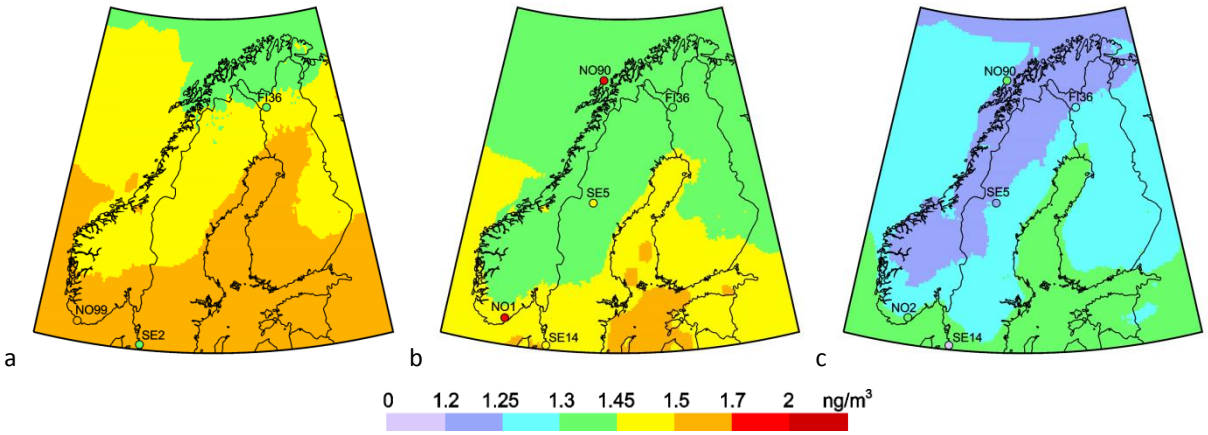

Fig. 4.5. *Spatial distribution of simulated Hg^0 concentration over Scandinavia in 2000 (a), 2010 (b) and 2019 (c). Circles show measured values in the same colour palette.*

The spatial distribution of Hg wet deposition is more complex and is largely determined by Hg atmospheric chemistry and the precipitation pattern. Elevated levels of wet deposition (10-15 g/km^2/y) occur over the Norwegian coast due to large annual precipitation and in other areas of Scandinavia (5-10 g/km^2/y) because of the effect of Hg^0 oxidation in the atmosphere to soluble Hg^{II} forms, which are easily scavenged by precipitation. In general, temporal changes of Hg wet deposition between 2000 and 2019 are smaller than spatial variability of the wet deposition levels over the region.

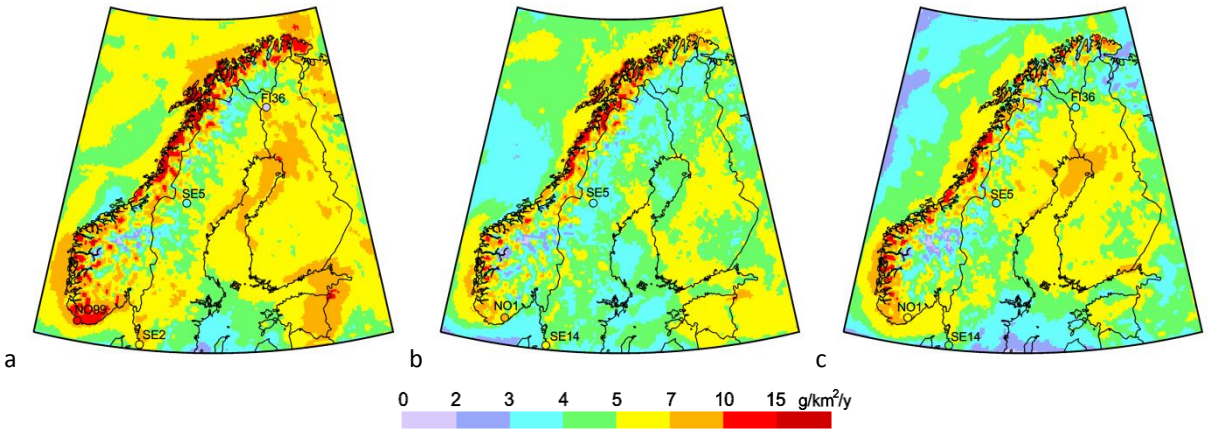

Fig. 4.6. *Spatial distribution of simulated Hg wet deposition over Scandinavia in 2000 (a), 2010 (b) and 2019 (c). Circles show measured values in the same colour palette.*

Figure 4.7 shows maps of simulated Hg total deposition in Norway in comparison with measurements of Hg concentration in moss for 2000 and 2015. The distribution of Hg deposition over the country partly follows that of wet deposition (Fig. 4.7a and 4.7c). High deposition fluxes (above 16 g/km^2/y) occur in the most southern part of the country due to the proximity to significant emission sources in Central Europe and over the Atlantic coast because of intensive precipitation and, consequently, large contribution of wet scavenging. Worth noting that elevated Hg deposition levels estimated over the coast in the most northern part of the country, which are due to the effect of the springtime atmospheric Hg depletion events (AMDEs). As a result, no significant north-south gradient of Hg deposition over territory of the country was found. The lowest deposition levels were estimated in the middle of the southern and the inland northern parts of the country due to relatively dry climate.

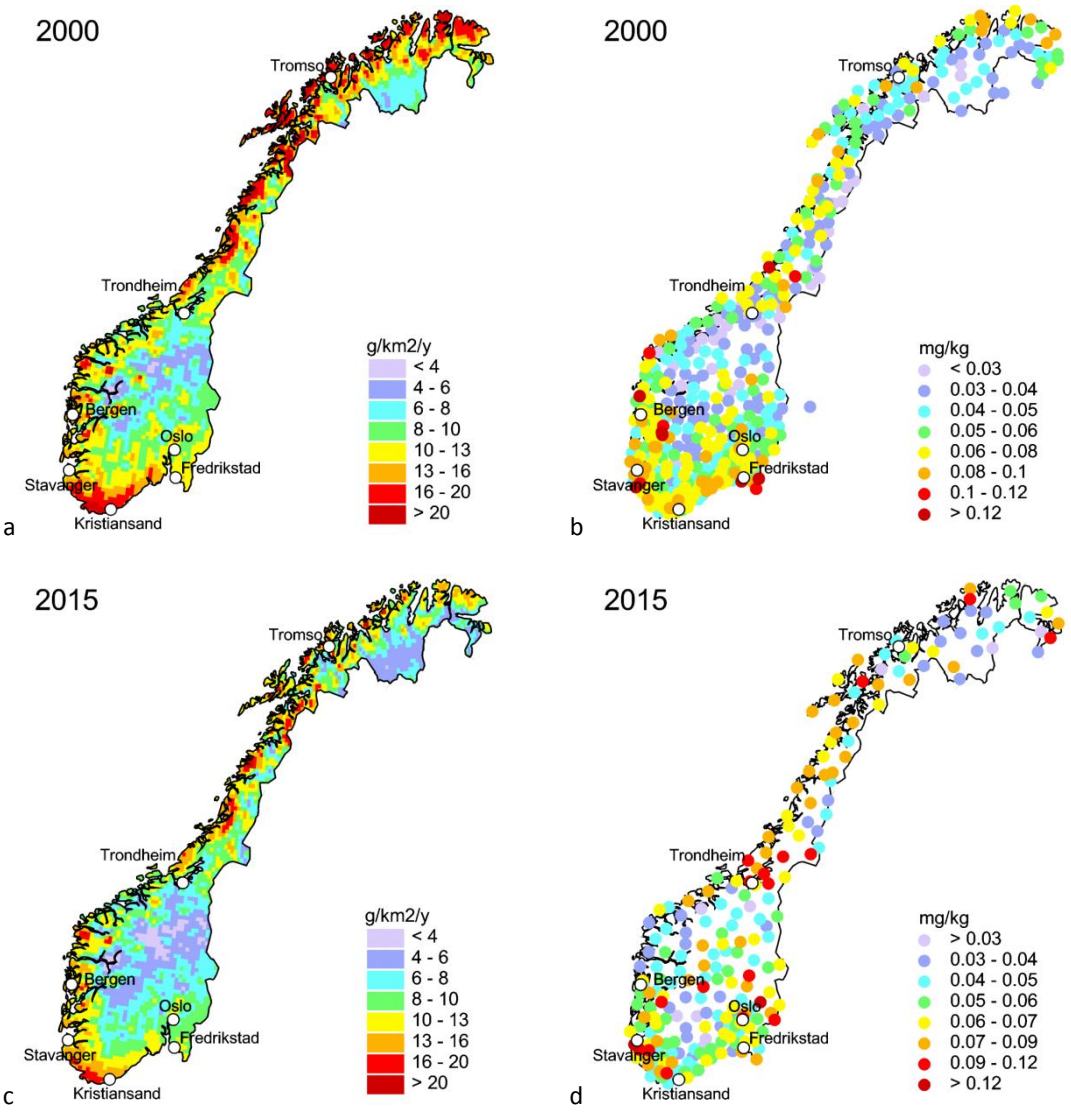

Fig. 4.7. *Spatial distribution of simulated Hg deposition over the territory of Norway (a, c) and measured Hg concentration in moss (b, d) in 2000 and 2015.*

In general, the modelling results agree with measurements of Hg in moss (Fig. 4.7b and 4.7d) in terms of areas with high and low Hg atmospheric loads. Elevated Hg concentrations in moss also observed in the southern part and along the coast including the most northern areas. Lower levels are found in the inland territories of the southern and northern parts of the country. There are also differences between the estimates of deposition and concentrations in moss patterns. For instance, high Hg levels in moss were observed in some locations in the southeast, around Oslo, which were not captured by the model. Additional analysis is needed to reveal the reasons of the deviations.

Consumption of fish and other seafood is one of the major pathways of human exposure to Hg pollution. Therefore, spatial variation of Hg deposition to marine regions of the North-East Atlantic and the Arctic was compared with Hg concentration in marine fish measured in these regions (Fig. 4.8). Mercury levels in fish generally correlate with Hg atmospheric loads. Both model and observations demonstrate higher Hg levels in the coastal waters of the North and Norwegian Seas, Skagerrak strait, and open waters of the North Atlantic. The lowest Hg deposition and concentration in fish levels are in

the Barents Sea. It should be noted that beside atmospheric deposition Hg levels in fish depend on many other factors that complicate the relationships.

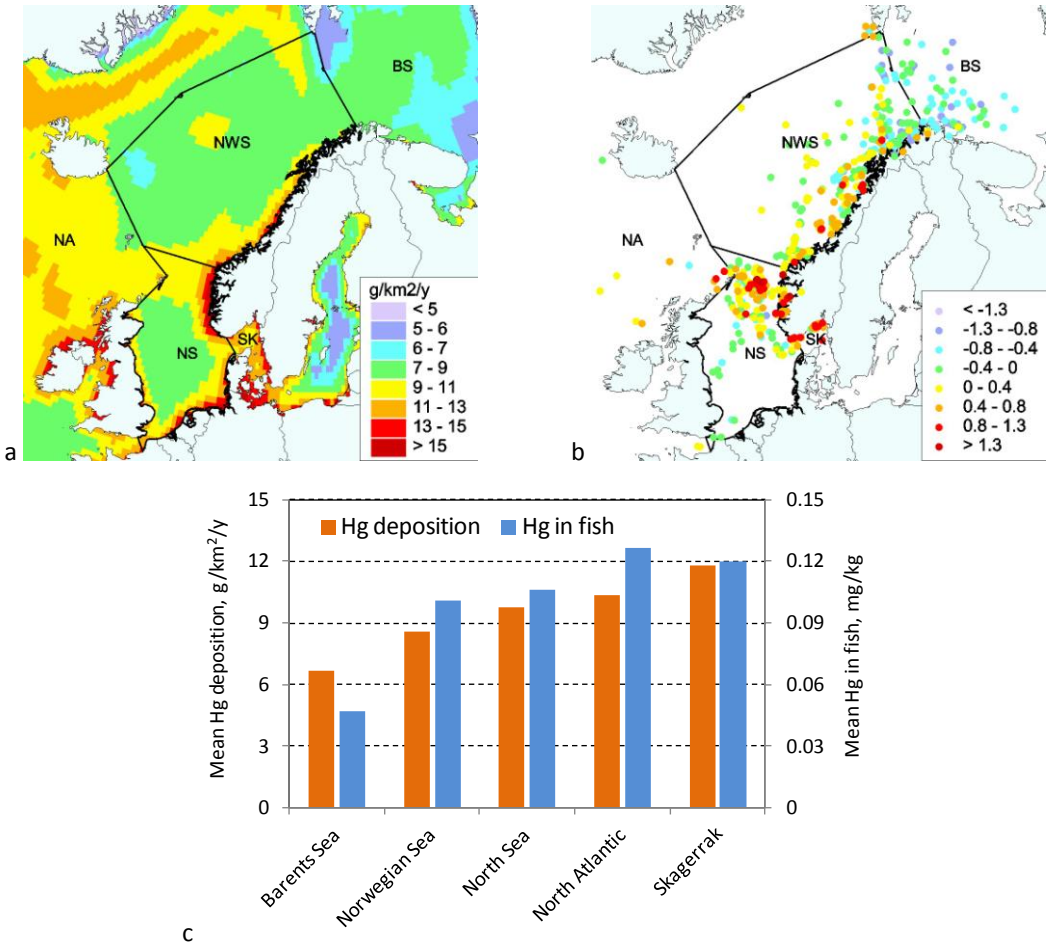

Fig. 4.8. *Spatial distribution of simulated Hg deposition over marine regions of the North East Atlantic and the Arctic adjacent to the Norwegian coast in 2015 (a) and measured Hg concentration in fish in 2006-2019 (scaled value of the log-transformed level across all fish species, Ho et al., 2021) (b). (c) – comparison of average levels of Hg deposition and concentration in fish in different marine regions.*

Long-term changes of Hg levels in Norway were studied using variety of data including model estimates, measurements in the atmosphere, mosses, and marine fish. Both modelling results and Hg atmospheric measurements show relatively small reduction (17%) of Hg^0 air concentration (Fig. 4.9a) over the past 30 years because of significant contribution of global emissions that have been slowly changing. Somewhat larger decrease over the period (30%) is demonstrated by Hg wet deposition measured and modelled at monitoring sites Birkenes/Lista located in the southern part of the country (Fig. 4.9b). Mercury wet deposition is stronger affected by regional emissions in Europe, which have been considerably reduced over the period.

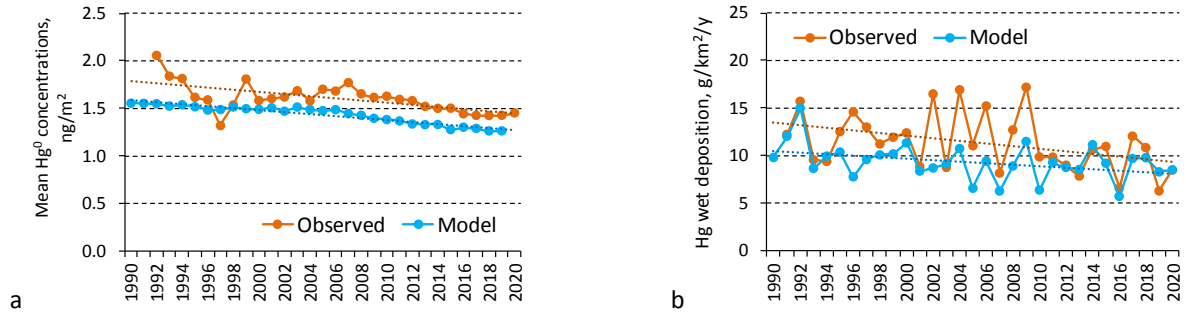

Fig. 4.9. *Long-term trends of measured (average over sites Birkenes/Lista, Andoya and Zeppelin) and simulated (average over Norway) Hg^0 air concentration (a) and wet deposition at site Birkenes/Lista (b).*

Average total (wet+dry) Hg deposition to the country (25%) undergoes slightly smaller decrease over the 30-years period because of the influence of slowly changing deposition levels in the northern part of the country (Fig. 4.10a). It is also confirmed by insignificant changes of Hg concentration in moss averaged over the territory of the country. Similar reduction rate was estimated for Hg deposition to the coastal area of the Norwegian Sea over the past 10 years (10%) (Fig. 4.10b). In contrast, Hg concentration in fish (*Greenland halibut*) caught in this region have decreased rapidly over the same period (60%). This difference shows importance of other factors, which can additionally affect Hg levels in fish including fish migration, complexity of food web, individual diet, etc.

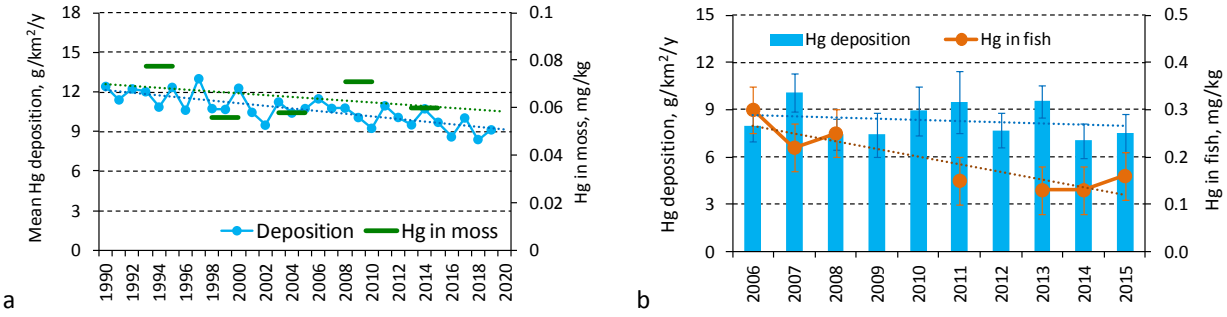

Fig. 4.10. *Long-term trends of average simulated Hg deposition and measured Hg concentration in moss in Norway (a) and Hg deposition over the Norwegian Sea in comparison with Hg concentration in fish (Greenland halibut, Bank et al., 2021).*

The performed country-scale study provides additional details of Hg pollution in Norway and could be useful for the effectiveness evaluation of national and international pollution reduction measures. Besides, further analysis of deviations between the modelling results and observations can help to improve further the modelling approaches.

4.4. PAH pollution: A case study for Poland

The case study for Poland continues a series of national scale case studies on PAHs [*Gusev et al.,* 2017; 2018; 2019] that were performed following the recommendation of the 2nd joint session of the Working Group on Effects and the Steering Body to EMEP held in 2017. The study was initiated in 2020 after the meeting of EMEP and national experts in modelling and emissions of PAHs (November, 2019). Main objectives of the study include:

1. Evaluation of the updated national PAH emission inventory reported to EMEP [*Bebkiewicz et al.*, 2020];
2. Analysis of PAH pollution levels and exceedances of air quality guidelines in Poland using modelling results and detailed measurements.

Polish inventory of national PAH emissions was substantially updated in 2019-2020 following the review recommendations of Task Force on Emission Inventories and Projections (TFEIP). Most of the updates were associated with the refinement of emission factors in the NFR category 1A4 related to the emissions from stationary combustion sources. Besides, time-series of total annual PAH emissions for the period 1990-2018 were updated on the basis of the EUROSTAT statistical data. These changes led to substantial increase of PAH emission estimates in the inventory submitted in 2020 comparing to the previous PAH emission estimates.

The first phase of the study was focused on the model assessment of B(a)P pollution in the country. using three different emission data sets, based on national inventories and emission scenarios. The model simulations with the scenario emissions allowed improving agreement between the model and measurements and indicated possible underestimation of national B(a)P emissions in Poland. The results were described in the EMEP Status Report on HMs and POPs [*Ilyin et al.*, 2021].

In the second phase of the study other 3 PAHs of the Protocol, namely, B(b)F, B(k)F, and I(cd)P, were considered. In particular, analysis and update of GLEMOS model parameterization for these 3 compounds was carried out. The GLEMOS model was used to evaluate previous and updated national emission inventories of 3 PAHs. Besides, exceedances of air quality guidelines for PAHs were estimated. Below in this section the outcome of the second phase of the study is briefly presented.

Refinement of GLEMOS model parameterization

As the initial step of the second phase, it was planned to analyze and update GLEMOS model parameterization for B(b)F, B(k)F, and I(cd)P. Similar to B(a)P these PAHs are semi-volatile compounds presenting in the atmosphere both in gaseous and particulate forms and undergo reactions with atmospheric reactants. The most significant processes influencing their transport and fate in the atmosphere include gas-particle partitioning and degradation.

In contrast to B(a)P, simplified parameterization of B(b)F, B(k)F, and I(cd)P gas-particle partitioning (GPP) and degradation was implemented in the GLEMOS model. In particular, it was based on the adsorption Junge-Pankow GPP scheme [*Junge*, 1977; *Pankow*, 1987]. The degradation was assumed

to take place only in the gaseous form of PAHs due to reaction with OH radical. These simplifications led to an overestimation of observed air concentrations, especially for the warm period of the year.

To improve performance of the model, the GPP parameterization was changed to the dual scheme that includes absorption into organic matter and adsorption to black carbon [*Dachs and Eisenreich*, 2000; *Lohmann and Lammel*, 2004]. Besides, parameterization of PAH degradation in particulate form was added based on the results of experimental studies [*Kahan and Donaldson*, 2006; *Kwamena et al.*, 2004, 2007]. Results of sensitivity model simulations showed noticeable improvement of model performance for B(b)F, B(k)F, and I(cd)P (Fig.4.11).

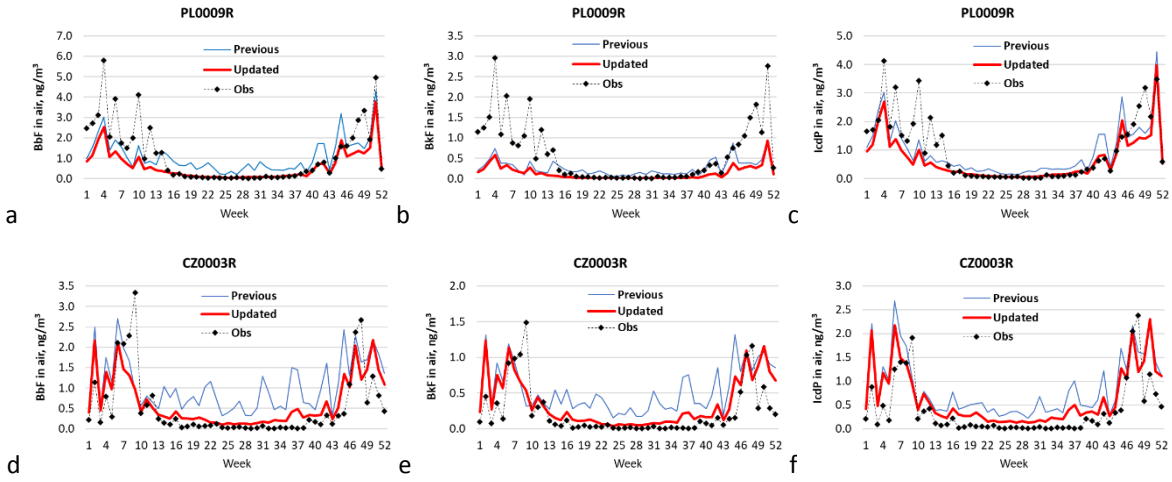

Fig. 4.11. *Seasonal variations of B(b)F (a,d), B(k)F (b,e), I(cd)P (c,f) air concentrations for 2018, simulated by the GLEMOS model on the basis of the previous and new model parameterizations, in comparison with observed concentrations at stations PL0009R (upper row) and CZ0003R (lower row).*

Model setup and input data

Model simulations for the PAH case study for Poland were carried out for the year 2018. Two datasets of gridded anthropogenic emissions for each of three considered PAHs (B(b)F, B(k)F, I(cd)P) were prepared for model simulations. The first dataset (*PL_OLD*) was constructed using the previous national emission inventory of Poland for EMEP (submission 2019). In the second dataset emissions of Poland were substituted by the new inventory (*PL_NEW*). For other EMEP countries emission data for 2018 provided by CEIP (submission 2020) was used. Spatial distributions of annual emissions of B(b)F, B(k)F, and I(cd)P used in model simulations are presented in Fig. 4.12.

It is seen that B(b)F and B(k)F emission estimates of PL_NEW inventory are higher comparing to PL_OLD inventory. On the contrary, PL_NEW inventory provided lower I(cd)P emissions in comparison to PL_OLD inventory.

Seasonal variations of PAH anthropogenic emissions for the GLEMOS model were generated for each emission source sector using monthly temporal factors, based on the TNO estimates of the MACC project [*Denier van der Gon et al.*, 2011].

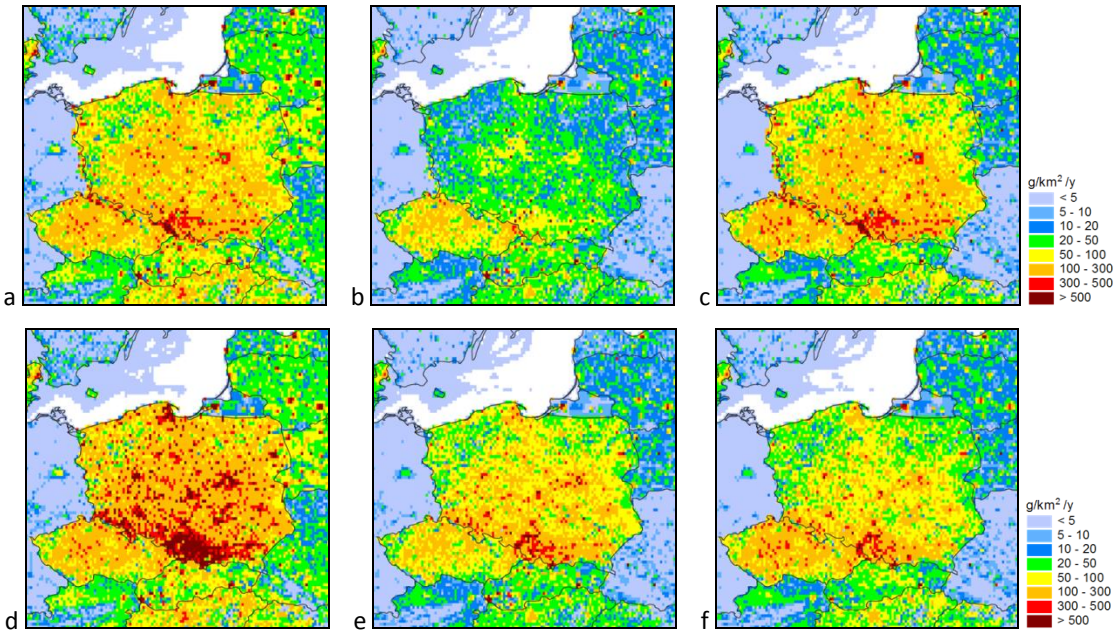

Fig. 4.12. *Spatial distribution of annual emission fluxes in 2018 according to PL_OLD inventory (a,b,c) and PL_NEW inventory (d,e,f) of B(b)F, B(k)F, and I(cd)P, respectively (spatial resolution 0.1°x0.1°).*

Modelling results and analysis

Results of model simulation were evaluated using measurement data of EMEP monitoring network and of EEA AQ e-reporting database. Annual mean modelled air concentrations of B(b)F, B(k)F, and I(cd)P for 2018, simulated using PL_OLD and PL_NEW emission datasets are shown in Fig. 4.13. The largest differences between the simulated air concentrations can be seen over the territory of Poland. Model simulations of B(b)F and B(k)F with PL_NEW emissions provided increased air concentrations whereas simulations for I(cd)P resulted in lower air concentrations compared to simulations with PL_OLD emissions.

Modelled air concentrations were compared with measurements of EMEP monitoring network and background rural, remote, and suburban stations of EEA AQ e-Reporting made in 2018. Statistical indicators of GLEMOS model performance in case of the use PL_OLD and PL_NEW emissions are illustrated in Fig. 4.14. The use of the updated national emission inventory leads to noticeable decrease of the model bias for B(b)F and B(k)F. Along with this, significant improvement of spatial correlation between the modelled and measured values is obtained. At the same time, model simulations of I(cd)P with updated emissions showed increase of model bias and decrease of spatial correlation compared to the simulations with the previous emissions.

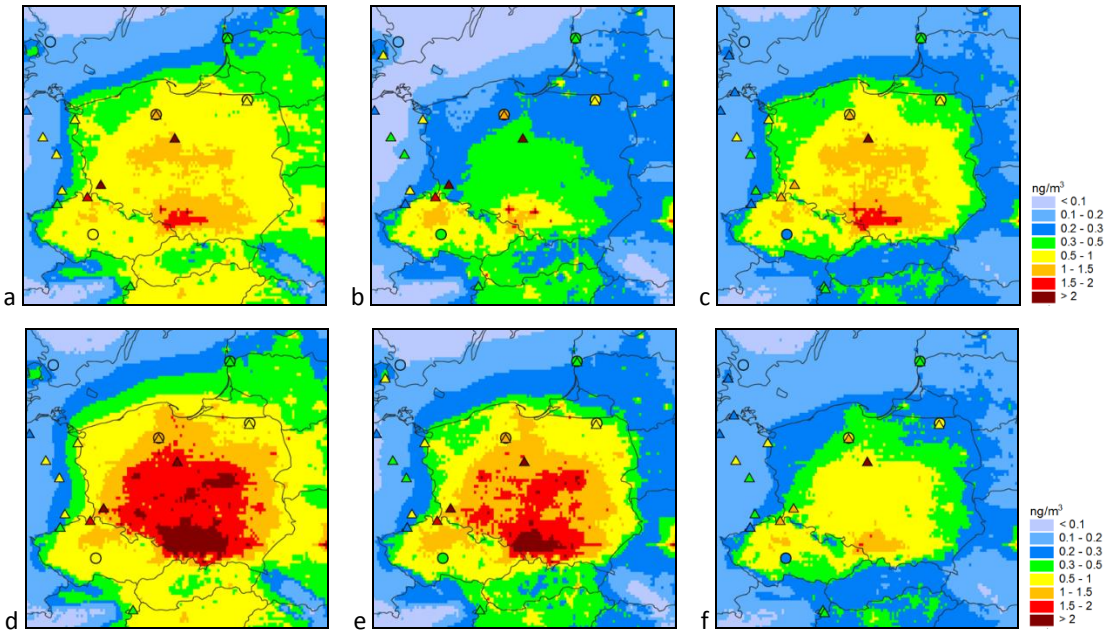

Fig. 4.13. *Annual mean modelled air concentrations of B(b)F, B(k)F, and I(cd)P in 2018 simulated using PL_OLD emissions (a,b,c) and PL_NEW emissions (d,e,f), respectively (spatial resolution 0.1°x0.1°). Maps of air concentrations are overlayed with annual mean observed concentrations of B(b)F, B(k)F, and I(cd)P for 2018 in the same scale as the modelling results (circles indicate EMEP stations, triangles – AQ e-reporting stations).*

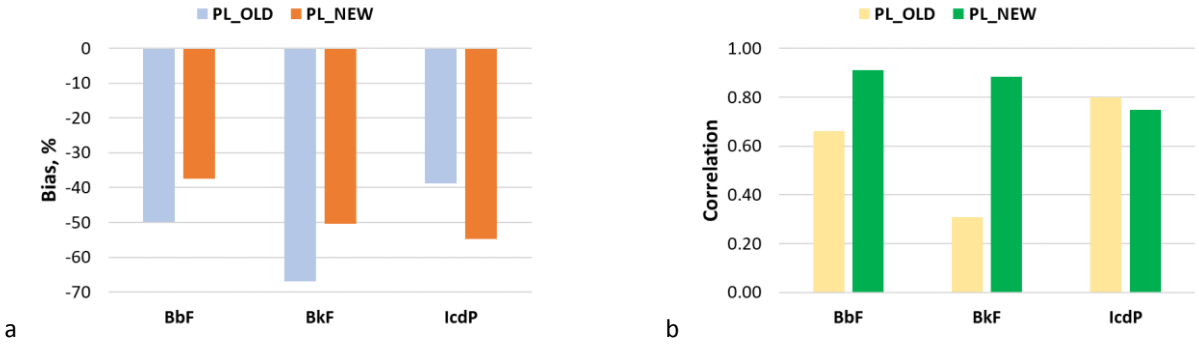

Fig. 4.14. *Mean relative bias (a) and spatial correlation (b) between the measured and modelled annual mean air concentrations of B(b)F, B(k)F, and I(cd)P for 2018 simulated using PL_OLD emissions and PL_NEW emissions.*

Results of model simulations with the new national emission inventory of 4PAHs for EMEP show that it allows to achieve better agreement with measurements for B(a)P, B(b)F, and B(k)F and improvement of accuracy of pollution assessment. At the same time, application of the new emissions for I(cd)P did not lead to improvement of model estimates. Furthermore, the study showed that modelling results still tend to underpredict observed air concentrations of the 4PAHs. Thus, further activities to reduce uncertainties of the model assessment of PAH pollution are required. They include refinement of emission estimates and model parameterizations of processes affecting PAH fate in the atmosphere. Possible future steps of the case study can include multi-model simulations, application of more detailed temporal and spatial disaggregation of PAH emissions, and co-operation with national experts in monitoring, modelling, and emissions.

4.5. Heavy metal and POP emissions from wildfires

Wildfires are the important source of atmospheric pollutants, such as particulate matter, carbon monoxide, oxides of nitrogen and sulphur, and other [*Andreae and Merlet*, 2001; *Urbanski et al*., 2009]. Besides, biomass burning is a contributor to the global pool of greenhouse gases [*Liu et al.*, 2014]. A number of studies also report about the effects of wildfire emissions on human health [*Reid et al*., 2016; *Requia et al.,* 2021].

It is reasonable to assume that heavy metals and POPs are emitted to the atmosphere due to wildfires. Some estimates of emissions of Hg from the fires are described in scientific literature [*Wiedinmyer and Friedli*, 2007; *Cinnirella and Pirrone*, 2006; *Friedli et al*., 2009; *De Simone et al.,* 2015; *Kumar et al*., 2018]. B(a)P global emissions from wildfires have been estimated in the study [*Luo et al*., 2020]. However, information on emissions of particulate metals like Pb and Cd, has not been found.

The objectives of this study are the following:

1) To overview the available databases with information on wildfires.
2) To estimate heavy metal and POP emissions from wildfires in the EMEP region.
3) To evaluate the effect of wildfires on air concentrations and deposition of selected heavy metals and POPs in the EMEP region.

Wildfire databases

Four global-scale databases on wildfires were considered (Table 4.2): GFED [*van der Werf et al.,* 2017], FINN [*Wiedinmyer et al*., 2011], GFAS [*Giglio et al*., 2006] and QFED [*Darmenov and da Silva*, 2015]. These databases are characterized by different spatial resolution, varying from 1 km (FINN) to 0.25° (GFED). Period of time covered by the databases starts in 2000s and finishes in 2020 or even spreads to present days. List of the data products varies between the databases. For further evaluation of heavy metal and POP emissions the most important characteristics are estimates of PM2.5 emissions and burnt biomass or combustion rate. Besides, the data on fire injection height available in the GFAS database can be important for distribution of emissions from wildfires with height.

Spatial distributions of PM2.5 emissions from wildfires in the EMEP region in 2020 derived from the considered databases are shown in Fig. 4.15. Similarities of the distributions include emissions in the southern and south-eastern parts of Europe (Portugal, Italy, the Balkan countries) and in the eastern part of the EMEP region. Nevertheless, intensity of the emissions from the wildfires differs between the databases. Generally, particulate matter emissions from FINN and QFED databases are higher than those from GFAS and GFED databases. Total annual emission of PM2.5 in the EMEP region in 2020 from FINN, GFAS, QFED and GFED databases are equal to 1.8, 0.8, 3.3 and 0.9 million tonnes, respectively.

Table 4.2. *Global biomass burning emission datasets.*

Data set	Spatial resolution	Time range and temporal resolution	Data products
GFED(*)	0.25°x0.25°	2000-2020; 3-h, daily, monthly	Burned area; Burnt mass; Emission factors, incl. PM2.5
FINN(**)	1x1 km^2	2002-2020; Daily	Burned area; Burnt mass; Emissions of species, incl. PM2.5
GFAS(***)	0.1°x0.1°	2003-present; Daily	Combustion rate; Burnt mass; Emission of species incl. PM2.5; Injection height
QFED(****)	0.1°x0.1°	2000-present; daily, monthly	Emission of species incl. PM2.5

(*)-Global Fire Emissions Database; http://www.globalfiredata.org

(**) - Fire INventory from NCAR; https://www2.acom.ucar.edu/modeling/finn-fire-inventory-ncar

(***) - Global Fire Assimilation System; http://modis-fire.umd.edu

(****) - Quick Fire Emissions Dataset; https://portal.nccs.nasa.gov/datashare/iesa/aerosol/emissions/QFED/v2.4r6/

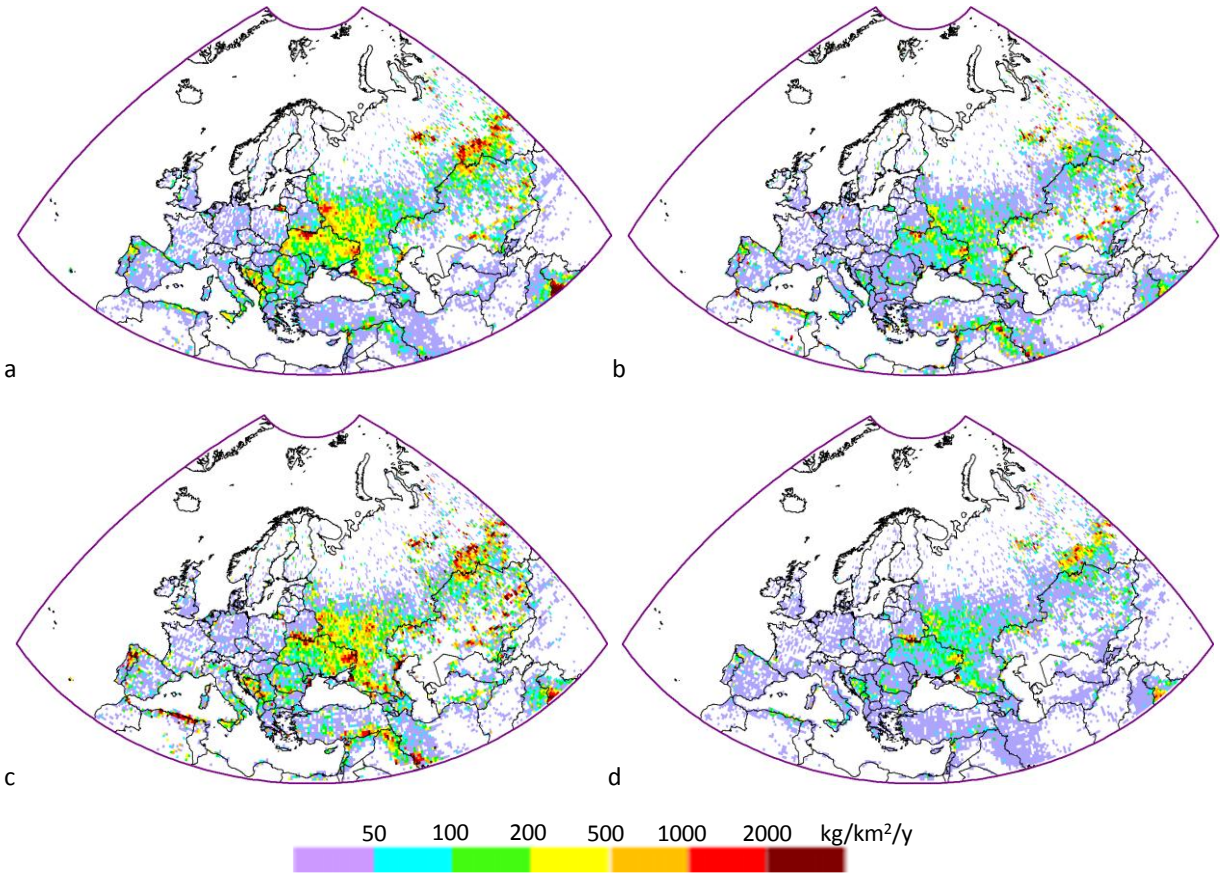

Fig. 4.15. *Annual emissions of PM2.5 in 2020, provided by wildfire databases FINN(a), GFAS(b), QFED(c) and GFED4(d).*

Emissions from wildfires are subject to strong seasonal variability. The highest emissions in 2020 are noted for April and for summer period (July-August) (Fig. 4.16). For the emissions from the FINN database a local maximum in October also takes place.

Among the available databases, FINN is characterized by the highest spatial resolution. Besides, this database is already used by MSC-W in modelling of wildfire emissions of particulate matter and acidifying compounds [*Simpson et al*., 2012]. Therefore, further pilot estimates of heavy metal and POP emissions were carried out basing on FINN database. Annual emissions of PM2.5 and burnt biomass vary substantially in the recent decade (Fig. 4.17). The highest intensity of wildfires took place in 2012, and the lowest in 2018. Year 2017 was selected for numerical experiments with the wildfire emissions.

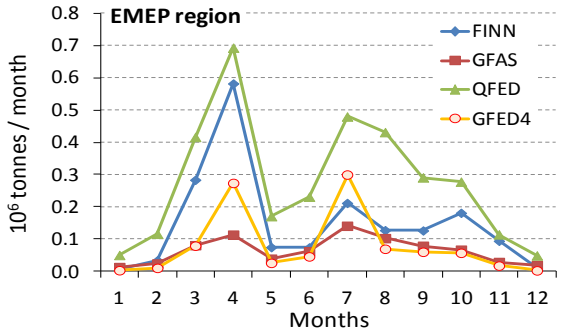

Fig. 4.16. *Monthly sums of PM2.5 emissions from wildfires in 2020 derived from FINN, GFAS, QFED and GFED4 databases.*

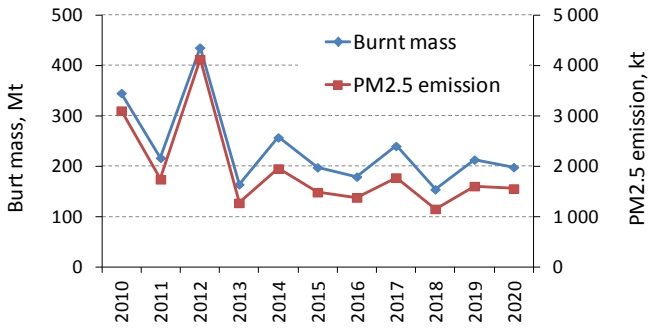

Fig. 4.17. *Annual values of burnt biomass and PM2.5 emissions caused by wildfires in the EMEP region.*

Emission of heavy metals and POPs in the EMEP region

This study was limited by pilot estimates of wildfire emissions of Pb and B(a)P. The source of B(a)P in the atmosphere is incomplete combustion of organic matter. Therefore, it is reasonable to suggest that B(a)P emission from wildfires (E_{BaP}) is proportional to biomass burnt during wildfires (*BM*):

$$E_{BaP} = BM \cdot EF_{BaP} \qquad [4.1]$$

Coefficient of proportionality EF_{BaP} in [4.1] is the emission factor. Data on burnt biomass is available in the databases on wildfire (Table 4.2). Information on emission factors for B(a)P compiled from peer-reviewed publications is summarized in Table 4.3. As seen, the emission factor varies from 0.1 for savannas vegetation to 1.59 mg/kg for pine wood. In current version of the parameterization of wildfire emissions a value of 0.5 mg/kg was used.

Spatial distribution of annual B(a)P emission from wildfires in 2017 is shown in Fig. 4.18a. There are areas of significant wildfire emissions in the southern and south-eastern parts of Europe (Portugal, southern Italy, the Balkan countries) as well as in the eastern part of the EMEP domain. Wildfire emissions in central and northern Europe are low compared to other parts of the EMEP domain. Annual emissions from anthropogenic sources are higher compared to those from the wildfires (Fig. 4.18b) in most of countries.

Table 4.3. *B(a)P emission factors for wildfires.*

Biomass/ecosystem type	Emission factor (mg/kg)	Reference
Pine with Greens	1	*Luo et al.*, 2020 and references therein
Pine	0.35	*Luo et al.*, 2020 and references therein
Fir	0.19	*Luo et al.*, 2020 and references therein
Pine wood	0.38 – 1.59	*Luo et al.*, 2020 and references therein
Wood fuel	0.693	*Luo et al.*, 2020 and references therein
Pine	0.712	*Luo et al.*, 2020 and references therein
Oak	0.245	*Luo et al.*, 2020 and references therein
Hard wood	0.14	*Luo et al.*, 2020 and references therein
Savanna	0.1	*Shen et al.*, 2013
Extratropical forest	0.35	*Lammel et al.*, 2013
Savanna, cropland (crop residues)	0.33	*Lammel et al.*, 2013

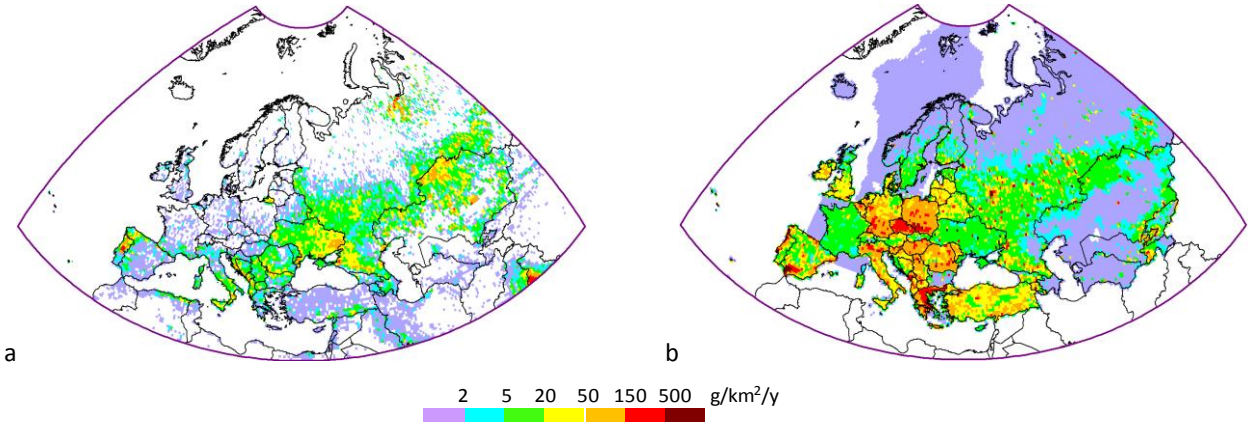

Fig. 4.18. *Spatial distribution of B(a)P emissions from wildfires (a) and anthropogenic sources (b) in 2017.*

Contribution of wildfires to total (wildfires and anthropogenic) annual emission of B(a)P in 2017 varies substantially among the EMEP countries. In 23 of 51 EMEP countries the contribution exceeds 5%, and in 7 countries it exceeds 25% (Fig. 4.19). The highest contribution is noted for Kazakhstan (around 60%) followed by Azerbaijan and Monaco.

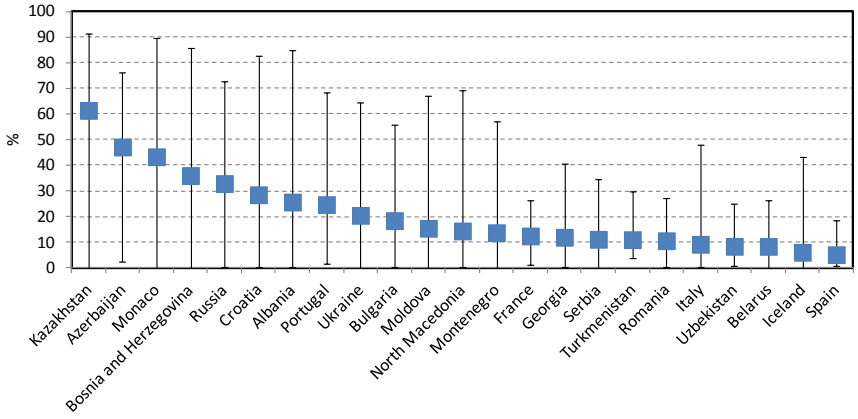

Fig. 4.19. *Contribution of wildfires to emissions of B(a)P in the EMEP countries in 2017. Whiskers indicate range between the highest and the lowest monthly-mean contributions to total emission. Only countries with the contribution exceeding 5% are shown.*

The whiskers in Fig. 4.19 indicate the range between the highest and the lowest monthly-mean contributions to total emission. Large difference between the lowest and the highest contributions means significant seasonal variability of wildfires and their contribution to total emission. Indeed, even if on annual time scale the contribution of wildfires to total emission of B(a)P is relatively low in most of the EMEP countries, on the monthly scale the situation may differ markedly. The highest anthropogenic emission of B(a)P takes place in winter because of predominant contribution of residential combustion sector in anthropogenic emissions. At the same time, the highest emissions from wildfires are expected in spring, summer and early autumn (Fig. 4.20). Therefore, in these seasons the contribution of wildfires to total emission is the highest. For example, in Italy maximum contribution of wildfires to total emission in 2017 occured in August (Fig. 4.20). Croatia and Portugal are characterized by two maximums in March and August and in August and October, respectively. In Bulgaria the contribution around 50% took place from July to October.

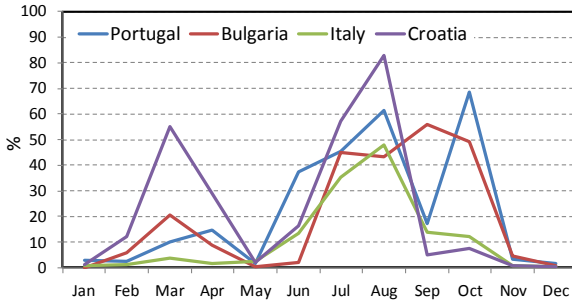

Fig. 4.20. *Monthly contribution of wildfire emissions to total B(a)P emission in 2017 in Portugal, Bulgaria, Italy and Croatia.*

Approach to estimate heavy metal emissions from wildfires differs from that used for B(a)P. Surface of parts of vegetation, such as leafs, stems, branches etc., serves as a receptor of metal deposition from the atmosphere. There are numerous studies reporting concentrations of heavy metals on leaves, needles , tree bark or forest floor [*Zsigmond et al.,* 2021; *Aboal et al.,* 2004; *Swislowski et al.,* 2020; *Parzych et al*., 2017; *Klink et al.,* 2017; *Brown et al*., 2017; *Madeijón et al*., 2004; *Bommarez et al*., 2021]. Therefore, during wildfires ash and particulate matter emitted to the atmosphere contains heavy metals previously deposited onto the vegetation. Therefore, it is assumed that emission of heavy metals due to the wildfires E_{HM} is proportional to emission of PM2.5 $E_{PM2.5}$:

$$E_{HM} = E_{PM2.5} \cdot C_{HM} \qquad [4.2]$$

Proportionality coefficient C_{HM} is concentration of particulate heavy metal (e.g., Pb or Cd) in particles in plumes from wildfire or in ash. Data on emission of PM2.5 are available in the databases on wildfires. Information on C_{HM} was found in peer-reviewed papers and summarized in Table 4.4.

Table 4.4. *Concentrations of Pb and Cd (mg/kg) in ash or PM2.5 particles of fire plumes.*

Pb	Cd	media	Region and year	Reference
87.4*	0.33	ash	Portugal, 2010	*Campos et al*., 2016
8.5**		ash	Australia, 2013	*Wu et al.*, 2017
94	0.6	ash	Portugal, 2011	*Silva et al*., 2015
10.75**		ash	Australia, 2011	*Kristensen et al*., 2014
10.7 – 21.4	0.08 – 0.09	ash	Australia, 2013	*Santín et al.*, 2015
38	0.55	ash	Greece, 2019	*Alexakis*, 2020
572*	4.9	ash	Australia, 1994-2004	*Iseley et al*., 2020
7 - 42		ash	USA, 2012	*Odigie and Flegal*, 2014
12 – 22		plume	Russia, Siberia, 2000-2003	*Самсонов et al.*, 2006
33.16**		plume	USA, California, 2017	*Kelly et al*., 2021

*mean; ** median

As follows from the Table 4.4, there is limited information on heavy metal concentrations in plumes or ash measured in Europe. For further numerical experiments aimed at evaluation of the effect of wildfires on heavy metal concentrations, a value of 90 mg/kg for Pb was selected as an average for available data of measurements in Portugal. However, it is very unlikely that Pb concentrations in ash in different parts of the EMEP region are the same as those measured in Portugal. Therefore, it was assumed that Pb concentrations in ash are proportional to modelled total Pb deposition flux. Estimated spatial distribution of Pb concentrations in ash is shown in Fig. 4.21. Relatively high concentrations (>90 mg/kg) take place in regions with elevated deposition fluxes such as Italy, Balkan region, north-western Germany, southern Poland and Turkey. Over most of Russia, Central Asia and Scandinavia the concentrations of Pb in ash are below 50 mg/kg.

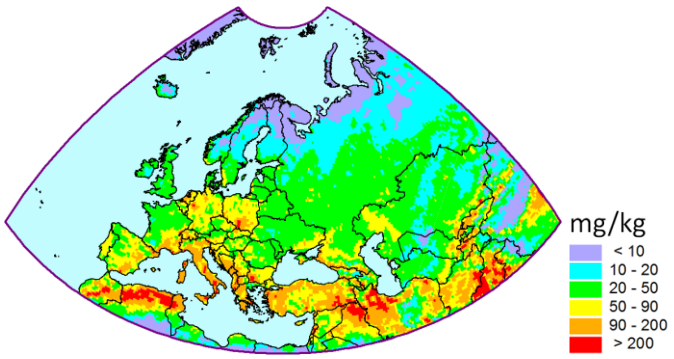

Fig. 4.21. *Concentrations of Pb in ash in the EMEP region in 2017.*

Combination of map of spatial distribution of PM2.5 emissions from wildfires and Pb concentrations in ash according to formula [4.2] results to the map of annual atmospheric emissions of Pb from wildfires in the EMEP region in 2017 (Fig. 4.22a). Areas of emissions from wildfires are noted for Portugal, southern Italy, the western part of the Balkan Peninsula and some regions in the eastern part of the EMEP domain. The central, western and northern parts of Europe are characterized by comparatively low emission of Pb from wildfires. Similar to B(a)P, emission of Pb from wildfires is much lower than the anthropogenic emission in most of the EMEP countries (Fig. 4.22b).

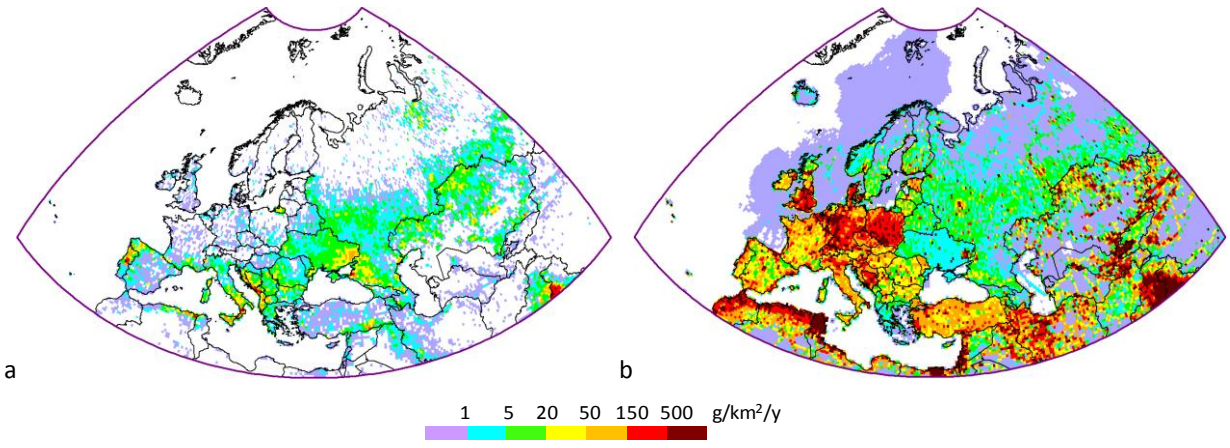

Fig. 4.22. *Spatial distribution of Pb emissions from wildfires (a) and anthropogenic sources (b) in 2017.*

Contribution of wildfire Pb emissions to total emission (wildfire and anthropogenic) on annual level exceeds 60% in Montenegro and Albania, and exceeds 5% in 11 EMEP countries (Fig. 4.23). Whiskers in the Fig.4.23 indicate the range between maximum and minimum monthly contributions of wildfire emissions. On monthly time scale these contributions can reach 20 – 90%.

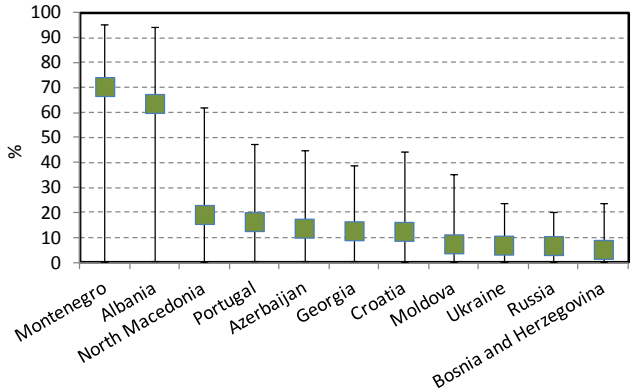

Fig. 4.23. *Contribution of wildfires to emissions of Pb in the EMEP countries in 2017. Whiskers indicate range between the highest and the lowest monthly-mean contributions to total emission. Only countries with the contribution exceeding 5% are shown.*

Model simulations of the pollution levels using wildfire emissions

Concentrations in air and total deposition fluxes of B(a)P and Pb were calculated for 2017 on the base of current stable version of GLEMOS model v2.2.2 (see Section 3.1). Two sets of the model simulations were performed: one without wildfire emissions (base case) and another one with included emissions from wildfires. To characterize the effect of wildfire emission on the pollution levels the contribution of wildfires to total concentration (base case and wildfire) was calculated.

Annual mean concentrations of B(a)P in air calculated with usage of wildfire emissions and contribution of wildfires to the concentrations are demonstrated in Fig. 4.24a and b, respectively. Areas of the highest contribution exceeding 75% are noted for the north-eastern part of Russia, numerous locations in Kazakhstan and in some non-EMEP countries (Algeria, Iran, west of China etc.). It is important to note that in these regions the concentrations of B(a)P are very low compared to the levels in Europe, hence even small increment of these levels in absolute terms results to the large relative increase. In southern and south-eastern Europe the contribution of wildfires to total concentration ranges mainly within 5 – 20%.

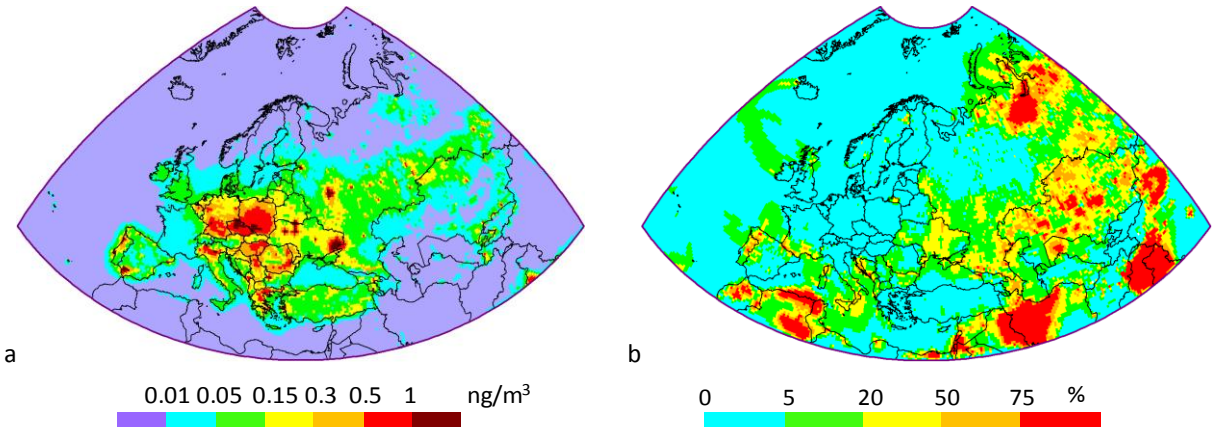

Fig. 4.24. *Annual mean concentration of B(a)P simulated with wildfire emissions included (a) and contribution of the wildfire emission to concentration (b) in 2017.*

The contribution on monthly time scale may differ substantially for particular months and countries. For example, August of 2017 is characterized by the most intensive wildfires. Large (> 75%) contribution of wildfires to total concentration is noted for Siberian and southern regions of Russia, most part of Kazakhstan and Ukraine, southern Italy, western part of the Balkan Peninsula and Portugal (Fig. 4.25a). In October when the intensity of wildfires is generally lower than in August, the contribution of the wildfires exceeds 50% in Portugal, and ranges from 20 to 50% in the southern part of Italy, south of Russia and over most of Kazakhstan (Fig. 4.25b).

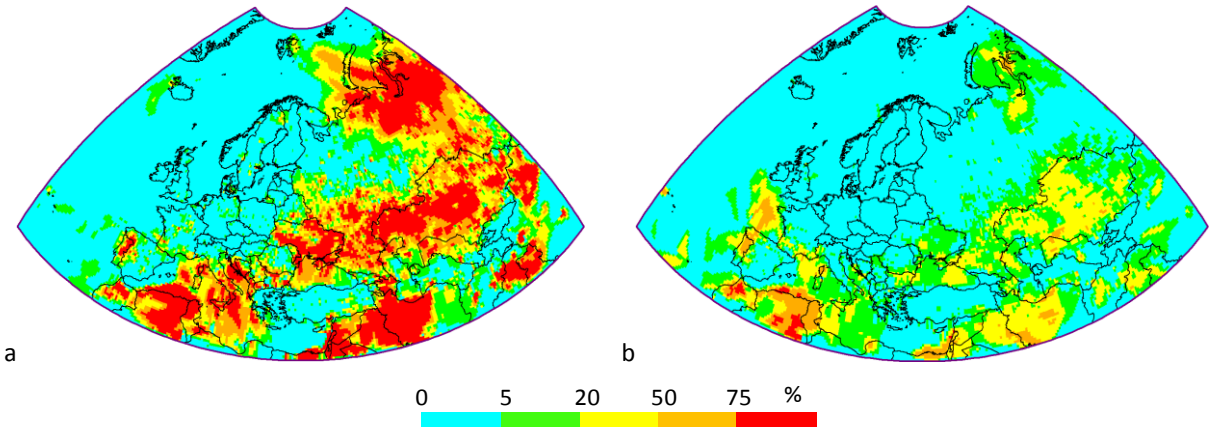

Fig. 4.25. *Monthly mean contribution of the wildfire emission to concentration of B(a)P in August (a) and October (b) in 2017.*

Contribution of wildfires to Pb annual mean concentrations in air in 2017 is relatively low. The contribution exceeds 5% in Portugal, north-western Spain, southern Italy, the Caucasus and western Siberian regions of Russia, and in a number of countries of the Balkan Peninsula (Fig. 4.26b). Contribution exceeding 15% in some locations of the western Siberia of Russia are caused by the effect of originally low concentrations in this region (Fig. 4.26a).

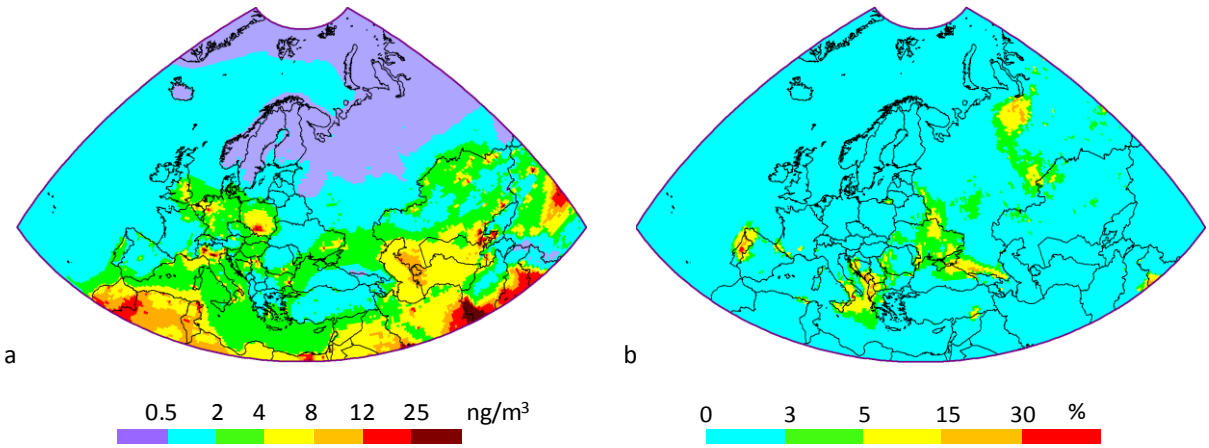

Fig. 4.26. *Annual mean concentration of Pb simulated with the usage of wildfire emissions (a) and contribution of the wildfire emission to concentration (b) in 2017.*

Much higher contribution takes place in certain months, e.g., in August and October (Fig. 4.27a,b). In August wildfires contribute more than 30% to Pb concentrations in Portugal, southern Italy, Albania, Montenegro, North Macedonia, southern Croatia and a number of locations in the eastern part of the EMEP region. It is interesting to note that significant contribution (15 – 30%) is noted for central part of Mediterranean Sea. Similar effect is seen over Iberian coast and Bay of Biscay in October. Transport of plumes from wildfires in Portugal resulted to substantial increase of Pb air concentrations over these aquatories (Fig. 4.27b). Therefore, wildfires can act as a considerable contributor to the marine pollution. Beside Portugal, large areas of significant (> 15%) contribution of wildfires to Pb air concentrations in October, 2017, took place in the southern and south-eastern parts of European Russia.

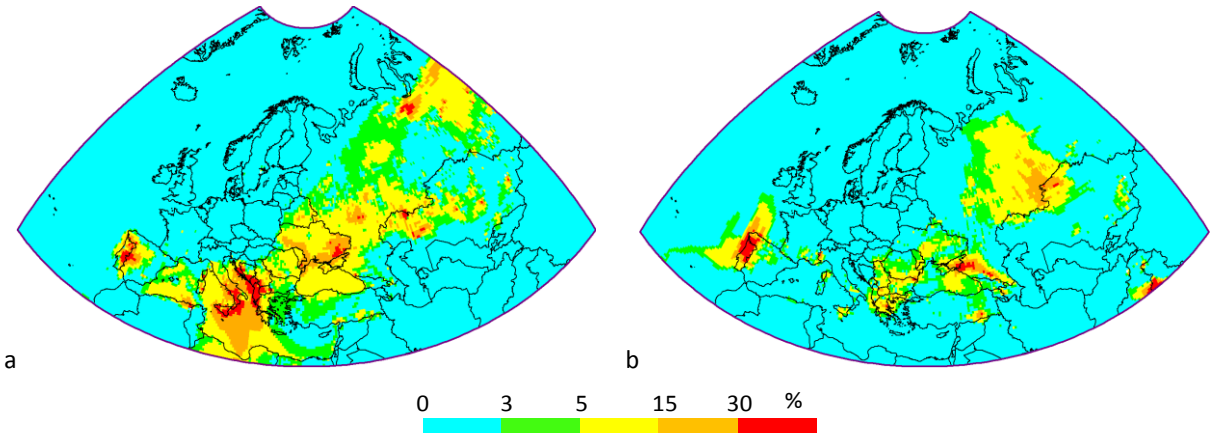

Fig. 4.27. *Monthly mean contribution of the wildfire emission to concentration of Pb in August (a) and October (b) in 2017.*

It is important to evaluate the effect of wildfires on modelled concentrations via comparison with measurements. Analysis of time series of modelled concentrations of Pb and B(a)P at particular stations demonstrated that in most cases the contribution of wildfires is revealed as one or several short-term episodes lasting for one or few days. Concentrations of B(a)P and Pb at measurement stations in southern Europe are observed mostly with weekly or monthly temporal resolution. This temporal resolution does not allow capturing short-term episodes of high modelled concentrations caused by wildfires. However, possible tracers of biomass burning such as carbon monoxide (CO), elemental carbon or particulate matter (e.g., PM2.5) are often measured with higher (e.g., daily) temporal resolution. Therefore, instead of direct comparison of modelled and observed concentrations of Pb and B(a)P, the time series of contribution of the wildfires were compared with the time series of biomass burning tracer species.

For the purposes of the evaluation the data on air concentrations from European Environmental Agency (EEA) data base AQ e-reporting (https://www.eea.europa.eu/data-and-maps/data/aqereporting-9) were used. At a number of stations episodes of high contribution from wildfires to concentrations of B(a)P coincide with increased levels of CO or PM2.5. For example, B(a)P contribution from wildfires reaching 0.25 ng/m^3 from 209 to 225 day of year 2017 correlates with the increased levels of PM2.5 and CO at Italian background urban station IT2110A (Fig. 4.28a). Similar

results are noted for other parts of Europe, for instance, for stations in Montenegro, e.g. ME0002A (Fig. 4.28b) and at some stations in Romania, e.g., RO0159A (Fig. 4.28c).

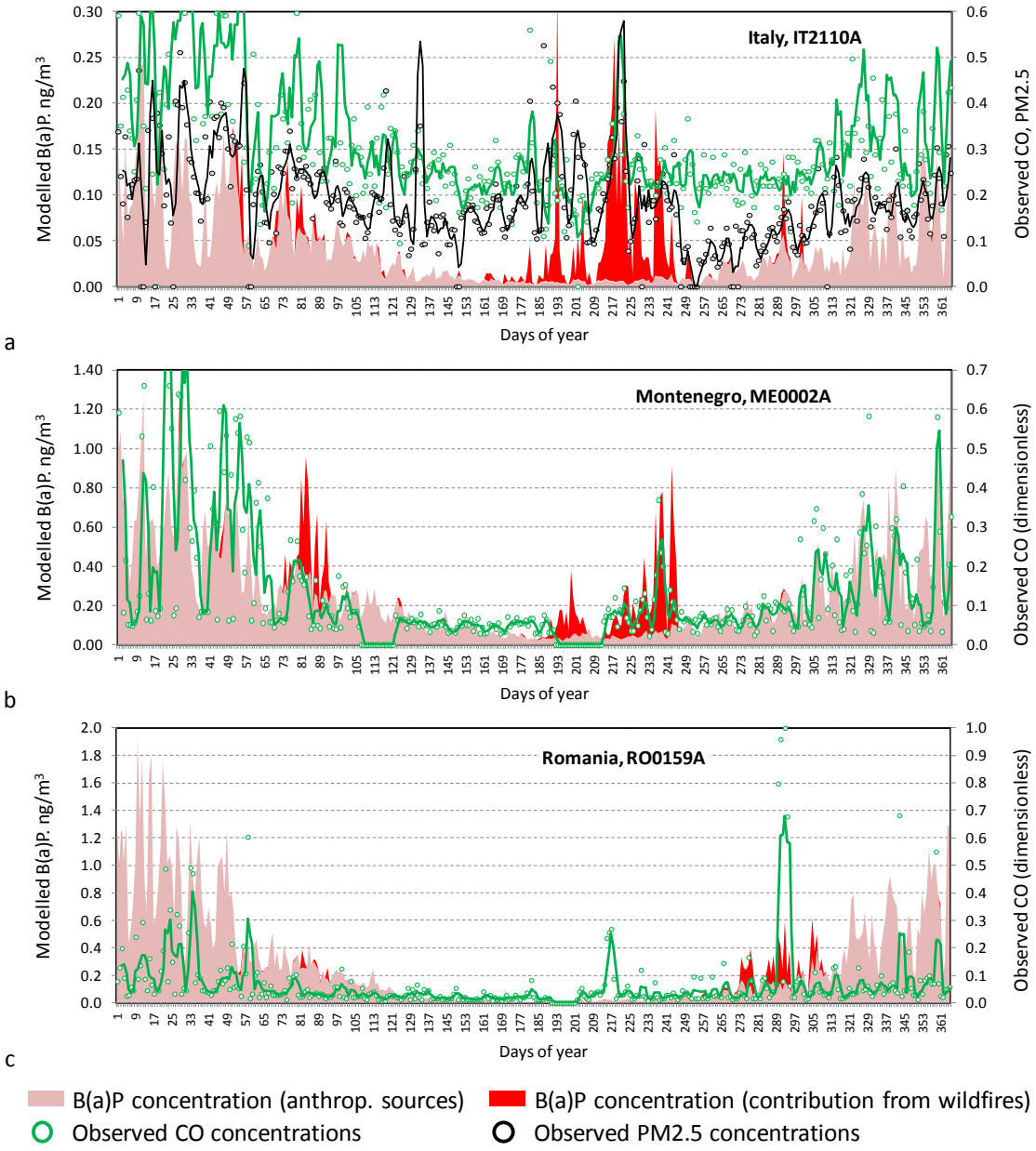

Fig. 4.28. *Modelled concentrations of B(a)P and observed concentrations of CO and PM2.5 and their trend at background urban station IT2110A(Italy, a), traffic urban station ME0002A (Montenegro, b) and background urban station RO0159A (Romania, c) in 2017.*

Similar results were obtained for Pb air concentrations. For example, peak of the wildfire component of Pb air concentration at Italian station IT0867A in the period from 239 to 245 day of year 2017 corresponds to peak of PM2.5 concentrations and increased level of CO (Fig. 4.29a). In another example Pb peak from wildfire in 240th day coincides with the peaks of CO and PM2.5 at Spanish station ES1138A (Fig. 4.29b). Since the contribution of wildfires to Pb air concentrations is lower than that to B(a)P concentrations, in Fig. 4.29 only wildfire component is shown.

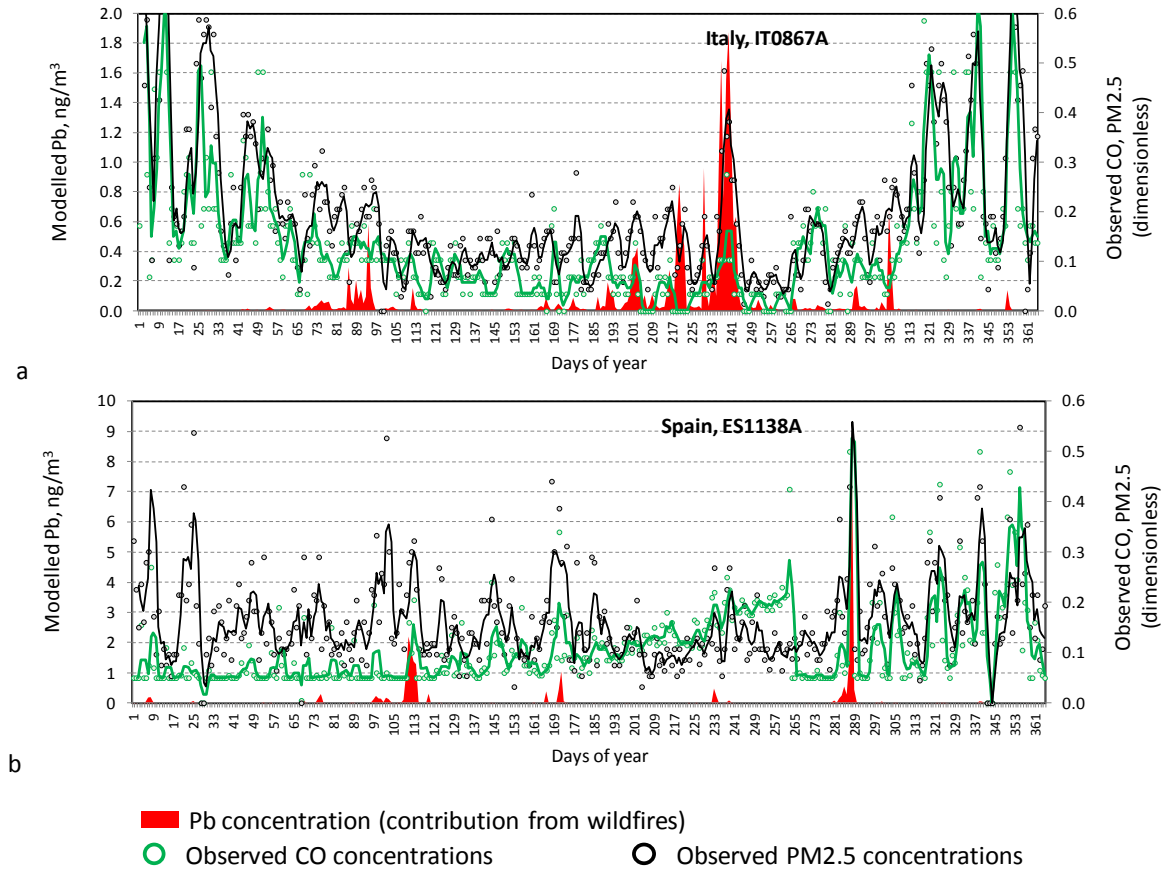

Fig. 4.29. *Modelled concentrations of Pb (contribution from wildfires) and observed concentrations of CO and PM2.5 and their trend at traffic urban station IT0876A (Italy, a) and traffic urban station ES1138A (Spain, b) in 2017.*

Comparison of time series of modelled B(a)P and Pb levels with the concentrations of CO and PM2.5 revealed that in a number of episodes with peaks of the tracer concentrations the contribution of wildfires is low or absent. It is explained by the fact that elevated concentrations of CO and PM2.5 are caused by numerous emission sources besides wildfires. Therefore, for more reliable evaluation of the modelled effect of wildfires on pollution levels larger set of the wildfire traces is needed. For example, measurement data on levoglucosan, which is produced by pyrolysis of cellulose, could serve as more reliable indicator of burning vegetation. In addition to this, at a number of stations there is also an opposite situation. Episodes of high Pb or B(a)P concentrations do not match with the corresponding peaks of the tracer concentrations. One of possible reason for this is inadequate vertical distribution of wildfire emissions. In current preliminary modelling tests Pb and B(a)P are emitted into the near-surface model layer. However, a number or studies indicate that the emission is distributed in the layer of hundreds or even thousands meters [*Sofiev et al*., 2012, *Shikwambana and Habarulema*, 2022; *Ke et al.,* 2021; *Wilkins et al*., 2022]. It results in dilution of the wildfire emission and decrease of air concentration near the emission source. Besides, as a rule, wind direction changes with altitude. Hence, direction of atmospheric transport of plumes from wildfires at higher altitude should differ from that near the surface. Therefore, location of wildfire emission sources in the lowest model layer can lead to overestimation of the pollutant air concentrations, especially in the vicinity of the sources.

Preliminary results of the presented study demonstrate that wildfires can be significant contributors to the Pb and B(a)P pollution levels in the EMEP region. However, further research is needed. In particular, it is important to carry out sensitivity analysis of modelling results to input parameters such as emission factors, vertical distribution of wildfire emissions, concentrations of heavy metals in emitted by wildfires particles etc. In addition to FINN database, other wildfire databases should be tested. Besides, more measurement data of potential wildfire tracers, e.g., levoglucosan and black carbon, are needed to the evaluation of the modelling results. Finally, the proposed approach can be tested for other heavy metals and POPs.

Chapter 5. CO-OPERATION

5.1. Subsidiary bodies of the Convention

5.1.1. Task Force on Measurements and Modelling

The EMEP Task Force on Measurements and Modelling (TFMM) held its 23rd meeting online in May 2022. During the meeting MSC-E provided participants with the information on research activities of the Centre in co-operation with national experts in the field of assessment of HM and POP pollution.

Mercury-related research activities were focused on the Arctic region. MSC-E participated in co-operative studies, which followed up the recent AMAP Hg Assessment 2021. Data products obtained in this work as a country-specific case study were used in the national Norwegian Mercury Assessment 2022 . The results of the study, including analysis of spatial distribution of Hg pollution levels in Norway, long-term trends of Hg air concentration and deposition to the country and trends in biota, were presented at the TFMM meeting. It was shown that spatial distribution of Hg deposition fluxes over Norway generally corresponded to that of Hg concentrations in mosses. Besides, it was demonstrated that spatial distribution of Hg deposition to waters of North Atlantic and the Arctic well correlated with concentrations of Hg in fish. Finally, it was indicated that the reduction of Hg concentrations in fish during the recent decade is stronger than the decline of atmospheric deposition.

Evaluation of the effect of wildfires on heavy metal and POPs pollution levels was another research activity presented at the meeting. Four available wildfire databases were examined. Emissions of Pb and B(a)P from the wildfires in the EMEP region were estimated. Contributions of wildfire emissions to concentrations of Pb and B(a)P were simulated using the GLEMOS model. The modelled effect of wildfires on the pollution levels was validated via comparison with concentrations of wildfire tracers such as CO and PM2.5. It was shown that wildfires can significantly contribute to air concentrations of toxic pollutants in particular countries in certain months. Further steps in model assessment of the effects of wildfires on heavy metal and POP pollution levels were suggested.

Main focus in the research activities on POPs was directed to the PAHs. The activities included participation in the Eurodelta-Carb multi-model assessment of B(a)P and a case study of PAH pollution in Poland. Preliminary results on B(a)P of several modelling groups (EMEP/MSC-E, CEIMAT, INERIS, ENEA, FMI) and their evaluation against measurements were presented. Similarities and differences between the annual mean concentrations and intra-annual variations obtained by participated models and observed levels were examined.

Results of the second phase of the country-scale study of PAH levels in Poland were demonstrated. It was shown that updated national inventory of PAH emissions (reported to EMEP) allowed to improve model assessment of pollution for B(b)F and B(k)F. At the same time, for I(cd)P no improvement was obtained comparing to the previously used national emission inventory.

Special attention was also paid to the contaminants of emerging concern (CECs). Current status of their monitoring, development of emission inventories and modelling approaches was presented. In particular, pilot model simulations of PBDE pollution, based on the expert estimates of emissions, reasonably well reproduced the observed levels and their long-term trends in the EMEP region. Further research and cooperation activities related to HM and POP pollution assessment were proposed.

5.1.2. Task Force on Hemispheric Transport of Air Pollution

MSC-E continues co-operation with the Task Force on Hemispheric Transport of Air Pollution (TF HTAP) on assessment of Hg and POP pollution. In particular, the Centre took part in the TF HTAP virtual meetings focused on global emissions and modelling of Hg (May 18, 2022, http://htap.org/event/global-emissions-and-modeling-of-mercury/) and POPs/CEC (May 25, 2022, http://htap.org/event/global-emissions-and-modeling-of-pops-cec/). The meetings were aimed at discussion of practical programs for fulfilment of the near-term plans of Hg and POP activities formulated at the TF HTAP Workshops (April 2021).

The meeting on Hg, which was attended by over 50 experts, reviewed the current state of knowledge and on-going activities within various national and international research groups focused on Hg pollution assessment. In particular, available global Hg emissions inventories and future projections were presented and discussed. New developments in Hg multi-media modelling, model applications for near-term and longer-term decision-making and model assessment of Hg pollution in particular regions (the Arctic) were also overviewed. It was agreed that near-term TF HTAP activities on Hg would benefit if formulated in line with the on-going effectiveness evaluation procedure performed under the Minamata Convention on Mercury (MCM). To facilitate further development of the activities program it was decided to form an *ad hoc* group of scientific experts and hold a number of planning meetings.

During the meeting on POPs, the outcome of recent assessments prepared under AMAP and Stockholm Convention in a field of monitoring and assessment of pollution levels in the Arctic and on the global scale was presented. In addition, development and application of global inventories for unintentionally emitted legacy POPs was overviewed. A number of experts presented results of monitoring studies and progress in the development of advanced modelling techniques to study pollution levels, transport and fate of the CECs and microplastics. Plans of near-term TF HTAP activities in line with on-going and future work of experts in POPs/CECs were discussed. It was agreed to consider opportunities of multi-pollutant studies of combustion-related POPs (e.g. PAHs, PCDD/Fs) and particulate matter, and to continue reviewing the progress in the studies of CECs and microplastics on global and regional scales.

5.1.3. Task Force on Technical and Economic Issues

In framework of cooperation with the Task Force on Technical and Economic Issues, MSC-E took part in the seventh TFTEI annual meeting held on October 29th, 2021. The meeting was devoted to the discussion of ongoing and future work of the task force experts related to the revision of the Gothenburg Protocol as well as to various aspects of PM and black carbon emissions. A representative of MSC-E briefly presented the outcome of the recent work carried out by MSC-E and experts from Poland, on the assessment of PAH pollution in the EMEP region that is summarized in the MSC-E Technical Report [*Gusev et al.*, 2021]. In particular, updated results on long-term changes in measured and modelled B(a)P air concentrations had been demonstrated, with emphasis on key emission source categories and exceedances of B(a)P air quality guidelines and population exposure. Besides, PAH pollution assessment on a national scale had been performed as a part of a case study for Poland, focusing on the analysis of B(a)P pollution in the country. Model simulations with updated national emission inventory and scenario emissions had allowed for the improvement of model assessment of B(a)P pollution. At the same time, possible underestimation of national B(a)P emissions in Poland had been indicated based on the results of a comparison of modelled and measured concentrations.

5.1.4 ICP-Vegetation

MSC-E continued cooperation with WGE. In particular, MSC-E took part in annual 35th online Task Force meeting of ICP-Vegetation. Information about comparison of long-term changes of modelled deposition fluxes and measured concentrations in mosses of Pb, Cd, Hg and Cu was demonstrated. Besides, similar information was presented for one of the second priority heavy metals, copper (Cu). Additional information about changes of POP levels in air and in mosses was shown both for legacy POPs like B(a)P, HCB and PCB-153, and for CECs included into the POP Protocol, such as BDE-99.

EMEP monitoring data are used for the evaluation of the modelling results and provide actual measurement information on annual, seasonal or even daily basis. Nevertheless, spatial density of the EMEP stations is relatively low providing few or several stations per country. Besides, there is a number of countries where EMEP monitoring stations are not available.

Along with the EMEP monitoring data measurements of heavy metals and POPs in mosses can be used as alternative measurement information. A number of moss species have no root system and consume nutrients from the atmospheric deposition [*Dołęgowska and Migaszewski,* 2014; *Rühling and Tyler*, 1973; *Harmens et al.,* 2010]. This property was used as a basis of using mosses in the biomonitoring of atmospheric pollution. Unlike the EMEP monitoring network, measurements in mosses are characterized by higher spatial density (Fig. 5.1). Besides, measurements in mosses are carried out in countries where the EMEP monitoring data are not available. However, measurements in mosses have lower temporal resolution compared to the EMEP data. According to up-to-date understanding of physiology of mosses and methodology of moss sampling it is assumed that

concentrations in mosses represent three-year accumulation of deposited heavy metals or POPs [*Harmens et al.*, 2010; *ICP-Vegetation*, 2015; *Schröder et al*., 2013].

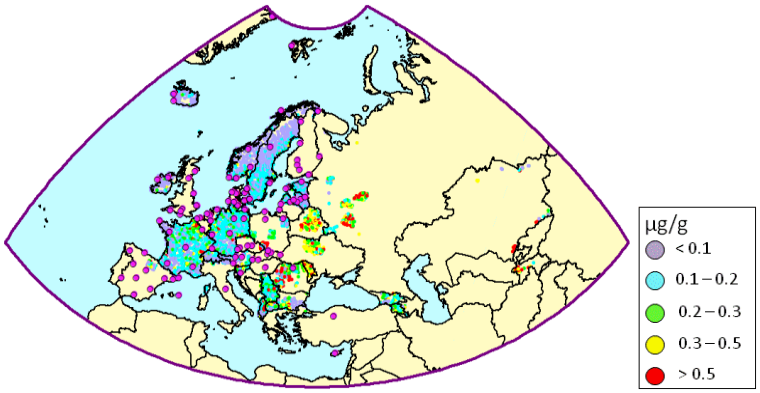

Fig. 5.1. *Spatial distribution of Cd concentrations measured in mosses in survey of 2015. Pink circles denote location of the EMEP monitoring stations measuring heavy metal levels in 1990 - 2020.*

Pan-European surveys of concentrations in mosses are carried out regularly every five years. Currently data on concentrations of heavy metals in mosses are available for 1990, 1995, 2000, 2005, 2010 and 2015 [*Frontasyeva et al*., 2020, *Harmens et al*., 2012, *Harmens et al.*, 2008]. The data from these six surveys are used in the analysis of long-term pollution changes of heavy metals between 1990 and 2015. Besides, moss measurements are used for biomonitoring of POPs since 2010. Therefore, changes of POP pollution between 2010 and 2015 can also be examined.

Long-term changes of heavy metals were estimated for countries where the measurements in mosses cover the period of at least 15 years. In the analysis we considered only the gridcells where measurements of different surveys overlapped. Periods of the analysis of changes for different countries may differ. Therefore the long-term difference between measured or calculated pollution levels is expressed as mean rate of change per year expressed in per cents.

The most significant reduction of deposition and concentrations in mosses takes place for Pb. In most of the considered countries the rate of pollution reduction is similar for concentrations in mosses and deposition and varies from 5% to 10% per year. Relatively low reduction is noted for Iceland. This country is known for low national emissions. Besides, due to its remoteness from main European emission sources the contribution of transboundary transport in absolute terms is also insignificant. Hence, the main contribution to Pb levels is made by secondary sources, especially, re-suspension from sea surface. Rate of Cd reduction varies mainly from 2% to 7% per year (Fig. 5.2b), and Hg reduction ranges from 1 to 3% per year (Fig. 5.2c). In France and North Macedonia the trends are contrasting with declining modelled deposition and increasing concentrations in mosses. Significant growth of Hg concentrations in mosses in France is explained by sharp two-fold increase between surveys of 2010 and 2015. Relatively low rate of Hg reduction is explained by significant contribution of non-EMEP natural, legacy and anthropogenic sources. Similar to Hg, changes of Cu are also relatively low, ranging typically from 1 to 2.5% per year (Fig. 5.2d). However, small changes of Cu levels are explained by low reduction of anthropogenic emissions of Cu in the EMEP region.

According to the available Cu emission data in the EMEP region, the overall reduction of Cu emission between 1990 and 2015 was around 10% [*CEP*, 2022; *Denier van der Gon et al.*, 2005].

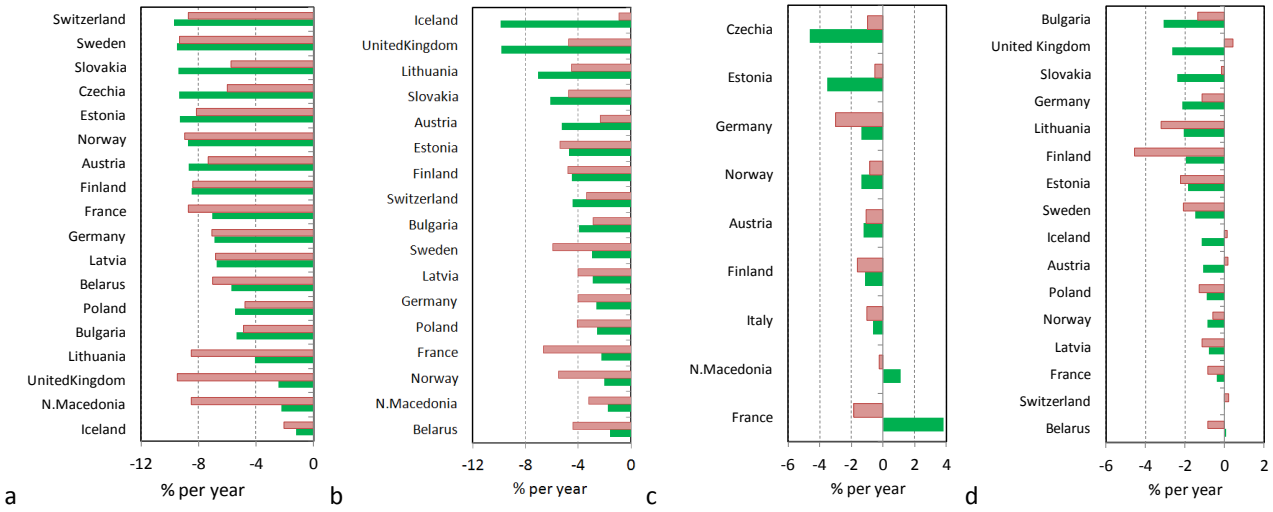

Fig. 5.2. *Mean rate of long-term change (% per year) of measured concentrations in mosses (green bars) and deposition flux (pink bars) of Pb (a), Cd (b), Hg (c) and Cu (d). Negative value means reduction, and positive value means increase.*

Long-term changes of total deposition and concentrations in mosses were analyzed for each country and each considered metal. Examples of comparison of the copper level changes in Estonia, Switzerland and Belarus are presented in Fig. 5.3. Concentrations in mosses and deposition in Switzerland exhibit relatively low changes over the period from 1990 to 2015 (Fig. 5.3a). This tendency is in line with pan-European trend of Cu emissions. One of the exceptions is Estonia. Until 2000 national emission of Estonia has been decreasing. The main countries-sources of Cu transboundary pollution in Estonia are Russia and Finland. Emissions in Russia were stable until 2000, and emissions of Finland also have been declining. As a result, deposition of Cu in Estonia has been decreasing between 1990 and 2000 that is confirmed by similar decline of concentrations in mosses (Fig. 5.3b). After 2000, emissions of Finland continued to decline, while the tendency of Estonian and Russian emissions changed to gradual increase. It resulted in slow increase of deposition in Estonia after 2000. Concentrations in mosses also demonstrated growth between 2005 and 2015. Belarus is one of the countries in the eastern part of the EMEP region where information on monitoring of heavy metal levels at the EMEP stations is limited. However, data on concentrations of Cu in mosses is available for 1995 an 2015. Comparison of the modelled and observed Cu pollution levels shows only minor changes between 1995 and 2015 (Fig. 5.3c).

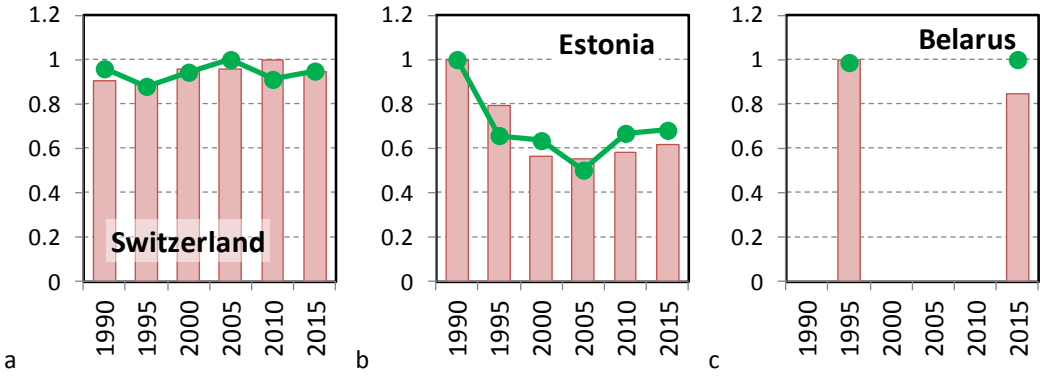

Fig. 5.3. *Mean concentrations in mosses and deposition fluxes (dimensionless form) of Cu in Switzerland (a), Estonia (b) and Belarus (c). Pink bars mean deposition flux and green lines mean concentrations in mosses.*

Analysis of long-term variability of concentrations in mosses and deposition in particular countries characterizes the status of the pollution changes on the whole. However, the data from moss surveys were used to investigate the changes at local scale. EMEP monitoring stations were selected as 'locations' to test this idea. Besides, information on the measured wet deposition from the EMEP stations was also involved into the analysis.

In most cases locations of moss sampling plots do not coincide with the locations of the EMEP monitoring stations. Median value of concentrations in mosses within 50-km radius was used as moss concentration value at the EMEP monitoring station. This approach was applied to all EMEP stations where wet deposition measurements were available, and the changes for all considered metals were estimated. Few examples in Fig. 5.4 demonstrate various aspects derived from this comparison.

At a number of stations, for example, Cd levels at station DE0001R (Westerland, Germany), the all three parameters (concentrations in mosses, modelled total deposition and observed wet deposition) demonstrate similar decreasing trend (Fig. 5.4a). It means that concentrations in mosses can be used for examination of long-term pollution trends not only at large scales such as countries but also at smaller (local) scales. At other stations concentrations in mosses can be used as a complement to the observed wet deposition for the purposes of verification of modelled deposition time series. For example, Cu wet deposition data at station DE0002R (Waldfoh, Germany) were available in the second half of the considered period. Nevertheless, measurement data from moss surveys for 1990-2000 period can be applied to evaluate long-term changes (Fig. 5.4b). At some stations significant discrepancies between temporal changes of concentrations in mosses, modelled and observed deposition fluxes are found. For example, long-term changes of modelled deposition agree well with the changes of concentrations in mosses at Estonian station EE0009R (Lahemaa). The both parameters demonstrate decline from 1990 to 2005, and then gradual increase to 2015 (Fig. 5.4c). However, the observed wet deposition demonstrates sharp 6-fold drop between 2010 and 2015. It is likely that this drop can be connected with the uncertainties of Cu measurements in precipitation and requires special investigation.

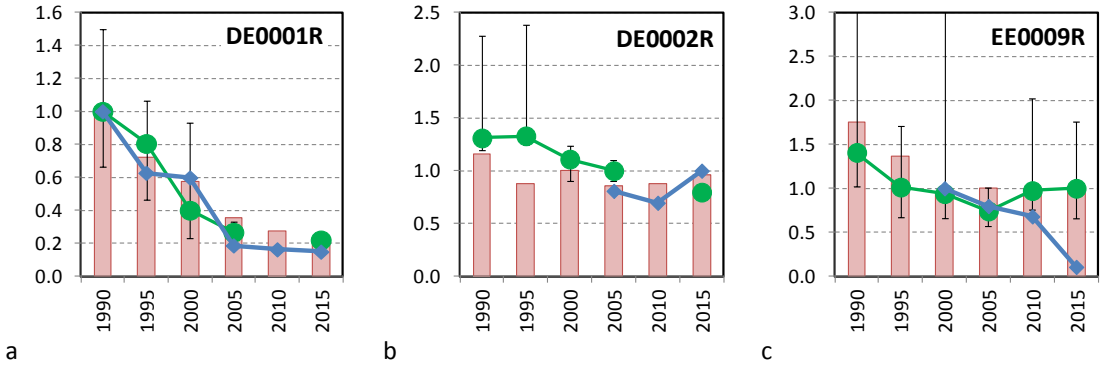

Fig. 5.4. *Mean concentrations in mosses, modelled deposition fluxes and observed wet deposition fluxes (dimensionless form) of Cd at station DE0001R (a) and Cu at stations DE0002R(b) and EE0009R(c). Pink bars mean modelled total deposition flux, green lines mean concentrations in mosses and blue lines mean observed wet deposition. Whiskers indicate a range of concentrations in mosses within 50-km radius around EMEP monitoring station.*

First measurements of POP concentrations in mosses under the coordination of ICP-Vegetation activity were carried out in survey of 2010. Currently measurements are available for surveys of 2010 and 2015. The data encompass a wide range of POP compounds including PAHs, PCBs, HCB, BDE and other species. For example, B(a)P data were available from Norway, France, Spain, Switzerland, Austria, Germany, Poland and Slovenia (Fig. 5.5).

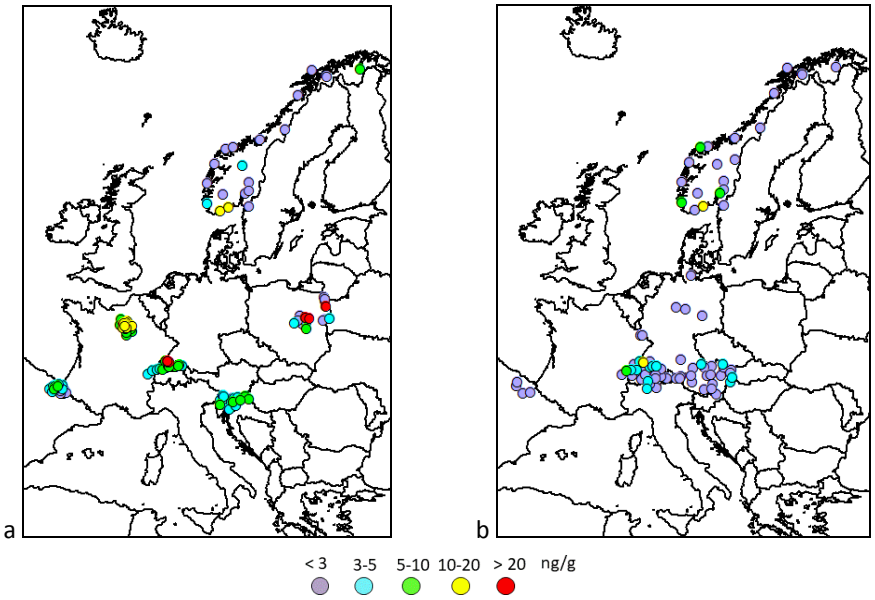

Fig. 5.5. *Concentrations of B(a)P measured in mosses in 2010 (a) and 2015 (b).*

Comparison of changes of pollution levels based on modelling results and observed concentrations in mosses between 2010 and 2015 was carried out for B(a)P, HCB, PCB-153 and BDE-99. The data on B(a)P from the both surveys were available for Norway and Switzerland, and on other pollutants – only for Norway. The change of B(a)P concentrations in mosses and modelled deposition in Switzerland is almost the same making up about 40% (Table 5.1). The changes of BDE-99 and PCB-

153 have the same direction, and the changes of B(a)P and HCB are contrasting for concentrations in mosses and modelled deposition.

Table 5.1. *Changes of concentrations in mosses and deposition of POPs in Norway and Switzerland between 2010 and 2015. Negative value means reduction, and positive value means increase of the pollution levels.*

Pollutant	Country	Change (moss), %	Change (modelled), %
B(a)P	Switzerland	-42	-43
B(a)P	Norway	-29	5
HCB	Norway	55	-22
BDE99	Norway	-68	-23
PCB-153	Norway	2	12

The changes of modelled and observed values were estimated for Norwegian EMEP stations Birkenes and Andoya. Example demonstrating concentrations in mosses and modelled and measured concentrations of B(a)P and BDE-99 at station Birkenes is shown in Fig. 5.6. Observed concentrations of B(a)P in air and mosses demonstrate decline between 2009 and 2015 (Fig. 5.6a). However, modelled air concentrations underestimate observed concentrations in air from 2009 to 2012 and agree well with the observed levels after 2012. It is probably that the underestimation is caused by the influence of unaccounted local emission sources. Concentrations in mosses and modelled and observed concentrations of BDE-99 in air exhibit distinct decline between 2009 and 2015 (Fig. 5.6b).

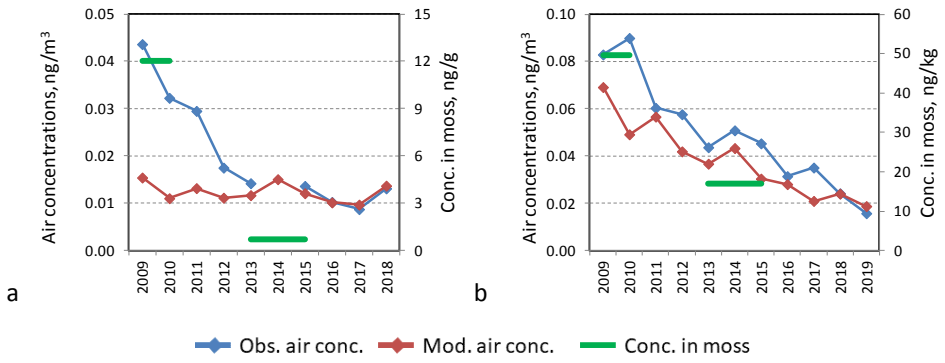

Fig. 5.6. *Modelled and observed concentrations in air and mosses of B(a)P (a) and BDE-99(b).*

The presented analysis showed that combined usage of the results of biomonitoring, atmospheric modelling and EMEP monitoring allows identifying and investigating long-term heavy metal and POP pollution changes in particular countries as well as at local scale. Results of modelling and biomonitoring demonstrate similar rates of Pb, Cd, Hg and Cu reduction in most of EMEP countries. The highest reduction is noted for Pb, and the lowest for Hg. Measurements in mosses, observations at the EMEP monitoring stations and modelling results demonstrate declining trend for BDE-99 and minor changes for PCB-153. For B(a)P and HCB the changes between modelled and the observed values are contrasting. Results of moss surveys are very useful for evaluation of long-term trends of heavy metals and POPs in the EMEP region. Further cooperation between EMEP and ICP-Vegetation is highly appreciated.

5.2. International organizations

5.2.1. Stockholm Convention

Co-operation and exchange of information on POP pollution with UNEP Stockholm Convention has been continued. MSC-E took part in the preparation of the 3rd Global Monitoring Report of the Stockholm Convention which compiled the most recent outcomes of research activities on monitoring and modelling of pollution levels and trends of legacy POPs as well as CECs. The contribution of the Centre included the results of model assessment of POP pollution levels and trends in the EMEP region.

Refinement of national POP emission inventories under the Stockholm Convention is of importance for the analysis of POP pollution in the EMEP countries. In particular, national inventories of legacy POPs and CECs emissions are being revised due to further development of the UNEP Standardized Toolkit and recalculations of national emission data. Updated information on emissions to the atmosphere and other environmental compartments complements model assessment for the EMEP region. Besides, collaboration with the activities under the Stockholm Convention Global Monitoring Plan (GMP) on the collection and analysis of global-scale monitoring data on POP concentrations in air and other compartments is important for the evaluation of GLEMOS modelling results.

5.2.2. Helsinki Commission

Regular evaluation of airborne pollution load of heavy metals and POPs to the Baltic Sea is carried out in the framework of long-term cooperation between EMEP and the Helsinki Commission (HELCOM). This year MSC-E continued collaboration with HELCOM based on the updated contract, which assumes evaluation of pollution levels and trends for extended list of heavy metals and POPs, including second priority metals and chemicals of emerging concern. In accordance with the updated contract the compilation of data on atmospheric emissions and model assessment of long-range transport, and deposition of copper, HCB, and BDE-99 for the period 1990-2019 is presented in the Joint report of the EMEP Centres for HELCOM [*Gauss et al.*, 2021]. In addition, a review of information on regulation, emissions, monitoring, and model assessment of SCCPs and PFOS is included in the report. Besides, information on emissions and modelling results on copper, HCB, and BDE-99 is also summarized in the Baltic Environment Fact Sheets, published on the HELCOM website (http://www.helcom.fi). In this section brief outline of MSC-E contribution to the Joint EMEP report is provided.

Long-term changes of Copper emissions and deposition to the Baltic Sea

Copper is essential trace element for biological systems. However, excess of copper can cause harmful effects for humans [*Gautam et al.*, 2014]. Copper is also toxic for aquatic organisms even at low concentrations and for soil microorganisms [*Gautam et al.*, 2014; *Flemming and Trevor*, 1989]. European Chemical Agency classified copper as toxic to aquatic life with long lasting effects

(Regulation (EC) No 1272/2008). Under the LRTAP Convention copper belongs to a group of so-called second priority metals, and Protocol on Heavy metals does not propose any restrictions on Cu emission. Nevertheless, Parties to the Convention regularly update their national Cu emission inventories and perform measurements of Cu concentrations in air and precipitation at the EMEP stations.

Annual emission of Cu in the HELCOM Contracting Parties in 2019 is almost the same as in 1990 (Fig. 5.7). The emission decreased by 12% from 1990 to 2000 and increased to the value of 1990 in the subsequent period (2001-2019). In particular countries long-term changes differ markedly from each other and from the HELCOM-mean tendency. For example, the most significant drop of Cu emissions is noted for Finland (74%), followed by Estonia (55%), and Sweden (39%), while emission in Denmark, Russia and Poland increased by 33%, 20% and 10%, respectively. Along with anthropogenic emission sources, Cu can be emitted to the atmosphere by natural and secondary sources. According to the expert estimates [*Pacyna and Pacyna*, 2001; *Nriagu*, 1989; *Rauch and Pacyna*, 2009] global-scale Cu anthropogenic emissions are comparable to the secondary emissions.

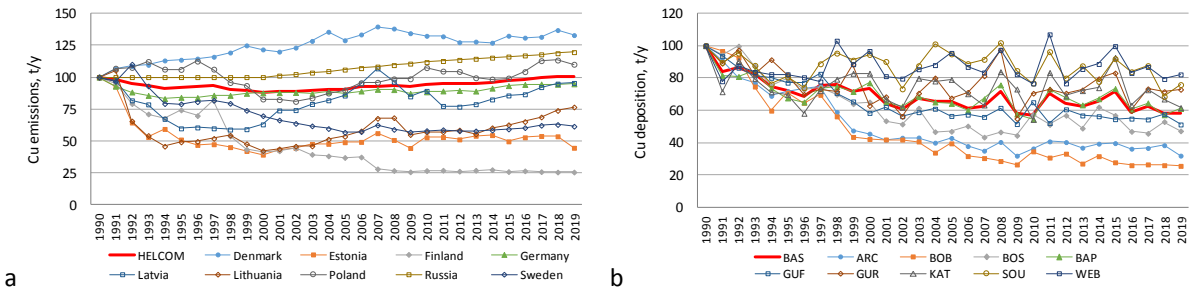

Fig. 5.7. *Relative changes of annual anthropogenic emissions of copper to the atmosphere from the HELCOM Contracting Parties (a) and of copper deposition to the Baltic Region and its sub-basins in the period 1990-2019 (% of 1990).*

Expert estimates of spatial distribution of copper anthropogenic emissions within the EMEP region were prepared by MSC-E using officially reported gridded PM2.5 emissions. The highest Cu anthropogenic emission flux in the Baltic region in 2019 is noted for the northern part of Germany, Denmark, the northern part of Poland, some regions of the southern part of Finland and on Russian coast of Gulf of Finland (Fig. 5.8a). Local areas of high emission are associated with large cities, e.g., St-Petersburg, Riga, Kaliningrad, Stockholm, Helsinki. Low emissions, except for particular local areas, occur along the eastern and south-eastern coast of Sweden, Latvia, Estonia, Lithuania, and the western coast of Finland.

Modelling of atmospheric transport and deposition of Cu over the EMEP region over long period of time was performed by MSC-E for the first time. Previous experience of Cu modelling includes model assessment of regional scale Cu pollution levels used for generation of boundary concentrations for fine resolution modelling over the area surrounding Italy [*Ilyin et al.*, 2017].

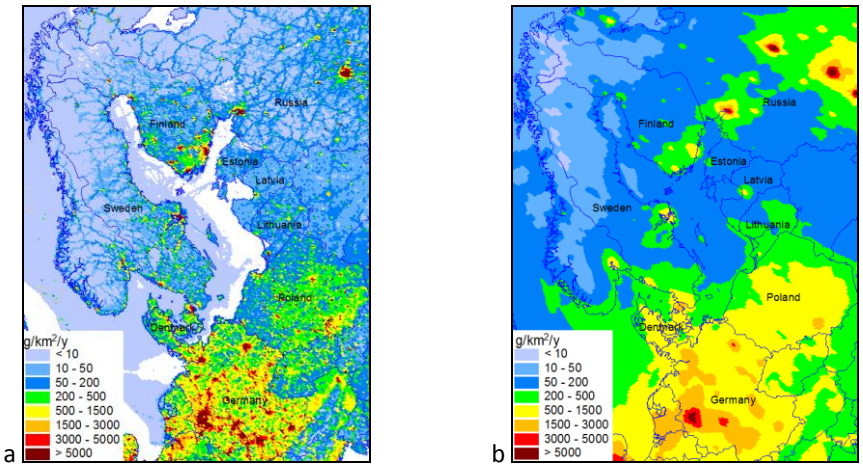

Fig. 5.8. *Anthropogenic emission (a) and total deposition flux (b) of Cu in the Baltic region in 2019.*

Atmospheric input of Cu to the Baltic Sea was calculated for the period from 1990 to 2019. Deposition of Cu to the Baltic Sea decreased by 42% (from 146 to 85 t) from 1990 to 2019 (Fig. 5.8b). The most substantial decline of copper deposition took place in the Bothnian Bay sub-basin (-74%), and the lowest one – in the Western Baltic sub-basin (-18%). The decline of Cu deposition to the Baltic Sea over considered period was non-uniform. In the period from 1990 to 1996, strong decline took place. Mean annual rate of deposition decline during this period was about 6.8 tonnes per year, while in the rest part of the considered mean annual decline rate of about 0.7 tonnes.

Changes of total copper deposition to the Baltic Sea in the period 1990-2019 do not follow the changes of anthropogenic emissions of HELCOM countries. Model simulations indicate that deposition from anthropogenic sources to the Baltic Sea declined from 1990 to 2019 approximately by 25%. The most significant contribution to these changes was made by the decline of copper emissions of Finland (by 74%). Besides, the decline of secondary emissions of Cu (about 75%) also contributed to the overall decline of deposition to the Baltic Sea.

Spatial distribution of Cu deposition in 2019 is similar to that of distribution of emissions (Fig. 5.8b). However, due to the dispersion in the atmosphere spatial gradients between regions with high and low emissions are smoothed. The highest deposition flux exceeding 1000 g/km^2/year is estimated for the Sound sub-basin of the Baltic Sea, where the highest emissions of the Baltic region occur. Significant deposition values (200 – 1000 g/km^2/y) are also noted for the Kattegat, Western Baltic and the western part of the Baltic Proper sub-basins. The lowest (below 100 g/km^2/y) deposition flux takes place in the Bothnian Bay sub-basin.

Modelled copper concentrations in air and wet deposition fluxes simulated for the period from 1990 to 2019 were compared with the values observed at the HELCOM monitoring stations. In general, the model tends to somewhat underestimate (by 30% on average) the observed concentrations in air in the beginning of the considered period (1990 - 1999), and somewhat overestimate (by 30% on average) in the end of the period (2010-2019). At most of the stations the ratio of modelled and observed concentrations lies within a factor of 2. The model performance for wet deposition differs for particular stations and years. In general, the agreement between the modelled and observed

deposition fluxes in the end of the considered period is much better than that in the beginning of the period.

In spite of second priority metals (e.g., Cu) are not currently regulated by the LRTAP Protocol on HMs, information on emissions and measurements of these metals is collected and reported by the EMEP countries. Model assessment of atmospheric input of selected second priority metals to the Baltic Sea is of importance for HELCOM. Besides, a number of researchers carry out modelling of pollution levels of the second priority metals on national scale in Europe [*Schaap et al.*, 2018; *González et al*., 2012; *Mircea et al*., 2013; *Dore et al.*, 2014]. Therefore, taking this into account, it could be reasonable to include assessment of these metals in the research activity within EMEP.

Long-term changes of HCB emissions and deposition to the Baltic Sea

HCB is known as a pollutant of global concern due to its long lifetime in air, significant potential to long-range transport, and persistence in the environment. HCB was widely used throughout the world as a fungicide or pesticide from the beginning of 1950s until 1970s, when its application for the agricultural purposes was banned or severely restricted. Contemporary levels of HCB pollution are likely supported by unintentional releases due to industrial and combustion processes. Along with anthropogenic emissions, additional contribution to HCB pollution levels is made by the secondary emission sources (re-volatilization from surface media). Secondary sources were formed due to long-term air-surface exchange and accumulation of HCB in the terrestrial and aquatic compartments as well as due to direct emissions to them. It is believed that contemporary secondary emissions are considerably larger comparing to the anthropogenic emissions [*Barber et al.*, 2005].

Atmospheric input of HCB to the Baltic Sea for the period from 1990 to 2019 was estimated using the GLEMOS model. The latest available official inventories of anthropogenic HCB emissions of the HELCOM and other EMEP countries have been used in the model computations. Analysis of officially reported national inventories of HCB releases shows that annual anthropogenic emissions of HCB in the HELCOM Contracting Parties have decreased during the period 1990-2019 by 98% (Fig. 5.9a). The most significant drop of HCB emissions is indicated for 2002 due to strong reduction of emission reported by Germany. For the subsequent period 2003-2019 no clear trend in HCB emission changes can be seen. Spatial distributions of anthropogenic HCB emissions in 2019 (Fig. 5.10a) indicates the most significant emission fluxes in the areas along the southern part of the Baltic Sea. To evaluate accumulation of HCB in the terrestrial and aquatic compartments and subsequent re-volatilization, spin-up global-scale model simulations were carried out for period 1945-2019 based on the updated MSC-E expert estimates of global historical HCB emissions [*Shatalov et al.*, 2010].

Model simulations indicate decrease of airborne input of HCB to the Baltic Sea by 95% in the period from 1990 to 2019 (Fig. 5.9b). The decrease of HCB deposition to the Baltic Sea was higher during the period 1990-2002 comparing to subsequent period 2003-2019. The highest total annual HCB deposition fluxes over the Baltic Sea in 2019 are estimated for the Gulf of Riga and Gulf of Finland sub-basins (Fig. 5.10b). The lowest deposition flux is obtained for the Bosnian Sea sub-basin. Due to substantial reduction of contemporary HCB anthropogenic emissions and accumulation of HCB in the

environmental compartments, the largest contribution to total annual deposition to the Baltic Sea in 2019 is made by secondary emission sources (re-volatilization from surface compartments).

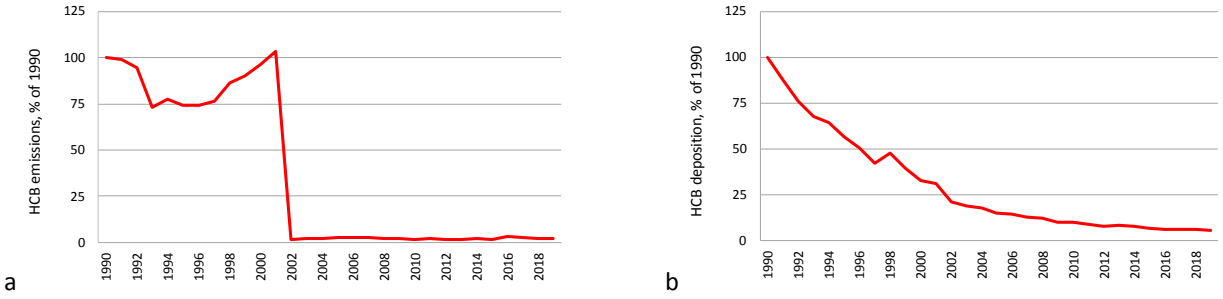

Fig. 5.9. *Anthropogenic emission (a) and total deposition flux (b) of HCB in the Baltic region in 2019.*

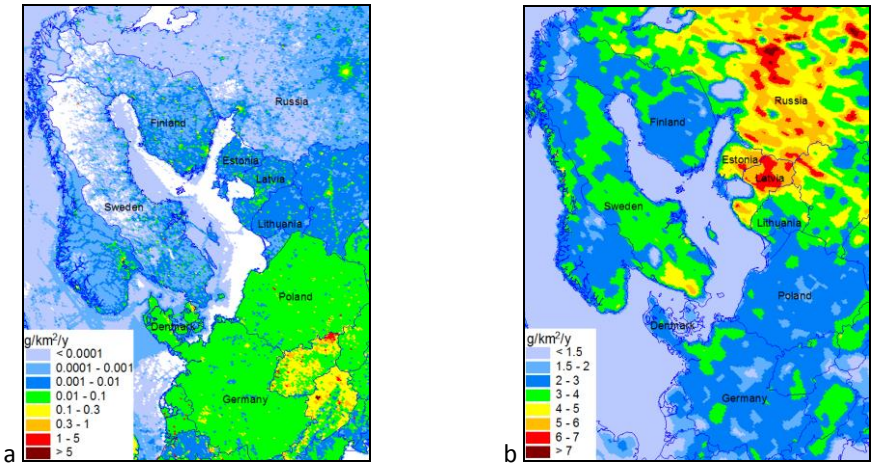

Fig. 5.10. *Anthropogenic emission (a) and total deposition flux (b) of HCB in the Baltic region in 2019.*

In spite of high uncertainties in the anthropogenic and secondary emissions of HCB, model estimates of regional scale HCB pollution levels show generally reasonable agreement with observed pollution levels.

Long-term changes of BDE-99 emissions and deposition to the Baltic Sea

A pilot model evaluation of polybrominated diphenyl ethers (PBDEs) atmospheric input to the Baltic Sea and its sub-basins was carried out for the period 2000-2019. PBDEs are a group of persistent toxic chemicals that were manufactured and used as flame retardants in various products including furniture, plastics, textiles, and electronic equipment during several past decades. They were produced for the commercial purposes in a form of technical mixtures such as penta-BDE, octa-BDE, and deca-BDE since 1970s. Due to the harmful properties their production and use were banned in the European Union and globally since early 2000s [*Abbasi et al.*, 2003].

Information on PBDE emissions to the environment is not currently reported on a regular basis by the EMEP countries. The construction of experimental scenario of long-term changes of BDE-99

emissions in the EMEP region was performed by MSC-E on the basis of TNO inventory of penta-BDEs emissions for 2000 [*Denier van der Gon et al.*, 2005]. The approach for estimating the emissions of selected PBDE congener BDE-99 was based on the results of the studies [*Palm et al.*, 2004; *La Guardia et al.*, 2006] performing analysis of chemical composition of penta-BDE emissions. Scenario of long-term variations of emissions was elaborated on the basis of estimates of temporal variations of penta-BDE emissions described in [*Birgul et al.*, 2012]. In addition, long-term measurements of BDE-99 at several EMEP monitoring sites were used. Similar approach was applied in this study to obtain estimates of BDE-99 emissions for the period 2000-2019 (Fig. 5.11a). Expert estimates of annual anthropogenic BDE-99 emissions for 2019 are shown in Figure 5.12a. It should be noted that this scenario is subject of high uncertainty. Nevertheless, it can be applied for preliminary analysis of contemporary levels of PBDE pollution on the basis of model predictions and measurements.

Long-term changes of atmospheric input and source allocation of selected PBDE congener (namely BDE-99) deposition to the Baltic Sea and its catchment area were estimated using model simulations on the basis of available PBDE emission expert estimates. Model predictions indicate that airborne input of BDE-99 to the Baltic Sea has declined by 91% in the period from 2000 to 2019 (Fig. 5.11b).

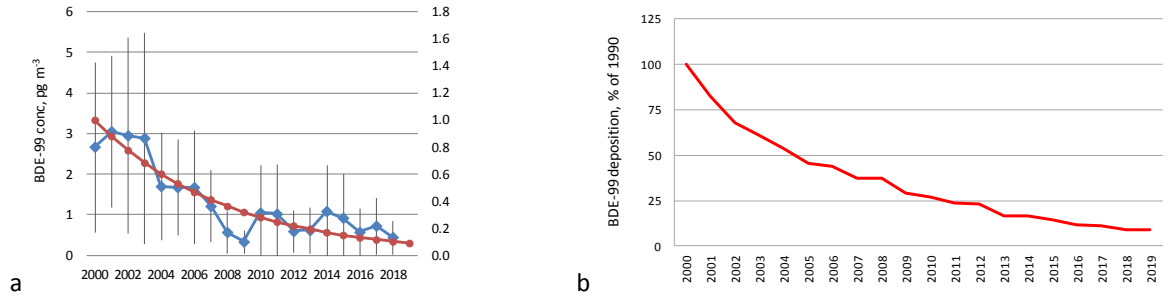

Fig. 5.11. *Averaged BDE-99 annual mean air concentrations observed the monitoring stations in Europe in period 2000-2019 and expert estimates of temporal changes of BDE-99 emissions in HELCOM countries relative to the emissions in 2000 (a). Whiskers indicate the range between minimum and maximum values of observed concentrations. Long-term changes of modelled total deposition flux of BDE-99 to the Baltic region in 2000-2019 in % of 2000 (b).*

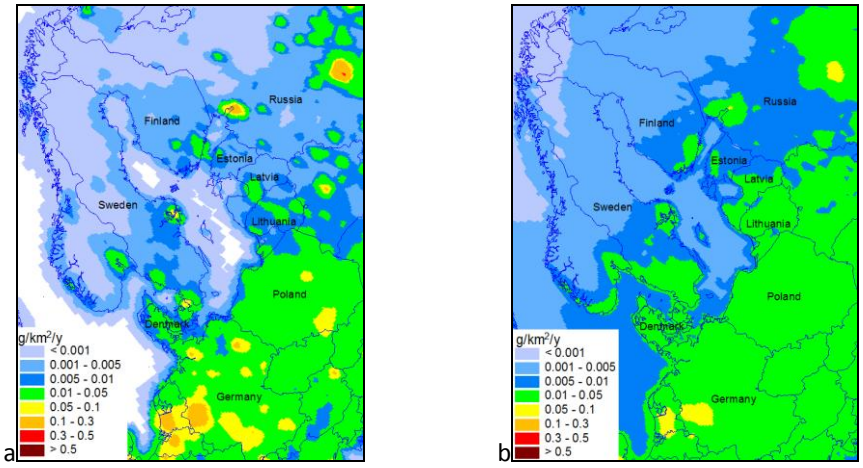

Fig. 5.12. *Spatial distribution of annual total anthropogenic emission (a) and total deposition fluxes (b) of BDE-99 in the Baltic region in 2019.*

According to results of model simulations the rates of decline of BDE-99 deposition to the Baltic Sea were different in the periods 2000-2005 and 2006-2019. In the period from 2000 to 2005, stronger decline is estimated. The subsequent period (2006-2019) is characterised by less intensive mean annual decline rate. Reduction of atmospheric input of BDE-99 to the Baltic Sea is connected with the realization of various abatement measures, which took place in the HELCOM countries as well as other EMEP countries. Spatial distribution of modelled BDE-99 deposition fluxes for 2019 are presented in Fig. 5.12b. The highest level of total annual BDE-99 deposition fluxes over the Baltic Sea in 2019 is estimated for the Sound sub-basin. The lowest deposition flux is obtained for the Bosnian Bay sub-basin.

5.2.3. OSPAR

In accordance with the contract between MSC-E and OSPAR Commission, model assessment of atmospheric inputs of selected heavy metals, including cadmium (Cd), lead (Pb), and mercury (Hg) to the maritime area of the Convention for the Protection of the Marine Environment of the North-East Atlantic (OSPAR) was carried out. The assessment covers the period from 1990 to 2019 and includes information on emissions in the OSPAR Contracting Parties (Norway, Sweden, Finland, Denmark, Germany, the Netherlands, Belgium, Luxemburg, France, Spain, Portugal, the United Kingdom, Ireland, Iceland and Switzerland), long-term trends of deposition to the OSPAR regions (Fig. 5.13), evaluation of modelling results against measurements and comparison with the results of previous assessment. Detailed description of the results prepared for the OSPAR Commission are presented in [*Ilyin et al*., 2022].

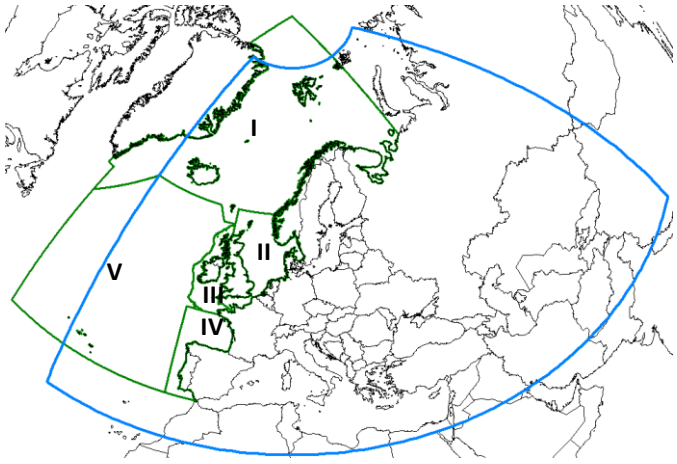

Fig. 5.13. *Borders of the EMEP domain (blue line) and OSPAR maritime area (green line) with indication of the OSPAR regions (I - V).*

Total annual atmospheric emissions of all the OSPAR countries have decreased by 96% for Pb, 73% for Cd and 83% for Hg from 1990 to 2019. The most significant emissions reduction occurred in the first third of the period. In 2019 total emissions of Pb, Cd and Hg made up 543, 36 and 23 t/y,

respectively. The largest contributions to total annual heavy metal emissions were made by Germany, Spain and the United Kingdom.

Deposition of Pb, Cd and Hg to the OSPAR maritime area decreased for the considered period. The largest decrease took place in the Greater North Sea (Region II). For example, reduction of Cd deposition made up 80% (Fig. 5.14), and the decline of Pb and Hg deposition was 87% and 45%, respectively. The Arctic Waters and Wider Atlantic regions are most remote from the main emission regions. Therefore, they are characterized by the lowest reduction of deposition, which made up around 60% for Pb, 35-40% for Cd and about 20% for Hg. In general, the decline of deposition to the OSPAR regions is lower than the emission reduction because of the effect of secondary and global sources.

Contribution of emission sources of the OSPAR Contracting Parties to deposition was estimated for 1995, 2005 and 2015. Contribution of the OSPAR countries to deposition is the largest for the Greater North Sea (Region II), while the lowest – to the Arctic Waters (Region I) and the Wider Atlantic (Region V). The major contributors to the Regions I, II, III are the United Kingdom, France and Germany, whereas the Regions IV and V are mostly affected by Spain, Portugal, France and the United Kingdom. However, contributions of particular OSPAR countries may change over the considered years.

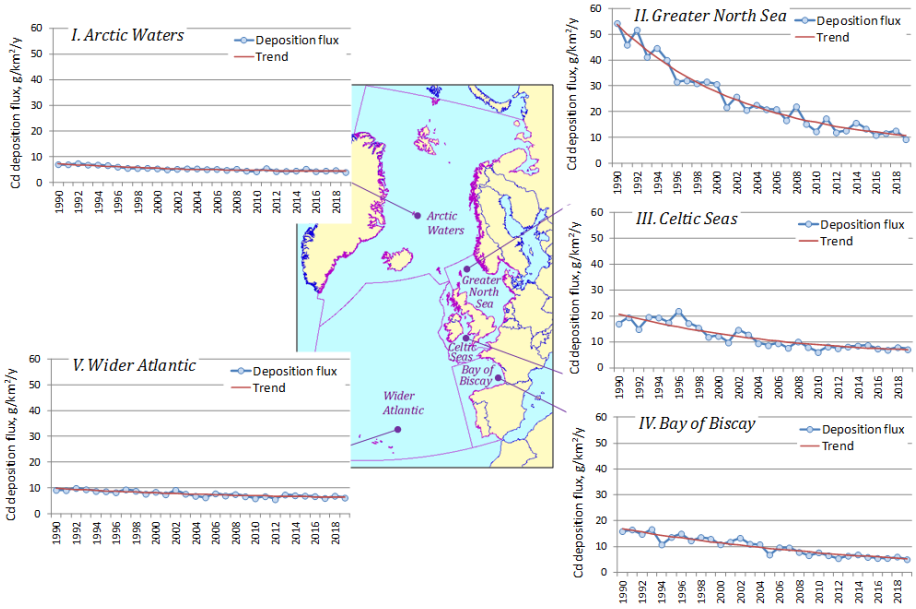

Fig. 5.14. *Time series of average annual Cd deposition flux to five regions of the OSPAR maritime area in the period 1990-2019. Blue line is model estimate, red line is trend approximation.*

Modelling results were evaluated via comparison with measurement data of the OSPAR Comprehensive Atmospheric Monitoring Programme (CAMP). At most of the monitoring stations modelled air concentrations and wet deposition of Pb and Cd agree with observations within a factor of two. Most of the modelled and observed wet deposition fluxes of Hg agree within ±40% (e.g., Fig. 5.15). Higher discrepancies between the modelled and observed Pb, Cd, and Hg values for the first

part of the period (1990-2000) are likely caused by uncertainties of measurements. At most of the stations with a long monitoring period both modelled and observed air concentrations and wet deposition fluxes demonstrate declining trend.

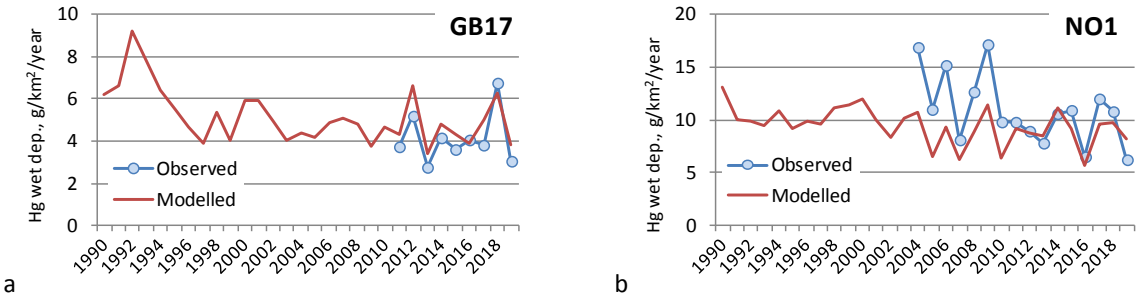

a b

Fig. 5.15. *Modelled and observed annual sum of wet deposition flux of Hg at station GB17 (Heigham Holmes, the United Kingdom) (a) and NO1 (Birkenes, Norway) (b) in the period 1990-2019.*

Current results were compared with the previous assessment covering the period from 1990 to 2006 [*OSPAR*, 2009]. The model estimates were revised due re-calculation of national emissions by the EMEP countries, updates of meteorological and other input data as well as refinement of the model parameterizations. The new modelling results show 10-30% lower average deposition of all three heavy metals to most of the OSPAR regions. The new results also demonstrate somewhat higher reduction rates for Pb and Cd deposition, whereas the slopes of Hg deposition trends changed insignificantly.

The results on the assessment of atmospheric pollution of the OSPAR maritime area by Pb, Cd and Hg were presented at the online meeting organized by OSPAR Commission. Spatial distribution of the heavy metal deposition, their long-term trends and contributions of the OSPAR Contracting Parties to pollution of the OSPAR regions were characterized. Comparison of modelled air concentrations, wet deposition fluxes and their long-term trends with measured values was demonstrated. Finally, it was shown that results of current assessment are comparable with the previously reported results. It is planned that current results of the assessment will be included into Quality Status Report of OSPAR in 2023.

6. MAIN CHALLENGES AND DIRECTIONS OF FUTURE RESEARCH

The Status Report summarizes main results of the EMEP activities on heavy metal and POP pollution assessment in 2022. It contains information on emissions, monitoring and model estimates of transboundary pollution of the EMEP countries performed in co-operation with national experts, Subsidiary Bodies of the Convention, and international organizations. Main challenges of the pollution assessment and directions of future research are outlined below.

- High PAH levels in the EMEP countries and slow pollution reduction are recognized as an important issue within the Convention that needs further scientific research. Detailed assessment of PAH pollution in the EMEP region will be continued with focus on population exposure to B(a)P and particulate matter from combustion sources as a part of the TFMM/EuroDelta-Carb multi-model intercomparison study.
- Pollution levels of Hg and some POPs in the EMEP region are largely affected by intercontinental atmospheric transport. Therefore, assessment of pollution levels, long-term trends and future projections for these contaminants should take into account emission changes in other continents. Cooperative activities on Hg and POP pollution assessment within TF HTAP will include collection and evaluation of global emission inventories, multi-model studies of Hg air-surface exchange as well as source apportionment of combustion-related POPs, and will be conducted in line with appropriate activities in other international bodies (Minamata and Stockholm Conventions, AMAP, etc.)
- Contaminants of emerging concern (CECs) comprise a large group of environmental pollutants that pose risk for human health and environment. Pollution assessment of CECs presents significant challenges due to insufficient knowledge of their sources, transport and fate in the environment. Preparatory work for the assessment of CEC long-range transport and fate will be continued collecting information on physical-chemical properties, releases and concentrations in different environmental media, and experimental model assessment of their pollution levels.
- Detailed analysis of pollution levels in individual EMEP countries being performed in co-operation with national experts involving variety of national data allows evaluation national emissions and monitoring data as well as improvement of the model assessment on both national and regional scales. The country-scale case studies on heavy metals and POPs have been successfully fulfilled for selected EMEP countries (Croatia, the Czech Republic, the Netherlands, Belarus, Germany, the UK, Spain, France, Norway and Poland) and will be continued in accordance with requests from other countries.
- Evaluation of adverse effects of heavy metal and POP pollution on human health and ecosystems is an important activity within the Convention coordinated by WGE. MSC-E will continue long-term co-operation with WGE focusing on joint analysis of heavy metal measurements in mosses in co-operation with ICP Vegetation, support of ICP Integrated Monitoring and ICP Forests with information on heavy metal deposition to various ecosystems as well as data exchange with TF Health on PAH pollution levels and exceedances of air quality guidelines.

- Toxic pollutants such as heavy metals, POPs and some CECs adversely affect marine ecosystems and biota. Assessment of atmospheric pollution of the marine environment with heavy metals and POPs will be performed in co-operation with HELCOM and OSPAR and will include model evaluation of long-term trends and source apportionment of atmospheric load of heavy metals (including metals of second priority) and POPs to the Baltic Sea and the North-East Atlantic.
- EMEP co-operation with other international organizations is an important activity aimed at dissemination of information and data exchange. MSC-E will continue collaboration with the UN Environment, AMAP, Stockholm and Minamata Conventions in relation to assessment of POP and Hg long-range transport and trends.

REFERENCES

Aas W., Nizzetto P.B., Pfaffhuber K.A. [2022] Heavy metals and POP measurements 2020, EMEP/CCC-Report 3/2022.

Abbasi G., L. Li, and K. Breivik [2019] Global Historical Stocks and Emissions of PBDEs. *Environ. Sci. Technol*. 2019, 53, 6330−6340.

Aboal J.R., Fernández J.A. and Carballeira A. [2004] Oak leaves and pine needles as biomonitors of airborne trace elements pollution. *Environmental and Experimental Botany* 51 (2004) 215–225.

Alexakis D.E. [2020] Contaminated Land by Wildfire Effect on Ultramafic Soil and Associated Human Health and Ecological Risk. Land 2020, 9, 409.

ALS [2013] Benzo(a)pyrene toxic equivalence quotient (TEQ) and aggregate organochlorine pesticides parameters, *EnviroMail* No. 59 Re-Release, July, 2013.

AMAP [2021] 2021 AMAP Mercury Assessment. Summary for Policy-makers. Arctic Monitoring and Assessment Programme (AMAP), Oslo, Norway. 16 pp.

AMAP/UNEP [2019] Technical Background Report for the Global Mercury Assessment 2018. Arctic Monitoring and Assessment Programme, Oslo, Norway/UN Environment Programme, *Chemicals and Health Branch*, Geneva, Switzerland. viii + 426 pp including E-Annexes.

Andreae M.O. and Merlet P. [2001] Emission of trace gases and aerosols from biomass burning. *Global Biogeochemical cycles*, Vol. 15, 4, 955-966.

Bailey R.E. [2001] Global hexachlorobenzene emissions. *Chemosphere* 43, 167-182.

Bank M.S., Frantzen S., Duinker A., Amouroux D., Tessier E., Nedreaas K., Maage A., & Nilsen B. M. [2021] Rapid temporal decline of mercury in Greenland halibut (Reinhardtius hippoglossoides). *Environmental Pollution*, 289, 11. doi:10.1016/j.envpol.2021.117843.

Barber J.L., Sweetman A.J., van Wijk D., Jones K.C. [2005] Hexachlorobenzene in the global environment: emissions, levels, distribution, trends and processes. *Sci. Tot. Environ*., 349, 1-44.

Bebkiewicz K., Z. Chłopek, A. Doberska, M. Kanafa, I. Kargulewicz, A. Olecka, J. Rutkowski, J. Skośkiewicz, S. Waśniewska, D. Zasina, M. Zimakowska-Laskowska, and M. Żaczek [2020] Poland's Informative Inventory Report 2020. Submission under the UN ECE Convention on Long-range Transboundary Air Pollution and Directive (EU) 2016/2284. Air pollutant emissions in Poland 1990–2018. Warsaw 2020.

Birgul et al. [2012] Atmospheric polybrominated diphenyl ethers (PBDEs) in the United Kingdom, *Environmental Pollution*, vol.169, pp. 105-111.

Blunden, J. and T. Boyer, Eds. [2021]. State of the climate in 2020. Special Supplement to the Bulletin of the American Meteorological Society Vol. 102, No. 8, August 2021.

Bogdal C., Müller C.E., Buser A.M., Quante M., Wang Z., Scheringer M., Gerecke A.C., Schmid P., Zennegg M., MacLeod M. and K.Hungerbühler [2014] Emissions of Polychlorinated Biphenyls, Polychlorinated Dibenzo-p-dioxins, and Polychlorinated Dibenzofurans during 2010 and 2011 in Zurich, Switzerland. *Environ. Sci. Technol.,* 48, 482−490.

Bommarez T., Cools N. and De Vos B. [2021] Heavy metals in forest floors and topsoils of ICP Forests Level I plots. Forest Soil Coordinating Centre of ICP Forests. Report of the Research Institute for Nature and Forest 2021 (5). Research Institute for Nature and Forest, Brussels. DOI: doi.org/10.21436/inbor.29316481.

Bossi R., Vorkamp K., Skov H. [2016] Concentrations of organochlorine pesticides, polybrominated diphenyl ethers and perfluorinated compounds in the atmosphere of North Greenland. *Environmental Pollution* 217, 4-10.

Breivik K., Alcock R., Li Y.-F., Bailey R.E., Fiedler H. and J.M.Pacyna [2004] Primary sources of selected POPs: regional and global scale emission inventories. *Environmental Pollution,* 128, 3–16.

Breivik K., Sweetman A., Pacyna J.M. and K.C.Jones [2007] Towards a global historical emission inventory for selected PCB congeners - A mass balance approach-3. An update. *Science of the Total Environment*, 377, 296-307.

Brown G., Luu I. and O'Sullivan G. [2017] Trace Metal Concentrations in Pine Needles at Varying Elevation in Proximity to Roadways in an Urban Environment. *Journal of Environmental Protection*, 2017, 8, 733-743.

Brubaker W.W., Hites R.A. [1998] OH reaction kinetics of gas-phase alpha- and gamma-hexachlorocyclohexane and hexachlorobenzene. *Environmental Science & Technology* 32, 766-769.

Campos I., Abrantes N., Keizer J.J., Vale C. and Pereira P. [2016] Major and trace elements in soils and ashes of eucalypt and pine forest plantations in Portugal following a wildfire. *Science of the Total Environment* 572 (2016) 1363–1376.

CEIP [2022]. WebDab. Officially reported emission data. https://www.ceip.at/webdab-emission-database/reported-emissiondata. Visited 01.04.2022.

CEIP Inventory Review Report 2022. S. Schindlbacher, B. Ullrich, R. Wankmueller: Inventory Review 2022. Review of emission data reported under the LRTAP Convention and NEC Directive, Stage 1 and 2 and review, Status of gridded and LPS data. Technical Report CEIP 04/2022. In preparation.

CEIP Uncertainties 2021. Uncertainties and recalculations of emission inventories submitted under CLRTAP, Technical Report CEIP 1/2021, Sabine Schindlbacher, Bradly Matthews, Bernhard Ullrich. Available at: https://www.ceip.at/fileadmin/inhalte/ceip/00_pdf_other/2021/uncertainties_and_recalculations_of_emission_inventories_submitted_under_clrtap.pdf.

Cinnirella S. and N. Pirrone [2006] Spatial and temporal distributions of mercury emissions from forest fires in Mediterranean region and Russian Federation. *Atmospheric Environment* 2006, 40, 7346–7361.

CLRTAP [2017]. Mapping critical loads for ecosystems, Chapter V of Manual on methodologies and criteria for modelling and mapping critical loads and levels and air pollution effects, risks and trends. UNECE Convention on Long-range Transboundary Air Pollution; accessed 04.03.2022 at https://www.umweltbundesamt.de/en/manual-for-modelling-mapping-critical-loads-levels?parent=68093.

Dachs J. and S. J.Eisenreich [2000] Adsorption onto Aerosol Soot Carbon Dominates Gas-Particle Partitioning of Polycyclic Aromatic Hydrocarbons. *Environ. Sci. Technol*. 2000, 34, 3690-3697.

Darmenov A. and da Silva A. [2015] *The Quick Fire Emissions Dataset (QFED): Documentation of versions 2.1, 2.2 and 2.4*, NASA Technical Report Series on Global Modeling and Data Assimilation NASA TM-2015-104606, Volume 38, http://gmao.gsfc.nasa.gov/pubs/docs/Darmenov796.pdf.

Dastoor A, Angot H,, Bieser J., Christensen J.H., Douglas T.A., Heimbürger-Boavida L-E., Jiskra M., Mason R.P, McLagan D.S., Obrist D. Outridge P.M., Petrova M.V., Ryjkov A., St. Pierre K.A., Schartup A.T., Soerensen A.L., Toyota K. Travnikov O., Wilson S.J.and Zdanowicz C. [2022]. Arctic mercury cycling. https://doi.org/10.1038/s43017-022-00269- w.

De Simone F., Cinnirella S., Gencarelli C.N., Yang X., Hedgecock I.M. and Pirrone N. [2015] Model Study of Global Mercury Deposition from Biomass Burning. *Environ. Sci. Technol*. 2015, 49, 6712–6721.

De Vries W, Groenenberg J.E. and Posch M. [2015b] Mass balance approaches to assess critical loads and target loads of metals for terrestrial and aquatic ecosystems. pp. 207-222. In: Critical loads and dynamic risk assessments. Nitrogen, acidity in terrestrial and aquatic ecosystems. Edited by W. de Vries, J-P. Hettelingh and M. Posch. *Envitornmental pollution* 25, Springer.

De Vries W., Posch M., Sverdrup H.U., Larssen T., de Wet H.A., Bobbink R. and Hettelingh J-P. [2015a] Geochemical indicators for use in the computation of critical loads and dynamic risk assessment. pp 15-58. In: Critical loads and dynamic risk assessments. Nitrogen, acidity in terrestrial and aquatic ecosystems. Edited by W. de Vries, J-P. Hettelingh and M. Posch. *Envitornmental pollution* 25, Springer.

De Wit H.A., Hettelingh J-P., and Harmens H. [2015] Trends in ecosystem and health responses to long-range transported atmospheric pollutants . Norwegian Institute for Water Research, 92p.

Denier van der Gon H.A.C., Hendriks C., Kuenen J., Segers A. and Visschedijk A. [2011] Description of current temporal emission patterns and sensitivity of predicted AQ for temporal emission patterns. EU FP7, MACC, deliverable report D_D-EMIS_1.3. TNO.

Denier van der Gon H.A.C., van het Bolsher M., Visschedijk A.J.H., Zanveld P.Y.J. [2005] Study to the effectiveness of the UNECE Persistent Organic Pollutants and cost of possible additional measures. Phase I: Estimation of emission reduction resulting from the implementation of the POP Protocol. TNO report B&AO-A R 2005/194. April, 2005.

Dołęgowska S. and M. Migaszewski Z. [2014]. Terrestrial mosses as trace element bioindicators: a review. Pp 25 – 69. In: Moss. Classification, development and growth and functional role in ecosystems. Ed. by: Mohamed J. ISBN: 978-1-63117-396-7, Nova Science Publishers, Inc.

Dore A.J., Hallsworth S., McDonald A.D., Werner M., Kryza M., Abbot J., Nemitz E., Dore C.J., Malcolm H., Vieno M., Reis S.

and Fowler D. [2014]. Quantifying missing annual emission sources of heavy metals in the United Kingdom with an atmospheric transport model. Science of the Total Environment 479–480 (2014) 171–180.

ECHA [2013]. Support document for identification of cadmium as a subs tance of very high concern becaus e of its CMR properties and because of its adverse effects nn kidney and bone tissues after prolonged exposure, which cause probable serious effects to human health which give rise to an equivalent level of concern to those of CMR and PBT/vPvB. 24 p.

ECHA [2018]. Support document for identi fication of lead (lead powder and lead massive) as a substance of very high concern because of i ts toxic for reproduction properties (article 57c). 7 p.

ECMWF [2022] Operational archive. https://www.ecmwf.int/en/forecasts/dataset/operational-archive. Accessed 27.05.2022

EMEP/EEA Guidebook 2013. EMEP/EEA air pollutant emission inventory guidebook – 2013. EEA Technical report No 12/2013. Available at: https://www.eea.europa.eu/publications/emep-eea-guidebook-2013.

EMEP/EEA Guidebook 2016. EMEP/EEA air pollutant emission inventory guidebook – 2016. EEA Technical report No 21/2016. Available at: https://www.eea.europa.eu/publications/emep-eea-guidebook-2016.

EMEP/EEA Guidebook 2019. EMEP/EEA air pollutant emission inventory guidebook – 2019. EEA Technical report No 13/2019. Available at: https://www.eea.europa.eu/publications/emep-eea-guidebook-2019.

Fiedler H. [2007] National PCDD/PCDF release inventories under the Stockholm Convention on Persistent Organic Pollutants, *Chemosphere,* 67, 96–108.

Flemming C.A. and Trevor J.T. [1989] Copper toxicity and chemistry in the environment: a review. *Water, Air, and Soil Pollution 44*: 143-158.

Friedl M., Sulla-Menashe D. [2019] MCD12Q1 MODIS/Terra+Aqua Land Cover Type Yearly L3 Global 500m SIN Grid V006 [Data set]. NASA EOSDIS Land Processes DAAC. Accessed 2021-05-14 from https://doi.org/10.5067/MODIS/MCD12Q1.006.

Friedli H.R., Arellano A.F., Cinnirella S. and Pirrone N. [2009] Initial Estimates of Mercury Emissions to the Atmosphere from Global Biomass Burning. *Environ. Sci. Technol*. 2009, 43, 3507–3513.

Frontasyeva M., Harmens H., Uzhinskiy A., Chaligava, O. and participants of the moss survey [2020]. Mosses as biomonitors of air pollution: 2015/2016 survey on heavy metals, nitrogen and POPs in Europe and beyond. Report of the ICP Vegetation Moss Survey Coordination Centre, Joint Institute for Nuclear Research, Dubna, Russian Federation, 136 pp. ISBN 978-5-9530-0508-1.

Gauss M., A. Gusev, W. Aas, V. Shatalov, I. Ilyin, O. Rozovskaya, H. Klein, A. Nyiri, N. Vulyh [2021] Atmospheric Supply of Nitrogen, Copper, HCB, BDE-99, SCCP and PFOS to the Baltic Sea in 2019 EMEP Centres Joint Report for HELCOM. MSC-W Technical Report 1/2021.

Gautam R.K., Sharma S.K., Mahiya S. and Chattopadhyaya M.C. [2014] CHAPTER 1: Contamination of Heavy Metals in Aquatic Media: Transport, Toxicity and Technologies for Remediation, in Heavy Metals In Water: Presence, Removal and Safety, 2014, ed. by Sharma S. pp. 1-24 DOI: 10.1039/9781782620174-00001.

Giglio L., Csiszar I. and Justice C.O. [2006] Global distribution and seasonality of active fires as observed with the Terra and Aqua MODIS sensors. *Journal of Geophysical Research*, 111:G02016, doi:10.1029/2005JG000142.

González M.A., Vivanco M.G., Palomino I., Garrido J.L., Santiago M. and Bessagnet B. [2012]. Modelling Some Heavy Metals Air Concentration in Europe. *Water Air Soil Pollut* 223:5227–5242.

Gusev A., I. Ilyin, V. Shatalov, O. Travnikov, N. Batrakova, O. Rozovskaya, I. Strijkina, K.Brevik, Nizzetto P.B., W. Aas, K. Mareckova, S. Poupa, C. Sosa, M. Tista, R. Wankmueller, F. Couvidat [2019] Assessment of transboundary pollution by toxic substances: Heavy metals and POPs. EMEP Status Report 2/2019, July 2019.

Gusev A., Ilyin I., Mantseva L., Rozovskaya O., Shatalov V. and Travnikov O. [2006]. Progress in further development of MSCE-HM and MSCE-POP models (implementation of the model review recommendations). EMEP/MSC-E Technical Report 4/2006.

Gusev A., O.Rozovskaya, V. Shatalov [2007] Modelling POP long-range transport and contamination levels by MSCE-POP model . EMEP/MSC-E Technical Report 1/2007.

Gusev A., O.Rozovskaya, V.Shatalov, N.Vulykh, P. Nizzetto, K. Breivik, and W.Aas [2017] Transboundary transport of Persistent Organic Pollutants with emphasis on PAHs: regional and national scale assessment and transition to the new EMEP grid. EMEP Status Report 3/2017.

Gusev A., O.Rozovskaya, V.Shatalov, N.Vulykh, W. Aas, K. Breivik, F. Couvidat, and M.G. Vivanco [2018] Persistent Organic Pollutants: assessment of transboundary pollution on global, regional, and national scales. EMEP Status Report 3/2018.

Gusev A., Rozovskaya O., Shatalov V., Vulykh N., Nizzetto P.B., Breivik K., Aas W. [2017] Transboundary transport of Persistent Organic Pollutants with emphasis on PAHs: regional and national scale assessment and transition to the new EMEP grid. EMEP Status Report 3.

Harmens H., Norris D. and the participants of the moss survey [2008]. Spatial and temporal trends in heavy metal accumulation in mosses in Europe (1990-2005). ICP Vegetation Programme Coordination Centre, Centre for Ecology and Hydrology, Bangor, UK, 51 p.

Harmens H., Norris D., Mills G., and the participants of the moss survey [2013]. Heavy metals and nitrogen in mosses: spatial patterns in 2010/2011 and long-term temporal trends in Europe. ICP Vegetation Programme Coordination Centre, Centre for Ecology and Hydrology, Bangor, UK, 63 pp.

Harmens H., Norris D.A., Steinnes E., Kubin E., Piispanen J., Alber R., Aleksiayenak Y., Blum O., Cos¸kun M., Damh M., De Temmerman L., Fernández J.A., Frolova M., Frontasyeva M., González-Miqueom L., Grodzinska K., Jeran Z., Korzekwa S., Krmar M., Kvietkus K., Leblond S., Liiv S., Magnússon S.H., Mankovská B., Pesch R., Rühling Å., Santamaria J.M., Schröder W., Spiric ., Suchara I., Thöni L., Urumov V., Yurukova L., echmeister H.G. [2010]. Mosses as biomonitors of atmospheric heavy metal deposition: Spatial patterns and temporal trends in Europe. Environmental Pollution 158 (2010) 3144 -3156.

Hettelingh J-P., Schütze G., de Vries W., Denier van der Gon H., Ilyin I., Reinds G.J., Slootweg J. and Travnikov O. [2015]. Critical loads of cadmium, lead and mercury and their exceedances in Europe. pp 523 – 546. In: Critical loads and dynamic risk assessments. Nitrogen, acidity in terrestrial and aquatic ecosystems. Edited by W. de Vries, J-P. Hettelingh and M. Posch. *Envitornmental pollution* 25, Springer.

HMCR [2021] Hydrometeorological Centre of Russia. The main peculiarities of atmospheric circulation and weather in the northern hemisphere. https://meteoinfo.ru/circulation-review. Accessed on December 2.

Ho Q.T., Bank M.S., Azad A.M., Nilsen B.M., Frantzen S., Boitsov S., Maage A., Kogel T., Sanden M., Froyland L., Hannisdal R., Hove H., Lundebye A. K., Ostbakken O.J.N., & Madsen L. [2021] Co-occurrence of contaminants in marine fish from the North East Atlantic Ocean: Implications for human risk assessment. *Environment International*, 157, 13. doi:10.1016/j.envint.2021.106858.

Hung H., Blanchard P., Halsall C.J., Bidleman T.F., Stern G.A., Fellin P., Muir D.C.G., Barrie L.A., Jantunen L.M., Helm P.A., Ma J., Konoplev A. [2005] Temporal and spatial variabilities of atmospheric polychlorinated biphenyls (PCBs), organochlorine (OC) pesticides and polycyclic aromatic hydrocarbons (PAHs) in the Canadian Arctic: Results from a decade of monitoring. *Science of The Total Environment* 342, 119-144.

Hung H., Kallenborn R., Breivik K., Su Y.S., Brorstrom-Lunden E., Olafsdottir K., Thorlacius J.M., Leppanen S., Bossi R., Skov H., Mano S., Patton G.W., Stern G., Sverko E., Fellin P. [2010] Atmospheric monitoring of organic pollutants in the Arctic under the Arctic Monitoring and Assessment Programme (AMAP): 1993-2006. Science of The *Total Environment 408, 2854-2873*.

ICP Vegetation [2020] Monitoring of atmospheric deposition of heavy metals, nitrogen and POPs in Europe using bryophytes monitoring manual 2020 survey. ICP Vegetation Programme Coordination Centre, CEH. Bangor, UK, and Moss Survey Coordination Centre, Joint Institute for Nuclear Research, Dubna, Russia. http://icpvegetation.ceh.ac.uk.

Ilyin I., N.Batrakova, A.Gusev, M.Kleimenov, O.Rozovskaya, V.Shatalov, I.Strizhkina, O.Travnikov, K.Breivik, H.L.Halvorsen, P.B.Nizzetto, K.A.Pfaffuffer, W.Aas, K.Mareckova, S.Poupa, R.Wankmueller, B.Ullrich, A.Degorska [2021]. Heavy metals and POPs: Pollution assessment of toxic substances on regional and global scales. EMEP Status Report 2/2021, 148 p. (https://en.msceast.org/reports/2_2022.pdf).

Ilyin I., Rozovskaya O., Travnikov O. and Aas W. [2017] Assessment of heavy metal transboundary pollution on regional and national scales, transition to the new EMEP grid. EMEP Status Report 2/2017., 95 p.

Ilyin I., Rozovskaya O., Travnikov O., Aas W. and K.A.Pfaffhuber [2018] Assessment of heavy metal transboundary pollution on global, regional and national scales. EMEP Status Report 2/2018.

Ilyin I., Travnikov O., Rozovskaya O. and I.Strizhkina [2022] Trends in deposition of heavy metals to the OSPAR maritime area. EMEP/MSC-E Technical Report 1/2022. 63 p.

JRC [2019] European Commission, Joint Research Centre (JRC) - Emission Database for Global Atmospheric Research, Global Air Pollutant Emissions (EDGARv5.0), Crippa et al. (2019), https://edgar.jrc.ec.europa.eu/index.php/dataset_ap50.

Junge C.E. [1977] Basic considerations about trace constituent in the atmosphere is related to the fate of global pollutant. In: Fate of pollutants in the air and water environment. Part I, I.H. Suffet (ed.) (Advanced in Environ. Sci. Technol., v.8, Wiley-Interscience, New York.

Kahan T.F., Kwamena N.-O.A., and Donaldson D.J. [2006] Heterogeneous ozonation kinetics of polycyclic aromatic hydrocarbons on organic films. *Atmospheric Environment*, 40(19), 3448–3459.doi:10.1016/j.atmosenv.2006.02.004.

Karcioglu O. and Arslan B. (Eds.) [2019]. Poisoning in the Modern World - New Tricks for an Old Dog?. London, United Kingdom, IntechOpen, 2019 [Online]. Available from: https://www.intechopen.com/books/7111 doi: 10.5772/intechopen.73906.

Ke Z., Wang Y., Zou Y., Song Y. and Liu Y. [2021] Global wildfire plumerise data set and parameterizations for climate model applications. *Journal of Geophysical Research*: Atmospheres, 126, e2020JD033085. https://doi.org/10.1029/2020JD033085.

Kelly R. L., Bian X., Feakins S.J., Fornace K.L., Gunderson T., Hawco N.J., Liang H., Niggemann J., Paulson S.E., Pinedo-Gonzalez P., West A.J., Yang S-C. and John S.G. [2021] Delivery of Metals and Dissolved Black Carbon to the Southern California Coastal Ocean via Aerosols and Floodwaters Following the 2017 Thomas Fire. Journal of Geophysical Research: *Biogeosciences*, 126, e2020JG006117. https://doi.org/10.1029/2020JG00611.

Keyte I., R Harrison, G. Lammel [2013] Chemical reactivity and long-range transport potential of polycyclic aromatic hydrocarbons – a review. http://dx.doi.org/10.1039/c3cs60147a.

Kim K., S.A. Jahan, E. Kabir E., R.J.C. Brown [2013] A review of airborne polycyclic aromatic hydrocarbons (PAHs) and their human health effects. http://dx.doi.org/10.1016/j.envint.2013.07.019.

Klink A., Polechonska L., Dambiec M. and Biales [2017] A Comparative Study on Macro- and Microelement Bioaccumulation Properties of Leaves and Bark of Quercus petraea and Pinus sylvestris. *Arch Environ Contam Toxicol*. DOI 10.1007/s00244-017-0439-0

Kristensen L.J., Taylor M.P., Odigie K.O., Hibdon S.A. and Flegal A.R. [2014] Lead isotopic compositions of ash sourced from Australian bushfires. *Environmental Pollution* 190 (2014) 159-165.

Kumar A., Wu S., Huang Y., Liao H. and Kaplan J.O. [2018] Mercury from wildfires: Global emission inventories and sensitivity to 2000–2050 global change. *Atmospheric Environment* 2018, 173, 6–15.

Kwamena N.-O.A., Clarke J.P., Kahan T.F., Diamond M.L., & Donaldson D.J. [2007]. Assessing the importance of heterogeneous reactions of polycyclic aromatic hydrocarbons in the urban atmosphere using the Multimedia Urban Model. *Atmospheric Environment*, 41(1), 37–50. doi:10.1016/j.atmosenv.2006.08.016.

Kwamena, N.-O. A., Thornton, J. A., & Abbatt, J. P. D. [2004] Kinetics of Surface-Bound Benzo[a]pyrene and Ozone on Solid Organic and Salt Aerosols. *The Journal of Physical Chemistry* A, 108(52), 11626–11634. doi:10.1021/jp046161x.

La Guardia M.J., R.C. Hale, and E. Harvey [2006] Detailed Polybrominated Diphenyl Ether (PBDE) Congener Composition of the Widely Used Penta-, Octa-, and Deca-PBDE Technical Flame-retardant Mixtures. *Environ. Sci. Technol*. 2006, 40, 6247-6254.

Lammel G., Heil A., Stemmler I. Dvorská A. and Klánová J. [2013] On the Contribution of Biomass Burning to POPs (PAHs and PCDDs) in Air in Africa. *Environ. Sci. Technol*. 2013, 47, 20, 11616–11624.

Liu K., Wang X., Wei N., Song Z., Li D. [2019] Accurate quantification and transport estimation of suspended atmospheric microplastics in megacities: Implications for human health. *Environment International* 132, 105127. https://doi.org/10.1016/j.envint.2019.105127.

Liu Y., Goodrick S. and Heilman W. [2014]. Wildland fire emissions, carbon, and climate: Wildfire–climate interactions. Forest Ecology and Management 317, pp. 80 - 95.

Lohmann R. and G. Lammel [2004] Adsorptive and Absorptive Contributions to the Gas-Particle Partitioning of Polycyclic Aromatic Hydrocarbons: State of Knowledge and Recommended Parametrization for Modeling. *Environ. Sci. Technol.*, 38, 14, 3793-3803, DOI: 0.1021/es035337q.

Luo J., Han Y., Zhao Y., Huang Y., Liu X., Tao S., Liu J., Huang T., Wang L., Chen K. and Ma J. [2020]. Effect of northern boreal forest fires on PAH fluctuations across the Arctic. *Environmental Pollution* 261 (2020) 114186.

Madeijón P., Marañón T., Murillo J.M. and Robinson B. [2004] White poplar (Populus alba) as a biomonitor of trace elements in contaminated riparian forests. *Environmental Pollution* 132 (2004) 145-155.

Melymuk L., Bohlin P., Sanka O., Pozo K., Klanova J. [2014] Current Challenges in Air Sampling of Semivolatile Organic Contaminants: Sampling Artifacts and Their Influence on Data Comparability. *Environmental Science & Technology* 48, 14077-14091.

Mircea M., Silibello C., Calori G., Costa M. P., Dirodi G., Radice P., Vitali L. and Zanini G. [2013]. A Study of Heavy Metals Pollution in Italy with the Atmospheric Modelling System of the MINNI project. E3S Web of Conferences, 1, 03003.

Mitra S., Chakraborty A.J., Tareq A. M., Emran T.B., Nainu F., Khusro A., Idris A.M., Khandaker M.U., Osman H., Alhumaydhi F.A. and Simal-Gandara J. [2022]. Impact of heavy metals on the environment and human health: Novel therapeutic insights to counter the toxicity. *Journal of King Saud University – Science* 34 (2022) 101865.

Naeem M., Ansari A.A. and Sarvajeet S.G. (Eds.) [2020]. Contaminants in Agriculture. Sources, Impacts and Management. Springer Nature Switzerland AG 2020. , 445 p.

Nriagu J.O. [1989] A global assessment of natural sources of atmospheric trace metals. *Nature*, 338: 47-49.

Odigie K.O. and Flegal A.R. [2014] Trace Metal Inventories and Lead Isotopic Composition Chronicle a Forest Fire's Remobilization of Industrial Contaminants Deposited in the Angeles National Forest. *PLOS ONE*, Volume 9, Issue 9, e107835.

OSPAR [2009] Trends in atmospheric concentrations and deposition of nitrogen and selected hazardous substances to the OSPAR maritime area. Monitoring and Assessment Series. OSPAR Commission. Available at https://www.ospar.org/about/publications/page21.

Pacyna J.M. and Pacyna E.G [2001]. An assessment of global and regional emissions of trace metals to the atmosphere from anthropogenic sources worldwide. *Environ. Rev*. 9: 269–298.

Pacyna J.M., Breivik K., Munch J., Fudala J. [2001] European atmospheric emissions of selected persistent organic pollutants, 1970-1995. *Atmospheric Environment* 37, 119-131.

Palm A., E. Brorström-Lundén, K. Breivik [2004] Transport and fate of polybrominated diphenyl ethers in the Baltic and Arctic regions. TemaNord 2004:554. Nordic Council of Ministers, Copenhagen 2004. ISBN 92-893-1074-X.

Pankow J.F. [1987] Review and comparative analysis of the theories on partitioning between the gas and aerosol particulate phases in the atmosphere. *Atmos. Environ*., v.21, pp.2275-2283.

Parzych A., Mochnacky S., Sobisz Z., Kurhaluk N. and Polláková N. [2017] Accumulation of heavy metals in needles and bark of Pinus species. Folia Forestalia Polonica, series A – Forestry, 2017, Vol. 59 (1), 34–44.

Platt S.M., Hov Ø., Berg T., Breivik K., Eckhardt S., Eleftheriadis K., Evangeliou N., Fiebig M., Fisher R., Hansen G., Hansson H.C., Heintzenberg J., Hermansen O., Heslin-Rees D., Holmén K., Hudson S., Kallenborn R., Krejci R., Krognes T., Larssen S., Lowry D., Lund Myhre C., Lunder C., Nisbet E., Nizzetto P.B., Park K.T., Pedersen C.A., Aspmo Pfaffhuber K., Röckmann T., Schmidbauer N., Solberg S., Stohl A., Ström J., Svendby T., Tunved P., Tørnkvist K., van der Veen C., Vratolis S., Yoon Y.J., Yttri K.E., Zieger P., Aas W., Tørseth K. [2022] Atmospheric composition in the European Arctic and 30 years of the Zeppelin Observatory, Ny-Ålesund. *Atmos. Chem. Phys*. 22, 3321-3369.

Poupa S. [2021] Methodologies applied to the CEIP GNFR gap-filling 2021. Part II: Heavy Metals (Cd, Hg, Pb) and Persistent Organic Pollutants (Benzo(a)pyrene, Benzo(b)fluoranthene, Benzo(k)fluoranthene, Indeno(1,2,3-cd)pyrene, Total polycyclic aromatic hydrocarbons, Dioxin and Furan, Hexachlorobenzene, Polychlorinated biphenyls). Technical Report CEIP 06/2021.

Pulles T., Kok H. and U.Quass [2006] Application of the emission inventory model TEAM: Uncertainties in dioxin emission estimates for central Europe. *Atmospheric Environment,* 40, 2321–2332.

Pulles T., Kok H., Quass U., Juery C. and J.Matejovicova [2005] Dioxin emissions in candidate countries. TNO Report R&I-A R 2005/054. Available at:http://ec.europa.eu/environment/archives/dioxin/pdf/rapport_2005.pdf.

Rauch J.N. and Pacyna J.M. [2009]. Earth's global Ag, Al, Cr, Cu, Fe, Ni, Pb, and Zn cycles. GLOBAL BIOGEOCHEMICAL CYCLES, VOL. 23, GB2001, doi:10.1029/2008GB003376.

Reid C.E., Brauer M., Johnston F.H., Jerrett M., John Balmes J.R. and Elliott C.T. [2016]. Critical Review of Health Impacts of Wildfire Smoke Exposure. *Environmental Health Perspectives.* Vol. 124,9, pp 1334 – 1343.

Requia W.J., Amini H., Mukherjee R.,. Gold D.R., and Schwartz J.D. [2021]. Health impacts of wildfire-related air pollution in Brazil: a nationwide study of more than 2 million hospital admissions between 2008 and 2018. NATURE COMM UNICATIONS, (2021)12:6555, https://doi.org/10.1038/s41467-021-26822-7.

Rice K.M, Walker E.M., Miaozong J. Wu, Gillette C. and Blough E.R. [2014]. Environmental Mercury and Its Toxic Effects . *J Prev Med Public Health* 2014; 47:74-83.

Rühling Å and Tyler G. [1973]. Heavy metal deposition in Scandinavia. *Water, Air and Soil Pollution* 2, pp 445-455.

Salminen R. (Chief-editor) [2005]. Geochemical Atlas of Europe. Part 1 - Background Information, Methodology and Maps. A contribution to IUGS/IAGC Global Geochemical Baselines. ISBN 951-690-913-2 (electronic version). http://weppi.gtk.fi/publ/foregsatlas/index.php.

Santín C., Doerr S.H., Otero X.L. and Chafer C.J. [2015]. Quantity, composition and water contamination potential of ash produced under different wildfire severities. *Environmental Research* 142 (2015) 297–308.

Schaap M., Hendriks C., Jonkers S. and Builtje P. [2018]. Impacts of Heavy Metal Emission on Air Quality and Ecosystems across Germany – Sources, Transport, Deposition and potential Hazards. Part 1: Assessment of the atmospheric heavy metal deposition to terrestrial ecosystems in Germany. ISSN 1862-4804 Dessau-Roßlau, December 2018. 81 p.

Schröder W., Pesch R., Hertel A., Schonrock S., Harmens H., Mills G. and Ilyin I. [2013]. Correlation between atmospheric deposition of Cd, Hg and Pb and their concentrations in mosses specified for ecological land classes covering Europe. *Atmospheric Pollution Research*, 4, (2013), 267-274.

SEDAC [2011] Global Rural-Urban Mapping Project, Version 1 (GRUMPv1): Urban Extents Grid (Africa). Palisades, NY: NASA Socioeconomic Data and Applications Center (SEDAC). Center for International Earth Science Information Network - CIESIN - Columbia University, International Food Policy Research Institute - IFPRI, The World Bank, and Centro Internacional de Agricultura Tropical - CIAT. 2011. (https://sedac.ciesin.columbia.edu/data/set/grump-v1-urban-extents/maps).

Shatalov V., Gusev A., Dutchak S., Rozovskaya O., Sokovykh V. and N.Vulykh [2010] Persistent Organic Pollutants in the Environment. EMEP Status Report 3/2010.

Shen H., Huang Y., Wang R., Zhu D., Li W., Shen G., Wang B., Zhang Y., Chen Y., Lu Y., Chen H., Li T., Sun K., Li B., Liu W., Liu J. and S.Tao [2013] Global atmospheric emissions of polycyclic aromatic hydrocarbons from 1960 to 2008 and future predictions. *Environ Sci Technol*., 2013, 47, 12, 6415-6424.

Shikwambana L. and Habarulema J.B. [2022]. Analysis of Wildfires in the Mid and High Latitudes Using a Multi-Dataset Approach: A Case Study in California and Krasnoyarsk Krai. *Atmosphere* 2022, 13, 428. https://doi.org/10.3390/atmos13030428.

Silva V., Pereira J.L., Campos I., Keizer J.J., Gonçalves F. and Abrantes N. [2015]. Toxicity assessment of aqueous extracts of ash from forest fires. *Catena* 135 (2015) 401–408.

Simpson D., Benedictow A., Berge H., Bergström R., Emberson L., Fagerli H., Flechard C. R., Hayman G. D., Gauss M., Jonson J. E., Jenkin M. E., Nyíri A., Richter C., Semeena V. S., Tsyro S., Tuovinen J.-P., Valdebenito Á. and Wind P. [2012] The EMEP MSC-W chemical transport model– technical description. *Atmos. Chem. Phys*., 12, 7825–7865.

Skamarock W.C., Klemp J.B., Dudhia J., Gill D.O., Barker D.M., Duda M.G., Huang X-Y., Wang W. and Powers J.G. [2008]. A Description of the Advanced Research WRF Version 3. NCAR/TN–475+STRNCAR TECHNICAL NOTE.

Sofiev M., Ermakova T. and Vankevich R. [2012] Evaluation of the smoke-injection height from wild-land fires using remote-sensing data. *Atmos. Chem. Phys.,* 12, 1995–2006, 2012.

Starek-Świechowicz, B., Budziszewska, B., & Starek, A. [2017] Hexachlorobenzene as a persistent organic pollutant: Toxicity and molecular mechanism of action. Pharmacological Reports, 69(6), 1232–1239. doi:10.1016/j.pharep.2017.06.013.

Strahler A., Muchoney D., Borak J., Friedl, M., Gopal S., Lambin E. and Moody A. [1999]. MODIS Land Cover Product. Algori thm Theoretical Basis Document (ATBD) Version 5.0. MODIS Land Cover and Land-Cover Change. Center for Remote Sensing, Department of Geography, Bos ton Universi ty, Bos ton, MA, 66 p.

Strizhkina I., Gusev A., O.Rozovskaya, Shatalov V., [2021a] Heavy metals and POPs: Pollution assessment of toxic substances on regional and global scales Part I. Supplementary materials for POPs. MSC-E Data Report 2/2022.

Strizhkina I., Ilyin I., Rozovskaya O., O.Travnikov, [2021b] Heavy metals and POPs: Pollution assessment of toxic substances on regional and global scales. Part II. Supplementary materials for heavy metals. MSC-E Data Report 1/2022.

Swislowski P., Kriz J. and Rajfur M. [2020]. The use of bark in biomonitoring heavy metal pollution of forest areas op the example of selected areas in Poland. *Ecol. Chem. Eng*, 2020;27(2):195-210.

Tørseth K., Aas W., Breivik K., Fjaeraa A.M., Fiebig M., Hjellbrekke A.G., Myhre C.L., Solberg S., Yttri K.E. [2012] Introduction to the European Monitoring and Evaluation Programme (EMEP) and observed atmospheric composition change during 1972-2009. *Atmospheric Chemistry and Physics* 12, 5447-5481.

Travnikov O., Batrakova N., Gusev A., Ilyin I., Kleimenov M., Rozovskaya O., Shatalov V., Strijkina I., Aas W., Breivik K., Nizzetto P.B., Pfaffhuber K.A., Mareckova K., Poupa S., Wankmueller R., Seussall K. [2020] Assessment of transboundary pollution by toxic substances: Heavy metals and POPs. EMEP Status Report 2/2020.

Travnikov O., Ilyin I. [2009] The EMEP/MSC-E mercury modeling system. In Mercury Fate and Transport in the Global Atmosphere, R. Mason, N. Pirrone, Eds. Springer, Boston, MA, pp. 571–587.

UNECE [1979] The 1979 Geneva Convention on Long-range Transboundary Air Pollution. United Nations Economic Commission for Europe. http://www.unece.org/env/lrtap/welcome.html.

UNECE [2014] Guidelines for reporting emission data under the Convention on Long-range Transboundary Air Pollution (ECE/EB.AIR/130). Available at: http://www.ceip.at/fileadmin/inhalte/emep/2014_Guidelines/ece.eb.air.125_ADVANCE_VERSION_reporting_guidelines_2013.pdf.

UNECE [2019] Monitoring strategy for the Cooperative Programme for Monitoring and Evaluation of the Long-range Transmission of Air Pollutants in Europe for the period 2020–2029. EB Decision 2019/1, ECE/EB.AIR/144/Add.1. URL: http://www.unece.org/fileadmin/DAM/env/documents/2019/AIR/EB_Decisions/Decision_2019_1.pdf.

Urbanski S.P., Hao W.M. and Baker S. [2009] Chemical composition of wildland fire emission. In: Bytnerowicz A., Arbaugh M., Riebau A. and Andersen C. (Editors). *Developments in Environmental Science*, Volume 8. pp 79 – 107.

van der Werf G.R., Randerson J.T., Giglio L., van Leeuwen T.T., Chen Y., Rogers B.M., Mu M., van Marle M.J.E., Morton D.C., Collatz G.J., Yokelson R.J., and Kasibhatla P.S. [2017]. Global fire emissions estimates during 1997–2016. *Earth Syst. Sci. Data*, 9, 697–720, 2017, https://doi.org/10.5194/essd-9-697-2017.

WHO [2000] Air Quality Guidelines - Second Edition. Chapter 5.11 Polychlorinated dibenzodioxins and dibenzofurans. https://www.euro.who.int/__data/assets/pdf_file/0017/123065/AQG2ndEd_5_11PCDDPCDF.pdf?ua=1.

WHO [2003] Concise International Chemical Assessment Document 55. Polychlorinated biphenyls: human health aspects. ISBN 92 4 153055 3; ISSN 1020-6167. https://www.who.int/ipcs/publications/cicad/en/cicad55.pdf?ua=1.

WHO [2017] Evolution of WHO air quality guidelines: past, present and future. Copenhagen. WHO Regional Office for Europe. (http://www.euro.who.int/__data/assets/pdf_file/0019/331660/Evolution-air-quality.pdf).

Wiedinmyer C. and H.Friedli [2007] Mercury Emission Estimates from Fires: An Initial Inventory for the United States. *Environ. Sci. Technol*. 2007, 41, 8092–8098.

Wiedinmyer C., S.K. Akagi, R.J. Yokelson, L.K. Emmons, J.A. Al-Saadi, J.J. Orlando and A. J. Soja. [2011] The Fire Inventory from Ncar (Finn): A High Resolution Global Model to Estimate the Emissions from Open Burning. *Geoscientific Model Development* 4, no. 3 (2011): 625-41.

Wilkins J.L., Pouliot G., Pierce T., Soja A., Choi H., Gargulinski E., Gilliam R., Vukovich J. and Landis M.S. [2022] An evaluation of empirical and statistically based smoke plume injection height parametrisations used within air quality models. *International Journal of Wildland Fire* 2022, 31, 193–211. https://doi.org/10.1071/WF20140.

Wong F., Hung H., Dryfhout-Clark H., Aas W., Bohlin-Nizzetto P., Breivik K., Mastromonaco M.N., Lunden E.B., Olafsdottir K., Sigurdsson A., Vorkamp K., Bossi R., Skov H., Hakola H., Barresi E., Sverko E., Fellin P., Li H., Vlasenko A., Zapevalov M., Samsonov D., Wilson S. [2021] Time trends of persistent organic pollutants (POPs) and Chemicals of Emerging Arctic Concern (CEAC) in Arctic air from 25years of monitoring. *The Science of the total environment* 775, 145109.

Wu L., Taylor M.P. and Handley H.K. [2017] Remobilisation of industrial lead depositions in ash during Australian wildfires. *Science of the Total Environment* 599–600 (2017) 1233–1240.

Zsigmond A.R., Száraz A. and Urák I. [2021] Macro and trace elements in the black pine needles as inorganic indicators of urban traffic emissions. *Environmental Pollution* 291 (2021) 118228.

Самсонов Ю.Н., Куценогий К.П., Макаров В.И., Иванов А.В., Иванов В.А. и Иванова Г.А. [2006] Аэрозольная эмиссия при лесных пожарах в бореальных лесах Сибири. Аэрозоли Сибири / [И.С.Андреева и др.]; отв. ред. К.П.Куценогий; Рос. акад. наук, Сиб. отд-ние, Ин-т химической кинетики и горения [и др.]. - Новосибирск: Изд-во СО РАН, 2006. - 548 с. - (Интеграционные проекты СО РАН; вып. 9). Стр. 282 – 299 (In Russian).

Reporting of priority heavy metals and POPs in EMEP East region

Table A1. Reporting of main heavy metals (Pb, Cd, Hg) in EMEP-East region since 2015

Reporting of main heavy metals (Pb, Cd, Hg)								
	2015	***2016***	***2017***	***2018***	***2019***	***2020***	***2021***	***2022***
Armenia	2008 - 2013 (only Pb, only a few sectors)	2014		2016	2017		2019	2020
Azerbaijan	1990 - 2013 (only Hg, only a few sectors)	1990-2014 (Pb, Cd: 1995-2014)	1990 - 2015 (Pb, Cd: 1995-2015)	1990 - 2016 (Pb, Cd: 1995-2016)	1995-2017 (Hg 1990-2017)			
Belarus	2013			2014-2016	2017	2018	2019	2020
Georgia	2007 - 2013 (no Hg)	2007-2014 (Cd, Hg: 2013-2014)	2007 - 2015	2007-2016	2007-2017		1990-2019	1990-2020
Kazakhstan		2013-2014	1990, 2000, 2005, 2010 - 2015	1990 - 2016		1990 - 2018	1990-2019	1990-2020
Kyrgyzstan		2014 (only Hg)	2015 (only Hg)		2017	2018		
Republic of Moldova	2013	1990-2014 (no emissions calculated for the waste sector)	1990 - 2015			1990 - 2017	1990-2019	
Russian Federation								2010-2020
Ukraine	2013	2014	2015	2016		2016, 2017, 2018	2019	2020
Turkey					1990 - 2017 *(just for very few IPPU categories)*	1990 - 2018 *(just for very few IPPU categories)*	1990-2019	1990-2020

Table A2. Reporting of POPs (PCDD/Fs, PAHs, HCB, PCBs) in EMEP East region since 2015

Reporting of POPs (PCDD/Fs, PAHs, HCB, PCBs)								
	2015	**2016**	**2017**	**2018**	**2019**	**2020**	**2021**	**2022**
Armenia		2014		2016 (only PCDD/Fs)	2017 (No HCB, no PCBs)		2019	2020
Azerbaijan	1995-2013	1995-2014 (no HCB, no PCBs)	1995-2015	1995-2016	1995 -2017 (HCB, PCBS no data for 2000)			
Belarus	2013			2014-2016	2017	2018	2019	2020
Georgia	2007-2013 (no HCB)	2007-2014 (PCDD/Fs) 2013-2014 (PAHs, HCB, PCBs)	2007-2015	2007-2016 (HCB only 2013-2016)	2007-2017		1990-2019	1990-2020
Kazakhstan		2013-2014	1990, 2000, 2005, 2010-2015	1990-2016		1990 -2018	1990-2019	1990-2020
Kyrgyzstan					2017	2018		
Republic of Moldova	2013	1990-2014 (no emissions calculated for the waste sector)	1990-2015			1990-2017	1990-2019	
Russian Federation								2010-2020
Ukraine	2013 (no PCDD/Fs)				2017	2017, 2018	2019	2020
Turkey								1990-2020

Annex A.2.

Significant changes (over ±15 %) between national totals used in models in year 2022 and national totals used in models in 2021

Data values represent the 'total national totals'. The column 'data sources' in the table below indicates the following four cases:

- *"reported"*: both 2019 and 2020 data are reported by country.
- *"gapfilled":* both 2019 and 2020 data are gap-filled by expert estimates
- *"new gapfilled":* 2019 data was reported by country and 2020 data had to be gap-filled by expert estimates (because it was not reported by country)
- *"new reported":* 2019 data was gap-filled, 2020 data is as reported by country

The indicator *"new"* in column *"% change"* indicates that the value has been either reported or gap-filled for the first time.

Component	Country	Data sources	Unit	2020 value	2019 value	% change	Value change
Cd	AM	reported	t	0.044	0.013	245%	0.032
B(a)P	AL	new gapfilled	t	0.642	0.021	3006%	0.622
B(a)P	BA	gapfilled	t	3.061	1.497	104%	1.564
B(a)P	CY	reported	t	0.146	0.115	27%	0.032
B(a)P	ES	new gapfilled	t	12.950	15.953	-19%	-3.003
B(a)P	FI	reported	t	5.987	7.311	-18%	-1.324
B(a)P	GB	reported	t	3.676	8.060	-54%	-4.384
B(a)P	IS	reported	t	0.008	0.012	-35%	-0.004
B(a)P	KZT	New reported	t	65.835	36.754	79%	29.080
B(a)P	LI	reported	t	0.002	0.003	-39%	-0.001
B(a)P	ME	reported	t	0.291	0.003	11131%	0.288
B(a)P	NO	reported	t	1.043	1.286	-19%	-0.242
B(a)P	PL	new gapfilled	t	82.685	62.160	33%	20.525
B(a)P	PT	new gapfilled	t	8.119	4.962	64%	3.157
B(a)P	RS	gapfilled	t	10.812	6.822	58%	3.990
B(a)P	SK	new gapfilled	t	7.553	6.117	23%	1.436
B(b)F	AL	new gapfilled	t	0.603	0.033	1725%	0.570
B(b)F	BA	gapfilled	t	4.073	1.943	110%	2.130
B(b)F	CY	reported	t	0.409	0.312	31%	0.097
B(b)F	FI	reported	t	4.748	5.704	-17%	-0.956
B(b)F	GB	reported	t	3.200	7.341	-56%	-4.141
B(b)F	IS	reported	t	0.031	0.039	-22%	-0.009
B(b)F	KZT	reported	t	137.247	52.573	161%	84.674
B(b)F	LI	reported	t	0.002	0.003	-39%	-0.001
B(b)F	MD	new gapfilled	t	4.763	6.798	-30%	-2.035
B(b)F	ME	reported	t	0.494	0.021	2303%	0.474
B(b)F	MT	reported	t	0.036	0.031	16%	0.005

Component	Country	Data sources	Unit	2020 value	2019 value	% change	Value change
B(b)F	NO	reported	t	2.407	3.418	-30%	-1.011
B(b)F	PL	new gapfilled	t	81.906	69.933	17%	11.973
B(b)F	PT	new gapfilled	t	6.172	4.187	47%	1.984
B(b)F	RS	new gapfilled	t	11.849	7.518	58%	4.332
B(b)F	SK	new gapfilled	t	7.513	6.400	17%	1.113
B(k)F	AL	gapfilled	t	0.226	0.010	2084%	0.216
B(k)F	BA	gapfilled	t	1.626	0.653	149%	0.973
B(k)F	CY	reported	t	0.173	0.132	31%	0.041
B(k)F	FI	reported	t	3.458	4.340	-20%	-0.882
B(k)F	GB	reported	t	1.509	3.018	-50%	-1.509
B(k)F	IS	reported	t	0.014	0.024	-42%	-0.010
B(k)F	KZT	reported	t	99.538	20.853	377%	78.684
B(k)F	LI	reported	t	0.003	0.005	-40%	-0.002
B(k)F	ME	reported	t	0.148	0.007	1882%	0.141
B(k)F	NO	reported	t	0.865	1.130	-23%	-0.265
B(k)F	PL	new gapfilled	t	37.570	32.046	17%	5.524
B(k)F	PT	new gapfilled	t	3.768	2.161	74%	1.607
B(k)F	RO	new gapfilled	t	7.767	6.615	17%	1.152
B(k)F	RS	new gapfilled	t	4.756	2.933	62%	1.823
B(k)F	SE	new gapfilled	t	0.938	0.792	18%	0.146
B(k)F	SK	new gapfilled	t	3.621	2.257	60%	1.364
Cd	AT	reported	t	0.942	1.162	-19%	-0.221
Cd	BG	reported	t	1.433	1.761	-19%	-0.328
Cd	ES	reported	t	5.604	7.363	-24%	-1.759
Cd	GB	reported	t	4.536	5.589	-19%	-1.053
Cd	GR	reported	t	1.438	1.720	-16%	-0.282
Cd	IS	reported	t	0.005	0.006	-26%	-0.002
Cd	LI	reported	t	0.003	0.004	-15%	-0.001
Cd	LT	reported	t	0.299	0.188	59%	0.111
Cd	MD	new gapfilled	t	0.396	0.732	-46%	-0.336
Cd	ME	reported	t	0.222	0.114	95%	0.108
Cd	MT	reported	t	0.044	0.007	516%	0.037
Cd	NL	reported	t	2.017	2.636	-23%	-0.619
Cd	TR	gapfilled	t	3.976	3.211	24%	0.765
Cd	UA	reported	t	5.804	8.434	-31%	-2.630
PCDD/F	BA	gapfilled	g I-TEQ	48.004	31.121	54%	16.882
PCDD/F	BY	reported	g I-TEQ	30.214	37.009	-18%	-6.795
PCDD/F	ES	reported	g I-TEQ	229.682	172.227	33%	57.456
PCDD/F	FI	reported	g I-TEQ	9.310	12.132	-23%	-2.821
PCDD/F	GB	reported	g I-TEQ	147.375	180.984	-19%	-33.610
PCDD/F	IS	reported	g I-TEQ	0.737	0.460	60%	0.277
PCDD/F	KZT	New reported	g I-TEQ	467.355	325.930	43%	141.425
PCDD/F	LI	reported	g I-TEQ	0.049	0.081	-40%	-0.033
PCDD/F	MC	reported	g I-TEQ	0.989	1.255	-21%	-0.266
PCDD/F	ME	reported	g I-TEQ	0.326	0.131	149%	0.195
PCDD/F	MT	reported	g I-TEQ	0.224	4.324	-95%	-4.100
PCDD/F	NL	reported	g I-TEQ	29.686	40.706	-27%	-11.020

Component	Country	Data sources	Unit	2020 value	2019 value	% change	Value change
PCDD/F	NO	reported	g I-TEQ	22.003	19.059	15%	2.944
PCDD/F	PT	reported	g I-TEQ	70.660	55.799	27%	14.862
PCDD/F	RS	reported	g I-TEQ	74.221	55.780	33%	18.440
PCDD/F	UA	gapfilled	g I-TEQ	235.833	806.569	-71%	-570.736
HCB	FR	reported	kg	22.073	29.794	-26%	-7.721
HCB	AT	reported	kg	14.590	17.219	-15%	-2.630
HCB	BG	reported	kg	0.276	1.582	-83%	-1.306
HCB	BY	reported	kg	0.920	1.112	-17%	-0.192
HCB	CY	reported	kg	0.044	0.023	91%	0.021
HCB	CZ	reported	kg	15.053	18.472	-19%	-3.419
HCB	DE	reported	kg	4.766	12.663	-62%	-7.897
HCB	EE	reported	kg	0.476	0.345	38%	0.132
HCB	GE	reported	kg	22.066	5.288	317%	16.778
HCB	GR	reported	kg	1.280	1.707	-25%	-0.427
HCB	HR	reported	kg	0.359	0.603	-40%	-0.244
HCB	HU	reported	kg	2.058	3.219	-36%	-1.161
HCB	IT	reported	kg	12.982	10.435	24%	2.547
HCB	KZT	reported	kg	32.664	7.934	312%	24.730
HCB	LI	reported	kg	0.001	0.001	-28%	0.000
HCB	LT	reported	kg	0.472	0.409	15%	0.063
HCB	LU	reported	kg	0.707	0.507	40%	0.200
HCB	MC	reported	kg	0.008	0.011	-31%	-0.003
HCB	MD	new gapfilled	kg	0.187	0.316	-41%	-0.129
HCB	MK	reported	kg	0.155	4.422	-96%	-4.266
HCB	MT	reported	kg	0.080	0.060	34%	0.020
HCB	PL	reported	kg	3.137	14.917	-79%	-11.780
HCB	PT	reported	kg	1.283	2.383	-46%	-1.100
HCB	SI	reported	kg	0.456	0.543	-16%	-0.087
HCB	UA	new gapfilled	kg	165.951	118.083	41%	47.868
Hg	FR	reported	t	2.377	3.000	-21%	-0.623
Hg	EE	reported	t	0.205	0.327	-37%	-0.122
Hg	GB	reported	t	3.366	4.009	-16%	-0.643
Hg	GE	reported	t	0.218	0.183	19%	0.035
Hg	GR	reported	t	0.811	1.183	-31%	-0.372
Hg	IE	reported	t	0.267	0.327	-18%	-0.060
Hg	LT	reported	t	0.265	0.147	81%	0.118
Hg	LU	reported	t	0.076	0.099	-23%	-0.023
Hg	MC	reported	t	0.001	0.001	51%	0.000
Hg	MD	new gapfilled	t	0.091	0.127	-28%	-0.035
Hg	MK	reported	t	0.165	0.211	-22%	-0.046
Hg	MT	reported	t	0.013	0.007	95%	0.006
Hg	NL	reported	t	0.495	0.591	-16%	-0.096
Hg	SI	reported	t	0.197	0.158	25%	0.040
Hg	TR	gapfilled	t	10.731	6.922	55%	3.809
I(cd)P	AL	reported	t	0.566	0.197	187%	0.369
I(cd)P	BA	gapfilled	t	2.786	0.728	283%	2.058
I(cd)P	CY	reported	t	0.124	0.096	29%	0.028

Component	Country	Data sources	Unit	2020 value	2019 value	% change	Value change
I(cd)P	ES	new gapfilled	t	7.004	8.650	-19%	-1.645
I(cd)P	FI	reported	t	4.045	4.955	-18%	-0.910
I(cd)P	GB	reported	t	2.067	4.636	-55%	-2.569
I(cd)P	IS	reported	t	0.008	0.011	-26%	-0.003
I(cd)P	KZT	reported	t	37.269	17.654	111%	19.615
I(cd)P	LI	reported	t	0.003	0.004	-41%	-0.002
I(cd)P	ME	reported	t	0.118	0.035	240%	0.084
I(cd)P	MT	reported	t	0.010	0.012	-17%	-0.002
I(cd)P	PL	new gapfilled	t	30.725	26.399	16%	4.326
I(cd)P	PT	new gapfilled	t	4.445	2.799	59%	1.646
I(cd)P	RO	new gapfilled	t	11.445	9.934	15%	1.511
I(cd)P	RS	new gapfilled	t	6.134	3.745	64%	2.390
I(cd)P	SI	new gapfilled	t	0.426	0.370	15%	0.056
I(cd)P	SK	new gapfilled	t	4.364	2.748	59%	1.617
I(cd)P	TM	gapfilled	t	0.378	3.023	-87%	-2.645
PAH	AL	gapfilled	t	2.038	0.261	679%	1.776
PAH	BA	gapfilled	t	11.546	4.820	140%	6.726
PAH	CY	reported	t	0.852	0.654	30%	0.198
PAH	ES	New reported	t	39.468	46.912	-16%	-7.444
PAH	FI	reported	t	18.239	22.309	-18%	-4.071
PAH	GB	reported	t	10.452	23.055	-55%	-12.603
PAH	IS	gapfilled	t	0.061	0.087	-30%	-0.026
PAH	KZT	gapfilled	t	339.888	127.834	166%	212.054
PAH	LI	reported	t	0.009	0.015	-40%	-0.006
PAH	MD	new gapfilled	t	13.809	16.867	-18%	-3.058
PAH	ME	reported	t	1.052	0.066	1490%	0.986
PAH	NO	reported	t	5.138	6.784	-24%	-1.646
PAH	PL	gapfilled	t	232.886	190.537	22%	42.349
PAH	PT	gapfilled	t	22.503	14.109	59%	8.394
PAH	RS	gapfilled	t	33.552	21.017	60%	12.534
PAH	SK	gapfilled	t	23.052	17.521	32%	5.531
PAH	TM	gapfilled	t	5.789	8.244	-30%	-2.455
Pb	AM	reported	t	1.197	0.797	50%	0.400
Pb	AT	reported	t	12.472	20.423	-39%	-7.951
Pb	BE	reported	t	11.787	14.591	-19%	-2.804
Pb	BG	reported	t	10.520	73.808	-86%	-63.288
Pb	EE	reported	t	4.217	11.374	-63%	-7.158
Pb	ES	reported	t	82.196	98.468	-17%	-16.272
Pb	GR	reported	t	6.202	7.875	-21%	-1.673
Pb	HU	reported	t	7.023	8.561	-18%	-1.538
Pb	IT	reported	t	155.825	198.974	-22%	-43.149
Pb	LT	reported	t	3.561	2.571	38%	0.990
Pb	LU	reported	t	1.239	1.460	-15%	-0.221
Pb	MC	reported	t	0.007	0.013	-50%	-0.007
Pb	MD	new gapfilled	t	1.673	2.684	-38%	-1.010
Pb	MK	reported	t	2.267	2.676	-15%	-0.409
Pb	RS	reported	t	34.980	47.367	-26%	-12.387

Component	Country	Data sources	Unit	2020 value	2019 value	% change	Value change
PCB	AT	reported	kg	16.206	34.814	-53%	-18.607
PCB	BE	reported	kg	8.727	14.260	-39%	-5.533
PCB	BG	reported	kg	2.408	3.099	-22%	-0.691
PCB	EE	reported	kg	0.562	0.438	28%	0.124
PCB	GB	reported	kg	705.103	488.764	44%	216.338
PCB	GR	reported	kg	43.920	35.496	24%	8.424
PCB	IS	reported	kg	0.015	0.032	-53%	-0.017
PCB	KZT	reported	kg	89.115	123.935	-28%	-34.820
PCB	LU	new gapfilled	kg	2.578	12.113	-79%	-9.535
PCB	LV	reported	kg	0.138	0.170	-19%	-0.032
PCB	MC	reported	kg	0.013	0.020	-34%	-0.007
PCB	MD	new gapfilled	kg	1.763	2.171	-19%	-0.408
PCB	ME	reported	kg	0.001	0.034	-98%	-0.033
PCB	MT	reported	kg	0.001	0.039	-99%	-0.038

Annex A.3.

Overview of heavy metals and POPs gap-filling in 2022

This chapter provides an overview of

Gap filling of heavy metals (Cd Hg, Pb)

Changes to previous year gap-filling:

- **Republic of Moldova did not report in 2022. 2020 data and was gap-filled with copy of 2019 data from previous reporting.**

	Cd	Hg	Pb
Albania	exp.	exp.	exp.
Armenia	R	R	R
Aral Lake	-	-	-
Asian Areas	exp.	exp.	exp.
Austria	R	R	R
Atlantic Ocean	-	-	-
Azerbaijan	exp.	exp.	exp.
Bosnia & Herzegovina	exp.	exp.	exp.
Baltic Sea	-	-	-
Belgium	R	R	R
Bulgaria	R	R	R
Black Sea	-	-	-
Belarus	R	R	R
Caspian Sea	-	-	-
Switzerland	R	R	R
Cyprus	R	R	R
Czechia	R	R	R
Germany	R	R	R
Denmark	R	R	R
Estonia	R	R	R
Spain	R	R	R
Finland	R	R	R
France	R	R	R
United Kingdom	R	R	R
Georgia	R	R	R
Greece	R	R	R
Croatia	R	R	R
Hungary	R	R	R
Ireland	R	R	R
Iceland	R	R	R
Italy	R	R	R
Kyrgyzstan	exp.	exp.	exp.
Kazakhstan	exp.	exp.	exp.

	Cd	Hg	Pb
Liechtenstein	R	R	R
Lithuania	R	R	R
Luxembourg	R	R	R
Latvia	R	R	R
Monaco	R	R	R
Republic of Moldova	exp.	exp.	exp.
Montenegro	R	R	R
Mediterranean Sea	-	-	-
North Macedonia	R	R	R
Malta	R	R	R
Netherlands	R	R	R
Norway	R	R	R
North Africa	exp.	exp.	exp.
North Sea	-	-	-
Poland	R	R	R
Portugal	R	R	R
Romania	R	R	R
Serbia	R	R	R
Russian Federation (RU)	exp.	exp.	exp.
Rest of Russian Federation in the EMEP domain (RFE)	exp.	exp.	exp.
Sweden	R	R	R
Slovenia	R	R	R
Slovakia	R	R	R
Tajikistan	exp.	exp.	exp.
Turkmenistan	exp.	exp.	exp.
Turkey	R+exp.	R+exp.	R+exp.
Ukraine	R	R	R
Uzbekistan	exp.	exp.	exp.

Gap filling of persistent organic pollutants (POPs)
Changes to previous year gap-filling:

- Albania: PAH gapfilled with 2019 data (in previous year reported data was used).
- Belgium: adjustment of the Indeno and PAH sector sum.
- Bulgaria: adjustment of the PAH sector sum.
- Germany: additional estimation of PAH compounds for iron and steel (reported as ‚not estimated') and adjustment of the PAH and compounds sector sum.
- Estonia: adjustment of the PAH sector sum.
- Spain: additional estimation of PAH compounds for iron and steel (reported as ‚not estimated') and adjustment of the PAH and compounds sector sum.
- Greece: use of reported B(a)P data (previously: adjustment)
- Hungary: adjustment of the PAH sector sum.
- Italy: additional estimation of PAH compounds for iron and steel and power plants (reported as ‚not estimated') and adjustment of the PAH and compounds sector sum.
- Kazakhstan: PCDD/F reported data is used (previously: TNO expert data extrapolation)
- Lithuania: adjustment of the PAH sector sum.
- Luxembourg: adjustment of PAH and compounds sector sum.
- Latvia: adjustment of the PAH sector sum.
- Moldova: additional estimation of PAH compounds for industrial production and sproduct use (reported as ‚not estimated') and adjustment of the PAH and compounds sector sum.
- Nort Macedonia: adjustment of the PAH sector sum.
- Malta: adjustment of the PAH sector sum.
- Poland: additional estimation of PAH compounds for iron and steel and product use (reported as ‚not estimated') and adjustment of the PAH and compounds sector sum.
- Portugal: additional estimation of PAH compounds for industrial production and shipping (reported as ‚not estimated') and adjustment of the PAH and compounds sector sum.
- Romania: additional estimation of PAH compounds for industrial production (reported as ‚not estimated') and adjustment of the PAH and compounds sector sum.
- Serbia: use of lately resubmitted data. Additional estimation of PAH compounds for industrial production (reported as ‚not estimated') and adjustment of the PAH and compounds sector sum.
- Sweden: additional estimation of PAH compounds for industrial production (reported as ‚not estimated') and adjustment of the PAH and compounds sector sum.
- Slovenia: additional estimation of PAH compounds for industrial production (reported as ‚not estimated') and adjustment of the PAH and compounds sector sum.
- Slovakia: : additional estimation of PAH compounds for industrial production and product use (reported as ‚not estimated') and adjustment of the PAH and compounds sector sum.
- Ukraine: PCDD/F expert estimate (previously: reported data). HCB: new expert estimate (lower emissions).

	B(a)P	B(b)F	B(k)F	PCDD/F	HCB	IP	PAH	PCB
Albania	exp.	exp.	exp.	exp.	R	R	exp.	R
Armenia	R	R	R	R	R	R	sum	R
Aral Lake	-	-	-	-	-	-	-	-
Asian Areas	-	-	-	-	-	-	-	-
Austria	R	R	R	R	R	R	R	R
Atlantic Ocean	-	-	-	-	-	-	-	-
Azerbaijan	exp.	exp.	exp.	exp.	exp.	exp.	exp.	exp.
Bosnia and Herzegovina	exp.	exp.	exp.	exp.	exp.	exp.	exp.	-
Baltic Sea	-	-	-	-	-	-	-	-
Belgium	R	R	R	R	R	sum	sum	R
Bulgaria	R	R	R	R	R	R	sum	R
Black Sea	-	-	-	-	-	-	-	-
Belarus	R	R	R	R	R	R	R	R
Caspian Sea	-	-	-	-	-	-	-	-
Switzerland	R	R	R	R	R	R	R	R
Cyprus	R	R	R	R	R	R	R	R
Czechia	R	R	R	R	R	R	sum	R
Germany	R+exp.	R+exp.	R+exp.	R+exp.	R	R+exp.	R+exp.	R
Denmark	R	R	R	R	R	R	R	R
Estonia	R	R	R	R	R	R	sum	R
Spain	R+exp.	R+exp.	R+exp.	R	R	R+exp.	R+exp.	R
Finland	R	R	R	R	R	R	R	R
France	R	R	R	R	R	R	R	R
United Kingdom	R	R	R	R	R	R	R	R
Georgia	R	R	R	R	R	R	sum	R
Greece	R	R	R	R	R	R	sum	R
Croatia	R	R	R	R	R	R	sum	R
Hungary	R	R	R	R	R	R	sum	R
Ireland	R	R	R	R	R	R	R	R
Iceland	R	R	R	R	R	R	sum	R
Italy	R+exp.	R+exp.	R+exp.	R	R	R+exp.	sum	R
Kyrgyzstan	exp.	exp.	exp.	exp.	exp.	exp.	exp.	exp.
Kazakhstan	R	R	R	R	R	R	sum	R
Liechtenstein	R	R	R	R	R	R	R	-
Lithuania	R	R	R	R	R	R	sum	R
Luxembourg	sum	sum	sum	R	R	sum	sum	R
Latvia	R	R	R	R	R	R	sum	R
Monaco	R	R	R	R	R	R	R	R
Republic of Moldova	R+exp.	R+exp.	R+exp.	R	R	R+exp.	R+exp.	R
Montenegro	R	R	R	R	R	R	R	R
Mediterranean Sea	-	-	-	-	-	-	-	-
North Macedonia	R	R	R	R	R	R	sum	R
Malta	R	R	R	R	R	R	sum	R
Netherlands	R	R	R	R	R	R	R	R

	B(a)P	B(b)F	B(k)F	PCDD/F	HCB	IP	PAH	PCB
Norway	R	R	R	R	R	R	R	R
North Africa	-	-	-	-	-	-	-	-
North Sea	-	-	-	-	-	-	-	-
Poland	R+exp.	R+exp.	R+exp.	R	R	R+exp.	sum	R
Portugal	R+exp.	R+exp.	R+exp.	R	R	R+exp.	sum	R
Romania	R+exp.	R+exp.	R+exp.	R	R	R+exp.	sum	R
Serbia	R+exp.	R+exp.	R+exp.	R	R	R+exp.	sum	R
Russian Federation	exp.	exp.	exp.	exp.	exp.	exp.	exp.	-
Russian Federation in the extended EMEP domain	exp.	exp.	exp.	exp.	exp.	exp.	exp.	-
Sweden	R+exp.	R+exp.	R+exp.	R	R	R+exp.	sum	R
Slovenia	R+exp.	R+exp.	R+exp.	R	R	R+exp.	sum	R
Slovakia	R+exp.	R+exp.	R+exp.	R	R	R+exp.	sum	R
Tajikistan	exp.	exp.	exp.	exp.	exp.	exp.	exp.	-
Turkmenistan	exp.	exp.	exp.	exp.	exp.	exp.	exp.	-
Turkey	exp.	exp.	exp.	exp.	exp.	exp.	exp.	-
Ukraine	exp.	exp.	exp.	exp.	exp.	exp.	exp.	R
Uzbekistan	exp.	exp.	exp.	exp.	exp.	exp.	exp.	-

R	*Reported/new reported*
sum	*Sum of sectors/components*
R+exp.	*Reported data plus expert estimates (e.g. PAH split)*
exp.	*Expert estimates*

Annex B.

Update of the assessment results with the new emission reporting data

The results of the model assessment of heavy metal and POP pollution levels, presented in the chapter 3 of this report, are based on the emission data for the previous year 2019, and the meteorology, chemical reactants, and land-cover data for the year 2020. This Annex presents the modelled deposition fluxes and atmospheric concentrations estimated based on the most recent emission data for 2020. The difference between the results presented in the Annex and those demonstrated in Chapter 3 is caused entirely by the changes in the emission data.

Relative difference between the modelling results based on emissions of 2020 and 2019 is calculated according to the following formula:

$$\Delta_{emis} = \frac{(Y_{2020} - Y_{2019})}{Y_{2019}} \cdot 100\%$$

Here Y_{2020} and Y_{2019} are modelled values (deposition flux or air concentration) in 2020 and 2019, respectively, and Δ_{emis} – relative difference between the results. Positive value of the difference means the increase of the pollution levels in 2020 relative to 2019, and vice versa.

Lead

Over most of the EMEP countries the changes of emission data lead to the decrease of Pb concentrations and deposition fluxes (Fig. B.1). The decline of air concentrations from 5% to 20% takes place over Spain, Portugal, Poland, Romania, Hungary, Slovakia, Czechia, Germany, Greece and most of France and Finland, and over the central part of Russia. In some countries, i.e., in Switzerland, Austria, the northern and southern parts of Italy, Bulgaria and the central regions of Russia the increase ranges in 20 – 50% limits, and sometimes even exceeds 50%. Major areas with increase of air concentrations is noted for a number of regions in Eastern Europe and Sicily and Calabria regions in the southern part of Italy. Spatial distribution of the difference of deposition fluxes is similar to that of air concentrations.

In most cases the reduction of the pollution levels is caused by the decrease of Pb emissions of sector B ("Industry"). Besides, in some countries, e.g., Finland and Ukraine, the reduction in other sectors such as A ("Public electricity and heat production"), C ("Other stationary combustion") and E ("Solvents") took place. In a number of countries (e.g., Russia, Ukraine, Italy) the changes are strongly associated with the changes of emission gridding (Chapter 1, Table 1.3), which results to the increase of emissions and pollution levels in some parts, and the decline in other parts of the countries.

It is worth mentioning that the changes of concentrations and deposition are in general lower than the changes of emissions. First of all, it is explained by the dispersion of the pollutants in the atmosphere. On one hand, it results to smaller changes in the vicinity of emission sources. On the other hand, the changes of the pollution levels due to transboundary transport occur even in the regions where emissions remain the same. Another reason is the effect of secondary emissions and transport from non-EMEP sources.

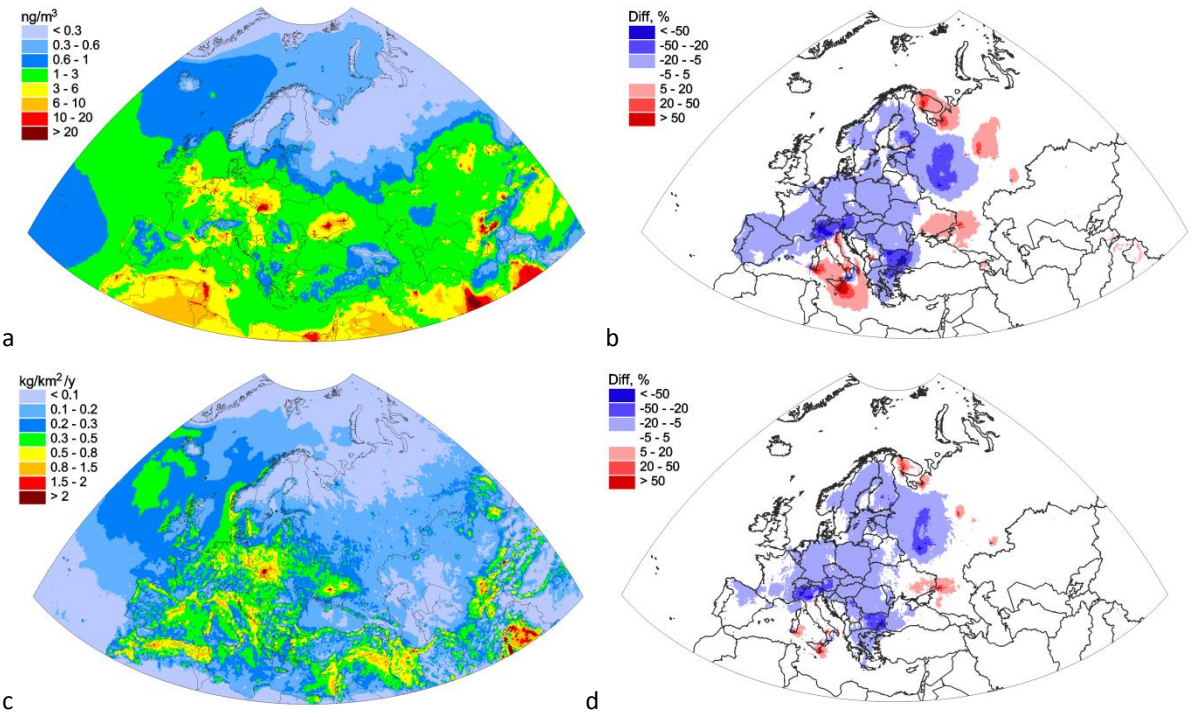

Fig. B.1. *Annual mean modelled air concentrations (a) and total deposition fluxes (c) of Pb based on the emissions data for 2020 and their relative changes (b and d) from the modelling results based on the emissions data for 2019.*

Cadmium

Decrease of Cd concentrations in air and deposition fluxes due to emission changes is noted for the United Kingdom, Ireland, Spain, Moldova and the southern parts of Italy, Norway and Finland (Fig. B.2). The highest decline exceeding 50% takes place over central part of European Russia and over northern Ukraine. Moderate increase (5 – 20%) of concentrations and deposition occurs in Poland, Lithuania, Turkey, Bosnia and Herzegovina and in numerous regions of Kazakhstan. Stronger increase (20 – 50% or even higher) was found for Montenegro, a number of regions in Italy and some areas in Russia.

The main emission sectors contributing to the decrease of modelled Cd pollution levels are “Other stationary combustion” (e.g., Finland, Italy, the United Kingdom, Spain, Moldova), “Industry” (e.g., Finland, Bulgaria, Italy, Poland, Spain), “Public electricity and heat production” (Finland, Lithuania), “Solvents” (Finland, Bulgaria, the United Kingdom, Lithuania). Increase of Cd emissions is related to sectors “Public electricity and heat production” (e.g., Bulgaria, Russia), “Industry” (e.g., Lithuania, Ukraine) and “Other stationary combustion” (e.g., Bulgaria, Lithuania, Montenegro). Similar to Pb, the changes in spatial distribution of emissions in a number of countries resulted to local increases or decreases of Cd pollution levels.

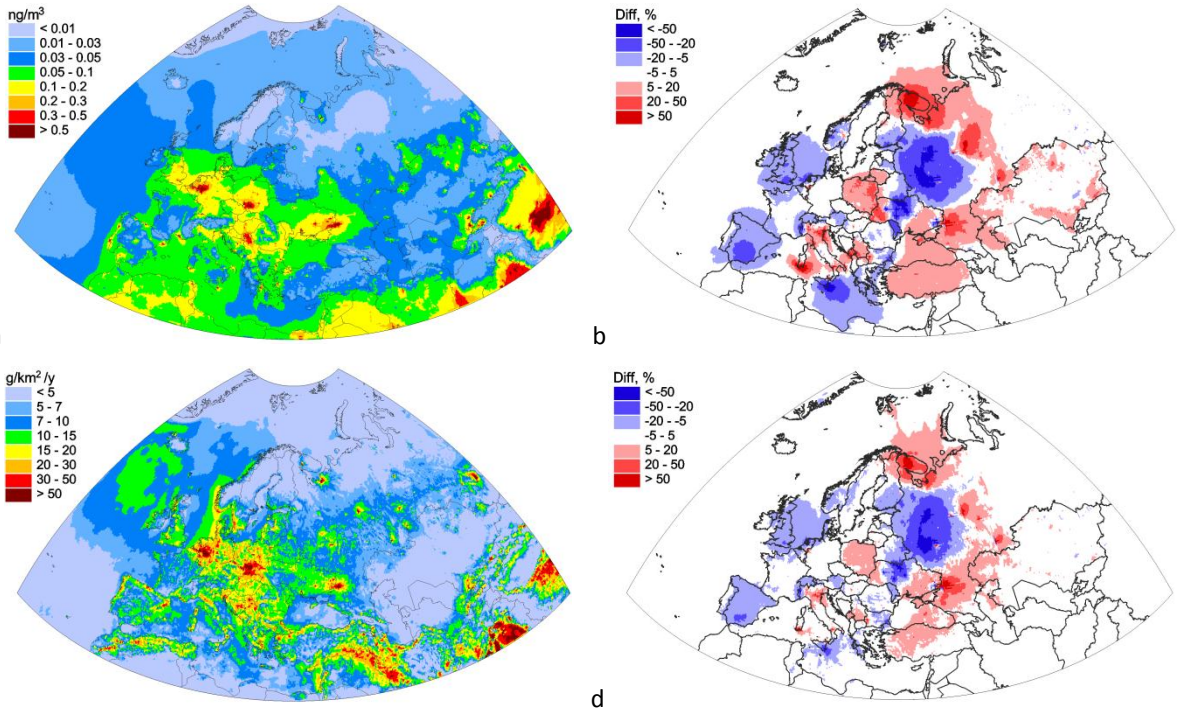

Fig. B. 2. *Annual mean modelled air concentrations (a) and total deposition fluxes (c) of Cd based on the emissions data for 2020 and their relative changes (b and d) from the modelling results based on the emissions data for 2019.*

Mercury

Modelled mean annual air concentrations and deposition fluxes of Hg in 2020 based on emissions and meteorological data for 2020 are shown in Fig B.3(a,d), and the relative changes - in Fig. B.3(c,d). In Turkey, the eastern part Ukraine and several regions in Italy the increase of air concentration was 1 – 10%, and the increase of deposition was mainly 5 – 20%, and in some gridcells from 20 to 50%. The change of Hg emission in sector J ("Waste") is responsible for the significant increase of Hg levels in Turkey, and to some extent – in Italy. The increase of sector "Industry" is the main contributor to the rise of Hg deposition and concentrations in Ukraine. Decrease of Hg air concentrations and deposition in the United Kingdom, central Russia, Switzerland, the northern part of Ukraine, and some regions of Germany and Italy. The decrease of Hg levels in Italy and the United Kingdom is mainly caused by "Industry" sector, and the decline in Germany is explained by "Public electricity and heat production" sector. The smaller changes of air concentrations compared to the changes of deposition are explained by large contribution to air concentrations of quite persistent elemental mercury caused by intercontinental transport.

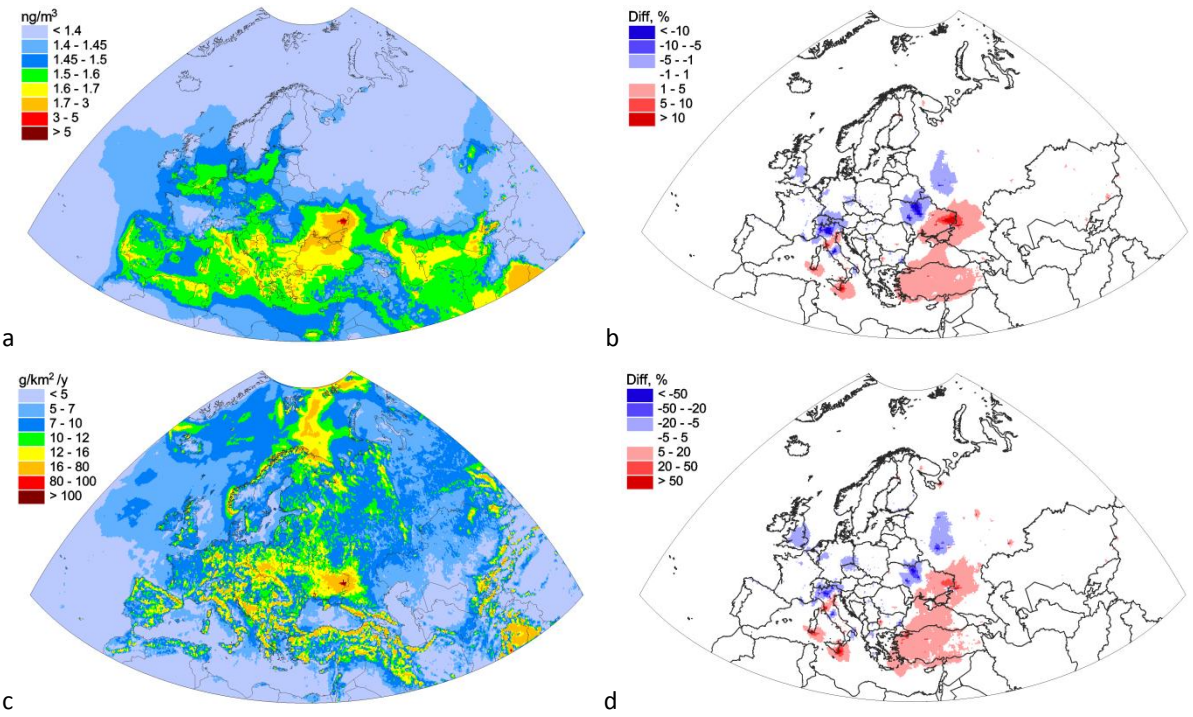

***Fig. B.3**. Annual mean modelled air concentrations (a) and total deposition fluxes (c) of Hg based on the emissions data for 2020 and their relative changes (b and d) from the modelling results based on the emissions data for 2019.*

PAHs

The modelling results for PAHs based on emissions for 2020 and 2019 are characterized by the large changes of the pollution levels. Besides the changes in total national emissions (Annex A.2), the methodology of PAH emission gridding was modified. It resulted in highly patchy spatial distribution of relative changes between the modelling results based on previous and updated emission data. In particular, relative differences of air concentrations and deposition fluxes in most of the EMEP countries are around ±20-50% and higher (Fig. B.4).

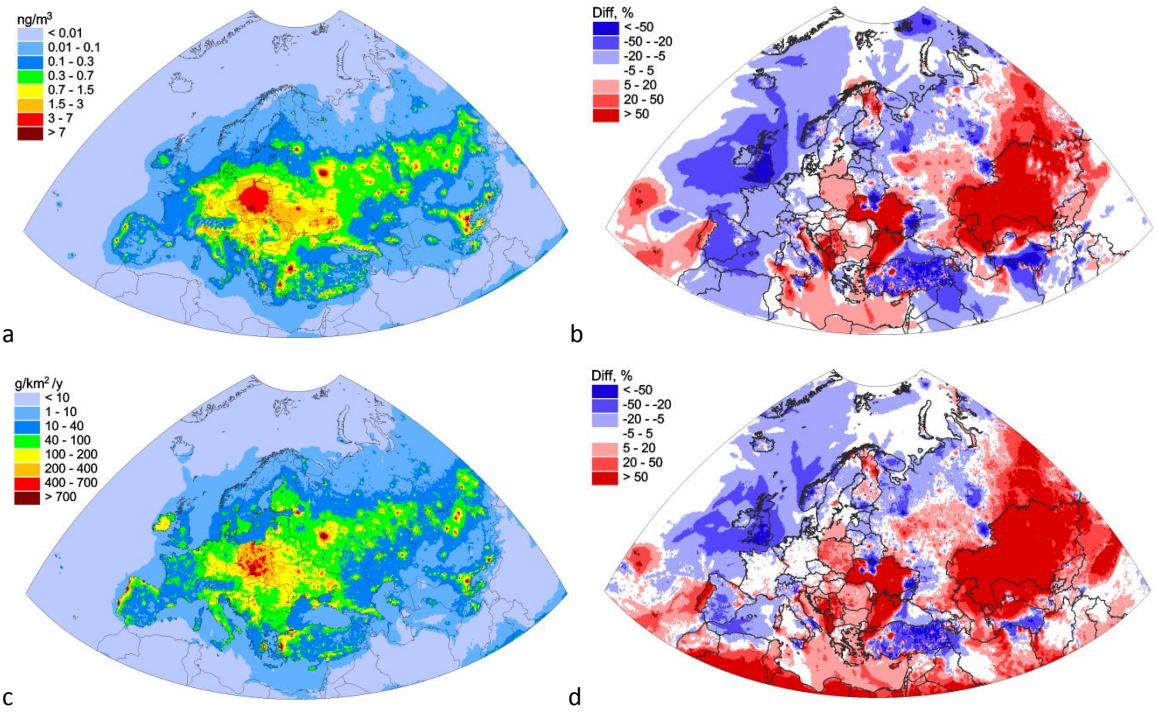

Fig. B.4. *Annual mean modelled air concentrations (a) and total deposition fluxes (c) of the sum of 4 PAHs, based on the emissions data for 2020, and their relative changes (b and d) from the modelling results based on the emissions data for 2019.*

PCDD/Fs and HCB

Emission data for PCDD/Fs and HCB, used in the model simulations for 2019, represents scenarios based on the usage of maximum level of the emissions in the EMEP countries [*Ilyin et al.*, 2021]. However, in order to carry out model assessment of pollution for 2020, official emission data prepared by CEIP were applied. Modelled PCDD/F and HCB air concentrations and deposition fluxes based on the input data related to 2020 are shown in Fig. B.5 and B.6, respectively.

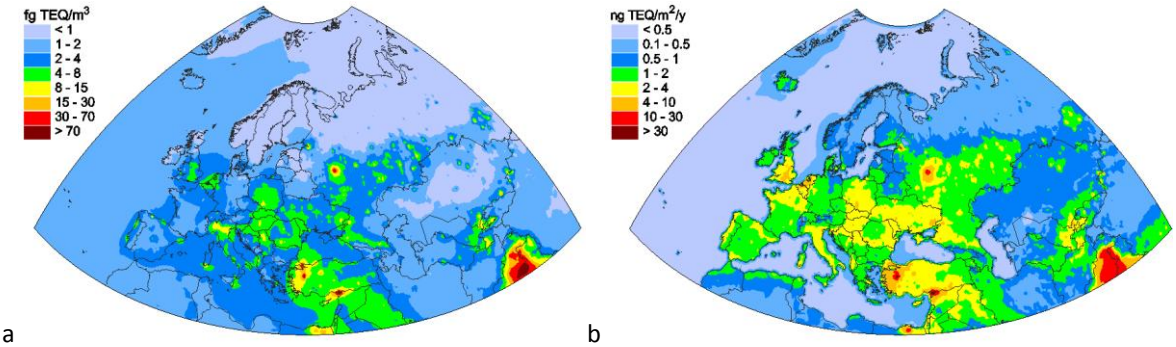

Fig. B.5. *Annual mean modelled air concentrations (a) and total deposition fluxes (b) of PCDD/Fs based on the emissions data for 2020.*

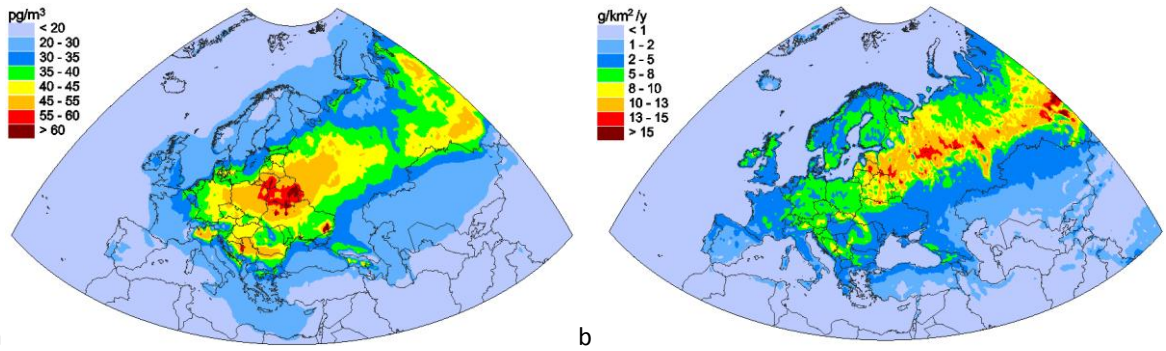

Fig. B.6. *Annual mean modelled air concentrations (a) and total deposition fluxes (b) of HCB based on the emissions data for 2020.*